The Synthesis and Analysis of Complex Poly(2-oxazoline) Architectures

Under the supervision of Prof. C. Remzi Becer.

A thesis submitted in partial fulfilment of the requirements for the degree of Doctor of Philosophy in Chemistry.

Graham Hayes

University of Warwick, Department of Chemistry

September 2022

Table of Contents

i. Acknowledgements

Thanks firstly must go to Remzi for his continued support and guidance throughout my PhD and beyond. Thanks also to the whole Becer group (past and present) who have been great to work with and who have always been available for help if needed. Special thanks to Ben for continually providing advice throughout my PhD and for proof-reading my thesis. Thanks must also go to Alessandra for proof-reading this entire thesis.

Next, I must give thanks to my family, particularly my parents Peter and Pamela, who have been so very supportive throughout my PhD, as well as agreeing to proof-read my thesis. The biggest thanks of all has to go to my wife Nathanya, who has always been there for me throughout this process offering guidance, support, friendship, and love. Without her I certainly would not be where I am today, and I am very grateful.

ii. Declaration

This thesis is submitted to the University of Warwick in support of my application for the degree of Doctor of Philosophy. It has been composed by myself and has not been submitted in any previous application for any degree. The experimental work contained in this thesis is original research carried out by the author, unless stated otherwise, in the Department of Chemistry at the University of Warwick. The work presented was carried out by the author except in the following instances:

Chapter 3: Advanced GPC measurements were performed by Ben Drain (Becer group, University of Warwick, Chemistry Department). TEM and DLS measurements were carried out by James Lefley (Becer group, University of Warwick, Chemistry department).

Chapter 4: Cell transfection, cell viability, and polyplex encapsulation efficiency were measured by Beatriz Dias Barbieri (Shattock Group, Faculty of Medicine, Department of Infectious Diseases, Imperial College London).

iii. Abstract

Poly(2-oxazoline)s are a diverse polymer type that are synthesised *via* the cationic ring-opening polymerisation of 2-oxazoline monomers. The diversity of this polymer class stems from the wide range of functionalities that can be installed at both polymeric chain ends, as well as the monomer R group. This potential functionality can be used to access complex polymeric architectures that have a wide range of possible applications. In **Chapter 1** of this thesis, a literature review of the synthesis and diversity of poly(2-oxazoline)s is firstly discussed, followed by discussion of some more complex poly(2-oxazoline) architectures. In **Chapter 2**, star polymers are synthesised using a bisfunctional 2-oxazoline monomer, and their potential for drug encapsulation is explored. Then, the same cross-linker is used to synthesise branched poly(2-oxazoline) structures. The analysis of these complex structures with advanced viscosity gel permeation chromatography is then discussed. In **Chapter 3**, poly(2-oxazoline)s are combined with acrylates to form hybrid block copolymers which can act as AB type macromonomers to form step-growth and cyclic polymers. The effect of various parameters on the ratio of step-growth to cyclic product is discussed, followed by advanced gel permeation chromatography analysis of the products and discussion on their aqueous self-assembly. In **Chapter 4**, a 2-oxazoline containing an amine on the R group is synthesised and polymerised to form statistical and block copolymers that can be glycosylated. These polymers are then tested for gene transfection and cell viability. Lastly in **Chapter 5**, a summary and conclusion are provided as well as an outlook on the future of poly(2-oxazoline)s.

iv. List of Schemes

v. List of Figures

vi. List of Tables

vii. Abbreviations

ATP	Adenosine triphosphate
ATRP	Atom transfer radical polymerisation
BHT	Butylated hydroxytoluene
BisOx	Bis-2-oxazoline
BMPA	2-bromo-2-methyl-propionic acid
BocAmineOx	Boc protected amine oxazoline
ButenylOx	2-Butenyl-2-oxazoline
CCS	Core cross-linked
CROP	Cationic ring opening polymerisation
Cu(0)-RDRP	Copper(0) mediated reversible deactivation radical polymerisation
CuAAC	Copper catalysed azide-alkyne cycloaddition
Đ	Dispersity
DHA	Dihydroxyanthraquinone
DIPEA	Diisopropylethylamine
dn/dc	Refractive index increment
DP	Degree of polymerisation
DLS	Dynamic light scattering
DMAP	4-Dimethylaminopyridine
DMF	Dimethylformamide
DMPA	2,2-dimethoxy-2-phenylacetophenone
DNA	Deoxyribonucleic acid
DPA	Diisopropylamine
EDAC	1-Ethyl-3-(3-dimethylaminopropyl)carbodiimide
EHA	Ethylhexyl acrylate
ESI-MS	Electrospray-ionisation mass spectrometry
EtOx	2-Ethyl-2-oxazoline
FDA	Food and Drug Administration
FTIR	Fourier transform infrared

GC	Gas chromatography
GPC	Gel permeation chromatography
HIV	Human immunodeficiency virus
HSKMC	Human skeletal muscle cells
IFN	Interferon
IPA	Isopropanol
IV	Intrinsic viscosity
LCST	Lower critical solution temperature
LNP	Lipid nanoparticle
LS GPC	Light scattering gel permeation chromatography
MA	Methyl acrylate
MALDI-TOF-MS	Matrix assisted laser desorption/ionisation time of flight mass spectrometry
Me_6TREN	Tris 2-(dimethylamino)ethylamine
MeOTs	Methyl tosylate
MeOx	2-Methyl-2-oxazoline
MRI	Magnetic resonance imaging
mRNA	Messenger ribonucleic acid
NMP	Nitroxide mediated polymerisation
NMR	Nuclear magnetic resonance
ORCA	Organic radical contrast agent
PDC	Polymer drug conjugate
PDI	Polydispersity index (*Đ*)
PDMAEMA	Poly(2-(dimethylamino)ethyl methacrylate)
pDNA	Plasmid DNA
PEG	Poly(ethylene glycol)
PEI	Poly(ethyleneimine)
pEtOx	Poly(2-ethyl-2-oxazoline)
PhOx	2-Phenyl-2-oxazoline
PMDETA	1,1,4,7,7-Pentamethyldiethylenetriamine
PMMA	Poly(methyl methacrylate)

pMeOx	Poly(2-methyl-2-oxazoline)
pPrOx	Poly(2-n-propyl-2-oxazoline)
PropTs	Propargyl p-toluenesulphonate
PrOx	2-n-Propyl-2-oxazoline
PTFE	Poly(tetrafluoroethylene)
RAFT	Reversible addition/fragmentation chain-transfer
RDRP	Reversible deactivation radical polymerisation
repRNA	Self-amplifying replicon ribonucleic acid
RI	Refractive index
RNA	Ribonucleic acid
ROMP	Ring-opening metathesis polymerisation
SARA-ATRP	Supplemental activator and reducing agent atom transfer radical polymerisation
saRNA	Self-amplifying ribonucleic acid
SARS-COV-19	Severe acute respiratory syndrome – Coronavirus 2019
SET-LRP	Single electron transfer living radical polymerisation
SI-ATRP	Surface-initiated atom transfer radical polymerisation
TEA	Triethylamine
TEM	Transmission electron microscopy
T_g	Glass transition temperature
THF	Tetrahydrofuran
TFE	Trifluoroethanol
T_m	Melting temperature
UCST	Upper critical solution temperature
UV	Ultra-violet

viii. List of Publications

Hayes, G. C.; Becer, C. R. Levulinic acid: a sustainable platform chemical for novel polymer architectures. *Polymer Chemistry* **2020**, *11* (25), 4068-4077

Hayes, G.; Drain, B.; Becer, C. R. Multiarm Core Cross-Linked Star-Shaped Poly(2-oxazoline)s Using a Bisfunctional 2-Oxazoline Monomer. *Macromolecules* **2022**, *55* (1), 146-155

Hayes, G. C.; Laurel, M.; MacKinnon, D.; Zhao, T.; Houck, H.; Becer, C. R. Polymers without petrochemicals: Sustainable routes to conventional monomers. *Chemical Reviews* **2022** (accepted).

Hayes, G.; Becer, C. R. Hyperbranched Poly(2-oxazoline)s via a Bisfunctional Crosslinker. *European Polymer Journal* **2022**, 181, 111678

Hayes, G.; Drain, B.; Lefley, J.; Becer, C. R. Hybrid Multiblock Copolymers of 2-Oxazoline and Acrylates via Cu Catalyzed Azide-Alkyne Cycloaddition Step-Growth Mechanism. *Macromolecules* **2022** (accepted).

Chapter 1. Introduction

1.1. Overview of Poly(2-oxazoline)s

Poly(2-oxazoline)s are a diverse class of polymeric structure that are synthesised from the cationic ring-opening polymerisation (CROP) of 2-oxazolines. Recent interest surrounding poly(2-oxazoline)s is due to their biocompatibility and their potential to replace current biomedical standards such as poly(ethylene glycol) (PEG). PEG is used as a 'stealth' polymer, so named because it can be used to deliver therapeutics into the human body whilst remaining undetected by the immune system.[1] However, recent literature suggests a growing proportion of the population presents some sort of immune response when exposed to PEG.[2] Poly(2-oxazoline)s are not only of interest due to their PEG-substitution potential; their biocompatibility makes them of interest for other therapeutic applications. Moreover, a variety of initiators, end-capping agents, and R groups are available allowing access to higher orders of polymeric architecture with related interesting properties and applications (**Scheme 1.1**).[3, 4] In this chapter, the synthesis, analysis, and applications of some of these complex structures including star polymers,[5] hyperbranched polymers,[6] block polymers,[7] and cyclic polymers[8] are discussed.

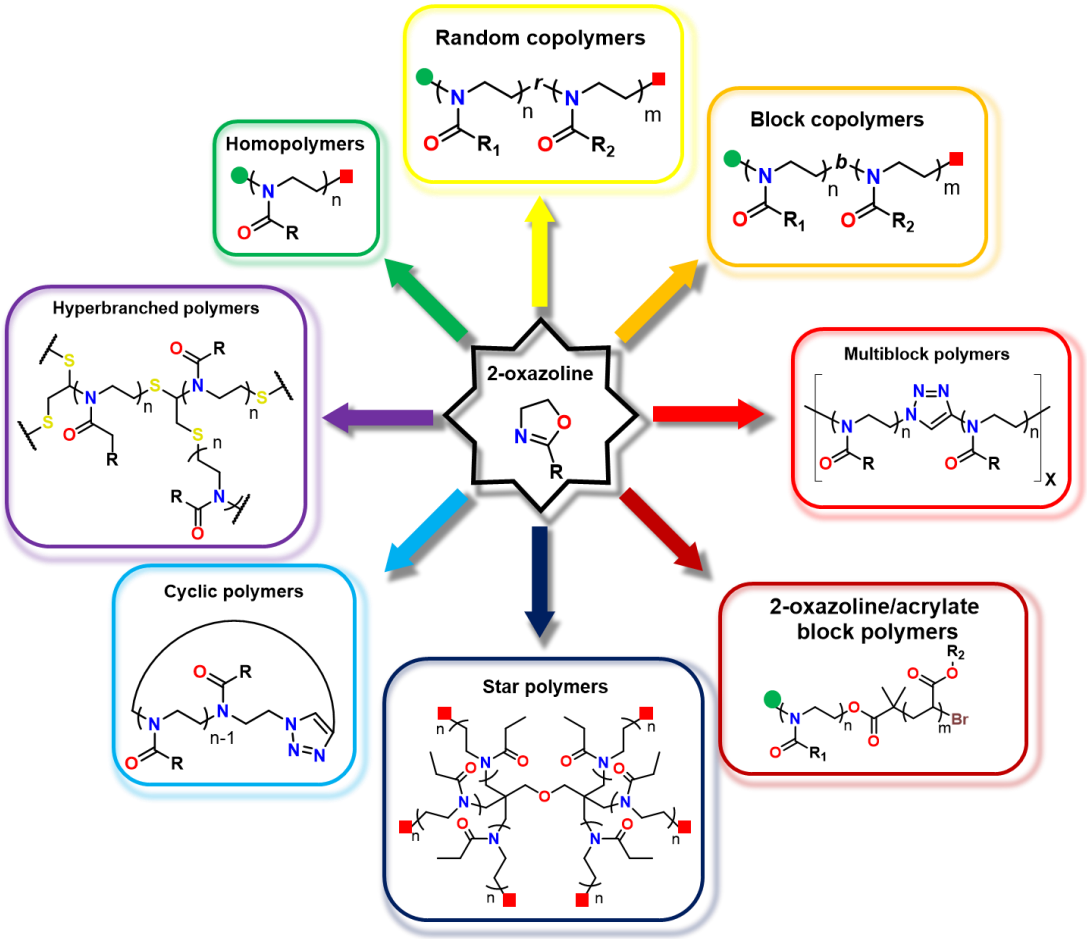

Scheme 1.1. Overview of some of the main architectures discussed in this thesis that are possible using the CROP of 2-oxazolines.

1.1.1. Synthetic Routes to 2-Oxazolines

The most common 2-oxazolines for CROP are 4,5-dihydroxyoxazoles, as substitution on the 4' and 5' positions on the 2-oxazoline ring can lead to issues with the polymerisation, due to steric hindrance and/or electronic effects.[9] There are three main methods that are typically used for the synthesis of poly(2-oxazoline)s (**Scheme 1.2.**). Firstly, they can be synthesised directly from non-activated carboxylic acids using 2-aminoethanol and a suitable Lewis acid.[10] This is a simple route with a wide range of potential starting materials, however harsh conditions are required making it incompatible with some functional groups that can be present on the carboxylic acids.

The second route is known as the Witte-Seeliger method, where a nitrile is reacted with 2-aminoethanol in the presence of a Lewis acid.[11] The third route is known as the Wenker method, and involves coupling a carboxylic acid or acid chloride with 2-chloroethylamine, followed by ring closure with a base.[12] Notably, a new fourth route to 2-oxazolines was discovered in 2022, where 2-chloroethyl isocyanate was reacted with a carboxylic acid in a one-pot setup with yields of up to 92% for a range of 2-oxazolines.[13]

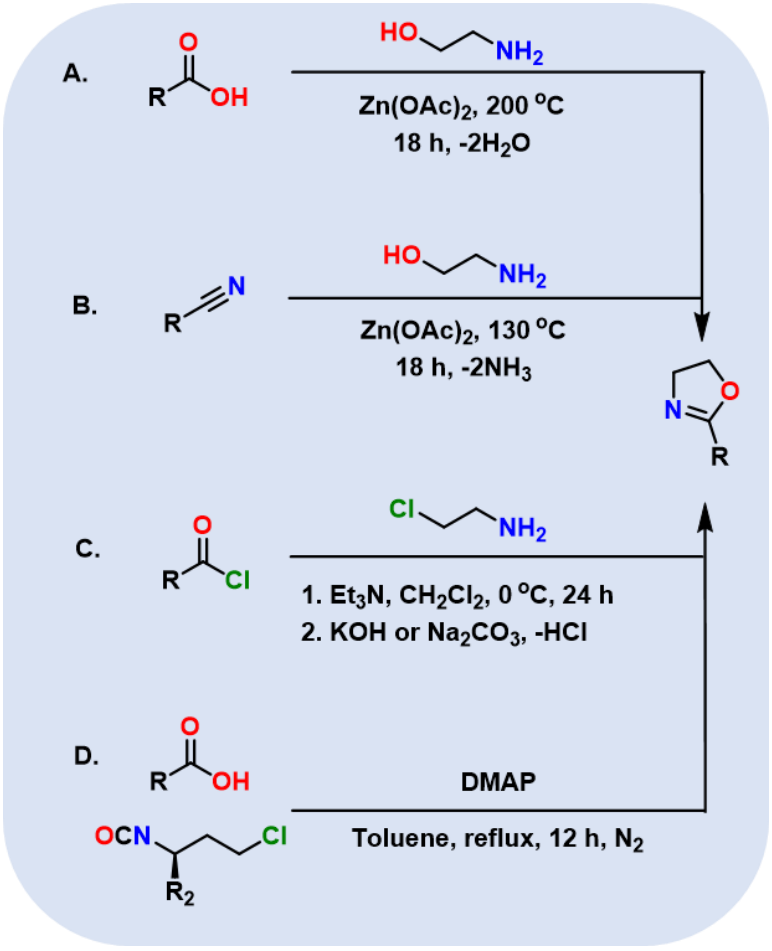

Scheme 1.2. Discussed synthetic routes to 2-oxazolines: (**A.**) From a non-activated carboxylic acid. (**B.**) The Witte-Seeliger method. (**C.**) The Wenker method. (**D.**) One-pot synthesis with 2-chloroethyl isocyanate.

1.1.2. CROP of 2-oxazolines

The CROP of 2-oxazolines is regarded as a living polymerisation technique and thus there are no termination reactions present in an ideal system. Moreover, to obtain well-controlled polymers, the initiation should be fast, and propagation should be constant. In this section, the kinetics of CROP are discussed, followed by a detailed discussion of the initiation, propagation, termination reactions, and chain transfer. It should be noted that a very thorough review article covering the chemistry of poly(2-oxazoline)s was published by Hoogenboom *et al*. in 2017.[14]

1.1.2.1. Kinetics of CROP

One of the main attributes of a living polymerisation is the absence of termination, and this results in the polymerisation following a first-order kinetic plot.[15] When termination is negligible, the concentration of propagating species is constant and so the polymerisation rate with respect to the log of the monomer concentration is a linear function of time (see **Equations 1.1** and **1.2**).

$$R_p = -\frac{d[M]}{dt} = k_p[P\cdot][M] \qquad \textbf{Equation 1.1}$$

$$ln\frac{[M]_0}{[M]} = k_p[P\cdot]t = k_p^{app}t \qquad \textbf{Equation 1.2}$$

Where R_p is the rate of polymerisation, [M] is the monomer concentration, k_p is the propagating rate constant, [P·] is the concentration of propagating species, t is time.

When the log of monomer conversion is plotted against time a linear trend is revealed, which is sensitive to any deviation from a constant [P·]. If the trend curves upwards, it is indicative of slow initiation, whilst if it curves downwards, it is indicative of termination reactions. The linear trend is not proof of a living polymerisation, as initiation and termination events may be occurring simultaneously at the same rate. When a polymerisation is living, the observed increase in molecular weight of the polymer should increase linearly with conversion if initiation is fast and there are no chain transfer reactions. If there are chain transfer reactions, the M_n/conversion plot will curve downwards, and if chain-chain coupling is present, the plot will curve upwards (**Figure 1.1.**).

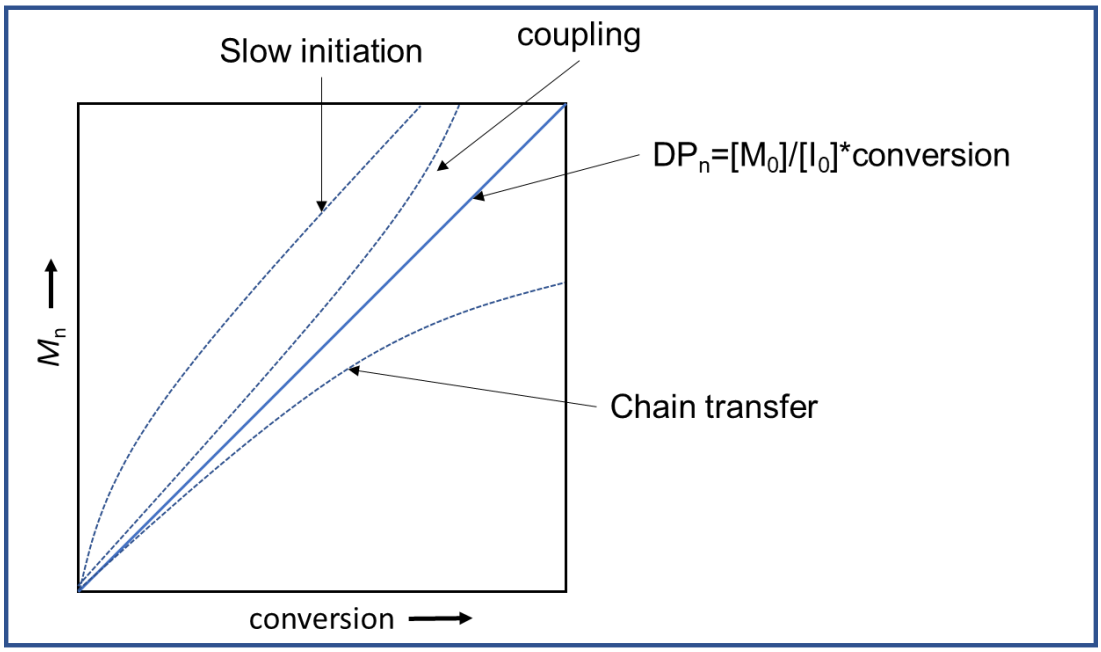

Figure 1.1. M_n/conversion plot with plots indicative of slow initiation, coupling, and chain transfer of CROP.

Schubert e*t al*. investigated the livingness of the CROP of various 2-oxazolines in 2005.[16] In this paper, they investigated the effect of microwave heating vs. conventional heating concluding there was no difference on the CROP. From **Figure 1.2**, the livingness of the CROP of 2-oxazolines can be observed by

the linear increase in log of monomer consumption over time and the linear molecular weight increase as a function of monomer conversion. Furthermore, the paper shows how monomer type and reaction temperature affect the reaction rate and serves as a useful reference for determining polymerisation times.

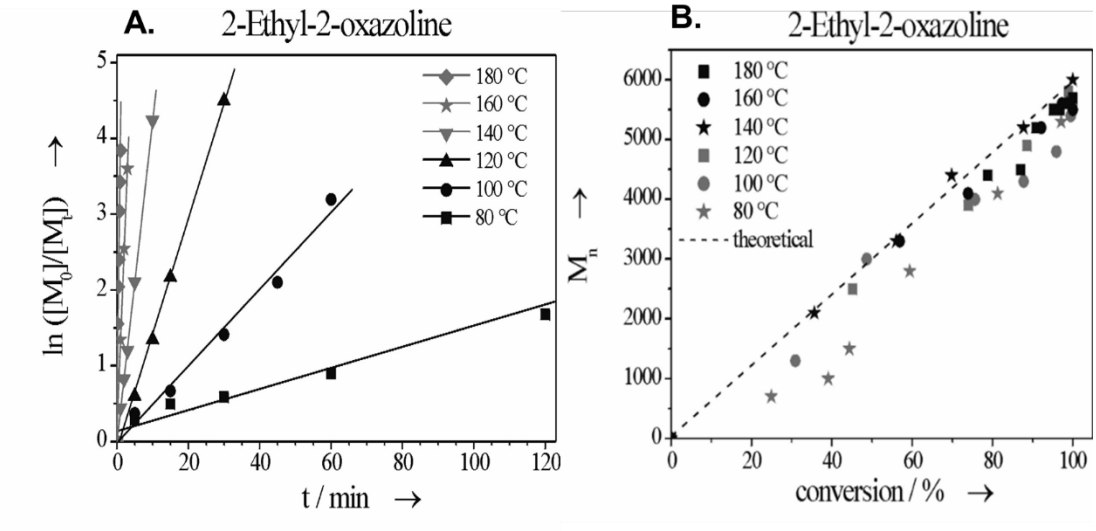

Figure 1.2. First order kinetic plots of 2-ethyl-2-oxazoline (EtOx) at various temperatures. The target degree of polymerisation (DP) was 60 and the reaction concentration was 4 M. **(A)** Semilogarithmic first order kinetic plot of EtOx at various temperatures **(B)** M_n increase as a function of monomer conversion. Figure reprinted from reference 16 with permission from the American Chemical Society (Copyright 2022).

1.1.2.2. Initiation, Termination, Propagation

The overall mechanism for the CROP of 2-oxazolines can be seen in **Scheme 1.3.** The initiation of the CROP of 2-oxazolines is commenced by the nucleophilic attack of the 2-oxazoline onto an electrophilic initiator, with the rate constant k_i.

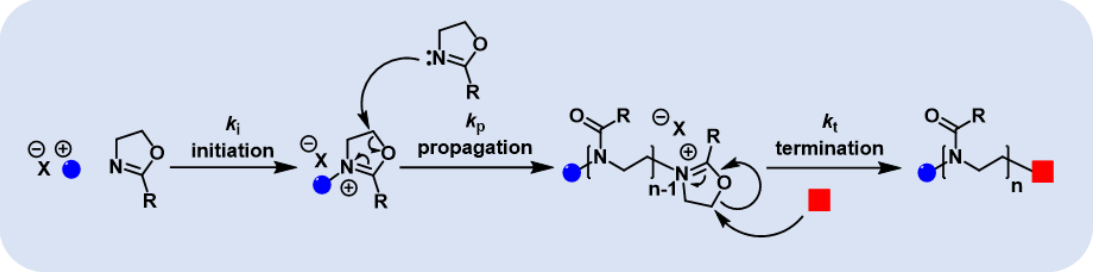

Scheme 1.3. Mechanism for the CROP of 2-oxazolines including initiation, propagation, and termination at the 5' position. The blue dot represents an electrophile, whilst the red square indicates a nucleophilic terminating species.

Typically, tosylates and triflates are used for initiation due to their stability and fast initiation.[17, 18] Nonetheless, there are various possible tosylates and triflates as well as other electrophiles available for initiation, and these will be discussed later in **Section 1.1.3**. Slow or incomplete initiation leads to a loss of control and deviation from the first order kinetics associated with the CROP of 2-oxazolines. The counter ion introduced by the initiator is very important as it influences the equilibrium between the active, cyclic, cationic species and the dormant covalent species (**Scheme 1.4.**).[14]

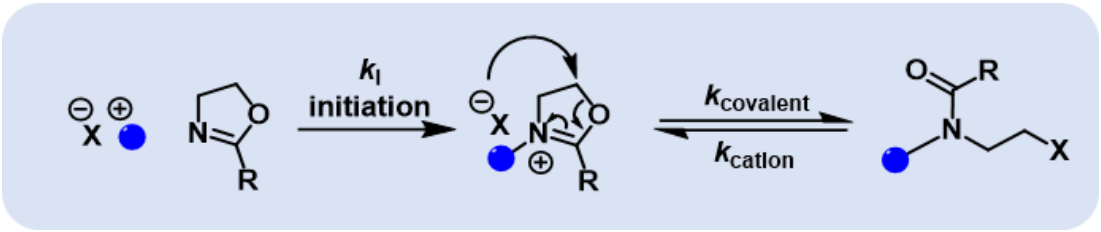

Scheme 1.4. Initiation of CROP with the resulting covalent/ionic equilibrium.

The propagation of the CROP of 2-oxazolines is a two-step mechanism. The first step is the addition of the first monomer to the initiation product. This is a slow process and thus is the rate determining step. Once the first addition is complete, the propagation rate (k_p) increases significantly, which is attributed to an intramolecular dipole interaction which stabilises the transition state.[19] The equilibrium between the covalent and cationic species determines the propagation rate, with the cationic species being responsible for propagation. Factors that alter this equilibrium include the solvent, counter ion, and monomer type. [20] To ensure that the propagation is fast, and the equilibrium is pushed towards the cationic species, counter ions that form stable anions such as tosylates are beneficial. The choice of solvent influences the

equilibrium, with solvents such as sulfolane[21] and chlorobenzene[22] favouring the formation of the cationic species, presumably due to their ability to solvate cationic species. Furthermore, the nucleophilicity of the 2-oxazoline itself is important, with less nucleophilic 2-oxazolines such as 2-phenyl-2-oxazoline (PhOx) propagating slowly due to the stabilising effect of the R group.[23]

The termination of 2-oxazoline chains can occur in the 2' and 5' position on the oxazolinium species. Some less nucleophilic species such as water terminate at both the 2' position and the 5' position (**Scheme 1.5.**)[24] however other more nucleophilic species such as thiolates terminate only at the thermodynamically favoured 5' position.[25] Like the initiation, functionalisation can be introduced by using an appropriate end-capping agent. As with the initiator, functional groups that can be installed by the terminating group will be discussed in **Section 1.1.3**.

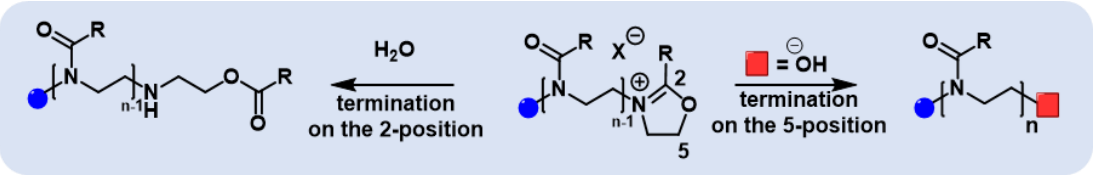

Scheme 1.5. Termination of the poly(2-oxazoline) chain at the 2' and 5' positions by water.

1.1.2.3. Chain Transfer Reactions

For an ideal living polymerisation, there are no unwanted termination or side-reactions. Nonetheless, for the CROP of 2-oxazolines, a chain transfer mechanism is known to occur for between 1/200 and 1/800 repeat units, [26] albeit at a much slower rate than propagation. Litt *et al.* first proposed that the root cause of this chain transfer is due to β-elimination.[26] The polymerisation

solvent is known to influence the degree of chain transfer, with some functional groups such as sulfoxides being more interfering than others.[27]

The proposed mechanism for this chain transfer can be seen in **Scheme 1.6**. Here, a 2-oxazoline monomer causes β-elimination on the living chain end halting the polymerisation and initiating a new chain with a hydride. The terminated chain can then reinitiate by coupling to a living chain end.

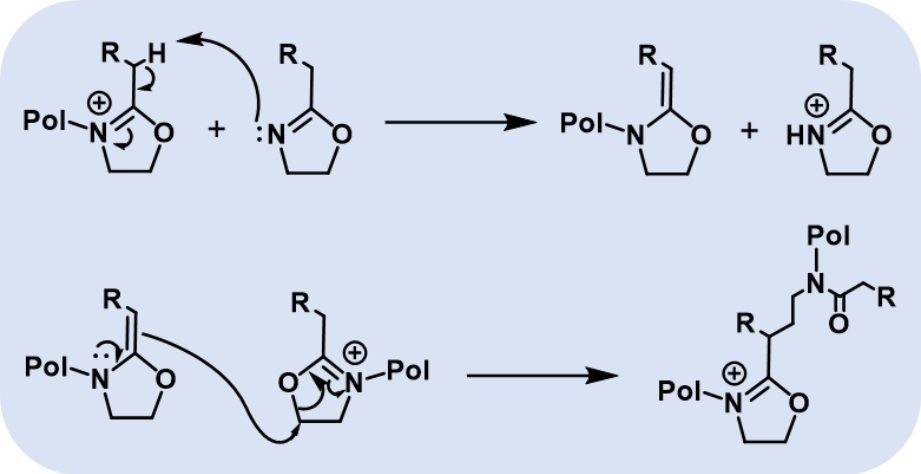

Scheme 1.6. Proposed chain transfer mechanism *via* β-elimination for the CROP of 2-oxazolines.

1.1.3. Versatility of Poly(2-oxazoline)s

One of main reasons for the attractiveness of 2-oxazolines is their chemical versatility. In the literature, there are many examples of different initiators,[28] termination groups,[14] and R groups.[29] These components are subject to intensive research in order to develop new poly(2-oxazoline) structures with useful physical properties. In this section, initiating and terminating groups for CROP are discussed, followed by a discussion of how the R group can be varied to access more complex architectures.

1.1.3.1. Types of Initiator

As mentioned earlier, electrophiles are used for the initiation of CROP. Previous examples that have been employed include alkyl tosylates,[17] alkyl triflates,[18] various Lewis acids,[30] and alkyl halide species[31] (**Figure 1.3.**). The most popular initiators are alkyl tosylates and alkyl triflates due to their stability and fast initiation.[17, 18] A further advantage of alkyl tosylates and triflates is the simple synthesis; a reaction between tosyl chloride and a suitable alcohol results in the desired tosylate product. Functional groups can easily be installed *via* this method, such as a propargyl moiety, sugar, or cholesteryl.[32, 33] Nonetheless, even tosylate based initiators can show poor initiation and a loss of control, such as 3-butynyl tosylate.[34] Interestingly, the only difference between 3-butynyl tosylate and the very commonly used and effective propargyl tosylate is an extra carbon between the alkynyl and the tosyl groups. One method to overcome poor initiation is to firstly form a oxazolinium salt by reacting one equivalent of initiator with one equivalent of a 2-oxazoline, which can then be used to initiate polymerisations.[35] Alkyl halides are also popular choices, with chlorides,[36] bromides,[37, 38] and iodides[19] all having been previously used. In fact, even molecular iodine can be used as an initiator.[39]

Multifunctional initiators are a common type of initiator for more complicated architectures such as star polymers. This type of initiator can be synthesised from a range of small molecules, including porphyrins,[40] pentaerythritol,[17] and cyclodextrins.[41] As well as this, initiators with diverse functionalities such as acetals,[42] esters,[43] and silanes[44] have also been used without demonstrating any side reaction, which highlights an area which could be developed further. For example, an ester introduced *via* the initiator could undergo

transesterification to develop more complex, biodegradable, poly(2-oxazoline) structures. Finally, even gold surfaces can be functionalised to act as an initiator to form brush-like layers.[45]

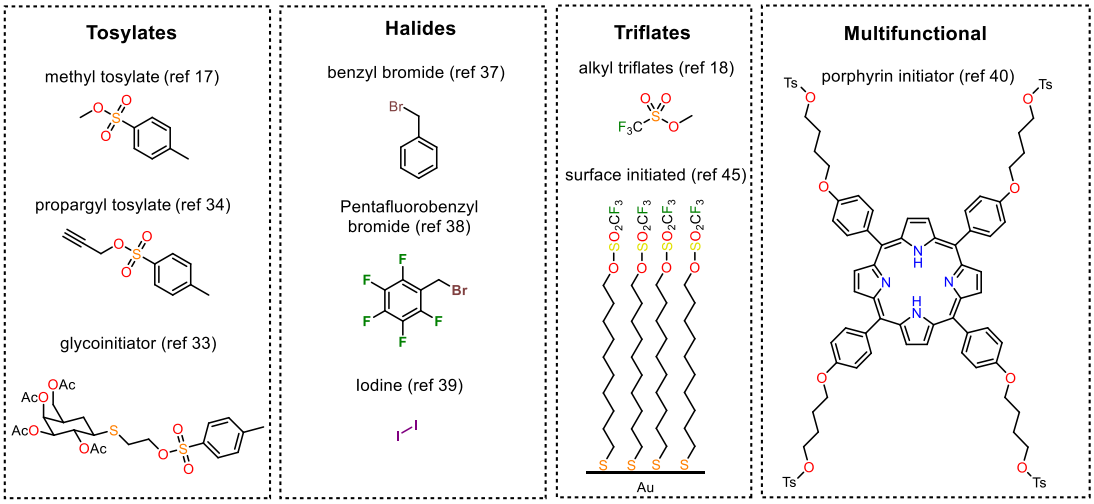

Figure 1.3. Some common and interesting examples of different types of initiator for CROP.

1.1.3.2. Types of Terminating Group

Terminating groups have an advantage compared to the initiator because they can be used to install functionalities that normally interfere with CROP. As mentioned in **Section 1.1.2.2,** poly(2-oxazoline)s can be terminated at the 2' position and the 5' position, depending on the nucleophilicity of the terminating agent. More nucleophilic terminating agents such as thiolates,[25] carboxylates,[46] and amines[47] are generally the terminating agents of choice because of their reliability in end-capping at the 5' position.

As mentioned, terminating poly(2-oxazoline) chains with water resulting in a mixture of products (**Scheme 1.5.**).The most reliable method to introduce an alcohol species at the 5' position is to use a methanolic potassium hydroxide solution.[48] Nonetheless, if there are esters or other groups present in the polymer that are susceptible to reaction with methanolic potassium hydroxide

and an alcohol is required at the chain end, other end-capping strategies are required such as the use of mercaptoethanol. Poly(2-oxazoline)s can be end-capped with carboxylates to allow access to various complex architectures. The carboxylate can be formed by deprotonating the appropriate carboxylic acid with a non-nucleophilic base such as DIPEA. Carboxylate forms of acrylic or methacrylic acid can be used as a terminating agent, to install a polymerisable vinylic end group, allowing access to acrylate/2-oxazoline brush copolymers.[49, 50] End-capping the polymer chain with a carboxylic acid containing a nitroxide,[51] trithiocarbonate,[52] or bromide,[53, 54] results in an oxazoline-macroinitiator structure for the initiation of reversible addition-fragmentation chain-transfer (RAFT) polymerisation, nitroxide mediated polymerisation (NMP), and copper(0) mediated reversible-deactivation radical polymerisation (Cu(0)-RDRP) (**Figure 1.4.**).

As well as carboxylates, amines are common end-capping agents. Primary,[55] secondary,[18] and tertiary[56] (yielding a quaternary, charged end-group) amines can all be employed to terminate polymer chains. Primary amines can potentially end-cap multiple polymer chains resulting in chain-chain coupling, and therefore the best strategy is to use a large excess of terminating agent to suppress this. A particularly useful way of installing functionality at the chain end is to end-cap the living polymer chains with sodium azide, resulting in an azide chain end that can undergo subsequent copper catalysed azide-alkyne cycloaddition (CuAAC).[57] This reaction has been used previously to create multiblock and cyclic polymers,[32] and is discussed further in **Section 1.3.1.1**. Another useful feature of terminating the polymer chain with an azide is that

this functionality can easily be reduced to a primary amine for further reaction.[58]

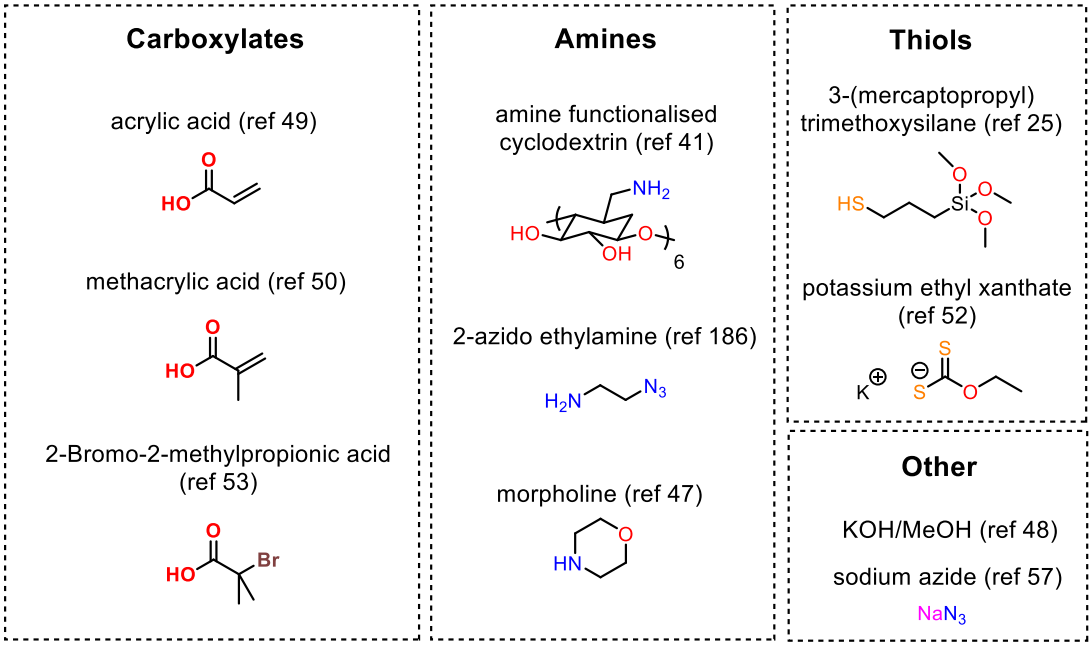

Figure 1.4. Some common and interesting terminating agents used for installing functionality on the poly(2-oxazoline) chain end.

1.1.3.3. Types of R Group

Of all the tuneable aspects of poly(2-oxazoline)s, the R group is the most diverse. In recent years, many different 2-oxazolines with various types of R group have been synthesised and successfully polymerised.[29] R groups must be tolerant to the CROP process, or else they may interfere and cause a loss of control. For example, primary amines attached to the R group will terminate living chains unless a protecting group is used.[59] CROP tolerant R groups include aliphatic chains,[60, 61] benzylic groups,[62] and functional groups containing oxygen,[63] silicon,[64] sulphur,[4] nitrogen,[65, 66] as well as fluorinated chains.[67]

The R group can be used in a variety of ways to functionalise poly(2-oxazoline)s or tune the physical properties of the polymer. Pendant reactive

moieties present on the R groups can undergo post-polymerisation functionalisation to introduce species that are not compatible with the CROP process. For example, poly(2-oxazoline)s with pendant alkenyl functionalities can be used to click on functionalities using thiol-ene click chemistry, such as thio-sugars.[68] As well as post-polymerisation modification, functional groups can be installed prior to modification, as long as they are tolerant to the CROP process. For example, previous work by Becer *et al.* developed two different 'inimers' which consisted of a poly(2-oxazoline) backbone with R groups containing initiators for either RAFT or Cu(0)-RDRP (**Figure 1.5.**).[69-71] They first developed a 2-oxazoline containing a primary alcohol which could then be linked to an initiator for another type of polymerisation *via* esterification. These inimers could then be polymerised to make poly(2-oxazoline) brushes with arms then synthesised either by RAFT or Cu(0)-RDRP. It must be noted that brush polymers where both the backbone and the arms are made from poly(2-oxazoline)s currently do not exist, although they will certainly have interesting properties making them suitable for various applications.

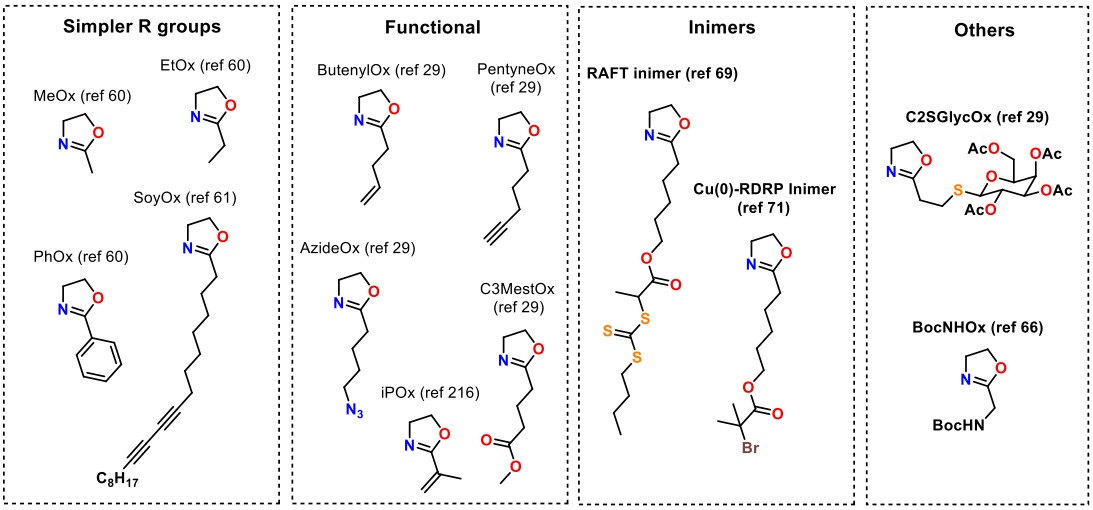

Figure 1.5. Some common and interesting 2-oxazoline R groups that have been used to synthesise functional poly(2-oxazoline)s.

As well as providing points to add functionality, the R group is critical for controlling the thermal and solution behaviours of the polymers. These features will be discussed in more detail in the following section.

1.1.3.4. Properties of Poly(2-oxazoline)s

1.1.3.4.1. Solution Behaviour

In solution, poly(2-oxazoline)s can respond to changes in pH and temperature, and this stimuli-responsiveness is of particular interest because of the associated non-toxicity of poly(2-oxazoline)s in humans.[72] If a polymer can demonstrate thermoresponsiveness or pH responsiveness *in vivo*, it can potentially be used for targeted drug delivery or other similar applications.

Some poly(2-oxazoline)s such as poly(2-ethyl-2-oxazoline) (pEtOx) demonstrate thermoresponsiveness in solution which is manifested as an upper critical solution temperature (UCST) or lower critical solution temperature (LCST) There is an important difference between the LCST and the cloud point – the LCST is the minimum temperature on the solubility boundary of a temperature vs composition plot, whilst the cloud point is any temperature that sits on the boundary. (**Figure 1.6.**).[73]

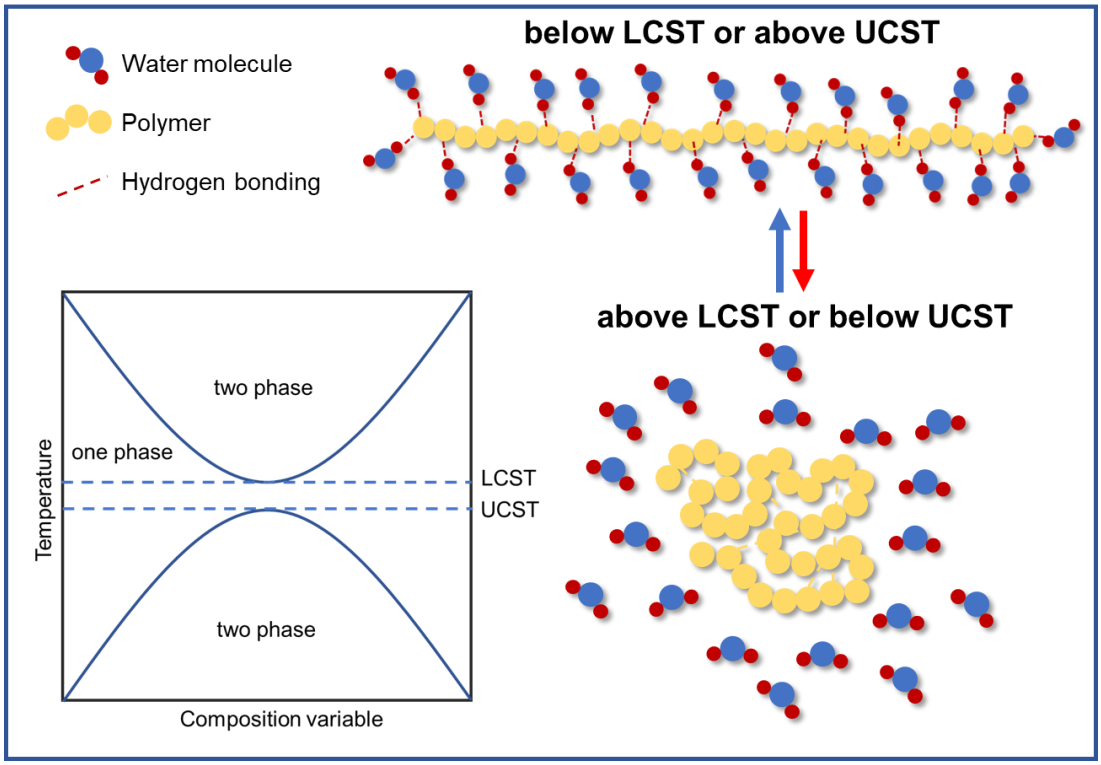

Figure 1.6. Phase diagram and visual representation of UCST and LCST behaviour.[74]

For the LCST, the polymer is completely soluble at low temperatures. When the polymer solution is heated, the Gibbs free energy of mixing becomes unfavourable, *i.e*., mixing is no longer spontaneous at elevated temperatures. At low temperatures, the polymer and solvent form a weak complex which is broken when the temperature is raised, and the polymer collapses in on itself forming an opaque mixture. For the UCST, the Gibbs free energy becomes negative when the temperature of the solution is raised. *i.e*., the greater thermal energy promotes miscibility of the polymer. Importantly, these phenomena are reversible and can be observed for the same polymer solution many times.[74]

There are several factors that affect the cloud point for poly(2-oxazoline)s. The degree of polymerisation (DP), polymer concentration in solution, and R group are the main contributors to variation in cloud point. Increasing the polymer

concentration and the DP have the effect of reducing the cloud point. For example, DP100 pEtOx has an LCST of 90.6 °C, whilst DP500 pEtOx has an LCST of 69.3 °C.[75] Plots of polymer concentration and polymer DP affecting the cloud point of pEtOx can be seen in **Figure 1.7.**

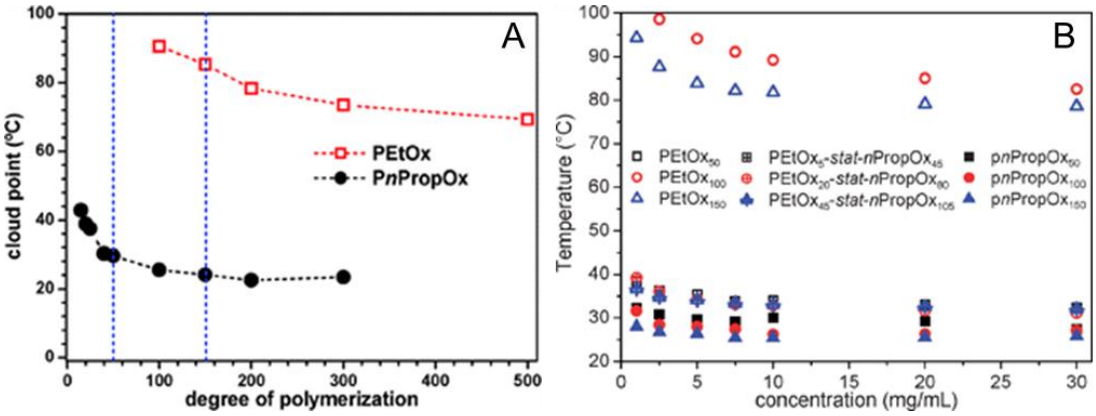

Figure 1.7. (A) Effect of increasing DP on cloud point. **(B)** Effect of polymer concentration on cloud point. Figure reprinted from reference 75, with permission from Royal Society of Chemistry (Copyright 2022).

The R group is instrumental in determining the polymer's solution behaviour. For example, whilst methyl, ethyl, propyl, and iso-propyl are water soluble, butyl chains and longer are insoluble.[76] The LCST of poly(2-oxazoline)s can be carefully tuned by combining different monomers, for example, copolymers of 2-ethyl-2-oxazoline (EtOx) and 2-cyclopropyl-2-oxazoline express LCSTs at a range of temperatures from 91 °C to 28 °C depending on the feed ratio of monomers.[77] In the literature, there are a wide range of examples of poly(2-oxazoline) copolymers where the feed ratio of monomers has been controlled in order to tune the LCST. For example, 2-isopropyl-2-oxazoline with 2-n-propyl-, 2-n-butyl-, and 2-n-nonyl-2-oxazoline,[78] or EtOx with a glycosylated 2-oxazoline.[79] Interestingly, the addition of Hofmeister salts can alter the LCST onset, and it appears that the effect largely follows the Hofmeister series.[80]

Poly(2-oxazoline)s expressing UCST behaviour are much less common than poly(2-oxazoline)s expressing LCST behaviour. Nonetheless, there are some examples of copolymers expressing UCST behaviour in the literature.[49] One example by Schubert *et al*. combined 2-nonyl-2-oxazoline with PhOx at various ratios to form quasi-block polymers, and subsequently demonstrated a range of UCSTs in ethanol/water.[81] As well as 2-nonyl-2-oxazoline, copolymers of EtOx and 2-methyl-2-oxazoline (MeOx) with PhOx demonstrate UCST behaviour in ethanol/water mixtures, with a 50:50 ratio of EtOx/PhOx demonstrating both UCST and LCST behaviour in a 40% ethanol solvent.[82]

Another type of stimuli responsiveness that poly(2-oxazoline)s exhibit is that of pH. Here, a change in pH induces some sort of alteration to the polymer structure or superstructure, which can be used for drug release for example. Examples of pH responsiveness may include degradation of specific parts of a polymer under a specific pH regime, such as polymers containing acyl guanidine which degrade as pH is decreased.[83] Another example is that of pH induced drug release demonstrated with poly(2-oxazoline) liposomes releasing doxorubicin at lower pH.[84]

1.1.3.4.2. Thermal Properties

Continuing from the solution behaviour of poly(2-oxazoline)s, the thermal properties are another feature that is worth considering, as they will have an impact on any potential applicability of 2-oxazoline polymers. It should be noted that a very thorough review on the thermal and crystalline properties of poly(2-oxazoline)s was recently published by Walach *et al*.[85] For poly(2-oxazoline)s with linear alkyl R groups, increasing the chain length of the alkyl chains reduces the glass transition temperature in a proportional manner.[86]

Once the alkyl length reaches around C_6, no glass transition temperature (T_g) is observed, presumably due to their large crystalline volume fraction. These linear polymers have a melting temperature (T_m) that is consistently around 120-140 °C, and the T_g increases with increasing DP. Common precursors for biobased poly(2-oxazoline)s are fatty acids such as those derived from soy beans, which can be used to generate a 2-oxazoline known as 'SoyOx'.[61] SoyOx is unsaturated and has an average of 17 carbons per alkyl chain. Homopolymers synthesised using SoyOx have T_m values that are extremely low compared to their saturated counterparts: ~88 °C for homopolymers of SoyOx, whilst poly(2-nonyl-2-oxazoline) has a T_m of around 150 °C. This is due to the unsaturated bonds in SoyOx disrupting any crystallinity. For short, branched alkyl chains, homopolymers exhibit an increased T_m and higher likelihood of crystallising compared to their linear counterparts. For example, poly(2-isopropyl-2-oxazoline) has a T_g of 70 °C and a T_m of 200 °C, whilst poly(2-n-propyl-2-oxazoline) has a T_g of around 40 °C and does not have a melting temperature.

1.2. Reversible Deactivation Radical Polymerisation

Reversible deactivation radical polymerisation (RDRP) is currently extremely popular, with various techniques being heavily researched. One of the main reasons RDRP is so popular is because of the wide range of monomers that can be polymerised in a well-controlled way. Monomers including acrylates, methacrylates, and styrenics can be polymerised,[87] and complex architectures such as star polymers,[88] multiblock polymers,[89] and cyclic polymers[89, 90] can be attained.[91] The main techniques used are RAFT, and atom transfer radical polymerisation (ATRP). A commonly used type of ATRP currently is Cu(0)-

RDRP, and this will be discussed further in **Section 1.2.1** as it has been used in **Chapter 3** of this thesis. All of these polymerisation techniques ideally follow the first order kinetics discussed in **Section 1.1.2.1**. Each technique has advantages and disadvantages, and polymers synthesised by each technique have a different end group that can be further functionalised. In **Figure 1.8**, the main attributes of RAFT and ATRP can be seen.[87]

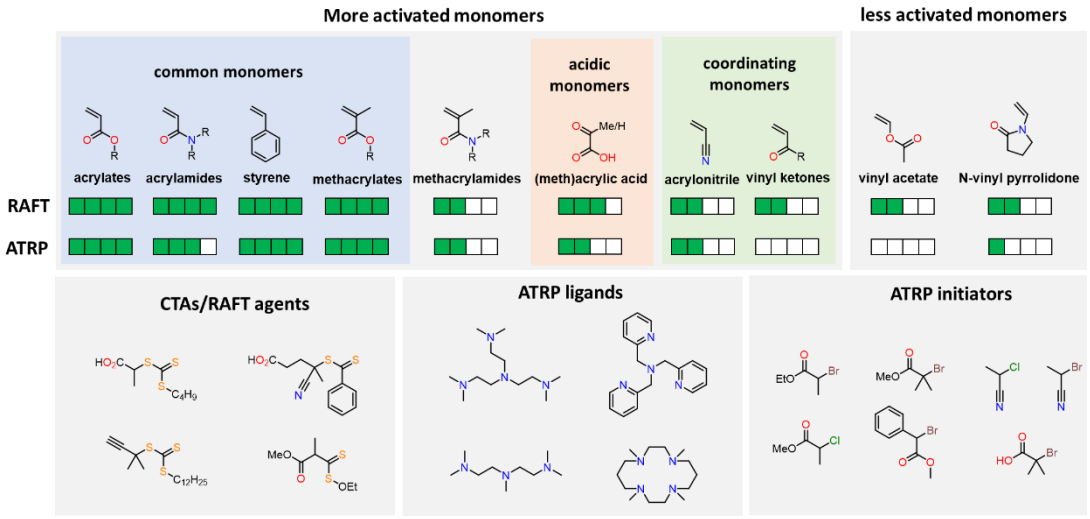

Figure 1.8. Comparison of common monomers for RAFT and ATRP, along with common initiators, ligands, and RAFT agents. Figure adapted from reference 87, with permission from Nature Reviews (Copyright 2022).

1.2.1. Cu(0)-RDRP

Cu(0)-RDRP is a type of ATRP. In this method of polymerisation, an initiator with a transferable atom, typically a halide, undergoes a redox reaction with an added transition metal catalyst. The initiator transfers the halide to a metal complex forming an oxidised metal deactivating species and a free radical that can undergo propagation with the monomer. The propagating chain end rapidly reacts with the oxidised metal complex to deactivate the polymer chain and reform the metal complex in its original oxidation state. This procedure repeats until the monomer is consumed and a polymer forms in a controlled

way. In Cu(0)-RDRP, there are two proposed mechanisms[92] – supplemental activation reversible addition atom transfer radical polymerisation (SARA-ATRP) proposed by Matyjaszewski,[93] and single electron transfer living radical polymerisation (SET-LRP) proposed by Percec.[94] Both mechanisms propose the same species, but their specific roles differ. The differences in the mechanisms can be seen in **Scheme 1.7.**

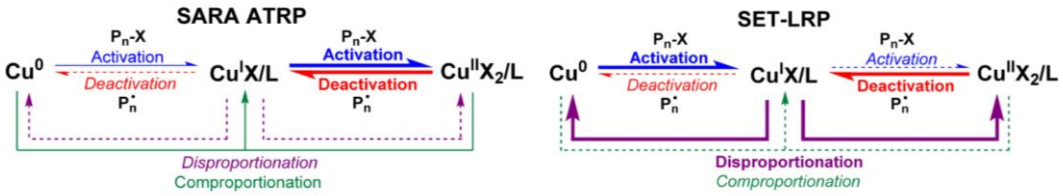

Scheme 1.7. Proposed mechanisms for Cu(0)-RDRP. Scheme adapted from reference 92 with permission from The Royal Society of Chemistry (Copyright 2022).

In SARA-ATRP, the Cu^{I} species is the main activator, whilst Cu^{0} acts as a reducing agent for Cu^{II} to generate supplemental activating species *via* comproportionation. In SET-LRP, Cu^{0} is the major activating species, which is regenerated by the disproportionation of Cu^{I} into Cu^{0} and Cu^{II}. Polymers formed *via* Cu(0)-RDRP possess a bromide on the chain end which allows for a wide range of functionalisation by simple substitution reactions. One example of this is with sodium azide, which forms an azide terminated polymer chain that can undergo further reaction *via* CuAAC.[95] This substitution chemistry has been used extensively in **Chapter 3** to generate multiblock copolymers.

1.3. Poly(2-oxazoline) Polymer Architectures

There are a wide range of different polymeric structures available when using 2-oxazoline monomers. In this section, the various polymer structures

synthesised in this thesis will be covered. Firstly, homopolymers and copolymers are discussed, followed by cyclic polymers, star polymers, and lastly hyperbranched polymers. It must be noted that other structures such as brush polymers are accessible with poly(2-oxazoline)s, but they have not been explored in this thesis and so are not covered in this section, however a thorough review was provided by Becer *et al*. in 2019 on brush polymers with 2-oxazolines.[96]

1.3.1. Homopolymers and Copolymers

Poly(2-oxazoline) homopolymers are the simplest type of oxazoline polymer, and consequently have been thoroughly researched in the last decades. Indeed, there are a vast range of different monomers that have been synthesised and successfully polymerised, as can be seen in the 2017 review by Hoogenboom *et al.* on poly(2-oxazoline)s.[29] Furthermore, homopolymers have important features such as useful solution, thermal, and surface properties.

Copolymers are structurally more complex than homopolymers and are of particular interest because they are a combination of different monomers, and so they can exhibit characteristics of the different components. Copolymers have a variety of forms ranging from random copolymers to statistical copolymers, through to block copolymers. One of the challenges associated with random copolymer synthesis of poly(2-oxazoline)s is that of monomer reactivities. Different 2-oxazoline R groups can affect the individual reactivities of the monomers due to steric and electrostatic effects, resulting in statistical and quasi-block polymers when different monomers are polymerised together.

Nonetheless, block polymers are of importance because they are effectively two different polymers connected covalently. This is significant because two separate homopolymers typically do not mix.[97] When they are linked together covalently, they form microphasic separations and can form self-assembled structures such as micelles and other nanostructures.[98]

1.3.1.1. Synthesis of Poly(2-oxazoline) Homopolymers and Copolymers

1.3.1.1.1. Poly(2-oxazoline) Homopolymers

The synthesis of linear homopolymers of 2-oxazolines is straightforward, and as mentioned earlier factors that affect polymerisation rate include monomer concentration, monomer type, initiator type, reaction temperature, and solvent.

One interesting area of 2-oxazoline homopolymers that has been developed is that of chiral polymers.[99] Here, chirality has been introduced through the addition of a methyl group at the 4' position on the oxazoline ring (**Scheme 1.8.**). The added steric hindrance of this group might be expected to reduce and interfere with the polymerisation leading to slow polymerisation and chain transfer, however no kinetic information was provided. Nonetheless, higher than expected values for *Đ* indicate some loss of control. For example, DP 50 poly(2,4-dimethyl-2-oxazoline) had a high *Đ* of 1.70.

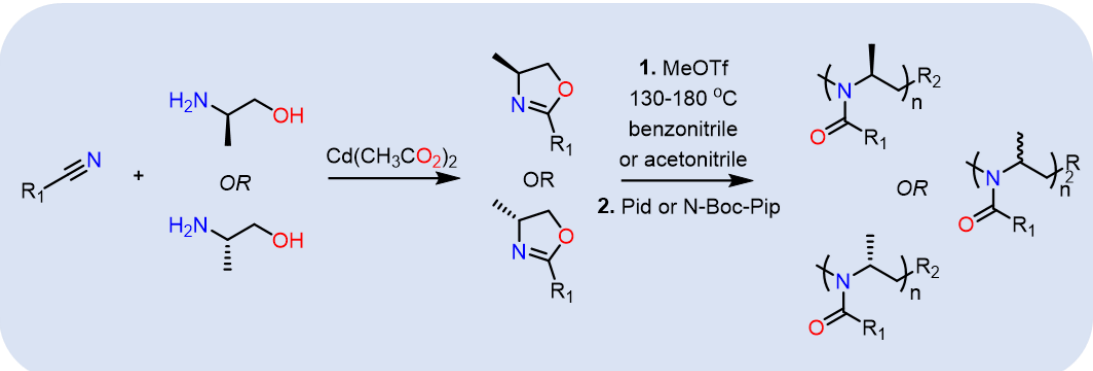

Scheme 1.8. Synthesis and polymerisation of chiral poly(2-oxazoline) homopolymers.[99]

Although homopolymers of poly(2-oxazoline)s are well-developed, well-defined polymers at molecular weights over 10 kDa are less reported. The reason for this is two-fold. Any impurities in the polymerisation system become even more problematic at high molecular weights and so monomer, solvent, and initiator purity are critical to obtain well-defined high molecular weight polymers. Secondly, chain-transfer reactions can occur resulting in unwanted dead chains and a loss of control. Hoogenboom *et al*. demonstrated that using chlorobenzene and low polymerisation temperatures of 40 °C allowed for access to well-controlled high molecular weight p(EtOx) with $M_{n(GPC)}$ values of up to 287.4 kDa and $Đ$ as low as 1.15 (**Figure 1.9.**).[100] However, the low temperature drastically increased polymerisation times, taking up to 28 days for 50% monomer conversion. Even then, the polymer peaks are not monomodal at the highest molecular weights, and it seems that one of the limits of the CROP of 2-oxazolines has been demonstrated, in that well-controlled polymers at extremely high molecular weight are not attainable.

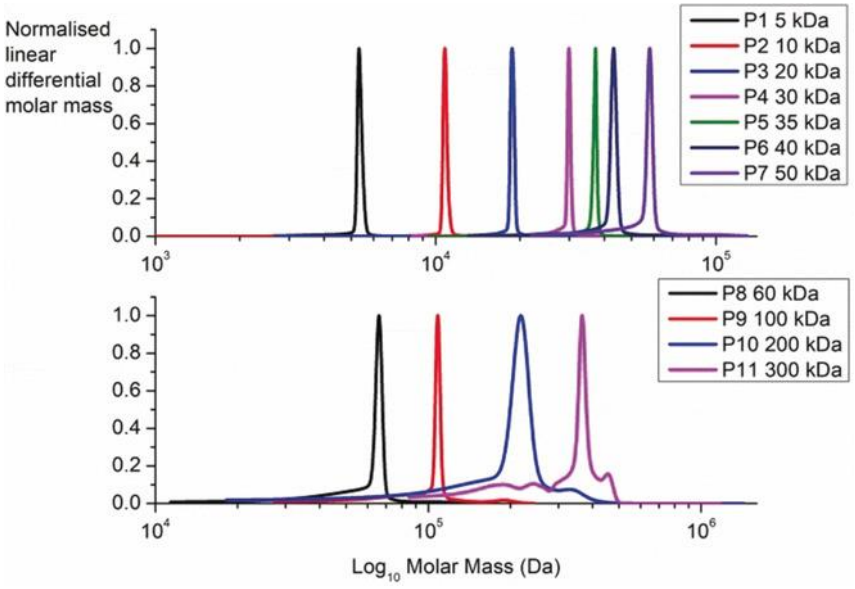

Figure 1.9. Gel permeation chromatography (GPC) traces of ultra-high molecular weight pEtOx from 5 kDa to 300 kDa. Figure reprinted from reference 100, with permission from John Wiley and Sons (Copyright 2022).

1.3.1.1.2. Random and Statistical Copolymers

When two or more 2-oxazoline monomers are combined in a polymerisation, it is not necessarily the case that a polymer will form with all monomers distributed completely randomly throughout. Monomers have different reactivities and this is due to influence from the R group. Electron donating R groups make the attacking monomer more nucleophilic and more reactive, but they also donate electron charge into the oxazolinium ring on the living polymer chain end, reducing the partial cationic nature on the 5' position making it less reactive. Furthermore, steric effects also influence the reactivity of the R group. These combined effects from the R group make predicting k_p difficult, however some trends can be seen. For example, it has been shown that 2-oxazolines with aliphatic R groups from methyl to octyl have largely comparable reactivities despite the difference in steric bulk (**Figure 1.10.**).[101] As the reactivity ratios of the monomers in a copolymerisation begin to deviate, the polymer composition will change from purely random, to a statistical polymer, to finally a quasi-block structure. The most notable example of this quasi-block type structure is when PhOx is combined with MeOx or EtOx.[102-104] PhOx polymerises at a much slower rate than MeOx or EtOx because the conjugation of the nitrogen and phenyl ring causes delocalisation of the nitrogen lone pair reducing its nucleophilicity. In a copolymerisation between PhOx and MeOx, the reactivity of MeOx has been shown to be around 500 times greater.[102]

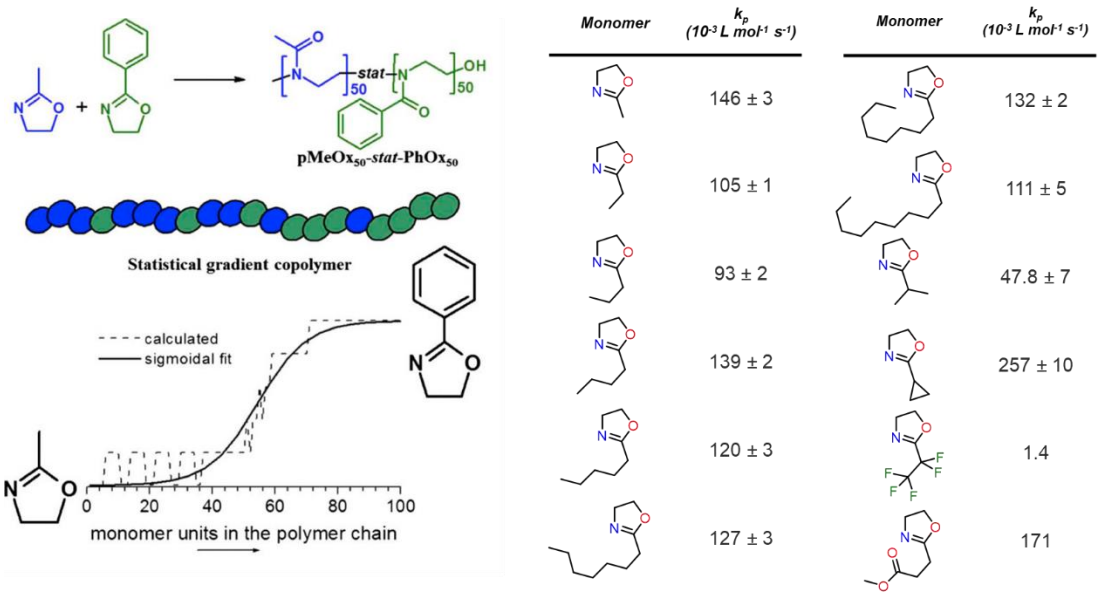

Figure 1.10. Plot demonstrating the polymer composition between MeOx and PhOx, and various monomers with their associated k_p values. Figure adapted from reference 104, with permission from The American Chemical Society (Copyright 2022).

1.3.1.1.3. Poly(2-oxazoline) Block Polymers

There are several approaches to the synthesis of poly(2-oxazoline) block copolymers. Firstly, and most commonly, is the sequential addition route where polymerisation of one monomer is allowed to reach full conversion before the next monomer is added. This route provides the most control over the polymerisation, however poly(2-oxazoline)s are limited to tetrablocks,[105, 106] and no example of a pentablock poly(2-oxazoline) has been reported (**Figure 1.11.**). The reason for this limitation is because extremely high end-group fidelity is required, and addition of subsequent blocks and sampling introduces the risk of contaminants being added. There are a wide range of examples of diblock[107, 108] and triblock poly(2-oxazoline)s in the literature, however.[109, 110]

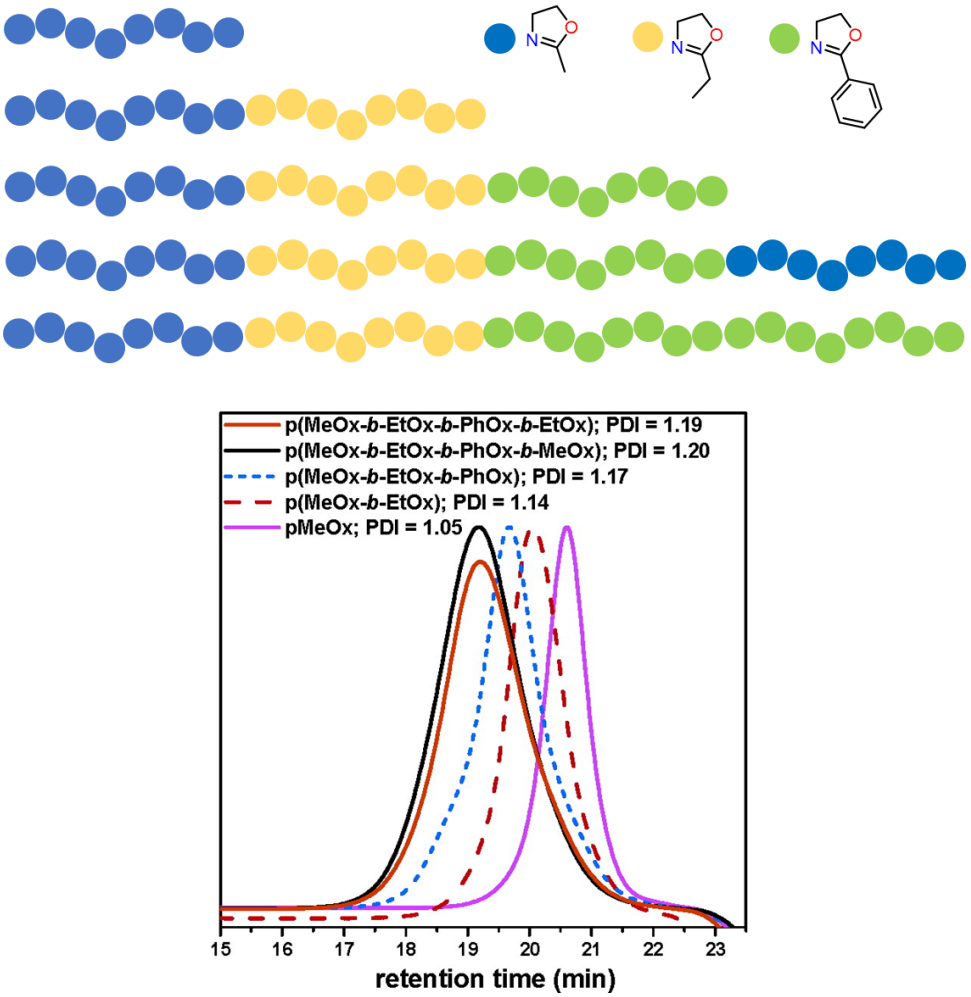

Figure 1.11. Simplified multiblock polymers and their associated GPCs. Figure adapted from reference 105, with permission from American Chemical Society (Copyright 2022).

A second method to multiblock poly(2-oxazoline)s is to link them using polymer-polymer coupling. This can be done by introducing two complementary groups at the α and Ω chain ends, which can react together in a combinatorial way.

Examples of this in the literature are much sparser than the sequential addition route, however examples include a pEtOx chain initiated with a pentafluorobenzyl bromide initiator and terminated with a bisthiol.[38] The pentafluorobenzyl and thiol can then react together to form a block polymer. Other examples include initiating the polymer chain with a propargyl group and terminating the polymer with an azide. These groups can then undergo CuAAC

to form poly(2-oxazoline) multiblock polymers.[111] One of the issues with this is the competing intramolecular cyclisation reaction however. Block polymers synthesised *via* polymer-polymer coupling are not limited to pure 2-oxazoline backbones, and this is discussed in the next section.

1.3.1.1.4. Poly(2-oxazoline) Blocks with other Types of Polymer

The use of heterofunctional initiators is an interesting way of combining poly(2-oxazoline)s with other polymerisation techniques. Previous examples of this include an initiator combining an acid bromide with a tertiary bromide that could be used to initiate both the CROP of 2-oxazolines (with the acid bromide) and ATRP of styrene (with the tertiary bromide),[112] and a RAFT agent combined with a tosylate to generate poly(2-oxazoline)-(meth)acrylate blocks (**Scheme 1.9.A**).[113] Separately, the living chain ends of poly(2-oxazoline)s can also be terminated with initiators to generate macroinitiators for different polymerisation techniques such as RAFT (**Scheme 1.9.B**)[52] and (Cu(0)-RDRP).[54, 114]

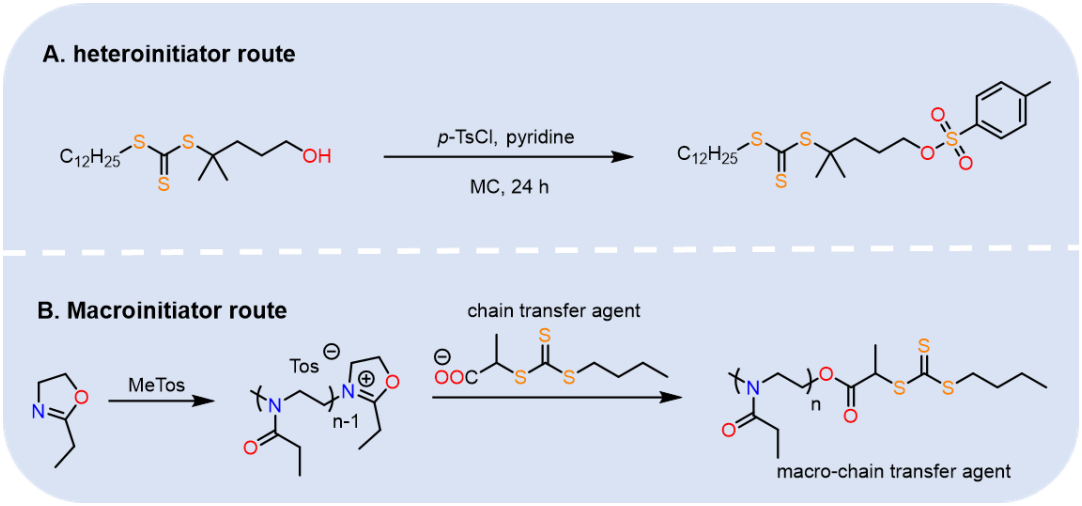

Scheme 1.9. (A) Synthesis of a tosylate-RAFT agent heteroinitiator.[113] **(B)** Synthesis of a poly(2-oxazoline) RAFT Macroinitiator.[52]

Another method that can be used to combine poly(2-oxazoline)s with acrylates is that of click chemistry. There are several methods used in the literature to combine poly(2-oxazoline)s with acrylates. Firstly, a poly(2-oxazoline) can be initiated with propargyl tosylate, installing a triple bond at the chain end which can then be combined with another polymer that is terminated with an azide using CuAAC. This method is highly suited to polymers synthesised *via* Cu(0)-RDRP as substitution of the terminal bromine with an azide is facile (**Scheme 1.10.A**).[95, 115] Opposingly, poly(2-oxazoline) chain ends can be terminated with an azide functionality which can then be conjugated onto polymers containing an alkyne functionality, for example, polymers synthesised using an alkyne functionalised RAFT agent (**Scheme 1.10.B**).[116] A third method involves end capping the poly(2-oxazoline) chain with (meth)acrylic acid to install an alkenyl functionality. This can then be combined with a thiol terminated polymer *via* thiol-ene click chemistry. This method is most suitable for polymers synthesised *via* RAFT polymerisation, as the RAFT agent can easily be reduced to a thiol on the chain end with an amine (**Scheme 1.10.C).**[117] The use of click chemistry to conjoin polymers is not restricted to acrylates, and a wide range of polymers have been linked to poly(2-oxazoline)s including pullulan,[118] poly(ethylene),[119] poly(lysine),[120] and poly(caprolactone).[121]

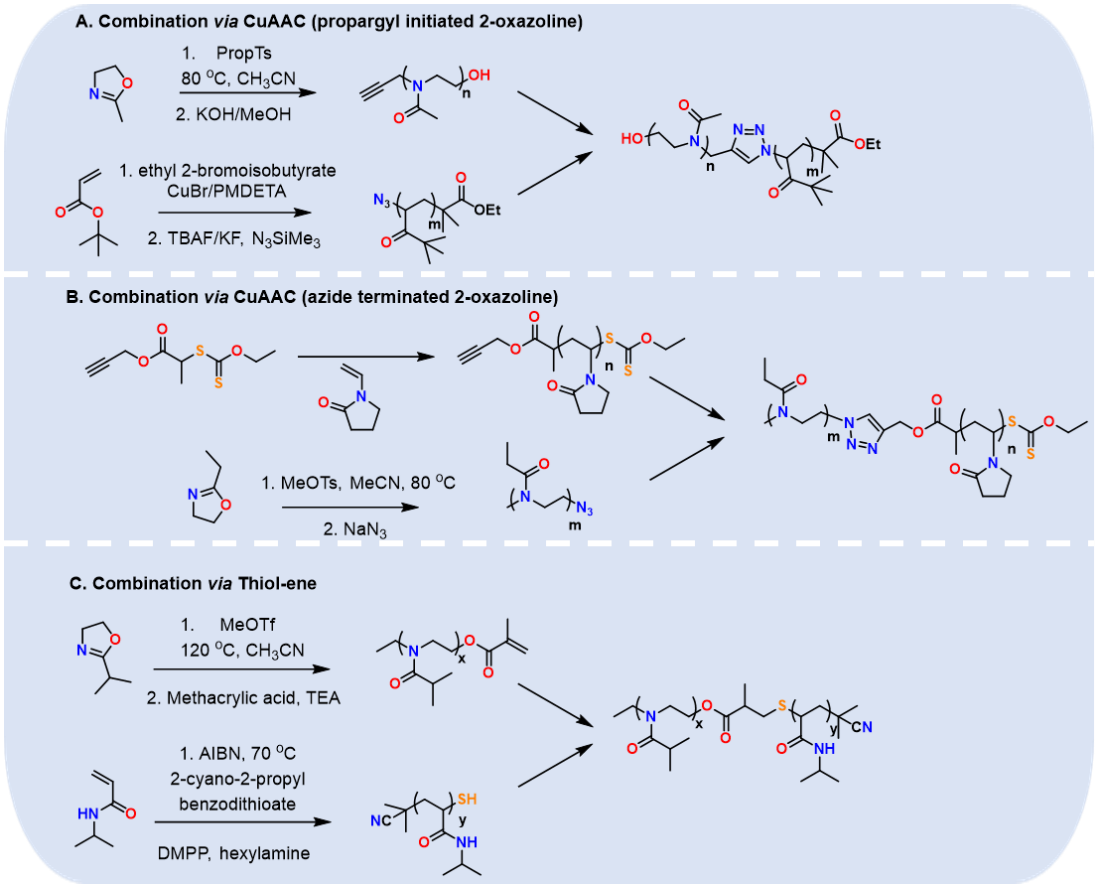

Scheme 1.10. Combination of poly(2-oxazoline) and poly(acrylate) *via*: **(A)** CuAAC using a propargyl initiated poly(2-oxazoline).[95] **(B)** CuAAC using an azide terminated poly(2-oxazoline). [116] **(C)** A poly(2-oxazoline) and poly(acrylate) *via* thiol-ene reaction.[117]

Interestingly, although diblocks of poly(2-oxazoline)s with acrylates have been synthesised *via* click chemistry previously, there are no examples of multiblock polymers combining both acrylates and 2-oxazolines in the literature. However, these polymers certainly have interesting properties, and are one of the focuses of **Chapter 3** of this thesis.

1.3.1.1.5. Hydrolysis of Poly(2-oxazoline)s

Frequently, poly(2-oxazoline)s are either partially or fully hydrolysed to form poly(ethylene imine) (PEI) or poly(2-oxazoline)-PEI copolymers, which are typically used for gene transfection.[122, 123] This route has an advantage over the ring opening polymerisation of aziridines, which produces randomly branched PEI that is not well defined. Further functionalisation of PEI with

groups such as sugars is of interest because this can allow for a more targeted delivery of ribonucleic acid (RNA),[124] however it is difficult to attain well-defined, functionalised PEI. There are two main methods to obtain functionalised PEI. Firstly, a copolymer is synthesised with monomers that have different hydrolysis rates ensuring that the monomer with the desired functional group is not preferentially hydrolysed, thus remaining on the polymer backbone. In the second method, the polymer is partially or fully hydrolysed and functionality is added post-hydrolysis *via* reaction with the secondary amines on the backbone, such as sugar moieties.[125] The first method is not ideal as the hydrolysis mechanism is not 100% selective towards one monomer, and the desired functional group needs to be stable to harsh hydrolysis conditions. The second method is limited to molecules that can react with secondary amines and cannot be used to access functionalised, charged block polymers.(**Scheme 1.11.**)

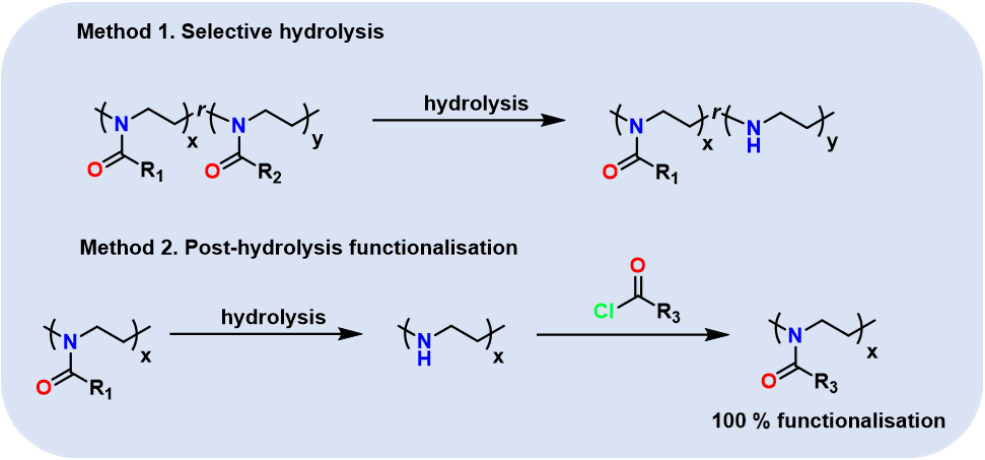

Scheme 1.11. Two main methods to functionalised, charged poly(2-oxazoline)s species.

It is possible to selectively hydrolyse a block polymer to yield a positively charged block polymer.[126] In this method, the hydrolysis rates of different R groups are exploited in order to preferentially hydrolyse one poly(2-oxazoline)

block to generate poly(2-oxazoline)-block-poly(ethylene imine) polymers. Generally, blocks are made using EtOx or 2-propyl-2-oxazoline with MeOx. The polymers are then hydrolysed, with the methyl R groups being preferentially hydrolysed.[127, 128] Subsequent functionalisation by reaction with the secondary amines reduces the charge density on the PEI block which may affect the transfection potential of the polymers. One potential method to avoid this issue is to use a 2-oxazoline that has a charged R group or contains a group that can be deprotected to yield a charged amine (**Scheme 1.12.**).[129,130] A similar approach was taken for **Chapter 4** of this thesis, where charged and glycosylated poly(2-oxazoline)s were synthesised and tested for transfection potential.

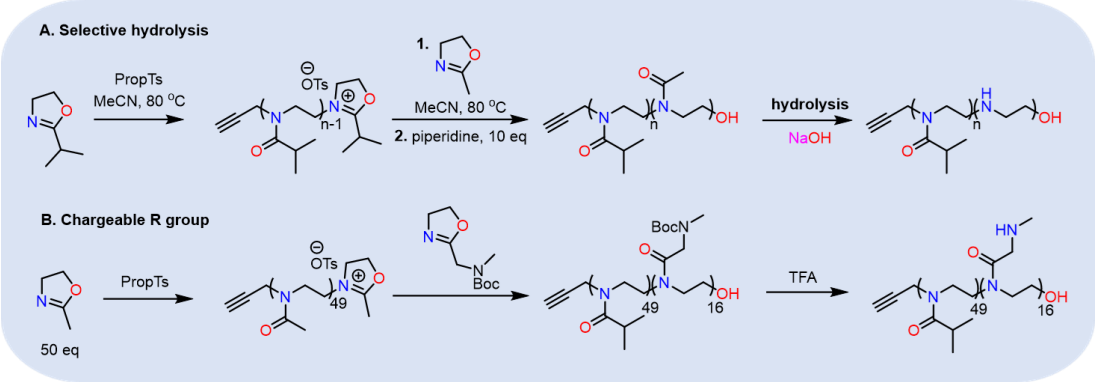

Scheme 1.12. Synthesis of charged block polymers *via*: **(A)** A hydrolysis route. **(B)** A monomer deprotection approach.[130]

1.3.1.2. Analysis of Homopolymers and Copolymers

The analysis of poly(2-oxazoline) homopolymers and random copolymers is relatively straightforward. During the polymerisation, monomer conversion is typically measured by gas chromatography (GC) or ^{1}H nuclear magnetic resonance spectroscopy (NMR), and GPC is used for polymer analysis. One of the issues with analysing poly(2-oxazoline)s with conventional GPC is that

due to their quasi-peptoid backbone structure, they can interact with the column and cause tailing to be observed in the GPC trace.[131, 132] This tailing can artificially increase the polymer dispersity, giving the false impression that the polymerisation was uncontrolled. For more detailed polymer analysis such as information on end-group fidelity, matrix assisted laser desorption/ionisation time of flight mass spectrometry (MALDI-TOF-MS) is a useful technique, and is commonly used for poly(2-oxazoline) homopolymers.[133] MALDI-TOF-MS can also be used to analyse random copolymers, however the analysis is much more complicated because of the extensive number of different polymer distributions.[134] A good example of how MALDI-TOF-MS can be used to analyse the end groups of a homopolymer can be seen in **Figure 1.12**.[135] Here, pEtOx was initiated with methacryloyl chloride, and terminated with a hydroxyl functionality. However, the major observed peak appears to be the hydride initiated peak attributed to chain transfer during the polymerisation.

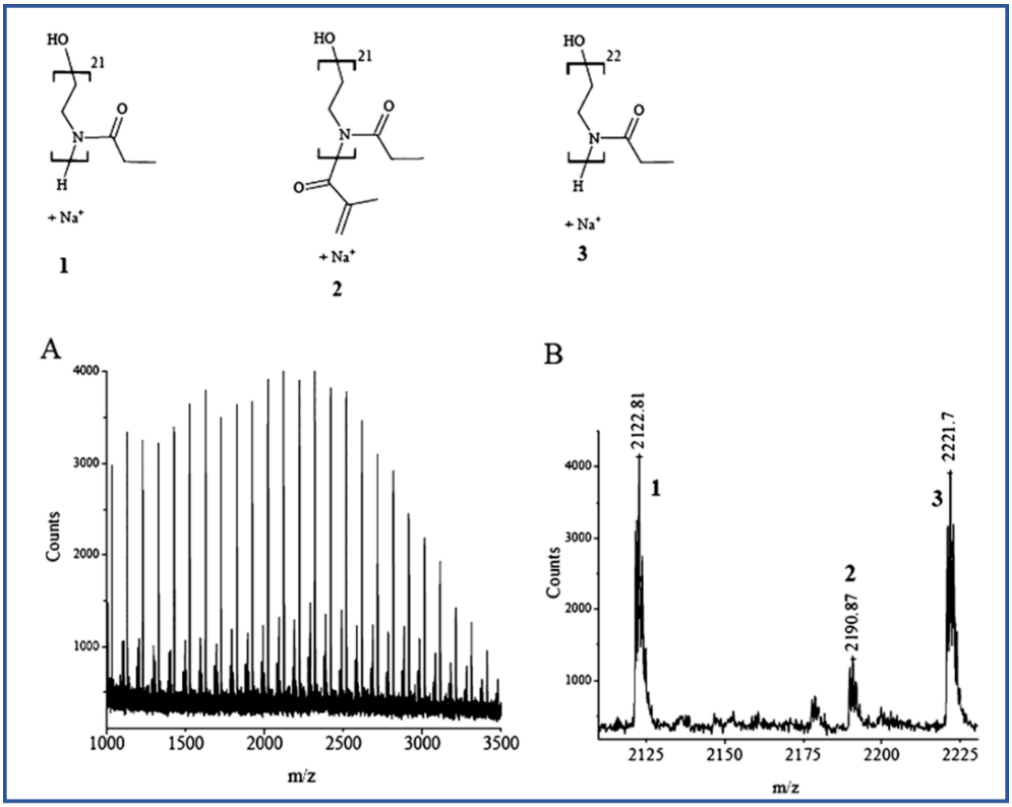

Figure 1.12. MALDI-TOF-MS of a poly(2-oxazoline) initiated with methacryloyl chloride. **(A)** shows the entire chromatogram. **(B)** shows a zoom of the two main distributions present. The structures at the top indicate the assigned end-groups for the distributions. Figure reprinted from reference 135, with permission from Taylor and Francis (Copyright 2022).

Like the analysis of homopolymers and random copolymers, block polymers are typically analysed using conventional GPC. Firstly, a sample of the first block is taken and analysed using GPC, before addition of the monomer for the second block. Then, once the subsequent monomer for the second block has been consumed, a sample can be taken to see the GPC shift to shorter retention time. As can be seen from **Figure 1.13**, both sides of the peak have shifted evenly with no additional tailing, indicating that high end-group fidelity is maintained upon addition of the second block monomer.

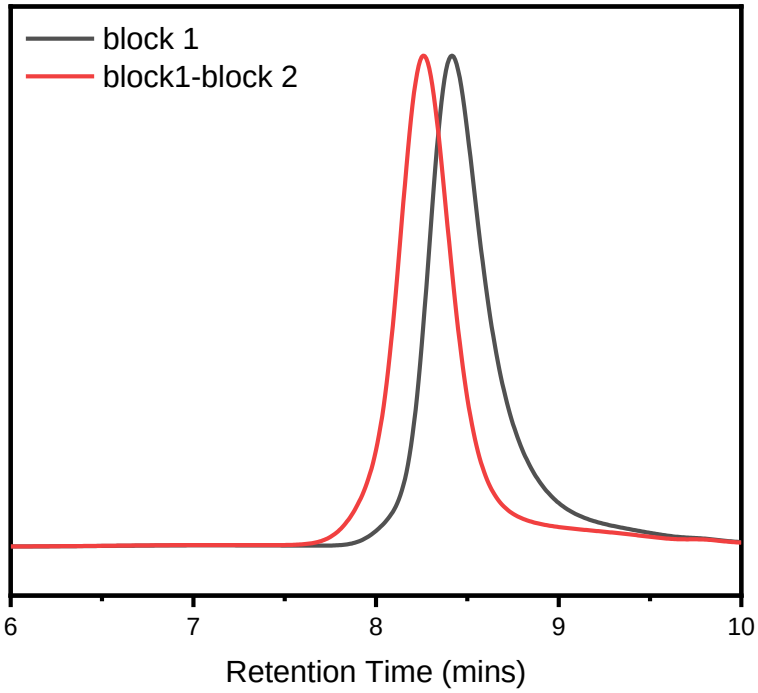

Figure 1.13. GPC shift to shorter retention time indicating block formation.

MALDI-TOF-MS can also be a useful tool for block polymer analysis. However, the analysis can be very complicated because block polymers have a wide range of potential molar masses. For example, consider a diblock polymer of DP10 methyl acrylate followed by a DP10 block of ethyl acrylate polymerised *via* Cu(0)-RDRP. The polymerisation of the first block will not be truly monodisperse, and so there will be some variation in the DP of the chains and thus the molecular mass of the polymers. Then, the ethyl acrylate block is polymerised from the first block, again with its own dispersity. This dramatically increases the number of potential molecular mass chains present in the sample making analysis much more difficult. The MALDI-TOF-MS of this polymer has been previously obtained and assigned by Haddleton *et al.* and can be seen in **Figure 1.14**.[136] As can be seen from the figure, there are many peaks making analysis difficult. Terpolymers and beyond will be even more complicated with many more peaks.

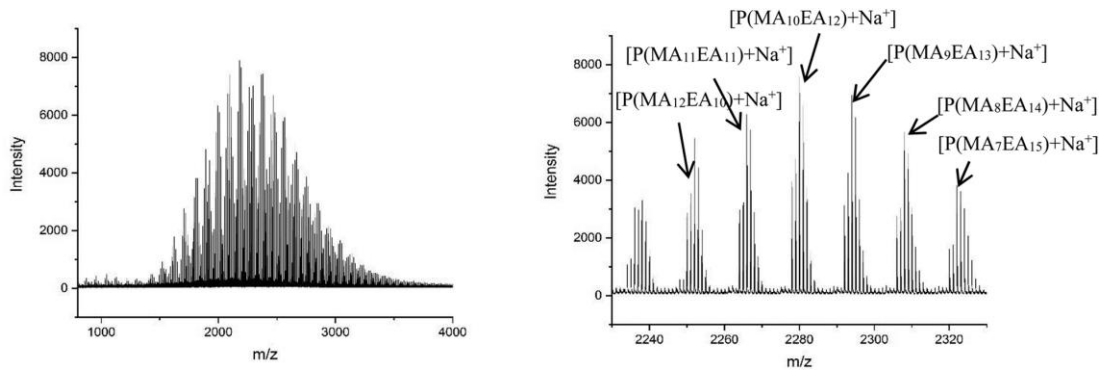

Figure 1.14. MALDI-TOF-MS of p(methyl acrylate)$_{10}$-*b*-p(ethyl acrylate)$_{10}$ (pMA$_{10}$-*b*-pEA$_{10}$), with zoomed region from 2220–2340 m/z region, showing the comonomer distribution for DP 22. Permission not required for reprint.

1.3.1.3. Applications of Homopolymers and Copolymers

1.3.1.3.1. Drug Delivery

One of the main potential applications of poly(2-oxazoline)s is as a replacement for PEG in drug formulation. PEG is currently used to provide stability, prevent protein coronas from forming,[137] and provide protection from the immune system.[138] However, an increasing proportion of the population express an immune response to PEG and so finding a replacement is of interest.[139] Meanwhile, poly(2-oxazoline)s have a quasi-peptide structure and have been shown to be largely non-toxic.[140, 141] Coupled with the tunability of various aspects of the polymer chain, poly(2-oxazoline)s have received much interest in recent years due to their potential to replace PEG for therapeutic applications.[142]

Polymer drug conjugates (PDCs) are polymeric species that have drugs attached with easily cleavable linkages. PDCs have been shown to improve the stability of drugs in physiological conditions and can quickly release their payload under an appropriate change in conditions. Indeed, *N*-(2-hydroxypropyl) methacrylamide-doxorubicin polymers have entered into

clinical trials as a PDC.[143] Previously, pEtOx has been investigated in conjunction with doxorubicin as a PDC, where the polymer was furnished with a doxorubicin molecule at the chain end.[144] A separate method used a copolymerisation route between EtOx and a 2-oxazoline containing a methyl ester. The methyl ester could undergo post polymerisation transesterification to add doxorubicin molecules along the polymer backbone, increasing the doxorubicin payload compared to conjugation of just one doxorubicin molecule at the chain end (**Scheme 1.13.**).[145] As well as these examples that use cleavable covalent bonds to conjugate drugs, the differences in reactivity ratios between 2-oxazoline monomers can be used to make amphiphilic gradient copolymers which can be self-assembled and used to encapsulate drugs. For example, EtOx can be combined with 2-(4-dodecyloxyphenyl)-2-oxazoline to yield gradient copolymers that can be self-assembled and loaded with curcumin, which is a highly coloured model drug.[146]

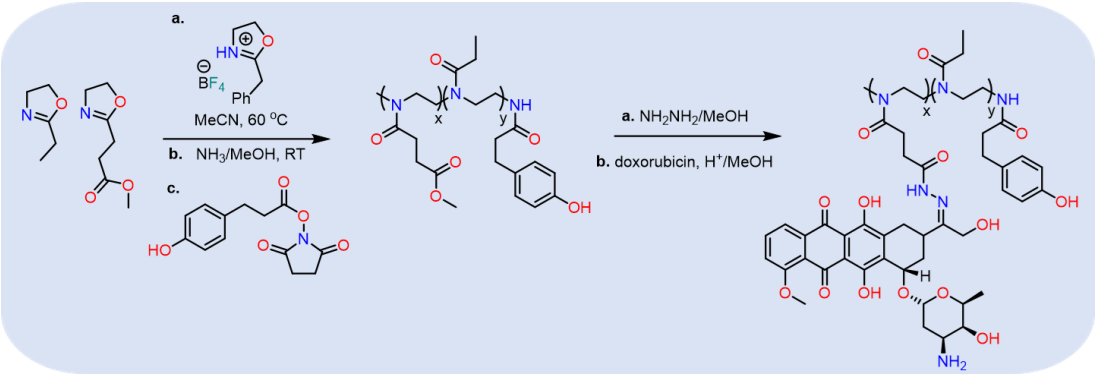

Scheme 1.13. Synthesis of a random poly(2-oxazoline) copolymer followed by conjugation with doxorubicin.[145]

Poly(2-oxazoline)s have been found to be very effective at forming layer by layer (LBL) self-assembled structures with tannic acid that can be used to encapsulate drugs such as doxorubicin and ciprofloxacin (**Scheme 1.14.**).[147, 148] These multi-layered structures are stabilised by a large amount of

hydrogen-bonding, which is disrupted when the pH of the system is raised above a certain critical pH and thus the self-assembled structure is disrupted releasing its drug payload. In a similar method, the large amount of hydrogen bonding that is available with tannic acid has also been used to stabilise poly(2-n-propyl-2-oxazoline)/gellum gum droplets that can be used for lipase delivery.[149]

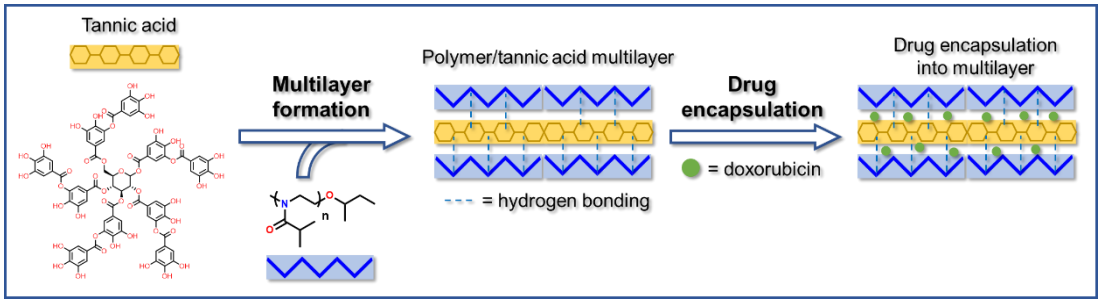

Scheme 1.14. Multilayer formation between poly(2-oxazoline)s and tannic acid, followed by doxorubicin encapsulation.[147]

One of the primary purposes of block poly(2-oxazoline)s is to form self-assembled structures by combining a hydrophilic monomer with a hydrophobic monomer. Typically, the hydrophilic monomer is either MeOx or EtOx, whilst the hydrophobic block is made from a long alkyl chain 2-oxazoline such as 2-nonyl-2-oxazoline.[150] Furthermore, the block length has been shown to be an important factor in the shape and size of the self-assembled structures.[151] The type of monomer used and the block length can determine the morphology of the self-assembled structure, with rod-like structures and spherical micelles amongst the available structures.[152] Due to the ability of block poly(2-oxazoline)s to self-assemble, many applications for this polymer architecture are concerned with drug encapsulation and delivery *via* a self-assembled polymeric carrier. For example, diblock poly(2-oxazoline)s made from pEtOx as the hydrophilic block and poly(2-butenyl-2-oxazoline) as the hydrophobic

block self-assemble into micelles in aqueous media. The hydrophobic block was found in the core of the micelle and thus they were able to encapsulate curcumin as a hydrophobic drug.[153] In a further example, a library of diblock polymers was synthesised by Kabanov *et al.* using various R groups including methyl, ethyl, butyl, *i*-propyl, and *N*-propyl in order to test their cellular uptake and cytotoxicity.[140] In this work, it was demonstrated that poly(2-oxazoline) blocks were well tolerated by mammalian cells, and all showed significantly higher drug delivery potential than homopolymers of EtOx, due to their ability to self-assemble. As well as diblock polymers, multiblocks such as triblock poly(2-oxazoline)s can be used for drug encapsulation. Triblocks with the hydrophobic segment as the central block have been shown to form rod like structures which are transformed into spherical micellar-like structures upon drug loading.[140] In this example, the hydrophobic block could be either a short butyl chain or a longer, more hydrophobic nonyl chain, with triblocks containing a central butyl core being able to load Paclitaxel at 45 wt%.[154]

1.3.1.3.2. Gene delivery

Gene therapy is a potent therapeutic technique, as it can be used to silence genes and prevent protein expression,[155] or used in vaccine delivery.[156] One of the problems with gene delivery is that the negatively charged RNA cannot easily pass through the hydrophobic cell membrane, and therefore a vector molecule is needed. For example, messenger ribonucleic acid (mRNA) vaccines against Covid-19 use non-viral nanoparticles as carriers.[157, 158] PEI derived from the hydrolysis of poly(2-oxazoline)s can be used as a positively charged polymer to combine with nucleic acids and improve their transfection.[123, 159, 160] Copolymers between pEtOx and PEI synthesised by

Becer *et al*. were used to transfect cells with different nucleic acids including plasmid DNA (pDNA), messenger RNA (mRNA), and self-amplifying replicon RNA (repRNA) (**Scheme 1.15.**).[161] In the study, they investigated the effects of polymer molecular weight and the PEI content within the polymer. For the pDNA and repRNA, fully hydrolysed polymers were found to show the best transfection, whilst polymers with 80% hydrolysis were found to be optimal for mRNA. However, the method of synthesis of the cationic polymers meant they were unable to test any structures other than various statistical copolymers between EtOx and PEI. The use of a 2-oxazoline with a chargeable R group would allow access to functional block polymers, which could then be tested for gene transfection.

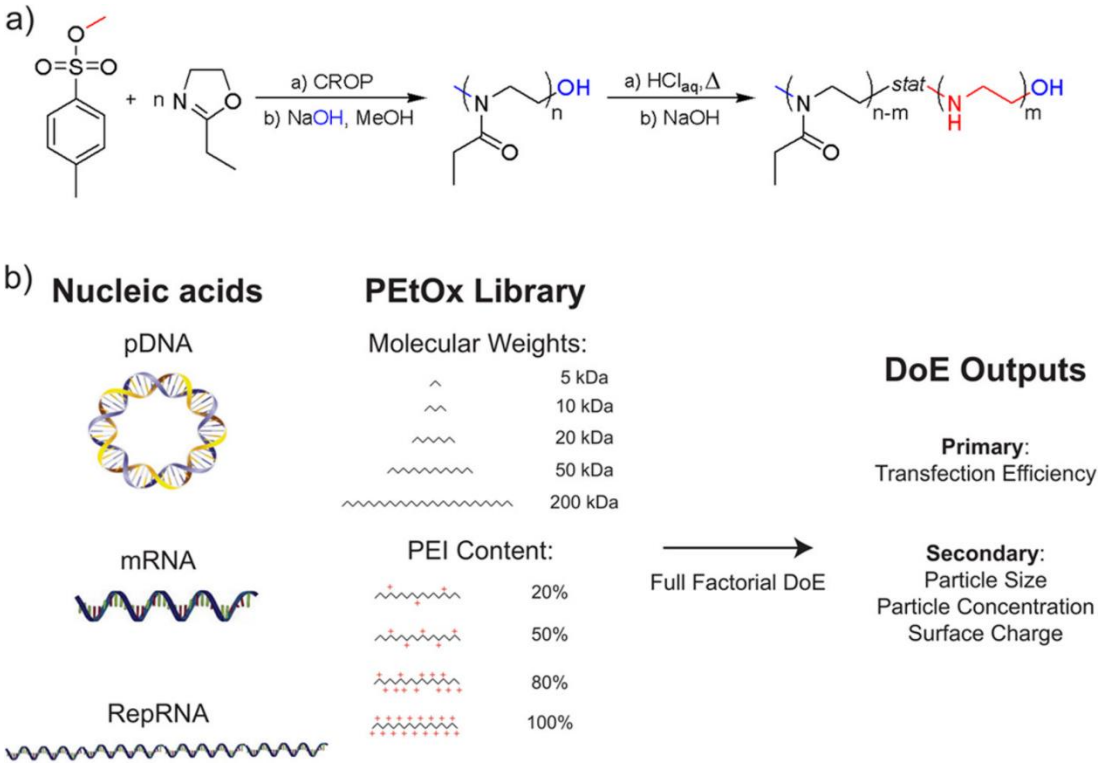

Scheme 1.15. (A) Cationic ring-opening polymerisation of EtOx and partial or full hydrolysis in aqueous HCl and **(B)** full factorial design of experiment parameters. Scheme reprinted from reference 161, with permission from the American Chemical Society (Copyright 2022).

1.3.1.3.3. Other Applications

Charged poly(2-oxazoline)s have also been shown to display potent antimicrobial and antifungal properties. For example, 2-oxazolines synthesised from boc-glycine and boc-γ-aminobutyric acid can be deprotected post-polymerisation to yield cationic amine homopolymers.[66, 162] These cationic polymers can enter bacteria and bind with deoxyribonucleic acid (DNA) causing the bacteria to form reactive oxygen species that cause the cell to burst. Further functionalisation of the cationic polymers to form poly(2-oxazoline)s with pendant guanidinium groups has also been performed, with the subsequent polymers showing promising antifungal properties.[163]

A final application of block poly(2-oxazoline)s is that of cell-imaging. Polymers containing fluorinated block segments can self-assemble and be used as contrast agents for magnetic resonance imaging (MRI).[164, 165] The fluorinated segment assembled into the cores of the polymer micelle, with the ^{19}F MRI studies showing high sensitivity to the micellar structures. Fluorinated triblocks containing hydrophilic, lipophilic, and fluorophilic segments have also been synthesised, however they are yet to be tested as contrast agents.[166]

1.3.2. Cyclic Polymers

Cyclic polymers are of scientific interest for several reasons. Their cyclic structure means they have smaller hydrodynamic volumes and lower viscosities in solution compared to linear polymers of the equivalent molecular weights. Furthermore, cyclic polymers can be less susceptible to degradation due to their lack of end groups. For example, cyclic proteins are protected from proteolytic enzymes that work at the chain ends.[167] Nonetheless, cyclic

polymers can be difficult to synthesise in good yield, as the synthesis has a competing step-growth polymerisation that can be difficult to suppress without high dilution. Finding conditions to maximise cyclisation is of interest because of this issue and this is one of the motivations of **Chapter 3**. In this section, synthetic methods of poly(2-oxazoline) cyclic polymers are discussed, followed by their analysis and potential applications.

1.3.2.1. Synthesis of Cyclic Polymers

The vast majority of literature based on cyclic poly(2-oxazoline)s uses CuAAC as the technique of choice for connecting the end-groups of poly(2-oxazoline)s (**Scheme 1.16**).[32, 168, 169] There are two main advantages to this. Firstly, it is simple to install the necessary reactive groups at the chain ends. An alkyne moiety can easily be installed at the α chain end with the use of a functional initiator such as propargyl tosylate. The azide can be introduced to the Ω chain end by using a suitable end capping group. In the literature, the two main end-capping agents used are sodium azide[170] and 2-azidoethylamine.[171] The main advantage of using 2-azidoethylamine is that it also introduces a secondary amine that can undergo further reaction, for example by linking the polymer to a nanoparticle.[169] The second advantage to using CuAAC is that it is fast, reliable, and very versatile. It can be performed in a wide range of solvents, which is helpful as the polymer may have limited solubility.[172]

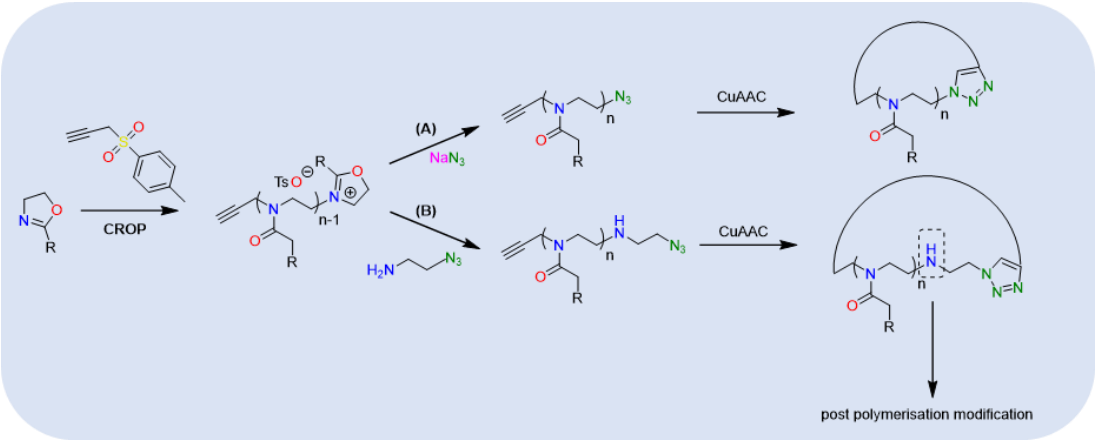

Scheme 1.16. Synthesis of cyclic poly(2-oxazoline)s *via* CuAAC. **(A)** End-capping with sodium azide. **(B)** End-capping with 2-azidoethylamine.[170, 171]

A second route to cyclic pEtOx was developed by Chen *et al*.[173] In their work, they used 2-bis(bromomethyl)benzene as a bis-initiator for CROP. Then they end capped both chain ends with potassium ethyl xanthate, before reducing the end groups to thiols with an amine. The free thiols could then react together in the presence of air to form a disulphide bridge thus forming a cyclic polymer.

The disadvantage to these routes is that the polymers can easily be coupled together to form multiblocks instead of cyclising. Even when the reaction is conducted under high dilution conditions, some polymers are likely to couple together and so a further purification step may be required. In order to tune the degree of cyclisation, the solvent polarity, reaction concentration, and block length have been shown to be critical.[174] For poly(fatty acid oxazoline), it has been demonstrated that cyclisation is favoured in more non-polar solvents whilst the competing step-growth is favoured in more polar solvents.[32] Furthermore, for cyclisation of poly(2-oxazoline)s using CuAAC, the amount of copper used has been shown to affect the degree of cyclisation, with more cyclisation at high copper concentrations.[32] This is thought to be due to a

ligating effect between the poly(2-oxazoline) backbone and the copper species.

Cyclic polymers are frequently used for coatings and biolubricants, and so having effective linking groups to various surfaces is beneficial. In fact, various methods have been developed to provide this linkage. Firstly, poly(glycidyl methacrylate) chains can be linked to a surface *via* surface-initiated atom transfer radical polymerisation (SI-ATRP). As mentioned earlier, poly(2-oxazoline)s end-capped with 2-azidoethylamine can be further reacted through the secondary amine introduced (**Scheme 1.17.**). Ring-opening the glycidyl rings using this secondary amine provides a simple method to functionalise surfaces with cyclic poly(2-oxazoline)s.[171] Other methods that have been employed include the addition of a nitrodopamine moiety to the cyclic poly(2-oxazoline) *via* the secondary amine functionality.[169] Nitrodopamines have been shown to be strong anchoring groups to metal surfaces,[175] and have been used to link cyclic poly(2-oxazoline)s to iron oxide nanoparticles[176] and titanium dioxide[8] surfaces. Lastly, Benetti *et al.* developed a method of linking cyclic pMeOx to cartilage by grafting onto a poly(glutamic acid) backbone with hydroxybenzaldehyde functionalities.[177]

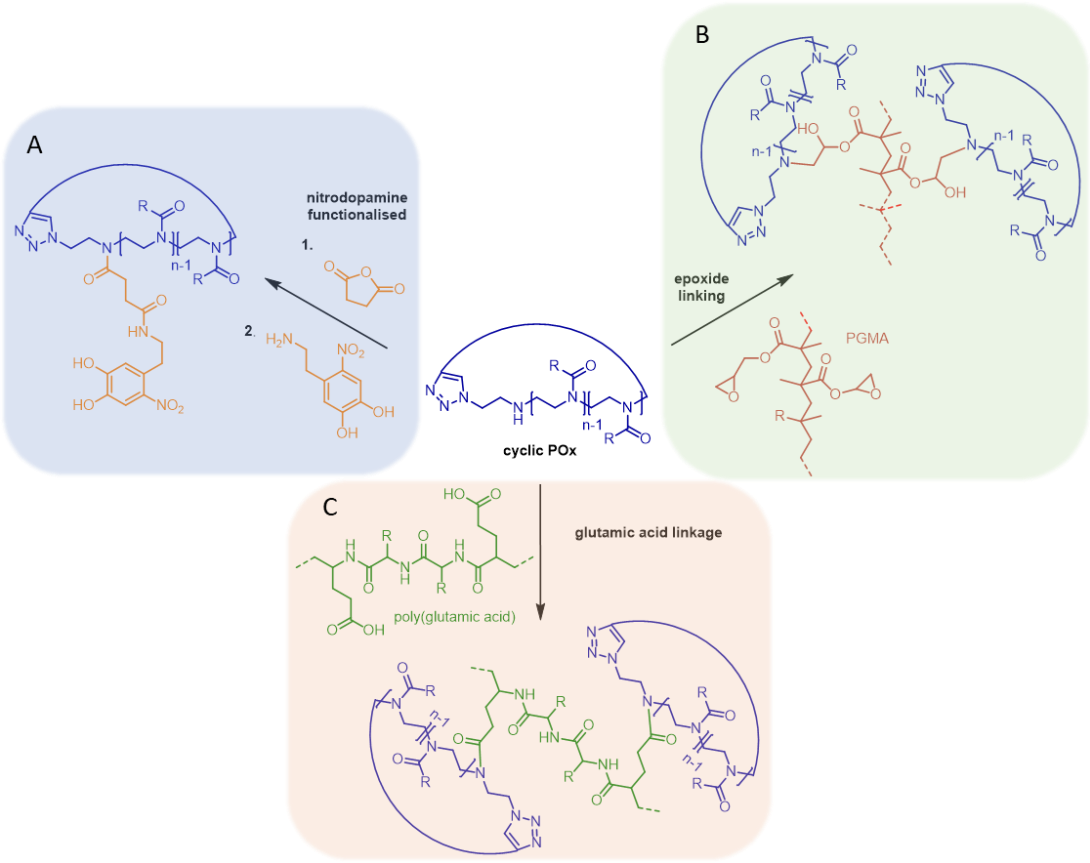

Scheme 1.17. Methods of functionalising cyclic poly(2-oxazoline)s. Note that in all cases, the end capping agent is 2-azidoethylamine. **(A)** Functionalisation with nitrodopamine.[169] **(B)** Linkage *via* epoxide ring opening.[171] **(C)** Linkage *via* amide formation.[177]

1.3.2.2. Analysis of Cyclic Polymers

The analysis of cyclic polymers is normally performed using conventional GPC methods as this is typically the most facile technique. If the hydrodynamic volume of a linear polymer and a cyclic polymer of equivalent molecular weight are compared, the cyclic polymer has a smaller hydrodynamic volume due to its more compact cyclic structure. This means that upon cyclising, the polymer peak in the GPC shifts to a longer retention time as it has a smaller size and thus takes longer to pass through the GPC column. Therefore, visualising cyclisation by GPC is simply a matter of observing a peak shift to longer retention time. Furthermore, due to the cyclic polymer having a smaller hydrodynamic volume compared to the linear equivalent at the same

molecular weight, it also has a lower intrinsic viscosity as it cannot inhibit solvent flow as effectively. This difference can be seen clearly when comparing linear poly(styrene) with cyclic poly(styrene) in a Mark-Houwink plot (**Figure 1.15.**) where the cyclic polymer has a lower intrinsic viscosity across the whole molecular weight range.[178]

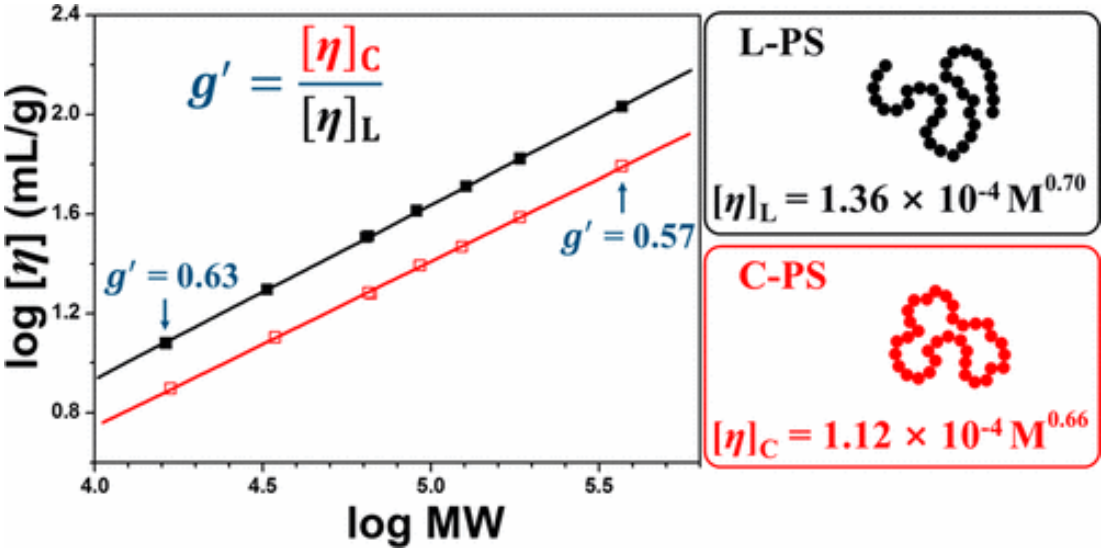

Figure 1.15. Difference in intrinsic viscosity between linear poly(styrene) (black) and cyclic poly(styrene) (red). Figure reprinted from reference 178, with permission from the American Chemical Society (Copyright 2022).

MALDI-TOF-MS can also be used to demonstrate cyclisation by CuAAC. In the case in **Figure 1.16**, the linear polymer chain was initiated with propargyl tosylate and terminated with an azide in order to undergo subsequent cyclisation *via* CuAAC.[168] Azides are not especially stable and, in this case, the terminal azide was reduced to an amine upon ablation with the instrument laser, releasing a molecule of nitrogen (*i.e.* reducing the polymer mass by 26). Upon cyclisation, the alkyne groups react with the azides forming the much more stable triazoles species, which could withstand the laser power and thus the expected mass (+Na) for the cyclic polymer can be seen.

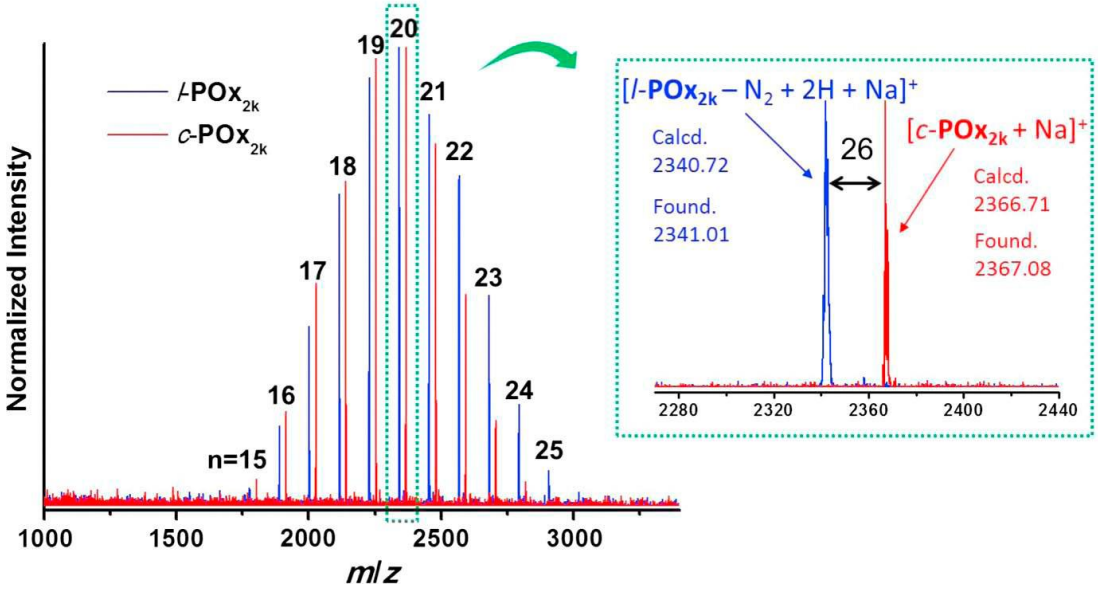

Figure 1.16. MALDI-TOF-MS spectrum of a linear polymer (blue) and the associated cyclic polymer (red). Figure reprinted from reference 168, with permission from Elsevier (copyright 2022).

1.3.2.3. Applications of Cyclic Polymers

1.3.2.3.1. Surface Coating

The more compact size and lower radius of gyration of cyclic polymers mean that they can be used to produce thinner, denser layers compared to a linear polymer of equivalent weight (**Scheme 1.18.**).[179, 180] The compact nature of the surface layers they form means they can be useful biolubricants and are effective at preventing protein contamination.[8, 171] In fact, most of the literature on cyclic poly(2-oxazoline) polymers is centred on their use as surface coatings. As well as preventing protein contamination, the dense cyclic polymer layers help to stabilise nanoparticles by preventing their aggregation, demonstrated by Benetti *et al.* when they showed that nanoparticles stabilised with cyclic polymers presented no aggregation even after a month later than the equivalent linear polymers had begun to aggregate.[181]

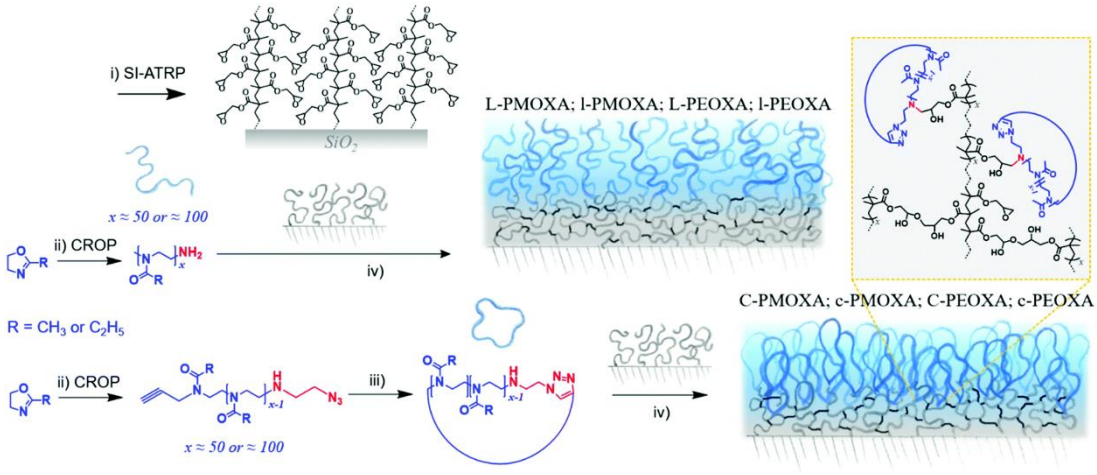

Scheme 1.18. Linear and cyclic poly(2-oxazoline)s and their attachment to a SiO_2 surface. The cyclic layer is thinner and denser than the analogous linear layer. Scheme reprinted from reference 179, with permission from The Royal Society of Chemistry. (Copyright 2022).

Brush polymers have also been shown to be effective at reducing friction, however interdigitation between brushes represents a major source of friction, especially at high pressures and low shear rates.[182, 183] Cyclic polymers have an advantage over brush polymers in this regard because they do not interdigitate to the same degree, and so are better at improving friction modulation.[184]

1.3.2.3.2. Gene Delivery

Lastly, cyclic PEI has been shown to be a promising improvement on linear PEI of the equivalent molecular weight for gene delivery.[185] In this case, the cyclic polymer was synthesised from a linear pEtOx that was subsequently cyclised *via* CuAAC, and then hydrolysed. The cyclic PEI was shown to be significantly less toxic than the current standard of gene delivery for polymers, which is 25 kDA PEI.[186] It is thought that the more compact structures of cyclic polymers result in an increase in charge density which improves transfection efficiency.

1.3.3. Star Polymers

A star polymer can be defined as a macromolecule that has three or more linear polymer arms radiating from a centralised branching point, or core. Within this definition, star polymers can be further classified by the method of synthesis, arm structure, and core structure. Star polymer have compact hydrodynamic volumes resulting in structures with lower viscosities compared to linear polymers of the equivalent molecular weight. Further details concerning the relationship between hydrodynamic volume, intrinsic viscosity, and molecular mass will be discussed later in the section on analysis of star polymers. Their low viscosities result in structures that can be used for rheology and viscosity modification, whilst the star cores can be used to encapsulate small molecules and so find applications for gene and drug delivery. In this section, the synthetic routes to star polymers are covered, followed by a more detailed examination of the analysis and applications of star polymers.

1.3.3.1. Synthesis of Star Polymers

There are three main approaches to star polymers synthesis, all of which are covered in this section, along with their associated advantages and disadvantages. These approaches are the core-first approach, arm-first approach, and the grafting-onto approach, and they will be discussed in this order (**Figure 1.17.**)**.** It should be noted that Qiao *et al*. provided a very thorough review on star polymers in 2016 covering synthesis, characterisation, and properties of star polymers.[187]

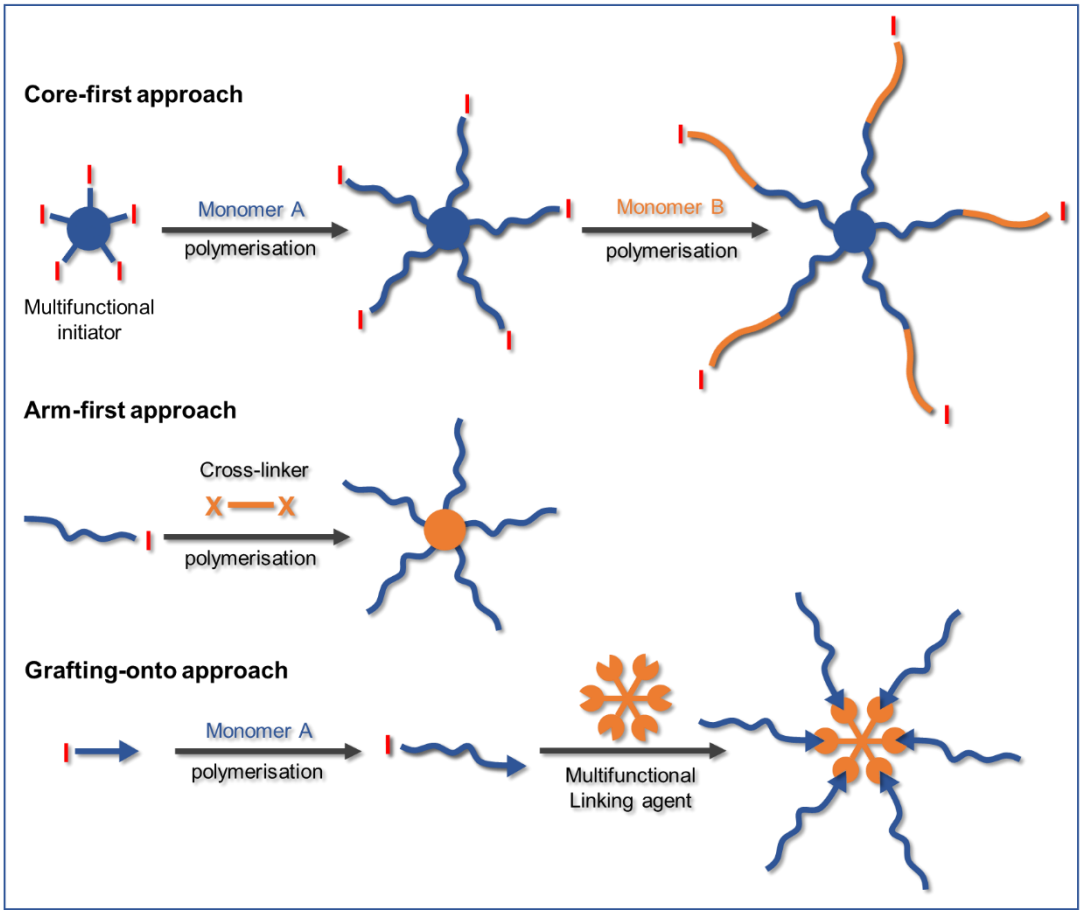

Figure 1.17. Schematic illustration of the core-first, arm-first, and grafting-onto approaches to star polymers.

1.3.3.1.1. Core-First Approach

The core-first approach uses a multifunctional initiator as the core, and the star arms form *via* polymerisation from the core. To ensure that the stars are well-defined, the initiation efficiency needs to be as close to 100% as possible, and the initiation rate should be much higher than the propagation rate. Advantages of the core-first approach include well-defined cores and simple purification from unreacted monomer *via* precipitation or dialysis. The small core size, limited number of arms, and difficulty directly analysing the arms are the main disadvantages.[187]

The core-first approach to poly(2-oxazoline) stars is well established, in part due to the ease of synthesis of the multi-initiator cores. Typically, an activated tosylate or triflate such as tosyl chloride or triflic anhydride is reacted with a multifunctional alcohol such as pentaerythritol to generate the initiator-core.[17, 188, 189] Although this is the most popular route, other cores have previously been used including metal cores with CROP initiators ligated to them.[190, 191] As all the arms form simultaneously from a central core, difficulty arises when determining whether all the arms are of the same length, or even if all arms have properly initiated. Nonetheless, techniques such as diffusion ordered nuclear magnetic resonance spectroscopy (DOSY NMR) and advanced GPC can be used to analyse the star polymers.[192] In fact, this is the ideal use of advanced GPC as the maximum number of potential arms is known.

1.3.3.1.2. Arm-First Approach

The arm-first approach is a convergent approach that involves the cross-linking of linear polymer arms to form a star (**Figure 1.17.**). The linear arms can be linked together with the use of a cross-linker or can be linked with the use of coupling chemistry, for example, through a short cross-linkable block.[193, 194] Conversely to the core-first approach, the arms can be characterised before star formation allowing for high levels of definition of the arms. Furthermore, this type of approach allows for the formation of stars with many arms, however the distribution of arms per star is more varied.[195, 196] Also, stars formed from this method can have very large cores that can contribute up to 30 *wt%* of the overall star, making them ideally suited to encapsulating small molecules.[187, 197] Nonetheless, stars synthesised *via* the

arm-first approach can suffer from poor arm-to-star conversion, as well as difficulty in analysing the core structure.

There are few examples in the literature of arm-first stars synthesised using the CROP of 2-oxazolines. Schlaad *et al*. synthesised pEtOx arms, followed by a block of poly(2-(3-butenyl)-2-oxazoline) which could undergo cross-linking *via* thiol-yne chemistry.[194] In a similar approach, the poly(2-(3-butenyl)-2-oxazoline) block was functionalised with charged thiols to form ionomer star structures.[198] A separate approach by Johnson *et al*. end-capped a poly(2-oxazoline) chain with a norbornene ring, which could then be cross-linked using ring opening metathesis polymerisation (ROMP) (**Scheme 1.19.**).[199] Lastly, a core cross-linked approach was recently developed using a bis-oxazoline to yield high molecular weight pEtOx stars, which is discussed in **Chapter 2**.[200]

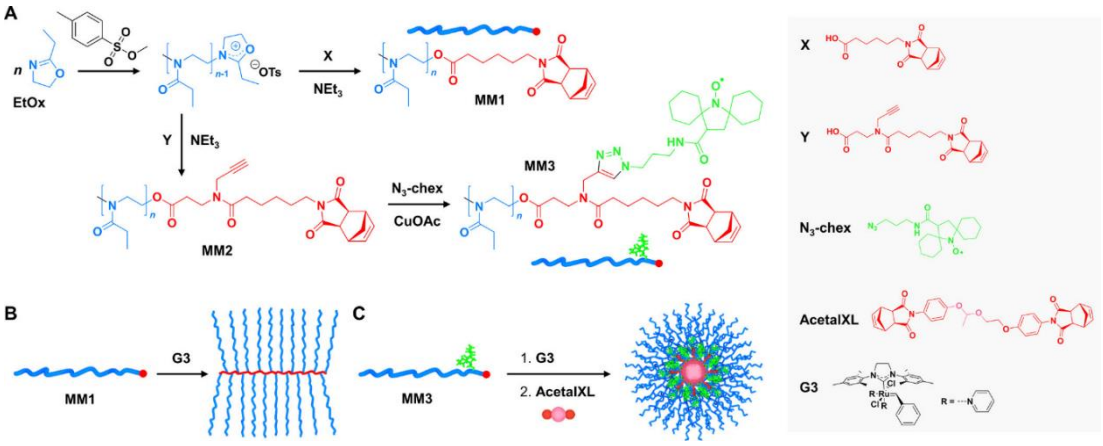

Scheme 1.19. (A) Synthesis of pEtOx-based norbornene-terminated macromonomers. **(B)** Graft-through ROMP of linear macromonomers to form bottlebrush polymers (BBPs). **(C)** Graft-through ROMP of branched macromonomers functionalised with N_3-chex to provide living BBPs, and subsequent addition of the cross-linker AcetalXL to form star polymers. Scheme reprinted from reference 199, with permission from American Chemical Society (Copyright 2022).

1.3.3.1.3. Grafting-onto Approach

The third method of star polymer synthesis is the 'grafting-onto' approach. This method offers the highest degree of control, as the core and the arms can be synthesised separately and then subsequently joined by some type of combinatorial chemistry, for example, click chemistry. This route has several disadvantages however – multiple purification steps are required, stars often have a small number of arms, lengthy reaction times are required, and an excess of arms are often required to ensure complete reaction.

Previous examples of this approach have used multifunctional polymer cores such as dendrimers, star shaped poly(ethylene oxide), and poly(ethyleneimine) (PEI) (**Scheme 1.20.**).[201-203]

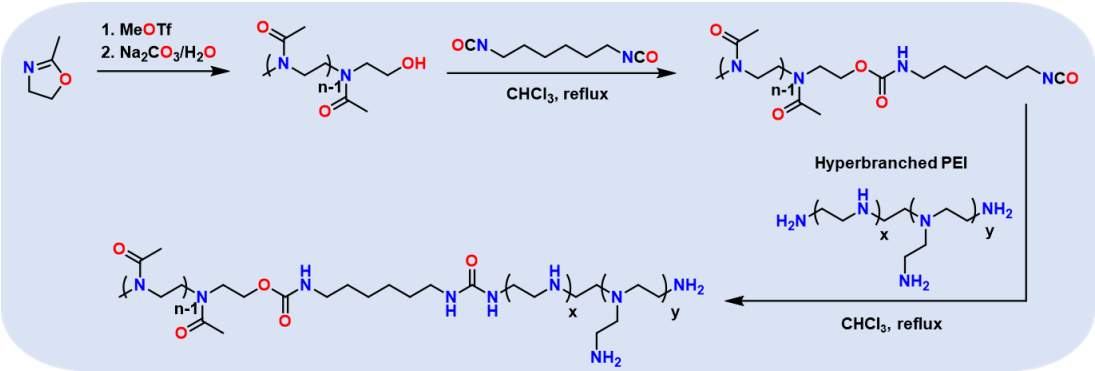

Scheme 1.20. Synthesis of star polymers *via* the grafting-onto approach using PEI as the core.[203]

Other examples use smaller molecules such as porphyrins to generate stars with fewer number of arms.[204] One of the advantages of combining the CROP of 2-oxazolines with the grafting-onto approach is that the pre-synthesised core can be directly injected into the CROP vessel to terminate the living chains. For example, PEI contains primary amines that can end-cap living chains to form a star, by direct injection into the arm polymerisation mixture.[203] Other examples use click reactions such as CuAAC to connect arms to a

functionalised core,[205, 206] and supramolecular interactions such as the cyclodextrin-adamantyl host-guest interaction have been used as a connecting mechanism.[207]

1.3.3.2. Analysis of Star Polymers

The analysis of star polymers can be difficult, as conventional GPC cannot provide information regarding the true number of arms per star, even if the core-first or grafting-onto approaches are used. As more arms are added to the star, the molecular weight of the star increases proportionally. However, the hydrodynamic volume does not increase proportionally as arms are added, due to an increase in branching. For example, three and a four-arm stars can have similar hydrodynamic volumes despite having a significant difference in molecular weight.[188] For the grafting-onto and core-first approaches, the number of arms can be estimated as the structure of the core is well-defined and the number of initiating sites or linking sites is known. Nonetheless, the initiators may not be 100% efficient in the arm-first approach, and for the grafting-onto approach, steric effects become prevalent and can prevent complete reaction between all the arms and the core. For the arm-first approach, there is no expected number of arms, and so this must be calculated using additional techniques such as light scattering or viscometric GPC.

1.3.3.2.1. Light Scattering GPC (LS GPC)

Light scattering is a useful technique for obtaining absolute molecular weights of polymers directly without calibration. In this technique, a laser is used to irradiate a sample. The sample scatters the light which is then collected by a

detector. The response from the detector is directly proportional to the molecular weight of the polymer due to the following equation:

$$R_\theta = Mw\ K \left(\frac{dn}{dc}\right)^2 \mathrm{c} \qquad \textbf{Equation 1.3}$$

Where R_θ is the detected scattered light, Mw is the molecular weight, *K* is a constant, dn/dc is the refractive index increment, and c is concentration.

This equation requires three assumptions. Firstly, that the dn/dc is constant across the sample. Secondly, that the sample is dilute and that there are no intermolecular interactions. Thirdly, that the scattering function P_Θ is equal to one if the polymer is below a size of ~ 10 nm.[208] The dn/dc of the sample is important as the intensity of scattered light is proportional to the square of it. Due to this relationship, light scattering is not suitable for samples with low dn/dc values. Furthermore, light scattering assumes that the dn/dc is constant throughout the sample and so the technique is not suitable for copolymers.

For a small particle, (less than 1/20th of the wavelength of the incident laser beam) the particle acts as a point and scatters light evenly in all directions. When the particles get larger relative to the laser wavelength, the particles act as a collection of points that cause destructive interference at high scattering angles, causing an apparent reduction in molecular weight at high angles, a phenomenon known as dissymmetry. The true molecular weight can only be calculated at the 0° angle, however this cannot be measured due to the inbound laser beam (**Figure 1.18.**).

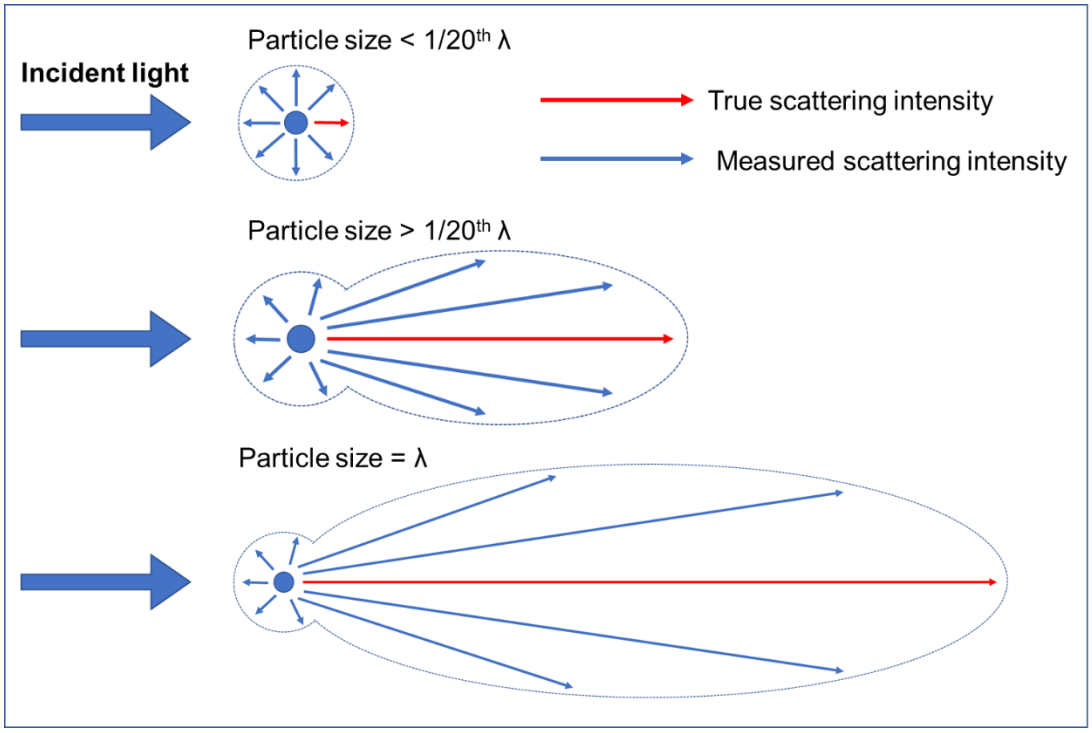

Figure 1.18. The effect of particles size on the degree of dissymmetry. Note that for particles with a size of less than 1/20th the wavelength of the incident light, there is no dissymmetry.

There are several different detector angles that can be used to collect light scattering data. Lower angle detectors provide more accurate information on molecular weight as there is less dissymmetry, but there is more noise from the incoming light source. High angle detectors such as a right-angle light scattering detector are less noisy, but are less accurate regarding the true molecular weight due to the dissymmetry issue.[209] If the scattered light is collected using more than one detector, this dissymmetry can be used to obtain size information about the particle *via* a partial Zimm plot.

LS GPC can be used to calculate the absolute molecular weight of star polymers; however, they need to be of appreciable size (over 15 nm) to generate high quality data. To calculate the average number of arms for an arm-first approach, the following equations are required:

$$N_{arms} = \frac{W_{arms} \times M_{w,star}}{M_{w,arms}}$$ **Equation 1.4**

Where $M_{w,star}$ and $M_{w,arms}$ are the weight average molecular weight of the star and arms as determined by LS-GPC. W_{arms} is the weight fraction of arms and is defined below in **Equation 1.5**.

$$W_{arms} = \frac{\left[\frac{Arm}{Crosslinker}\right] \times M_{w,arms} \times conv_{arms}}{M_{w,CL} \times conv_{CL} + \left[\frac{Arm}{Crosslinker}\right] \times M_{w,arms}}$$ **Equation 1.5**

Where [arm/cross-linker] is the molar ratio of arm to cross-linker, $conv_{arms}$ is the arm to star conversion, $M_{w,CL}$ are the weight average molecular weight of the cross-linker and $conv_{CL}$ is the cross-linker conversion.

One of the main problems with using light scattering for star polymer analysis is that the radius of gyration (R_g) cannot be calculated for particles with a size of under 10 nm as they act as a point and scatter light in all directions, and so do not show dissymmetry. This means that generally, the R_g of the arms cannot be calculated as they are too small. The ultimate result of this is that the number of arms per star as a function of molecular weight cannot be calculated. The R_g of a star is smaller than a linear reference of equivalent molecular weight due to the degree of branching present. This fact can be used to calculate *g*, the geometric branching factor (**Equation 1.6**) which can then be used to calculate the number of arms (**Equation 1.7**)

$$g = \left(\frac{R^2_{g,branched}}{R^2_{g,linear}}\right)_{MW}$$ **Equation 1.6**

Assuming a polydisperse star, **Equation 1.7** gives the number of arms, f, at each value of g and hence the number of arms at each molecular weight.

$$g = \frac{3f}{(f+1)^2}$$ **Equation 1.7**

In order to calculate the number of arms per star as a function of molecular weight, viscosity GPC can be a more useful technique, and is explained in the next section.

1.3.3.2.2. Viscosity GPC

All polymers increase the viscosity of solutions because they disrupt laminar flow of solvent and thus increase resistance to flow. For this reason, the hydrodynamic volume of a polymer is related to its intrinsic viscosity. For a given molecular weight, polymers with a smaller volume inhibit flow less, and so increase viscosity less than for a larger volume polymer. Branching in a polymer effectively decreases the hydrodynamic volume of a polymer (and the associated viscosity) whilst maintaining the molecular weight of the polymer.[210] The hydrodynamic volume of a polymer is therefore related to its intrinsic viscosity multiplied by its molecular mass. To measure viscosity, a four-capillary bridge viscometer is typically used (**Figure 1.19.**).[211] In this detector, the solvent line splits and flows down two paths. Both paths are identical, except one has a delay column that holds the sample so there is pure solvent on that side of the bridge. The inlet pressure and differential pressure between the two lines are then used to calculate intrinsic viscosity.

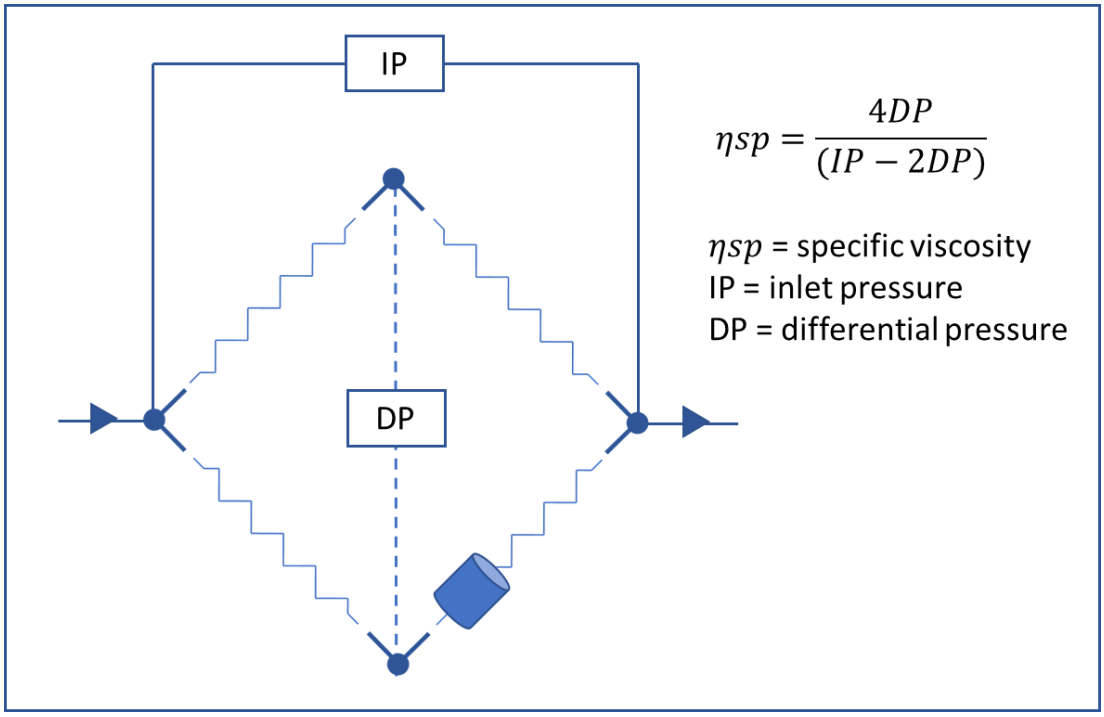

Figure 1.19. Simplified diagram of a 4-capillary bridge viscometer. The GPC eluent splits down both branches before a delay column holds the sample allowing for calculation of the intrinsic viscosity.

Using viscosity GPC for star polymer analysis relies on the fact that the lower the viscosity of a star polymer at a given molecular weight, the higher the degree of branching and therefore the more arms it has. For example, a linear polymer of 5 kDa molecular weight will have a higher viscosity compared to a 3-arm star of the same molecular weight and polymer type.

To calculate the number of arms per star, firstly the intrinsic viscosity (IV) needs to be calculated. This is calculated by using the specific viscosity combined with the concentration as obtained from the refractive index (RI) detector. The IV is then obtained using **Equation 1.8**:

$$[\eta] = \lim_{C \to 0} \frac{\eta_{sp}}{C} \qquad \textbf{Equation 1.8}$$

Where [η] is the intrinsic viscosity, η_{sp} is the specific viscosity and C is the concentration.

The discrepancy in intrinsic viscosity of a linear sample compared to an equivalent molecular weight star polymer can be used to calculate the degree of branching, or number of arms. This calculation requires the geometric branching factor g which is calculated from the R_g of the linear polymer and the branched polymer in question (**Equation 1.6**). However, the radius of gyration is measured by light scattering data and as mentioned, this is only suitable for polymers with an Rg over 10 nm. In cases where the R_g is smaller than 10 nm, the branching ratio g' can be calculated instead from the intrinsic viscosities of the linear reference and branched polymer (**Equation 1.9**).

$$g' = \left(\frac{IV(branched)}{IV(linear)}\right)_{MW} \qquad \textbf{Equation 1.9}$$

The relationship of the geometric branching factor g to the branching ratio g' is as follows:

$$g' = g^{\varepsilon} \qquad \textbf{Equation 1.10}$$

ε is a structural factor that has a value of between 0.5 and 1.5 and depends on numerous factors such as the solvent and type of branching.[188, 212] To calculate the number of arms (f) from g, **Equation 1.7** is used.

Guégan *et al*. used a core-first approach to generate poly(2-oxazoline) stars with various numbers of arms, and showed that the theoretical number of arms can be used to calculate a more accurate value of ε.[188] For the arm-first approach, the theoretical number of arms is not known, however literature data suggests a value of 0.75 is suitable for ε. [213, 214] Using the viscosity data, a Mark-Houwink plot can be generated to visually observe the change in viscosity across the molecular weight of a sample. As can be seen in **Scheme**

1.21, as the number of arms per star increases, the viscosity of the system decreases. The linear gradient of each star indicates that the number of arms per star remains constant across the system. The gradient of the Mark-Houwink plots gives information about the solvation of the polymer in solution. For a polymer in a theta solvent, the gradient should be ~0.5.

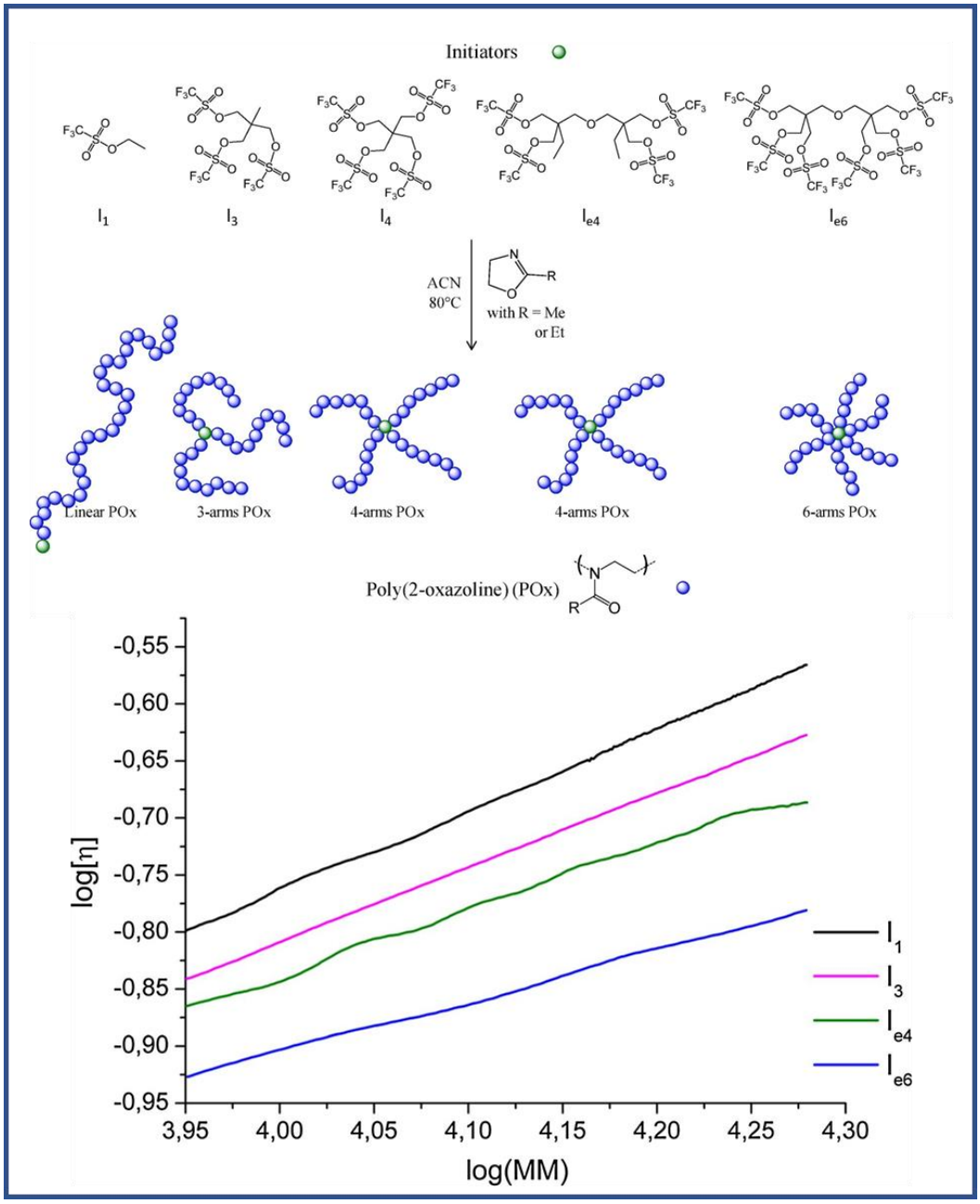

Scheme 1.21. Structures of initiators used by Guégan *et al.* for the synthesis of linear, 3-arm, 4-arm, and 6-arm polymers *via* the arm-first approach (top), and the Mark-Houwink plots of the different stars (bottom). Scheme adapted from reference 188, with permission from Elsevier (Copyright 2022).

1.3.3.3. Applications of Star Polymers

The unique structures of star polymers result in several useful properties that make them ideal for a range of applications. Their branched structures and protected cores make them ideal for small molecule encapsulation, and so stars are used frequently for drug encapsulation and gene delivery. Furthermore, their low relative viscosities due to branching result in potential viscosity modification applications. In this section, a few of the main applications of star polymers will be discussed.

1.3.3.3.1. Drug Delivery

One of the most popular applications of star polymers is drug delivery. Star polymers are ideal for this application because small molecules can be loaded into the star structure and thus protected from degradation in the body. This results in drugs being able to circulate for longer in the body without being excreted. Previously, stars have been used to encapsulate therapeutic molecules such as doxorubicin,[215, 216] irinotecan,[217] folic acid,[218] and alendronic acid.[219] Star polymers do not disintegrate upon dilution due to their cross-linking, which provide them with an advantage over other types of polymeric structures for drug delivery such as micelles. Nonetheless, this can also be a disadvantage as they can be difficult to biodegrade and as such can reside in the body for a prolonged time. There are few examples of poly(2-oxazoline) star polymers that have been used for drug encapsulation as most of the literature is focussed on the synthesis of them, however a four-arm star based on a pentaerythritol core with poly(caprolactone)-pEtOx arms (**Scheme 1.22.**) were shown to be able to encapsulate a hydrophobic model drug.[205]

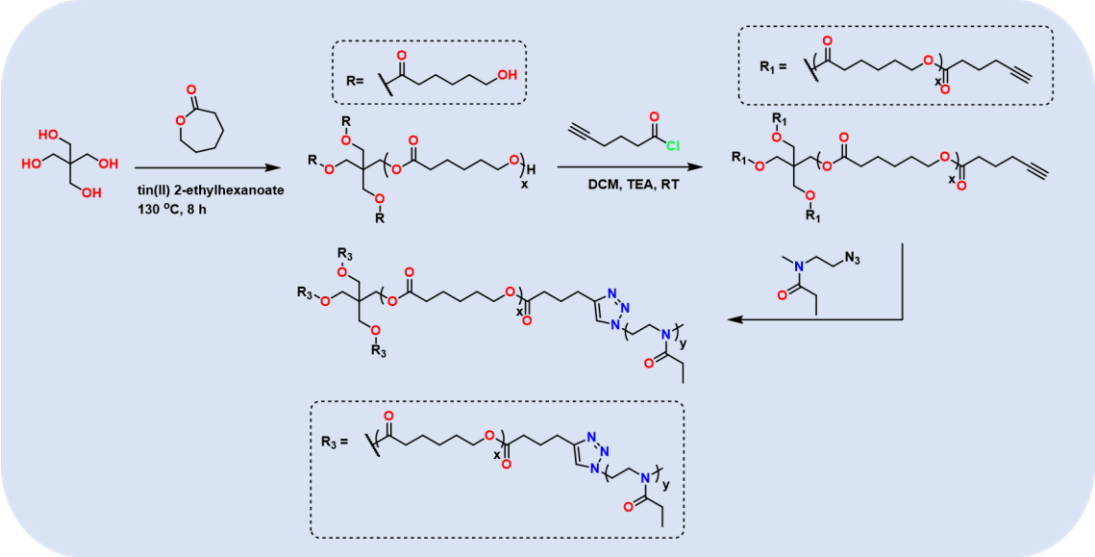

Scheme 1.22. Synthesis of poly(caprolactone)-pEtOx four-arm star polymers *via* a core-first approach.[205]

1.3.3.3.2. Gene Delivery

As well as drug delivery, star polymers have also been explored for gene delivery. The star polymer structure can be used to prevent proteins from aggregating with nucleic acids, thus increasing the lifetime of them in the body. Previously, star polymers have been used to deliver RNA to macrophage cells[220] and protect DNA for delivery into plants.[221] Regarding poly(2-oxazoline) star polymers for gene delivery, there are limited examples, however four-arm pMeOx stars have demonstrated the ability to effectively transfect plasmid DNA.[222] Another example used a cyclodextrin core furnished with hydroxyl moieties to generate poly(lactic acid) stars. The end groups were then functionalised with a tertiary bromine for ATRP, which was then used to polymerise a block of poly(dimethylamino ethyl methacrylate) (PDMAEMA) followed by a block of pEtOx end capped with a methacrylic acid. (**Scheme 1.23.**) Again, these star polymers were shown to be able to transfect plasmid DNA.[223]

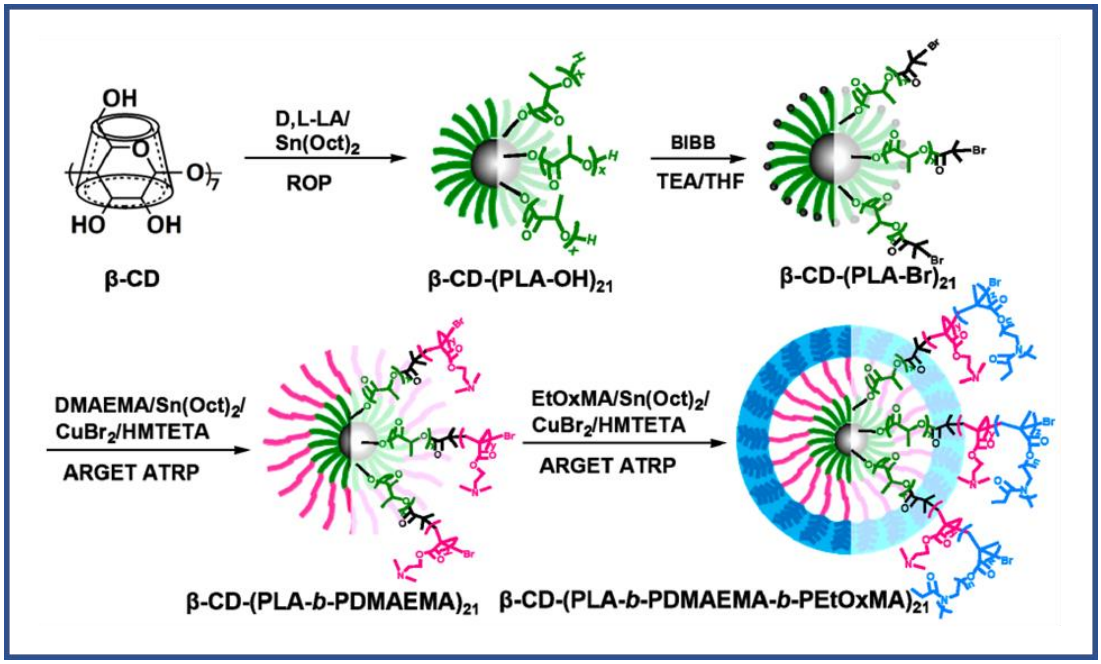

Scheme 1.23. Synthesis of triblock star polymers with a block of methacrylic acid end-capped pEtOx. Stars here were used for plasmid DNA transfection studies. Scheme taken from reference 221. Permission not required for reprint.

1.3.3.3.3. Contrast Agents

MRI is one of the most valuable diagnostic techniques available currently due to its ability to accurately generate 3D representations of the human body in a non-invasive manner. MRI often requires a contrast agent to enhance the difference between native water protons and cell matter. One of the key issues currently is that contrast agents use paramagnetic metals which can have toxicity issues. For this reason, there is a lot of research into metal free contrast agents such as organic radical contrast agents (ORCAs). Star polymers are ideal structures for contrast agents as the ORCA can be encapsulated into the core and thus protected from degradation. Nitroxides can be used as a contrast agent, however they have poor *in vivo* stability. The stability of the nitroxide can be improved by combining it into a star polymer as demonstrated by Johnson *et al*. who formed PEG and poly(2-oxazoline) core cross-linked stars *via* ROMP (**Scheme 1.19**).[199, 224, 225] Another approach used a

fluorescent 4-arm initiator for Cu(0) RDRP that could undergo aggregation induced emission, had low cytotoxicity and a long *in vivo* lifetime.[226]

1.3.4. Hyperbranched Polymers

Hyperbranched polymers are highly branched, soluble, three-dimensional macromolecular structures. Their branched nature endows them with attractive characteristics such as large numbers of functional groups, intramolecular cavities, and low viscosities. Dendrimers are a notable type of hyperbranched polymer in that they are perfectly branched with a spherical symmetry about the core of the structure and are very well-defined. Hydrogels differ from hyperbranched polymers because they tend to have much more cross-linking and are thus insoluble.

1.3.4.1. Synthesis of Hyperbranched Polymers

The synthesis of dendrimers can be performed by one of two methods: a divergent or a convergent approach. In the divergent approach, the synthesis begins at the core and the dendrons (arms) are grown in a stepwise manner, uniformly. Each addition to the dendrons is known as a 'generation.' This approach is the most common approach, however, it can be difficult to detect any defects in the arms, and multiple purification steps are required.[227] The second approach is a convergent approach, which first synthesises the arms and then attaches them to a core.[228] This route is similar to the arm-first approach seen with star polymers, however, has the difficulty of increasing steric hindrance around the core as arms are added. Notably, dendrimers have been used as cores in the grafting-onto approach for star polymer synthesis.[201]

To bypass the difficulty in synthesising dendrimers, branched polymers can be synthesised using a cross-linker. This method produces randomly branched polymers that possess many similar characteristics to dendrimers such as intramolecular cavities, and low viscosities. However, these branched polymers are less defined than dendrimers. The most common method of synthesising hyperbranched polymers with a cross-linker is known as the Strathclyde method, which uses a chain transfer agent to control branching.[229] It must be noted that currently, hyperbranched poly(2-oxazoline)s that have been synthesised with a cross-linker do not exist, however there are a wide range of hydrogels that have been reported.[230, 231]

One method of creating hyperbranched polymers has been demonstrated with an AB_2 monomer. In this method, a 2-oxazoline with a diphenol as the R group was used as the monomer, where the phenolic hydroxyl groups could ring open the 2-oxazoline.[232] A second method synthesised three-arm star polymers using 1,3,5-tris(bromomethyl)benzene as an initiator which were then terminated with potassium ethyl xanthate.[233] The chains could then be reduced with butylamine and then coupled together to form hyperbranched polymers. Similarly, Perrier *et al*. initiated pEtOx chains with propargyl tosylate and end-capped them with potassium ethyl xanthate.[6] The xanthate groups were then be reduced to thiols, which could then be used in a thiol-yne click reactions with the propargyl group on the α chain end to form hyperbranched polymers as multiple thiols can be attached per propargyl group (**Scheme 1.24.**).

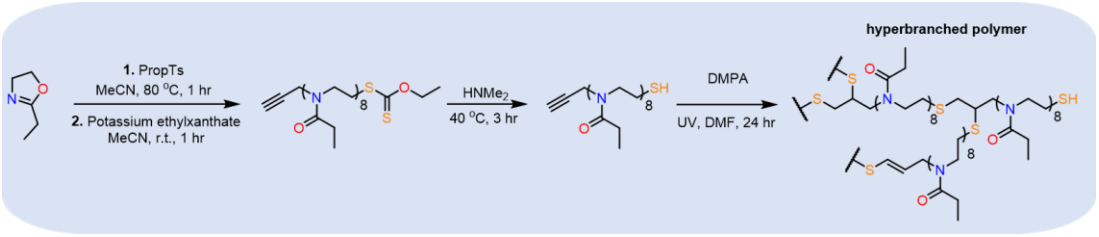

Scheme 1.24. Synthesis of branched poly(2-oxazoline)s *via* a thiol-yne click reaction approach.[6]

1.3.4.2. Analysis of Hyperbranched Polymers

A useful value to compare the degree of branching between polymers is the Zimm branching factor, or g'. The Zimm branching factor is the ratio of the intrinsic viscosity (IV) of a linear, non-branched reference (see **Equation 1.9**) with a branched polymer at each slice of the GPC chromatogram. As g' tends towards one, the degree of branching in the branched polymer reduces to that of a linear sample at the same molecular weight, *i.e.,* there is no branching present. As g' tends towards zero, the branching increases *ad infinitum.* To calculate g', a linear reference is required to compare to the branched polymers. In **Figure 1.20**, a linear poly(methyl methacrylate) (PMMA) can be seen with a branched PMMA, along with g'. The g' value can be seen to decrease as the branched polymer increases in molecular weight, which indicates that the higher molecular weight polymeric species have more branching.[234] At the low molecular weight, g' tends towards 1, indicating that the intrinsic viscosity of the branched polymer and linear reference are similar and so there is minimal branching present.

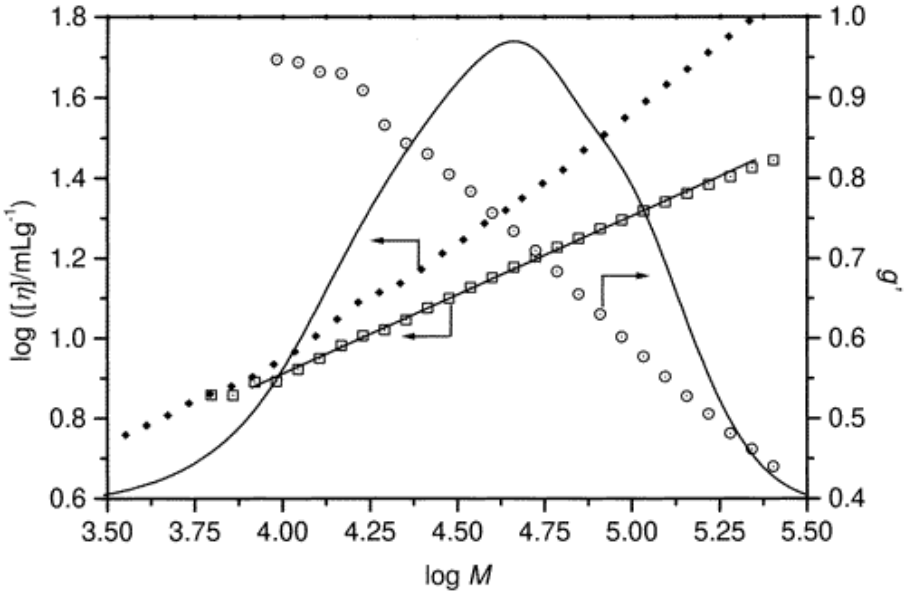

Figure 1.20. Mark-Houwink plot of branched PMMA (white squares), linear PMMA (black squares), g' contraction factor (white circles), and RI signal (black line). Figure reprinted from reference 234, with permission from American Chemical Society (Copyright 2022).

1.3.4.3. Applications of Hyperbranched Polymers

As with the other types of poly(2-oxazoline) architecture, hyperbranched poly(2-oxazoline)s have been explored mainly for biomedical usage. A comparison of the biodistribution of hyperbranched poly(2-oxazoline)s with PEG suggested that although PEG and hyperbranched pMeOx showed no discernible difference in their cellular association in the liver, hyperbranched pEtOx showed increased association with cells in the immune system, such as dendrocytes.[235] Hyperbranched PEI coupled with poly(2-oxazoline)s has been shown to be an effective DNA transfection vector, with similar transfection efficiencies to commercial 25 kDa PEI, and lower associated toxicity.[6] There are limited examples of hyperbranched poly(2-oxazoline)s in the literature, and so applications of these polymers are hard to come by. Nonetheless, there are examples of other types of hyperbranched polymer with real applicability. For example, hyperbranched polymers that have long chain conjugation from linking phenyl rings can be used for various electronic

and optical applications. For example, **Scheme 1.25.** shows the formation of a conjugated hyperbranched polymer *via* a Wittig reaction.[236]

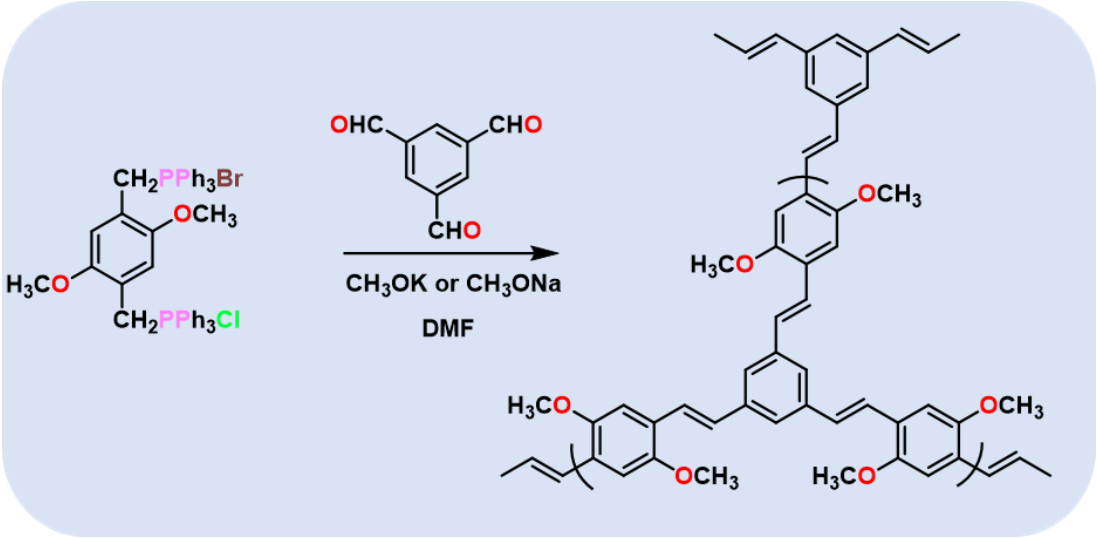

Scheme 1.25. Formation of conjugated hyperbranched polymers *via* Wittig Reaction.[236]

As well as potential optical applications, other hyperbranched polymers containing PEG sections show promise as solid electrolytes, as the ethylene glycol segments demonstrate good ion transport and solvation ability.[237] Hyperbranched polymers can also be used as toughening agents, compatibilisers, and dispersing agents.[238]

1.4. Summary

In this chapter, the synthesis, analysis, and properties of different poly(2-oxazoline) architectures have been discussed in detail. From simple homopolymers through to random and block copolymers, cyclic polymers, and star polymers, the adaptability of the CROP of poly(2-oxazoline)s has been demonstrated. Homopolymers and copolymers have been shown to be promising drug and gene delivery agents, whilst block polymers can be used to self-assemble and encapsulate small molecules. Cyclic polymers form

dense layers that make excellent materials for surface coatings, whilst star polymers have interesting viscosity behaviour and the ability to encapsulate drugs. Clearly, the various poly(2-oxazoline) structures discussed here are diverse, and are particularly suited as therapeutic devices, whether that be biolubrication, drug delivery, gene delivery, or other. Building on this introductory summary of the synthesis, analysis, and applications of the various types of poly(2-oxazoline)s discussed, this thesis will demonstrate four separate advanced polymeric architectures concerning poly(2-oxazoline)s. **Chapter 2** is concerned with the synthesis of core cross-linked poly(2-oxazoline) star polymers and their potential for drug encapsulation, followed by an investigation into the synthesis of branched polymers using the same cross-linker. In **Chapter 3**, multiblock and cyclic poly(2-oxazoline)-poly(acrylate) block polymers have been synthesised, with the reaction conditions optimised to favour either cyclisation or step-growth. In **Chapter 4**, statistical and block copolymers combining a charged amine oxazoline with a glycosylated oxazoline have been synthesised and used for RNA transfection studies.

1.5. References

1. Suk, J. S.; Xu, Q.; Kim, N.; Hanes, J.; Ensign, L. M., *Advanced Drug Delivery Reviews* **2016,** *99*, 28-51.
2. Yang, Q.; Lai, S. K., *WIREs Nanomedicine and Nanobiotechnology* **2015,** *7* (5), 655-677.
3. Jana, S.; Hoogenboom, R., *Polymer International* **2022,** *71* (8), 935-949.
4. Kempe, K.; Lobert, M.; Hoogenboom, R.; Schubert, U. S., *Journal of Polymer Science Part A: Polymer Chemistry* **2009,** *47* (15), 3829-3838.
5. Hawker, C. J.; Frechet, J. M.; Grubbs, R. B.; Dao, J., *Journal of the American Chemical Society* **1995,** *117* (43), 10763-10764.
6. Cook, A. B.; Peltier, R.; Zhang, J.; Gurnani, P.; Tanaka, J.; Burns, J. A.; Dallmann, R.; Hartlieb, M.; Perrier, S., *Polymer Chemistry* **2019,** *10* (10), 1202-1212.
7. Hwang, D.; Ramsey, J. D.; Makita, N.; Sachse, C.; Jordan, R.; Sokolsky-Papkov, M.; Kabanov, A. V., *Journal of Controlled Release* **2019,** *307*, 261-271.
8. Morgese, G.; Trachsel, L.; Romio, M.; Divandari, M.; Ramakrishna, S. N.; Benetti, E. M., *Angewandte Chemie International Edition* **2016,** *55* (50), 15583-15588.
9. Lambermont-Thijs, H. M. L.; Fijten, M. W. M.; van der Linden, A. J.; van Lankvelt, B. M.; Bloksma, M. M.; Schubert, U. S.; Hoogenboom, R., *Macromolecules* **2011,** *44* (11), 4320-4325.
10. M. Beck, P. B., U. Eicken, H. Fischer, W. E. Fristad, B. Hase and H.-J. Krause, *Angewandte Makromolekulare Chemie.* **1994,** *223* (217).
11. Witte, H. S., W., *Justus Liebigs Ann. Chem* **1974,** *6*, 996-1009.
12. Wenker, H., *Journal of the American Chemical Society* **1938,** *60* (9), 2152-2153.
13. Zhu, J.; Zhou, M.; Jiang, W.; Zhou, Y.; Song, G.; Liu, R., *Tetrahedron Letters* **2022,** *91*, 153637.
14. Verbraeken, B.; Monnery, B. D.; Lava, K.; Hoogenboom, R., *European Polymer Journal* **2017,** *88*, 451-469.
15. Szwarc, M., *Journal of Polymer Science Part A: Polymer Chemistry* **1998,** *36* (1), 9-15.
16. Wiesbrock, F.; Hoogenboom, R.; Leenen, M. A. M.; Meier, M. A. R.; Schubert, U. S., *Macromolecules* **2005,** *38* (12), 5025-5034.
17. Hoogenboom, R.; Fijten, M. W. M.; Kickelbick, G.; Schubert, U. S., *Beilstein Journal of Organic Chemistry* **2010,** *6*, 773-783.

18. Zhang, N.; Huber, S.; Schulz, A.; Luxenhofer, R.; Jordan, R., *Macromolecules* **2009,** *42* (6), 2215-2221.

19. Saegusa, T.; Ikeda, H., *Macromolecules* **1973,** *6* (6), 808-811.

20. Dworak, A., *Macromolecular Chemistry and Physics* **1998,** *199* (9), 1843-1849.

21. Vergaelen, M.; Verbraeken, B.; Monnery, B. D.; Hoogenboom, R., *ACS Macro Letters* **2015,** *4* (8), 825-828.

22. Monnery, B. D.; Shaunak, S.; Thanou, M.; Steinke, J. H. G., *Macromolecules* **2015,** *48* (10), 3197-3206.

23. Fijten, M. W. M.; Hoogenboom, R.; Schubert, U. S., *Journal of Polymer Science Part A: Polymer Chemistry* **2008,** *46* (14), 4804-4816.

24. Nuyken, O.; Maier, G.; Groß, A.; Fischer, H., *Macromolecular Chemistry and Physics* **1996,** *197* (1), 83-95.

25. Mero, A.; Fang, Z.; Pasut, G.; Veronese, F. M.; Viegas, T. X., *Journal of Controlled Release* **2012,** *159* (3), 353-361.

26. Litt, M.; Levy, A.; Herz, J., *Journal of Macromolecular Science: Part A - Chemistry* **1975,** *9* (5), 703-727.

27. Levy, A.; Litt, M., *Journal of Polymer Science Part A-1: Polymer Chemistry* **1968,** *6* (1), 63-72.

28. Guillerm, B.; Monge, S.; Lapinte, V.; Robin, J.-J., *Macromolecular Rapid Communications* **2012,** *33* (19), 1600-1612.

29. Glassner, M.; Vergaelen, M.; Hoogenboom, R., *Polymer International* **2018,** *67* (1), 32-45.

30. Tomalia, D. A.; Sheetz, D. P., *Journal of Polymer Science Part A-1: Polymer Chemistry* **1966,** *4* (9), 2253-2265.

31. Paulus, R. M.; Becer, C. R.; Hoogenboom, R.; Schubert, U. S., *Macromolecular Chemistry and Physics* **2008,** *209* (8), 794-800.

32. Drain, B. A.; Beyer, V. P.; Cattoz, B.; Becer, C. R., *Macromolecules* **2021,** *54* (12), 5549-5556.

33. Weber, C.; Czaplewska, J. A.; Baumgaertel, A.; Altuntas, E.; Gottschaldt, M.; Hoogenboom, R.; Schubert, U. S., *Macromolecules* **2012,** *45* (1), 46-55.

34. Fijten, M. W. M.; Haensch, C.; van Lankvelt, B. M.; Hoogenboom, R.; Schubert, U. S., *Macromolecular Chemistry and Physics* **2008,** *209* (18), 1887-1895.

35. Cesana, S.; Auernheimer, J.; Jordan, R.; Kessler, H.; Nuyken, O., *Macromolecular Chemistry and Physics* **2006,** *207* (2), 183-192.

36. Saegusa, T.; Kobayashi, S.; Yamada, A., *Die Makromolekulare Chemie* **1976,** *177* (8), 2271-2283.

37. Cirpan, A.; Alkan, S.; Toppare, L.; David, G.; Yagci, Y., *European Polymer Journal* **2001,** *37* (11), 2225-2229.

38. Zhao, T.; Drain, B.; Yilmaz, G.; Becer, C. R., *Polymer Chemistry* **2021,** *12* (44), 6392-6403.

39. Guillerm, B.; Monge, S.; Lapinte, V.; Robin, J.-J., *Macromolecules* **2010,** *43* (14), 5964-5970.

40. Jin, R.-H.; Motoyoshi, K.-I., *Journal of Porphyrins and Phthalocyanines* **1999,** *03* (01), 60-64.

41. Pereira, G.; Huin, C.; Morariu, S.; Bennevault-Celton, V.; Guégan, P., *Australian Journal of Chemistry* **2012,** *65* (8), 1145-1155.

42. Einzmann, M.; Binder, W. H., *Journal of Polymer Science Part A: Polymer Chemistry* **2001,** *39* (16), 2821-2831.

43. Giardi, C.; Lapinte, V.; Charnay, C.; Robin, J. J., *Reactive and Functional Polymers* **2009,** *69* (9), 643-649.

44. Hrkach, J. S.; Matyjaszewski, K., *Macromolecules* **1992,** *25* (8), 2070-2075.

45. Jordan, R.; Ulman, A., *Journal of the American Chemical Society* **1998,** *120* (2), 243-247.

46. Christova, D.; Velichkova, R.; Goethals, E. J., *Macromolecular Rapid Communications* **1997,** *18* (12), 1067-1073.

47. Volet, G.; Deschamps, A.-C. L.; Amiel, C., *Journal of Polymer Science Part A: Polymer Chemistry* **2010,** *48* (11), 2477-2485.

48. Diab, C.; Akiyama, Y.; Kataoka, K.; Winnik, F. M., *Macromolecules* **2004,** *37* (7), 2556-2562.

49. Concilio, M.; Nguyen, N.; Becer, C. R., *Polymer Chemistry* **2021,** *12* (30), 4359-4371.

50. Romio, M.; Grob, B.; Trachsel, L.; Mattarei, A.; Morgese, G.; Ramakrishna, S. N.; Niccolai, F.; Guazzelli, E.; Paradisi, C.; Martinelli, E.; Spencer, N. D.; Benetti, E. M., *Journal of the American Chemical Society* **2021,** *143* (45), 19067-19077.

51. Marx, L.; Volet, G.; Amiel, C., *Journal of Polymer Science Part A: Polymer Chemistry* **2011,** *49* (22), 4785-4793.

52. Krieg, A.; Weber, C.; Hoogenboom, R.; Becer, C. R.; Schubert, U. S., *ACS Macro Letters* **2012,** *1* (6), 776-779.

53. Menezes, R. N. L. d.; Felisberti, M. I., *Polymer Chemistry* **2021,** *12*, 4680-4695.

54. Tran, H.; Bergman, H. M.; de la Rosa, V. R.; Maji, S.; Parenti, K. R.; Hoogenboom, R.; Campos, L. M., *Journal of Polymer Science Part A: Polymer Chemistry* **2019,** *57* (12), 1349-1357.

55. Aoi, K.; Motoda, A.; Okada, M.; Imae, T., *Macromolecular Rapid Communications* **1997,** *18* (10), 945-952.

56. Waschinski, C. J.; Herdes, V.; Schueler, F.; Tiller, J. C., *Macromolecular Bioscience* **2005,** *5* (2), 149-156.

57. Volet, G.; Lav, T.-X.; Babinot, J.; Amiel, C., *Macromolecular Chemistry and Physics* **2011,** *212* (2), 118-124.

58. Osawa, S.; Ishii, T.; Takemoto, H.; Osada, K.; Kataoka, K., *European Polymer Journal* **2017,** *88*, 553-561.

59. Hartlieb, M.; Pretzel, D.; Kempe, K.; Kellner, C.; Paulus, R.; Gottschaldt, M.; Schubert, U., *Soft Matter* **2013,** *9*, 4693-4704.

60. Kempe, K.; Rettler, E. F. J.; Paulus, R. M.; Kuse, A.; Hoogenboom, R.; Schubert, U. S., *Polymer* **2013,** *54* (8), 2036-2042.

61. Hoogenboom, R.; Thijs, H. M. L.; Fijten, M. W. M.; Schubert, U. S., *Journal of Polymer Science Part A: Polymer Chemistry* **2007,** *45* (23), 5371-5379.

62. Kranenburg, J. M.; Tweedie, C. A.; Hoogenboom, R.; Wiesbrock, F.; Thijs, H. M. L.; Hendriks, C. E.; Van Vliet, K. J.; Schubert, U. S., *Journal of Materials Chemistry* **2007,** *17* (26), 2713-2721.

63. Levy, A.; Litt, M., *Journal of Polymer Science Part A-1: Polymer Chemistry* **1968,** *6* (7), 1883-1894.

64. Cai, G.; Litt, M. H., *Journal of Polymer Science Part A: Polymer Chemistry* **1992,** *30* (4), 659-669.

65. Hartlieb, M.; Pretzel, D.; Kempe, K.; Fritzsche, C.; Paulus, R. M.; Gottschaldt, M.; Schubert, U. S., *Soft Matter* **2013,** *9* (18), 4693-4704.

66. Zhou, M.; Qian, Y.; Xie, J.; Zhang, W.; Jiang, W.; Xiao, X.; Chen, S.; Dai, C.; Cong, Z.; Ji, Z.; Shao, N.; Liu, L.; Wu, Y.; Liu, R., *Angewandte Chemie International Edition* **2020,** *59* (16), 6412-6419.

67. Miyamoto, M.; Aoi, K.; Saegusa, T., *Macromolecules* **1991,** *24* (1), 11-16.

68. Kempe, K.; Hoogenboom, R.; Schubert, U. S., *Macromolecular Rapid Communications* **2011,** *32* (18), 1484-1489.

69. Kim, J.; Cattoz, B.; Leung, A. H. M.; Parish, J. D.; Becer, C. R., *Macromolecules* **2022,** *55* (11), 4411-4419.

70. Beyer, V. P.; Cattoz, B.; Strong, A.; Schwarz, A.; Becer, C. R., *Macromolecules* **2020,** *53* (8), 2950-2958.

71. Kim, J.; Waldron, C.; Cattoz, B.; Becer, C. R., *Polymer Chemistry* **2020,** *11* (42), 6847-6852.

72. Schlaad, H.; Diehl, C.; Gress, A.; Meyer, M.; Demirel, A. L.; Nur, Y.; Bertin, A., *Macromolecular Rapid Communications* **2010,** *31* (6), 511-525.

73. Hoogenboom, R.; Schlaad, H., *Polymer Chemistry* **2017,** *8* (1), 24-40.

74. Clark, E. A.; Lipson, J. E. G., *Polymer* **2012,** *53* (2), 536-545.

75. Hoogenboom, R.; Thijs, H. M. L.; Jochems, M. J. H. C.; van Lankvelt, B. M.; Fijten, M. W. M.; Schubert, U. S., *Chemical Communications* **2008,** (44), 5758-5760.

76. Lambermont-Thijs, H. M. L.; Kuringen, H. P. C. v.; Put, J. P. W. v. d.; Schubert, U. S.; Hoogenboom, R., *Polymers* **2010,** *2* (3), 188-199.

77. Glassner, M.; Lava, K.; de la Rosa, V. R.; Hoogenboom, R., *Journal of Polymer Science Part A: Polymer Chemistry* **2014,** *52* (21), 3118-3122.

78. Huber, S.; Jordan, R., *Colloid and Polymer Science* **2008,** *286* (4), 395-402.

79. Kempe, K.; Neuwirth, T.; Czaplewska, J.; Gottschaldt, M.; Hoogenboom, R.; Schubert, U. S., *Polymer Chemistry* **2011,** *2* (8), 1737-1743.

80. Bloksma, M. M.; Bakker, D. J.; Weber, C.; Hoogenboom, R.; Schubert, U. S., *Macromolecular Rapid Communications* **2010,** *31* (8), 724-728.

81. Hoogenboom, R.; Lambermont-Thijs, H. M. L.; Jochems, M. J. H. C.; Hoeppener, S.; Guerlain, C.; Fustin, C.-A.; Gohy, J.-F.; Schubert, U. S., *Soft Matter* **2009,** *5* (19), 3590-3592.

82. Hoogenboom, R.; Thijs, H. M. L.; Wouters, D.; Hoeppener, S.; Schubert, U. S., *Soft Matter* **2008,** *4* (1), 103-107.

83. Van Guyse, J. F. R.; Xu, X.; Hoogenboom, R., *Journal of Polymer Science Part A: Polymer Chemistry* **2019,** *57* (24), 2616-2624.

84. Xu, H.; Hu, M.; Yu, X.; Li, Y.; Fu, Y.; Zhou, X.; Zhang, D.; Li, J., *European Journal of Pharmaceutics and Biopharmaceutics* **2015,** *91*, 66-74.

85. Oleszko-Torbus, N.; Utrata-Wesołek, A.; Bochenek, M.; Lipowska-Kur, D.; Dworak, A.; Wałach, W., *Polymer Chemistry* **2020,** *11* (1), 15-33.

86. Rettler, E. F. J.; Kranenburg, J. M.; Lambermont-Thijs, H. M. L.; Hoogenboom, R.; Schubert, U. S., *Macromolecular Chemistry and Physics* **2010,** *211* (22), 2443-2448.

87. Truong, N. P.; Jones, G. R.; Bradford, K. G. E.; Konkolewicz, D.; Anastasaki, A., *Nature Reviews Chemistry* **2021,** *5* (12), 859-869.

88. Gao, H.; Matyjaszewski, K., *Macromolecules* **2006,** *39* (9), 3154-3160.

89. Khan, M.; Guimarães, T. R.; Choong, K.; Moad, G.; Perrier, S.; Zetterlund, P. B., *Macromolecules* **2021,** *54* (2), 736-746.

90. Stamenović, M. M.; Espeel, P.; Baba, E.; Yamamoto, T.; Tezuka, Y.; Du Prez, F. E., *Polymer Chemistry* **2013,** *4* (1), 184-193.

91. Matyjaszewski, K.; Spanswick, J., *Materials Today* **2005,** *8* (3), 26-33.

92. Konkolewicz, D.; Wang, Y.; Krys, P.; Zhong, M.; Isse, A. A.; Gennaro, A.; Matyjaszewski, K., *Polymer Chemistry* **2014,** *5* (15), 4396-4417.

93. Matyjaszewski, K.; Coca, S.; Gaynor, S. G.; Wei, M.; Woodworth, B. E., *Macromolecules* **1997,** *30* (23), 7348-7350.

94. Percec, V.; Guliashvili, T.; Ladislaw, J. S.; Wistrand, A.; Stjerndahl, A.; Sienkowska, M. J.; Monteiro, M. J.; Sahoo, S., *Journal of the American Chemical Society* **2006,** *128* (43), 14156-14165.

95. Tan, L.; Bai, L.; Zhu, H.; Zhang, C.; Chen, L.; Wang, Y.; Cheradame, H., *Journal of Materials Science* **2015,** *50* (14), 4898-4913.

96. Drain, B. A.; Becer, C. R., *European Polymer Journal* **2019,** *119*, 344-351.

97. Eagan, J. M.; Xu, J.; Di Girolamo, R.; Thurber, C. M.; Macosko, C. W.; LaPointe, A. M.; Bates, F. S.; Coates, G. W., *Science* **2017,** *355* (6327), 814-816.

98. Legros, C.; De Pauw-Gillet, M.-C.; Tam, K. C.; Taton, D.; Lecommandoux, S., *Soft Matter* **2015,** *11* (17), 3354-3359.

99. Luxenhofer, R.; Huber, S.; Hytry, J.; Tong, J.; Kabanov, A. V.; Jordan, R., *Journal of Polymer Science Part A: Polymer Chemistry* **2013,** *51* (3), 732-738.

100. Monnery, B. D.; Jerca, V. V.; Sedlacek, O.; Verbraeken, B.; Cavill, R.; Hoogenboom, R., *Angewandte Chemie International Edition* **2018,** *57* (47), 15400-15404.

101. Hoogenboom, R.; Fijten, M. W. M.; Thijs, H. M. L.; van Lankvelt, B. M.; Schubert, U. S., *Designed Monomers and Polymers* **2005,** *8* (6), 659-671.

102. Hoogenboom, R.; Thijs, H. M. L.; Fijten, M. W. M.; van Lankvelt, B. M.; Schubert, U. S., *Journal of Polymer Science Part A: Polymer Chemistry* **2007,** *45* (3), 416-422.

103. Milonaki, Y.; Kaditi, E.; Pispas, S.; Demetzos, C., *Journal Of Polymer Science Part A Polymer Chemistry* **2012,** *50* (6), 1226-1237.

104. Hoogenboom, R.; Thijs, H. M. L.; Wouters, D.; Hoeppener, S.; Schubert, U. S., *Macromolecules* **2008,** *41* (5), 1581-1583.

105. Hoogenboom, R.; Wiesbrock, F.; Leenen, M. A. M.; Thijs, H. M. L.; Huang, H.; Fustin, C.-A.; Guillet, P.; Gohy, J.-F.; Schubert, U. S., *Macromolecules* **2007,** *40* (8), 2837-2843.

106. Fustin, C.-A.; Thijs-Lambermont, H. M. L.; Hoeppener, S.; Hoogenboom, R.; Schubert, U. S.; Gohy, J.-F., *Journal of Polymer Science Part A: Polymer Chemistry* **2010,** *48* (14), 3095-3102.

107. Stafast, L. M.; Weber, C.; Kuchenbrod, M. T.; Hoeppener, S.; Behnke, M.; Schubert, S.; Mehmetaj, K.; Press, A. T.; Bauer, M.; Schubert, U. S., *ACS Applied Polymer Materials* **2022,** *4* (5), 3417-3425.

108. Daubian, D.; Gaitzsch, J.; Meier, W., *Polymer Chemistry* **2020,** *11* (6), 1237-1248.

109. Monnery, B. D.; Hoogenboom, R., *Polymer Chemistry* **2019,** *10* (25), 3480-3487.

110. Lübtow, M. M.; Mrlik, M.; Hahn, L.; Altmann, A.; Beudert, M.; Lühmann, T.; Luxenhofer, R., *Journal of Functional Biomaterials* **2019,** *10* (3).

111. Drain, B. A.; Beyer, V. P.; Cattoz, B.; Becer, C. R., *Macromolecules* **2021,** *54* (12), 5549-5556.

112. Becer, C. R.; Paulus, R. M.; Höppener, S.; Hoogenboom, R.; Fustin, C.-A.; Gohy, J.-F.; Schubert, U. S., *Macromolecules* **2008,** *41* (14), 5210-5215.

113. Yu, Y. C.; Cho, H. S.; Yu, W.-R.; Youk, J. H., *Polymer* **2014,** *55* (23), 5986-5990.

114. Menezes, R. N. L. d.; Felisberti, M. I., *Polymer Chemistry* **2021,** *12* (32), 4680-4695.

115. Guillerm, B.; Monge, S.; Lapinte, V.; Robin, J.-J., *Journal of Polymer Science Part A: Polymer Chemistry* **2013,** *51* (5), 1118-1128.

116. Willersinn, J.; Schmidt, B. V. K. J., *Polymers* **2017,** *9* (7), 293.

117. Zhou, Y.; Wu, P., *Polymer* **2018,** *153*, 250-261.

118. Willersinn, J.; Schmidt, B. V. K. J., *Journal of Polymer Science Part A: Polymer Chemistry* **2017,** *55* (22), 3757-3766.

119. Rudolph, T.; von der Lühe, M.; Hartlieb, M.; Norsic, S.; Schubert, U. S.; Boisson, C.; D'Agosto, F.; Schacher, F. H., *ACS Nano* **2015,** *9* (10), 10085-10098.

120. Osawa, S.; Osada, K.; Hiki, S.; Dirisala, A.; Ishii, T.; Kataoka, K., *Biomacromolecules* **2016,** *17* (1), 354-361.

121. Ozkose, U. U.; Yilmaz, O.; Alpturk, O., *Polymer Bulletin* **2020,** *77* (11), 5647-5662.

122. Oleszko-Torbus, N.; Mendrek, B.; Kowalczuk, A.; Utrata-Wesolek, A.; Dworak, A.; Walach, W., *Materials* **2020,** *13* (15).

123. Jeong, J. H.; Song, S. H.; Lim, D. W.; Lee, H.; Park, T. G., *Journal Of Controlled Release* **2001,** *73* (2-3), 391-399.

124. Blakney, A. K.; Liu, R.; Yilmaz, G.; Abdouni, Y.; McKay, P. F.; Bouton, C. R.; Shattock, R. J.; Becer, C. R., *Polymer Chemistry* **2020,** *11* (22), 3768-3774.

125. Blakney, A. K.; Abdouni, Y.; Yilmaz, G.; Liu, R.; McKay, P. F.; Bouton, C. R.; Shattock, R. J.; Becer, C. R., *Biomacromolecules* **2020,** *21* (6), 2482-2492.

126. Delecourt, G.; Plet, L.; Bennevault, V.; Guegan, P., *ACS Applied Polymer Materials* **2020,** *2* (7), 2696-2705.

127. van Kuringen, H. P. C.; de la Rosa, V. R.; Fijten, M. W. M.; Heuts, J. P. A.; Hoogenboom, R., *Macromolecular Rapid Communications* **2012,** *33* (9), 827-832.

128. Delecourt, G.; Plet, L.; Bennevault, V.; Guégan, P., *ACS Applied Polymer Materials* **2020,** *2* (7), 2696-2705.

129. Hertz, D.; Leiske, M.; Wloka, T.; Traeger, A.; Hartlieb, M.; Kessels, M.; Schubert, S.; Qualmann, B.; Schubert, U., *Journal of Polymer Science Part A: Polymer Chemistry* **2018,** *56* (12), 1210-1224.

130. He, Z.; Miao, L.; Jordan, R.; S-Manickam, D.; Luxenhofer, R.; Kabanov, A. V., *Macromolecular Bioscience* **2015,** *15* (7), 1004-1020.

131. Hoogenboom, R.; Fijten, M. W. M.; Schubert, U. S., *Journal of Polymer Science Part A: Polymer Chemistry* **2004,** *42* (8), 1830-1840.

132. Hoogenboom, R.; Fijten, M. W. M.; Meier, M. A. R.; Schubert, U. S., *Macromolecular Rapid Communications* **2003,** *24* (1), 92-97.

133. Altuntaş, E.; Weber, C.; Kempe, K.; Schubert, U. S., *European Polymer Journal* **2013,** *49* (8), 2172-2185.

134. Park, J.-S.; Kataoka, K., *Macromolecules* **2007,** *40* (10), 3599-3609.

135. Weber, C.; Becer, R. C.; Baumgaertel, A.; Hoogenboom, R.; Schubert, U. S., *Designed Monomers and Polymers* **2009,** *12* (2), 149-165.

136. Town, J. S.; Jones, G. R.; Haddleton, D. M., *Polymer Chemistry* **2018,** *9* (37), 4631-4641.

137. Su, G.; Jiang, H.; Xu, B.; Yu, Y.; Chen, X., *Molecular Pharmaceutics* **2018,** *15* (11), 5019-5030.

138. Harris, J. M.; Chess, R. B., *Nature Reviews Drug Discovery* **2003,** *2* (3), 214-221.

139. Garay, R. P.; El-Gewely, R.; Armstrong, J. K.; Garratty, G.; Richette, P., *Expert Opinion on Drug Delivery* **2012,** *9* (11), 1319-1323.

140. Luxenhofer, R.; Sahay, G.; Schulz, A.; Alakhova, D.; Bronich, T. K.; Jordan, R.; Kabanov, A. V., *Journal of Controlled Release* **2011,** *153* (1), 73-82.

141. Luxenhofer, R.; Han, Y.; Schulz, A.; Tong, J.; He, Z.; Kabanov, A. V.; Jordan, R., *Macromolecular Rapid Communications* **2012,** *33* (19), 1613-1631.

142. Bauer, M.; Lautenschlaeger, C.; Kempe, K.; Tauhardt, L.; Schubert, U. S.; Fischer, D., *Macromolecular Bioscience* **2012,** *12* (7), 986-998.

143. Hopewell, J. W.; Duncan, R.; Wilding, D.; Chakrabarti, K., *Human & Experimental Toxicology* **2001,** *20* (9), 461-470.

144. Li, J.; Zhou, Y.; Li, C.; Wang, D.; Gao, Y.; Zhang, C.; Zhao, L.; Li, Y.; Liu, Y.; Li, X., *Bioconjugate Chemistry* **2015,** *26* (1), 110-119.

145. Sedlacek, O.; Monnery, B. D.; Mattova, J.; Kucka, J.; Panek, J.; Janouskova, O.; Hocherl, A.; Verbraeken, B.; Vergaelen, M.; Zadinova, M.; Hoogenboom, R.; Hruby, M., *Biomaterials* **2017,** *146*, 1-12.

146. Datta, S.; Jutková, A.; Šrámková, P.; Lenkavská, L.; Huntošová, V.; Chorvát, D.; Miškovský, P.; Jancura, D.; Kronek, J., *Biomacromolecules* **2018,** *19* (7), 2459-2471.

147. Cagli, E.; Ugur, E.; Ulusan, S.; Banerjee, S.; Erel-Goktepe, I., *European Polymer Journal* **2019,** *114*, 452-463.

148. Haktaniyan, M.; Atilla, S.; Cagli, E.; Erel-Goktepe, I., *Polymer International* **2017,** *66* (12), 1851-1863.

149. Sharma, V.; Paramasivam, G.; Vergaelen, M.; Hoogenboom, R.; Sundaramurthy, A., *ACS Applied Bio Materials* **2021,** *4* (9), 7134-7146.

150. Schulz, A.; Jaksch, S.; Schubel, R.; Wegener, E.; Di, Z.; Han, Y.; Meister, A.; Kressler, J.; Kabanov, A. V.; Luxenhofer, R.; Papadakis, C. M.; Jordan, R., *ACS Nano* **2014,** *8* (3), 2686-2696.

151. Sedlacek, O.; Bardoula, V.; Vuorimaa-Laukkanen, E.; Gedda, L.; Edwards, K.; Radulescu, A.; Mun, G. A.; Guo, Y.; Zhou, J.; Zhang, H.; Nardello-Rataj, V.; Filippov, S.; Hoogenboom, R., *Small* **2022,** *18* (17), 2106251.

152. Wilson, P.; Ke, P. C.; Davis, T. P.; Kempe, K., *European Polymer Journal* **2017,** *88*, 486-515.

153. Raveendran, R.; Mullen, K. M.; Wellard, R. M.; Sharma, C. P.; Hoogenboom, R.; Dargaville, T. R., *European Polymer Journal* **2017,** *93*, 682-694.

154. Luxenhofer, R.; Schulz, A.; Roques, C.; Li, S.; Bronich, T. K.; Batrakova, E. V.; Jordan, R.; Kabanov, A. V., *Biomaterials* **2010,** *31* (18), 4972-4979.

155. Hannon, G. J., *Nature* **2002,** *418* (6894), 244-251.

156. Park, K. S.; Sun, X.; Aikins, M. E.; Moon, J. J., *Advanced Drug Delivery Reviews* **2021,** *169*, 137-151.

157. Polack, F. P.; Thomas, S. J.; Kitchin, N.; Absalon, J.; Gurtman, A.; Lockhart, S.; Perez, J. L.; Pérez Marc, G.; Moreira, E. D.; Zerbini, C.; Bailey, R.; Swanson, K. A.; Roychoudhury, S.; Koury, K.; Li, P.; Kalina, W. V.; Cooper, D.; Frenck, R. W.; Hammitt, L. L.; Türeci, Ö.; Nell, H.; Schaefer, A.; Ünal, S.; Tresnan, D. B.; Mather, S.; Dormitzer, P. R.; Şahin, U.; Jansen, K. U.; Gruber, W. C., *New England Journal of Medicine* **2020,** *383* (27), 2603-2615.

158. Baden, L. R.; El Sahly, H. M.; Essink, B.; Kotloff, K.; Frey, S.; Novak, R.; Diemert, D.; Spector, S. A.; Rouphael, N.; Creech, C. B.; McGettigan, J.; Khetan, S.; Segall, N.; Solis, J.; Brosz, A.; Fierro, C.; Schwartz, H.; Neuzil, K.; Corey, L.; Gilbert, P.; Janes, H.; Follmann, D.; Marovich, M.; Mascola, J.; Polakowski, L.; Ledgerwood, J.; Graham, B. S.; Bennett, H.; Pajon, R.; Knightly, C.; Leav, B.; Deng,

W.; Zhou, H.; Han, S.; Ivarsson, M.; Miller, J.; Zaks, T., *New England Journal of Medicine* **2020,** *384* (5), 403-416.

159. Bauer, M.; Tauhardt, L.; Lambermont-Thijs, H. M. L.; Kempe, K.; Hoogenboom, R.; Schubert, U. S.; Fischer, D., *European Journal Of Pharmaceutics And Biopharmaceutics* **2018,** *133*, 112-121.

160. Mees, M.; Haladjova, E.; Momekova, D.; Momekov, G.; Shestakova, P. S.; Tsvetanov, C. B.; Hoogenboom, R.; Rangelov, S., *Biomacromolecules* **2016,** *17* (11), 3580-3590.

161. Blakney, A. K.; Yilmaz, G.; McKay, P. F.; Becer, C. R.; Shattock, R. J., *Biomacromolecules* **2018,** *19* (7), 2870-2879.

162. Zhou, M.; Jiang, W.; Xie, J.; Zhang, W.; Ji, Z.; Zou, J.; Cong, Z.; Xiao, X.; Gu, J.; Liu, R., *ChemMedChem* **2021,** *16* (2), 309-315.

163. Jiang, W.; Zhou, M.; Cong, Z.; Xie, J.; Zhang, W.; Chen, S.; Zou, J.; Ji, Z.; Shao, N.; Chen, X.; Li, M.; Liu, R., *Angewandte Chemie International Edition* **2022,** *61* (17), e202200778.

164. Kaberov, L. I.; Kaberova, Z.; Murmiliuk, A.; Trousil, J.; Sedláček, O.; Konefal, R.; Zhigunov, A.; Pavlova, E.; Vít, M.; Jirák, D.; Hoogenboom, R.; Filippov, S. K., *Biomacromolecules* **2021,** *22* (7), 2963-2975.

165. Kolouchova, K.; Sedlacek, O.; Jirak, D.; Babuka, D.; Blahut, J.; Kotek, J.; Vit, M.; Trousil, J.; Konefał, R.; Janouskova, O.; Podhorska, B.; Slouf, M.; Hruby, M., *Biomacromolecules* **2018,** *19* (8), 3515-3524.

166. Kaberov, L. I.; Verbraeken, B.; Riabtseva, A.; Brus, J.; Radulescu, A.; Talmon, Y.; Stepanek, P.; Hoogenboom, R.; Filippov, S. K., *Macromolecules* **2018,** *51* (15), 6047-6056.

167. Craik, D. J., *Science* **2006,** *311* (5767), 1563-1564.

168. Jung, Y.; Kim, J.-H.; Jang, W.-D., *European Polymer Journal* **2017,** *88*, 605-612.

169. Schroffenegger, M.; Leitner, N. S.; Morgese, G.; Ramakrishna, S. N.; Willinger, M.; Benetti, E. M.; Reimhult, E., *ACS Nano* **2020,** *14* (10), 12708-12718.

170. Trachsel, L.; Romio, M.; Zenobi-Wong, M.; Benetti, E. M., *Macromolecular Rapid Communications* **2021,** *42* (7), 2000658.

171. Yan, W.; Divandari, M.; Rosenboom, J.-G.; Ramakrishna, S. N.; Trachsel, L.; Spencer, N. D.; Morgese, G.; Benetti, E. M., *Polymer Chemistry* **2018,** *9* (19), 2580-2589.

172. Tornøe, C. W.; Christensen, C.; Meldal, M., *The Journal of Organic Chemistry* **2002,** *67* (9), 3057-3064.

173. Ali, M. W.; Muhammad, Z.; Jia, Q.; Li, L.; Saleem, M.; Siddiq, M.; Chen, Y., *Polymer Chemistry* **2020,** *11* (25), 4164-4171.

174. Huettner, N.; Goldmann, A. S.; Hoogenboom, R.; Dargaville, T. R., *Polymer Chemistry* **2022,** *13* (27), 3975-3980.

175. Morgese, G.; Causin, V.; Maggini, M.; Corrà, S.; Gross, S.; Benetti, E. M., *Chemistry of Materials* **2015,** *27* (8), 2957-2964.

176. Willinger, M.; Reimhult, E., *The Journal of Physical Chemistry B* **2021,** *125* (25), 7009-7023.

177. Morgese, G.; Cavalli, E.; Rosenboom, J.-G.; Zenobi-Wong, M.; Benetti, E. M., *Angewandte Chemie International Edition* **2018,** *57* (6), 1621-1626.

178. Jeong, Y.; Jin, Y.; Chang, T.; Uhlik, F.; Roovers, J., *Macromolecules* **2017,** *50* (19), 7770-7776.

179. Hadziioannou, G.; Cotts, P. M.; ten Brinke, G.; Han, C. C.; Lutz, P.; Strazielle, C.; Rempp, P.; Kovacs, A. J., *Macromolecules* **1987,** *20* (3), 493-497.

180. Arrighi, V.; Gagliardi, S.; Dagger, A. C.; Semlyen, J. A.; Higgins, J. S.; Shenton, M. J., *Macromolecules* **2004,** *37* (21), 8057-8065.

181. Morgese, G.; Shirmardi Shaghasemi, B.; Causin, V.; Zenobi-Wong, M.; Ramakrishna, S. N.; Reimhult, E.; Benetti, E. M., *Angewandte Chemie International Edition* **2017,** *56* (16), 4507-4511.

182. Klein, J.; Kumacheva, E.; Mahalu, D.; Perahia, D.; Fetters, L. J., *Nature* **1994,** *370* (6491), 634-636.

183. Schorr, P. A.; Kwan, T. C. B.; Kilbey, S. M.; Shaqfeh, E. S. G.; Tirrell, M., *Macromolecules* **2003,** *36* (2), 389-398.

184. Divandari, M.; Trachsel, L.; Yan, W.; Rosenboom, J.-G.; Spencer, N. D.; Zenobi-Wong, M.; Morgese, G.; Ramakrishna, S. N.; Benetti, E. M., *ACS Macro Letters* **2018,** *7* (12), 1455-1460.

185. Cortez, M. A.; Godbey, W. T.; Fang, Y.; Payne, M. E.; Cafferty, B. J.; Kosakowska, K. A.; Grayson, S. M., *Journal of the American Chemical Society* **2015,** *137* (20), 6541-6549.

186. Taranejoo, S.; Liu, J.; Verma, P.; Hourigan, K., *Journal of Applied Polymer Science* **2015,** *132* (25).

187. Ren, J. M.; McKenzie, T. G.; Fu, Q.; Wong, E. H. H.; Xu, J.; An, Z.; Shanmugam, S.; Davis, T. P.; Boyer, C.; Qiao, G. G., *Chemical Reviews* **2016,** *116*, 6743-6836.

188. Plet, L.; Delecourt, G.; Hanafi, M.; Pantoustier, N.; Pembouong, G.; Midoux, P.; Bennevault, V.; Guégan, P., *European Polymer Journal* **2020,** *122*, 109323.

189. Luxenhofer, R.; Bezen, M.; Jordan, R., *Macromolecular Rapid Communications* **2008,** *29* (18), 1509-1513.

190. McAlvin, J. E.; Fraser, C. L., *Macromolecules* **1999,** *32* (5), 1341-1347.

191. McAlvin, J. E.; Scott, S. B.; Fraser, C. L., *Macromolecules* **2000,** *33* (19), 6953-6964.

192. Huin, C.; Eskandani, Z.; Badi, N.; Farcas, A.; Bennevault-Celton, V.; Guégan, P., *Carbohydrate Polymers* **2013,** *94* (1), 323-331.

193. Ferreira, J.; Syrett, J.; Whittaker, M.; Haddleton, D.; Davis, T. P.; Boyer, C., *Polymer Chemistry* **2011,** *2* (8), 1671-1677.

194. Brummelhuis, N. t.; Schlaad, H., *Polymer Chemistry* **2011,** *2* (5), 1180-1184.

195. Uchiyama, M.; Satoh, K.; McKenzie, T. G.; Fu, Q.; Qiao, G. G.; Kamigaito, M., *Polymer Chemistry* **2017,** *8* (38), 5972-5981.

196. Monaco, A.; Drain, B.; Becer, C. R., *Polymer Chemistry* **2021,** *12* (36), 5229-5238.

197. Sulistio, A.; Widjaya, A.; Blencowe, A.; Zhang, X.; Qiao, G., *Chemical Communications* **2011,** *47* (4), 1151-1153.

198. ten Brummelhuis, N.; Secker, C.; Schlaad, H., *Macromolecular Rapid Communications* **2012,** *33* (19), 1690-1694.

199. Alvaradejo, G. G.; Nguyen, H. V. T.; Harvey, P.; Gallagher, N. M.; Le, D.; Ottaviani, M. F.; Jasanoff, A.; Delaittre, G.; Johnson, J. A., *ACS Macro Letters* **2019,** *8* (4), 473-478.

200. Hayes, G.; Drain, B.; Becer, C. R., *Macromolecules* **2022,** *55* (1), 146-155.

201. Lambermont-Thijs, H. M. L.; Fijten, M. W. M.; Schubert, U. S.; Hoogenboom, R., *Australian Journal of Chemistry* **2011,** *64* (8), 1026-1032.

202. Rudolph, T.; Crotty, S.; Von der Lühe, M.; Pretzel, D.; Schubert, U. S.; Schacher, F. H., *Polymers* **2013,** *5* (3), 1081-1101.

203. Zhang, C.; Liu, S.; Tan, L.; Zhu, H.; Wang, Y., *Journal of Materials Chemistry B* **2015,** *3* (27), 5615-5628.

204. Rudolph, T.; Crotty, S.; Schubert, U. S.; Schacher, F. H., *e-Polymers* **2015,** *15* (4), 227-235.

205. von der Ehe, C.; Kempe, K.; Bauer, M.; Baumgaertel, A.; Hager, M. D.; Fischer, D.; Schubert, U. S., *Macromolecular Chemistry and Physics* **2012,** *213* (20), 2146-2156.

206. Bullet, J.-R.; Korchagina, E. V.; Winnik, F. M., *Macromolecules* **2021,** *54* (13), 6161-6170.

207. Schmidt, B. V. K. J.; Rudolph, T.; Hetzer, M.; Ritter, H.; Schacher, F. H.; Barner-Kowollik, C., *Polymer Chemistry* **2012,** *3* (11), 3139-3145.

208. Podzimek, S., *Journal of Applied Polymer Science* **1994,** *54* (1), 91-103.

209. Wyatt, P. J., *Analytica Chimica Acta* **1993,** *272* (1), 1-40.

210. Zimm, B. H.; Kilb, R. W., *Journal of Polymer Science* **1959,** *37* (131), 19-42.

211. Massey, J. A.; Kulbaba, K.; Winnik, M. A.; Manners, I., *Journal of Polymer Science Part B: Polymer Physics* **2000,** *38* (23), 3032-3041.

212. Balke, S. T.; Mourey, T. H.; Robello, D. R.; Davis, T. A.; Kraus, A.; Skonieczny, K., *Journal of Applied Polymer Science* **2002,** *85* (3), 552-570.

213. Bohdanecky, M., *Macromolecules* **1977,** *10* (5), 971-975.

214. Adam, M.; Delsanti, M., *Macromolecules* **1977,** *10* (6), 1229-1237.

215. Li, M.; Guo, J.-W.; Wen, W.-Q.; Chen, J.-K., *Nanomaterials* **2019,** *9* (4), 547.

216. Braunová, A.; Chytil, P.; Laga, R.; Šírová, M.; Machová, D.; Parnica, J.; Říhová, B.; Janoušková, O.; Etrych, T., *Journal of Controlled Release* **2020,** *321*, 718-733.

217. England, R. M.; Moss, J. I.; Gunnarsson, A.; Parker, J. S.; Ashford, M. B., *Biomacromolecules* **2020,** *21* (8), 3332-3341.

218. Zhao, F.; Yin, H.; Zhang, Z.; Li, J., *Biomacromolecules* **2013,** *14* (2), 476-484.

219. Chen, H.; Li, G.; Chi, H.; Wang, D.; Tu, C.; Pan, L.; Zhu, L.; Qiu, F.; Guo, F.; Zhu, X., *Bioconjugate Chemistry* **2012,** *23* (9), 1915-1924.

220. Cheng, H.; Fan, X.; Wu, C.; Wang, X.; Wang, L.-J.; Loh, X. J.; Li, Z.; Wu, Y.-L., *Macromolecular Rapid Communications* **2019,** *40* (5), 1800207.

221. Whitfield, R.; Anastasaki, A.; Truong, N. P.; Cook, A. B.; Omedes-Pujol, M.; Loczenski Rose, V.; Nguyen, T. A. H.; Burns, J. A.; Perrier, S.; Davis, T. P.; Haddleton, D. M., *ACS Macro Letters* **2018,** *7* (8), 909-915.

222. Rasolonjatovo, B.; Pitard, B.; Haudebourg, T.; Bennevault, V.; Guégan, P., *European Polymer Journal* **2017,** *88*, 689-700.

223. Lin, W.; Yao, N.; Li, H.; Hanson, S.; Han, W.; Wang, C.; Zhang, L., *Polymers* **2016,** *8* (11), 397.

224. Nguyen, H. V. T.; Chen, Q.; Paletta, J. T.; Harvey, P.; Jiang, Y.; Zhang, H.; Boska, M. D.; Ottaviani, M. F.; Jasanoff, A.; Rajca, A.; Johnson, J. A., *ACS Central Science* **2017,** *3* (7), 800-811.

225. Nguyen, H. V. T.; Detappe, A.; Gallagher, N. M.; Zhang, H.; Harvey, P.; Yan, C.; Mathieu, C.; Golder, M. R.; Jiang, Y.; Ottaviani, M. F.; Jasanoff, A.; Rajca, A.; Ghobrial, I.; Ghoroghchian, P. P.; Johnson, J. A., *ACS Nano* **2018,** *12* (11), 11343-11354.

226. Guan, X.; Meng, L.; Jin, Q.; Lu, B.; Chen, Y.; Li, Z.; Wang, L.; Lai, S.; Lei, Z., *Macromolecular Materials and Engineering* **2018,** *303* (6), 1700553.

227. Rauch, F.; Endres, P.; Friedrich, A.; Sieh, D.; Hähnel, M.; Krummenacher, I.; Braunschweig, H.; Finze, M.; Ji, L.; Marder, T. B., *Chemistry – A European Journal* **2020,** *26* (57), 12951-12963.

228. Grayson, S. M.; Fréchet, J. M. J., *Chemical Reviews* **2001,** *101* (12), 3819-3868.

229. Gao, Y.; Zhou, D.; Lyu, J.; A, S.; Xu, Q.; Newland, B.; Matyjaszewski, K.; Tai, H.; Wang, W., *Nature Reviews Chemistry* **2020,** *4* (4), 194-212.

230. Zahoranová, A.; Kroneková, Z.; Zahoran, M.; Chorvát Jr, D.; Janigová, I.; Kronek, J., *Journal of Polymer Science Part A: Polymer Chemistry* **2016,** *54* (11), 1548-1559.

231. Kelly, A. M.; Hecke, A.; Wirnsberger, B.; Wiesbrock, F., *Macromolecular Rapid Communications* **2011,** *32* (22), 1815-1819.

232. Böhme, F.; Clausnitzer, C.; Gruber, F.; Grutke, S.; Huber, T.; Pötschke, P.; Voit, B., *High Performance Polymers* **2001,** *13* (2), S21-S31.

233. Ali, M. W.; Cheng, S.; Si, J.; Siddiq, M.; Ye, X., *Journal of Polymer Science Part A: Polymer Chemistry* **2019,** *57* (19), 2030-2037.

234. Simon, P. F. W.; Müller, A. H. E.; Pakula, T., *Macromolecules* **2001,** *34* (6), 1677-1684.

235. Humphries, J.; Pizzi, D.; Sonderegger, S. E.; Fletcher, N. L.; Houston, Z. H.; Bell, C. A.; Kempe, K.; Thurecht, K. J., *Biomacromolecules* **2020,** *21* (8), 3318-3331.

236. Yang, J.; He, Q.; Lin, H.; Fan, J.; Bai, F., *Macromolecular Rapid Communications* **2001,** *22* (14), 1152-1157.

237. Xinling, W.; Jianjun, C.; Ling, H.; Xiaozhen, T., *Journal of Polymer Science Part B: Polymer Physics* **2001,** *39* (19), 2225-2230.

238. Gao, C.; Yan, D., *Progress in Polymer Science* **2004,** *29* (3), 183-275.

Chapter 2. Multiarm Core Cross-linked Star Shaped Poly(2-Oxazoline)s and Hyperbranched Polymers Using a Bisfunctional 2-Oxazoline Monomer

Part of this chapter has been published in the following article:

Hayes, G.; B. Drain., C.R. Becer. Macromolecules, 2022. 55(1): p. 146-155.

Part of this chapter has been published in the following article:

Hayes, G.; Becer, C.R.; *European Polymer Journal,* 2022. 181, 111678.

2.1. Introduction

Branched polymers are a very interesting class of polymeric structure with unique properties. Branching can be used to synthesise very large polymeric species with interesting solution behaviour due to their unusually low intrinsic viscosities relative to their molecular weights. In this chapter, the synthesis and analysis of star polymers and hyperbranched polymers made from poly(2-oxazoline)s are discussed.

Star shaped polymers are a unique type of complex three-dimensional structure that have fascinating properties leading to a wide range of potential applications.[1-5] The extent of branching possible from star polymers result in low viscosity systems with high degrees of flexibility.[6-8] These features can be exploited to use star polymers for viscosity modification,[9-11] or to encapsulate small molecules such as drugs for therapeutic applications.[12-14] Furthermore, the capacity for drug encapsulation and release can be further enhanced by the method of star synthesis employed, and the monomer class chosen for the arms.[15]

In **Chapter 1**, the three main approaches to star polymer synthesis were discussed: the core-first, the grafting-onto, and the arm-first or core cross-linked (CCS) approach. As mentioned, the core-first approach has the disadvantages of producing stars which are small in size, with a limited number of arms that are difficult to characterise.[16, 17] The grafting-onto approach is the least suitable for industrial applications as multiple purification steps and long reaction times are often required.[18] Stars synthesised *via* the CCS method have the disadvantage of being less well-defined and thus more challenging

to analyse. On the other hand, the CCS method allows for the synthesis of stars with hundreds of well-defined arms and large cores making them highly suited for drug encapsulation applications.[19-22] Star polymers *via* a core cross-linked approach have previously been synthesised using a variety of monomers and polymerisation techniques.[23] However, research into poly(2-oxazoline) star polymers is sparse with few literature examples.[16, 24-26]

As well as star polymers, dendrimers are another intriguing class of branched polymer. Dendrimers are monodisperse, perfectly branched, globular polymeric structures. Dendrimers have many potential applications, but due to their extremely high definition they are most useful for biomedical purposes which demand clarity of chemical structure.[27, 28] Nonetheless, dendrimers can be expensive, often requiring difficult and laborious synthetic techniques.[29] Hyperbranched polymers on the other hand are often much easier to synthesise with fewer synthetic steps, and can often be synthesised in a one-pot system.[30] Like dendrimers, hyperbranched polymers also exhibit valuable properties such as high solubility, low viscosity, possession of internal cavities for small molecule storage and transport, and an abundance of functional groups.[31]

Hyperbranched polymers have previously been synthesised with controlled polymerisation techniques using multifunctional vinyl monomers as cross-linkers and a chain transfer agent to control the degree of cross-linking.[32-34] This type of branched polymer synthesis is known as the ‘Strathclyde method’, and is one of the easiest and most common ways to make branched polymers.[35, 36] Previous polymerisation techniques using similar approaches to the Strathclyde method include reversible addition fragmentation chain-

transfer (RAFT) polymerisation,[37] copper-mediated reversible deactivation radical polymerisation (Cu(0)-RDRP),[38] and nitroxide mediated polymerisation (NMP).[39] However, there are limited examples of hyperbranched poly(2-oxazoline)s in the literature, and there are none that use a bis-oxazoline cross-linker. The reason for this is because gelation is extremely prevalent and difficult to control without the use of a chain-transfer agent, of which there is no analogue in the cationic ring opening polymerisation (CROP) of 2-oxazolines. Nonetheless, poly(2-oxazoline) hydrogels have previously been synthesised using a bis-oxazoline cross-linker.[40, 41] The synthesised hydrogels were used for biomedical applications such as drug storage agents,[42] and deoxyribonucleic acid (DNA) binding matrices.[43] The main advantage of a branched polymer compared to a hydrogel is that it is soluble, which makes polymer characterisation easier. It also means branched polymers can be used as homogenous catalysts[44] and can also be mixed as a plasticiser.[45]

In this chapter, core cross-linked star polymers were synthesised using 2-oxazolines. This was performed by synthesising poly(2-ethyl-2-oxazoline) (pEtOx) arms with various lengths and cross-linking them with a bis 2-oxazoline (BisOx) cross-linker to create star shaped polymers (**Scheme 2.1.**). Furthermore, a systematic study of various parameters was carried out, altering the number of equivalents of cross-linker, the polymerisation concentration, and the degree of polymerisation (DP) of the arms. The formed stars were then analysed using advanced gel permeation chromatography (GPC) to elucidate structural information including the average number of arms per star as a function of molecular weight. Finally, the obtained star shaped polymers were compared for their drug encapsulation potential by

encapsulating dihydroxyanthroquinone (DHA) as a model compound. Separately, the BisOx cross-linker was also used to form hyperbranched polymers, with various end-capping agents tested to control the degree of cross-linking.

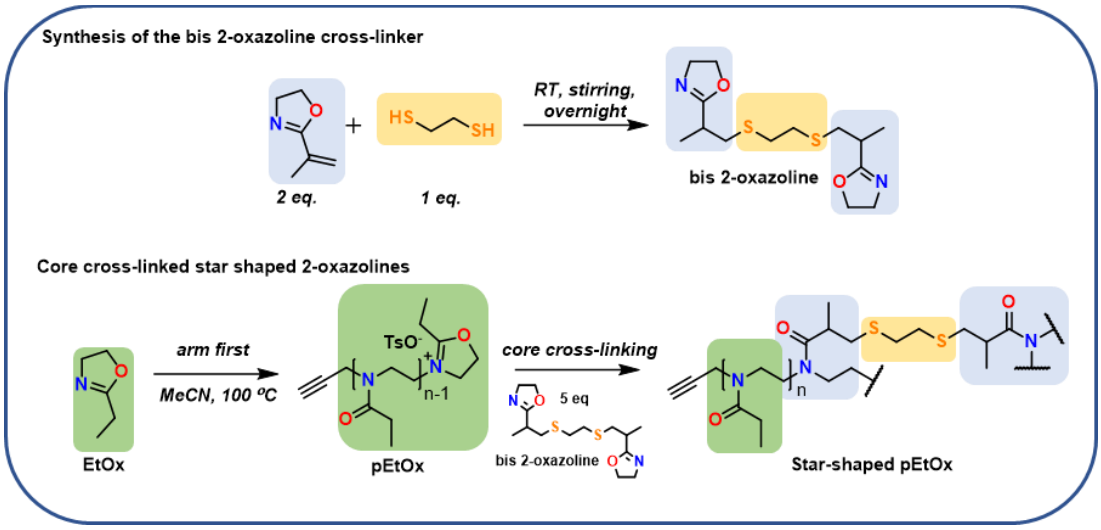

Scheme 2.1. Schematic representation of the synthesis of BisOx cross-linker (top), and the cationic ring opening polymerisation of 2-ethyl-2-oxazoline followed by core cross-linking using the BisOx cross-linker to obtain multiarm star shaped polymers (bottom).

2.2. Results and Discussion

2.2.1. Multiarm Core Cross-linked Star Shaped Poly(2-Oxazoline)s

2.2.1.1. Synthesis of Star Polymers *via* CROP of 2-Oxazolines

As discussed in **Chapter 1**, the structure of 2-oxazolines allows for further polymer functionalisation and tunability *via* their R group. In this case, the R group was exploited to create a bis 2-oxazoline (BisOx) cross-linker *via* a highly efficient thiol-ene click reaction between 2-isopropenyl-2-oxazoline (iPOx) and 1,2-ethanedithiol. No catalyst was required given that iPOx acts as a Michael acceptor, and no purification was required resulting in a straightforward, efficient synthetic route to the cross-linker. This click reaction

was carried out in bulk at room temperature, highlighting a synthetic technique that could easily be scaled up. The progress of the reaction was followed by ^{1}H nuclear magnetic resonance (NMR) spectroscopy to ensure complete conversion **(Figure 2.1.**). Furthermore, the BisOx product was analysed by ^{13}C NMR spectroscopy (**Figure 2.15, additional data**), Fourier transform infrared spectroscopy (FTIR) (**Figure 2.16, additional data)**, and electrospray ionisation mass spectrometry (ESI-MS) (**Figure 2.17, additional data**).

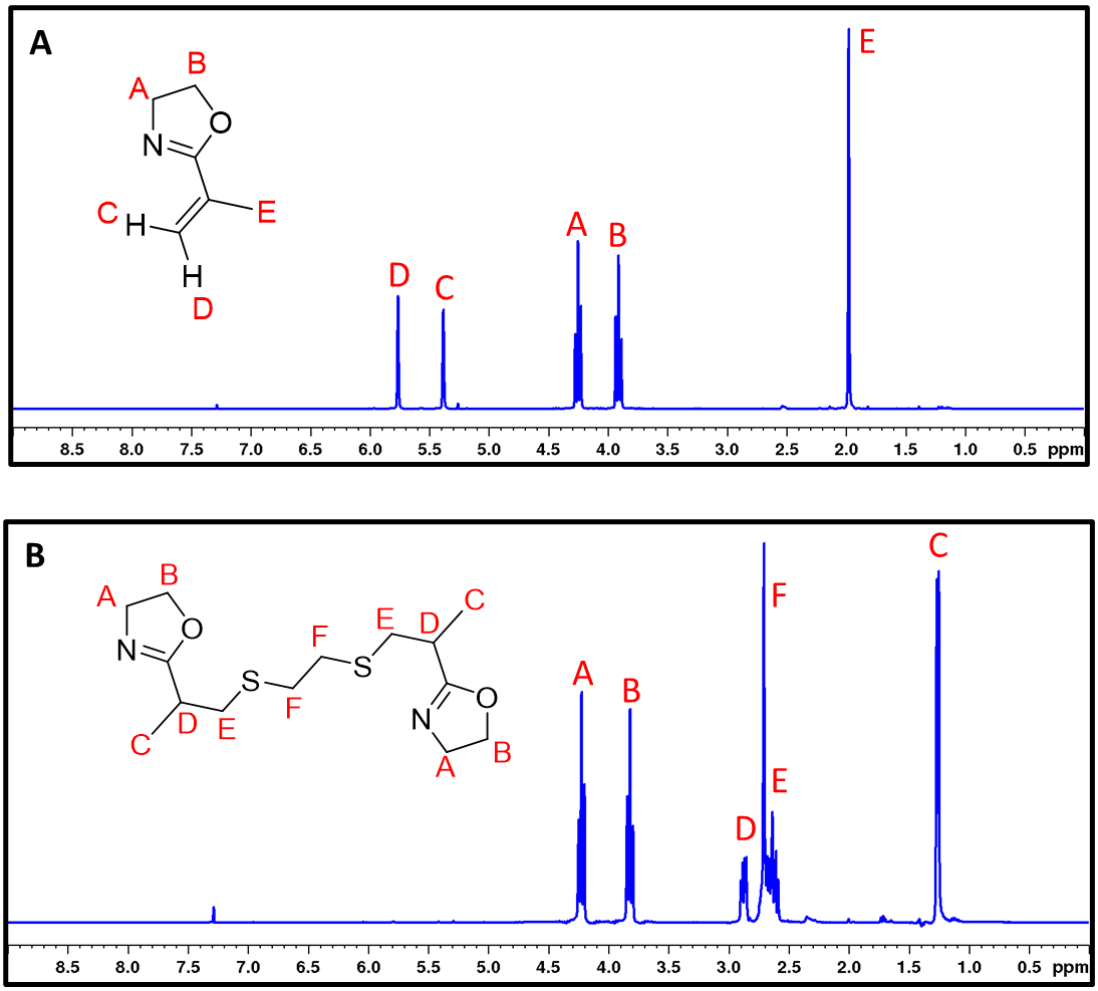

Figure 2.1. ^{1}H NMR spectra of: **(A)** starting material, 2-isopropenyl-2-oxazoline and **(B)** the BisOx product. Reaction progress was monitored by the disappearance of isopropenyl double bond peaks at 5.38 ppm and 5.76 ppm (C and D). All spectra were measured using $CDCl_3$ as the solvent.

The arm-first approach for star polymer synthesis was selected for two reasons. Firstly, the method of synthesis is straightforward as it can be

performed in one pot, and the formed stars can easily be separated from residual monomer by simple precipitation. Secondly, the arm-first approach has the flexibility to create stars with a wide variety of arm numbers and core sizes which allows for investigation into the optimum conditions for drug encapsulation. The fact that one of the main applications of this class of stars is biomedical in nature,[46] coupled with the advantages of using 2-oxazolines (non-toxicity, stealth behaviour, and stimuli-responsivity) provides a synergistic effect that makes this type of star particularly exciting.

For the synthesis of CCS polymers, a systematic approach was taken with the initial aim being to produce large stars with a high number of arms, whilst maximising arm conversion. Arms were synthesised using 2-ethyl-2-oxazoline (EtOx), with a range of degrees of polymerisation (DP) from 25-100 and a range of monomer concentrations from 2 M – 0.5 M. Once quantitative monomer conversion for the arms was reached, BisOx was then injected at 5-20 equivalents to tune the core size. EtOx and BisOx conversions were monitored by ^{1}H NMR spectroscopy, where in each case full consumption of both EtOx and BisOx were observed by the disappearance of the corresponding 2-oxazoline ring peaks at 3.7 and 4.2 ppm (**Figure 2.2.**). The range of polymers synthesised and their features are listed in **Table 2.1.**

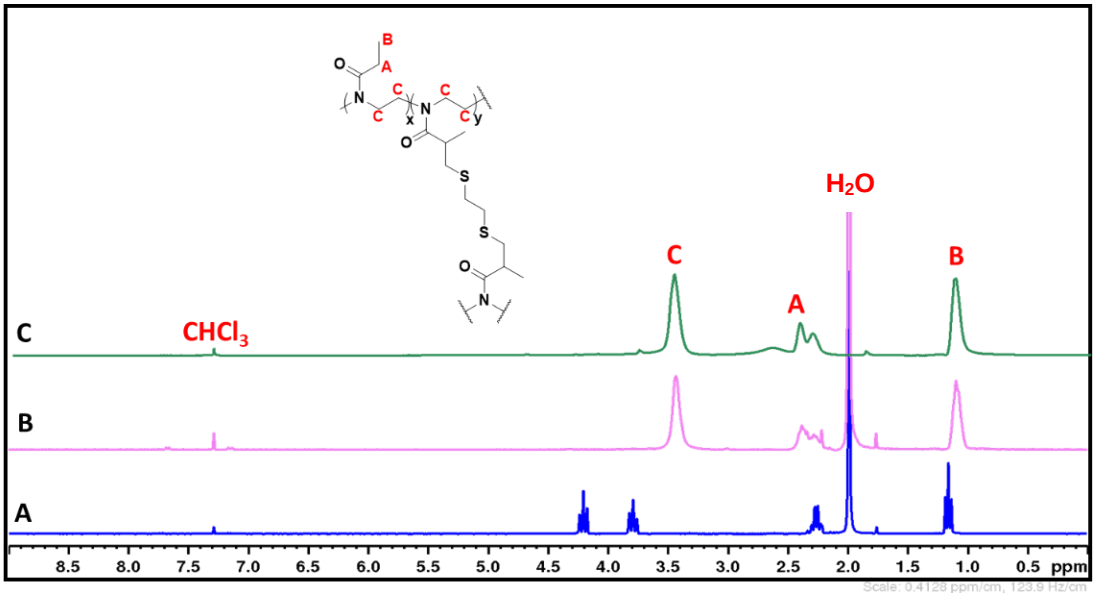

Figure 2.2. ^{1}H NMR Spectra of **S100-3**: **(A)** Initial reaction mixture before arm formation (T_0). **(B)** Reaction mixture after arm formation. **(C)** After addition and consumption of cross-linker. Note the peaks for the BisOx cross-linker are obscured by the main poly(2-ethyl-2-oxazoline) peaks. All spectra were measured using $CDCl_3$ as the solvent.

Table 2.1. List of linear and star shaped polymers prepared *via* CROP. Polymers are sorted by their arm DPs firstly, then sorted by amount of cross-linker, and finally by [M]. Gel column highlights limits to the star synthesis, Y means gelation occurred due to excessive cross-linker or high reaction concentration, whereas N means no gelation occurred and the star polymers are formed.

Entry	*EtOx DP*	*BisOx DP*	*Conc [EtOx]*	*Gel*	*Rel. DHA Encap.[a] (%)*	*Arm Conv.[b] (%)*	*N_{arms}[c]*	*Hydrodynamic Size (nm)[d]*
L1	100	N.D.	N.D.	N.D..	N.D.	N.D.	N.D.	N.D.
S25-1	25	5	0.5	N	57	74	61	9.5
S25-2	25	5	2.0	N	47	77	124	9.3
S25-3	25	10	0.5	Y	N.D.	N.D.	N.D.	N.D.
S50-1	50	5	0.5	N	35	28	7	5.8
S50-2	50	5	1.0	N	47	82	6	6.4
S50-3	50	5	2.0	N	42	30	11	5.8
S50-4	50	10	0.5	N	100	45	60	9.3
S50-5	50	10	1.0	N	62	74	107	12.0
S50-6	50	10	2.0	N	50	57	877	25.8
S50-7	50	20	0.5	N	55	73	213	8.7
S50-8	50	20	1.0	Y	N.D.	N.D.	N.D.	N.D.
S100-1	100	5	0.5	N	38	11	7	5.8
S100-2	100	5	2.0	N	31	53	8	7.4
S100-3	100	10	0.5	N	38	69	108	15.1
S100-4	100	10	2.0	N	35	74	169	15.8
S100-5	100	20	0.5	N	75	81	1002	28.5
S100-6	100	20	2.0	Y	N.D.	N.D.	N.D.	N.D.

[a] Calculated by a relative method described in **Section 2.2.1.6**.
[b] Calculated following GPC integration method described in **Section 2.2.1.2.**
[c] Average number of arms as calculated assuming a polydisperse model with ε=0.75.
[d] Measured by dynamic light scattering (DLS) (intensity setting).

2.2.1.2. Star Polymer Analysis and Characterisation

One of the challenges of using the arm-first approach to form star polymers *via* the CROP of poly(2-oxazoline)s is that a certain proportion of arms generally remain unincorporated and there are two main reasons for this. Firstly, a certain proportion of chains will be terminated by impurities (such as water in CROP) and therefore unable to react further with the cross-linker. It must be noted that this is not a significant factor for CROP if the arm monomer (EtOx in this case) and initiator have been purified and dried rigorously. Indeed CCS polymers prepared *via* other polymerisation techniques such as RAFT polymerisation or Cu(0)-RDRP still show residual arms.[47, 48] Secondly, as the star formation progresses and more arms are incorporated into each star, steric bulk increases around the core resulting in arms being unable to access the core. A further purification step is required to obtain pure star polymers, and so maximising arm conversion is highly desirable. The relative arm conversion percentage was calculated using a GPC chromatogram integration method (**Figure 2.3.**).

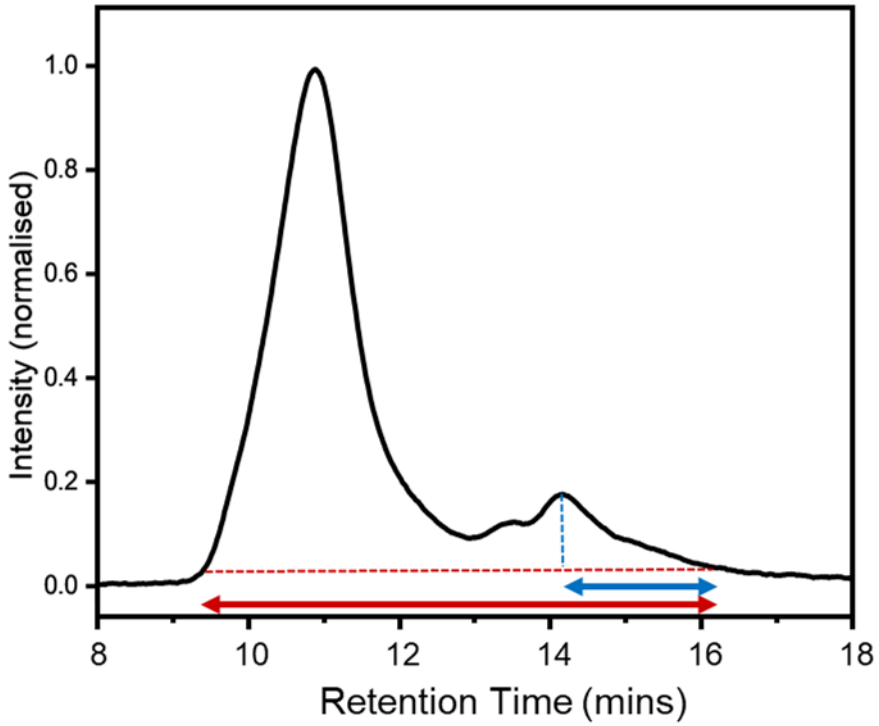

Figure 2.3. GPC trace of **S100-5** highlighting areas used for arm conversion calculation. The blue area indicates half of the residual arm whilst the red area is the total area. In this case, the arm conversion was calculated at 81%. Sample was measured on a DMF GPC instrument.

From the areas in **Figure 2.3**, the arm conversion was calculated using the following equation:

$$residual\ arm\ \% = \frac{2(blue\ area)}{red\ area} \times 100 \qquad \textbf{Equation 2.1}$$

It must be noted that this method does not provide an absolute conversion value but is useful for providing an estimate that can be used to compare different reaction conditions. Two main assumptions are required when using this method. Firstly, it is assumed that the peaks are Gaussian in nature. Secondly, the specific refractive index increment (dn/dc) for both the arms and star polymers is similar. The refractive index intensity is directly proportional to mass concentration, and so the star peak is much more intense compared to the equivalent molar concentration of arms, due it the stars having much larger molecular weights. It is possible to calculate the arm conversion by

dividing both peaks by their respective $M_{n(GPC)}$ values to obtain their molar concentrations. The arm conversion can then be calculated by multiplying the number of moles of star polymer by the average number of arms per star as derived from the Mark-Houwink plot (to calculate the number of moles of arms incorporated in the star polymers), and comparing to the molar concentration of leftover arms. There is considerable error associated with this method however. Due to the compact nature of the star polymer, the $M_{n(GPC)}$ value will be significantly underestimated, and there is error associated with the number of arms per star calculation, as mentioned.

A second challenge of preparing star polymers *via* the arm-first approach is the difficulty in analysing the formed stars and their core structures. The precursor arms are generally simple to analyse by GPC and ^{1}H NMR spectroscopy; however, elucidating detailed information such as the number of arms per star is more difficult due to the random nature of the core formation mechanism. As discussed in **Chapter 1**, light scattering GPC can be used to analyse star polymers, but only provides an average number of arms per star if the size of the linear arm is below ~10 nm. This is because polymers with a size below 10 nm do not show dissymmetry and thus their radius of gyration (R_g) cannot be obtained by light scattering. The ultimate result of this is that the geometric branching factor, g, and subsequently number of arms per star as a function of molecular weight cannot be calculated with light scattering. To measure the number of arms as a function of the molecular weight of the star, viscosity GPC can be used instead. Viscometric analysis provided by advanced GPC can be used to create a Mark-Houwink plot, which gives branching information allowing for indirect measurement of the number of

arms per star polymer. The star formation is deemed to begin where the Mark-Houwink plot deviates to a lower viscosity compared to the linear reference (**Figure 2.4.**). As branching increases in the star polymer, the hydrodynamic volume of the star increases but not to the same extent as its molecular weight, resulting in an overall reduction in intrinsic viscosity (see section on star polymer analysis in **Chapter 1** for more information). The difference between the intrinsic viscosities of the linear reference and star polymer can be used to calculate the geometric branching ratio g' (**Equation 2.2**).

$$g' = \left(\frac{IV(branched)}{IV(linear)}\right)_{MW} \qquad \textbf{Equation 2.2}$$

The relationship of *g'* to the geometric branching factor, g, is as follows:

$$g' = g^{\varepsilon} \qquad \textbf{Equation 2.3}$$

Where ε is a structural factor that can be calculated experimentally when the number of arms is known by using the core-first approach to star polymers.[16]. However, this is not possible for arm-first stars where the number of arms is much less certain due to the more random nature of the core formation. In this chapter, a literature value of 0.75 was used.[49,50] To calculate the number of arms (*f*) from *g*, the following equation is required which assumes a polydisperse system:

$$g = \frac{3f}{(f+1)^2} \qquad \textbf{Equation 2.4}$$

The number of arms, *f*, can then be plotted against the star molecular weight to give a visual representation of number of arms as a function of the molecular weight of each star.

Core cross-linked stars generally have some residual arms left and these can be used as an internal calibration and overlapped with a linear reference polymer to ensure analytical accuracy. Furthermore, a line of best fit has to be extrapolated from the linear reference to allow for an accurate estimate of IV_{linear} at high molecular weights, which is necessary for calculating the degree of branching in the star polymers and thus the number of arms at high molecular weight (**Figure 2.4.**). There is a known chain transfer reaction that occurs for between 1 in 200 to 1 in 800 repeat units for the CROP of poly(2-oxazoline)s resulting in a branched structure, and so high molecular weight poly(2-oxazoline)s that are truly linear are not achievable.[51] For this reason, a lower molecular weight linear sample is required which can then be extrapolated mathematically.

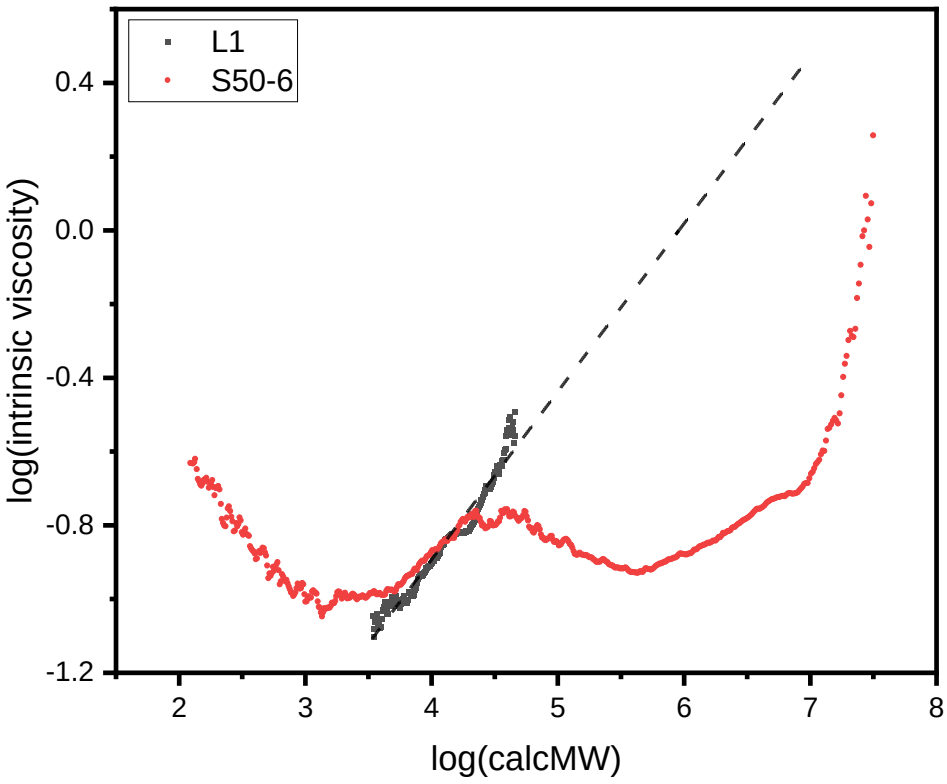

Figure 2.4. Mark-Houwink plot showing the linear reference (**L1**) and extrapolated line of best fit (in black) with **S50-5** (in red) as an example star polymer. Samples were measured on a DMF GPC instrument.

As well as advanced GPC analysis, dynamic light scattering (DLS) measurements were carried out to provide evidence for particle formation and to determine any correlations between star size and the number of arms.

2.2.1.3. The Effect of Arm Length on Star Formation

The arm length is an important variable in the synthesis of star polymers because it has been shown to affect arm to star conversion and the number of arms per star.[52, 53] To cover a wide range of arm lengths, DP25 (**S25-1** to **S25-3**), DP50 (**S50-1** to **S50-8**), and DP100 (**S100-1** to **S100-6**) arms were synthesised and tested. Initially, it was found that the arm length was an important parameter for the stars' ability to incorporate cross-linker. It must be noted that when incorporation of cross-linker is discussed, it refers to the amount of cross-linker that can be taken up by the whole system before gelation occurs, and not how much cross-linker can be absorbed into each individual star core. If shorter arms were combined with too much cross-linker, an insoluble gel-like structure formed that could not be analysed, presumably because the shorter arms cannot sufficiently stabilise the cross-linked core in solution. These insoluble samples are indicated in the Gel column in **Table 2.1.** and marked as Y. Increasing the arm length allowed for more cross-linker to be incorporated, however DP25 arms could only stabilise 5 equivalents of cross-linker across the whole concentration range tested (**S25-2**). DP50 and DP100 arms at low concentration could stabilise up to 20 equivalents of BisOx (**S50-7**, **S100-5**)**.**

The arm length was analysed by comparing **S25-1**, **S50-1**, and **S100-1** which were chosen given that DP25 arms could not stabilise more than 5 equivalents

of cross-linker. **Figure 2.5.** shows the GPC analysis of these three stars and the arm functionality plot. For the stars **S25-1**, **S50-1**, **S100-1**, the arm conversion decreases from 74%, 28% and 11%, respectively. It is quite likely that the longer arms have much more steric bulk than the short arms and when a small amount of cross-linker is used, the formed cores are very sterically hindered preventing arms from being incorporated. In fact, by observing **Figure 2.5.A**, it can be seen that stars formed from DP50 and DP100 arms have very similar hydrodynamic volumes, suggesting that the effect of steric hindrance of the arms is most pronounced from DP25 to DP50 and not as much from DP50 to DP100.

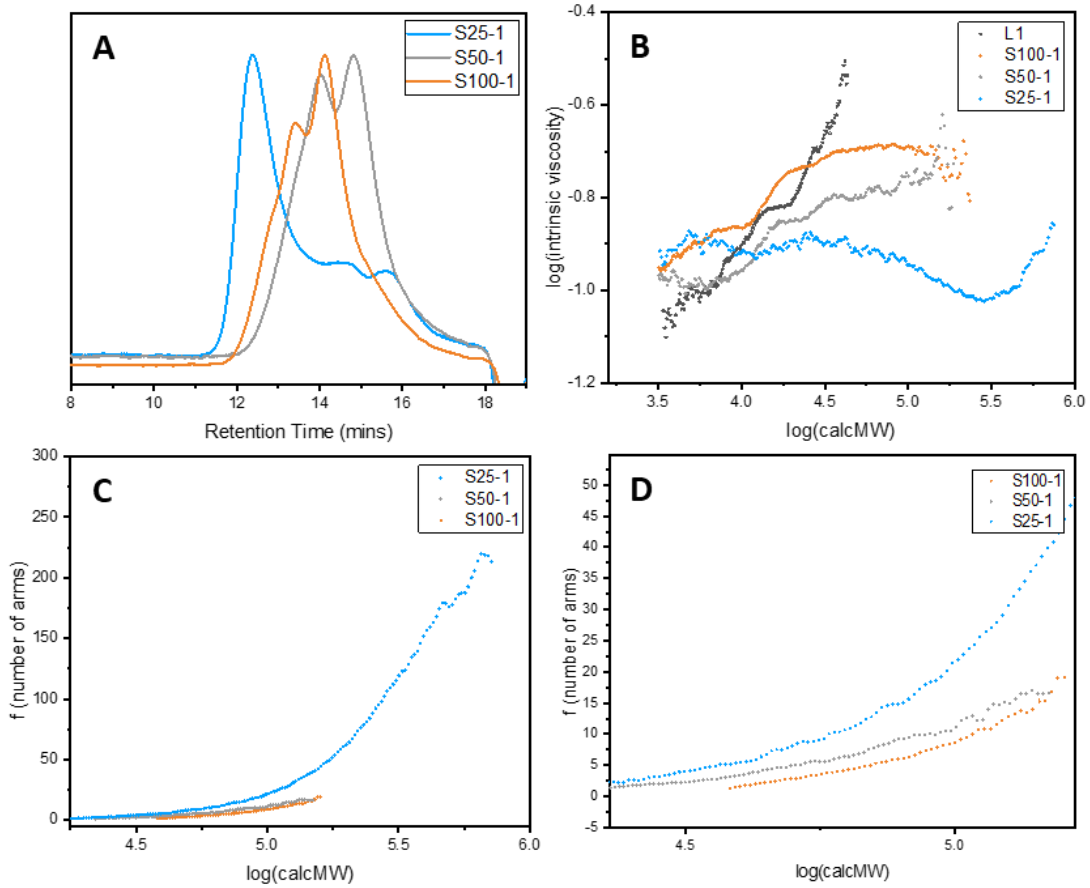

Figure 2.5. Plots showing the influence of arm length (DP=25, 50, and 100) on star formation. **(A)** Hydrodynamic volume of stars as measured by GPC RI. **(B)** Mark-Houwink plots of stars. **(C)** Number of arms, f, as a function of log(MW) (Assuming a polydisperse model with ε=0.75).

(D) Zoomed into region of (C) at lower log(calcMW) for better comparison. All samples were measured on a DMF GPC instrument.

By observing the stars' Mark-Houwink plot (**Figure 2.5.B)**, the star polymer structures can be analysed. All three stars have a lower viscosity than the linear reference, which is indicative of branching. **S25-1** (blue trace in **Figure 2.5.B)** shows the biggest drop in viscosity and almost reaches molecular weights of log6 Da demonstrating that even small arms and small amounts of cross-linker can form very large structures. **S100-1** and **S50-1** form similar molecular weight structures of around log5 (100 kDa); however, **S100-1** has fewer arms as can be seen from its higher viscosity. A possible reason why **S100-1** has formed structures that are as heavy as **S50-1** despite having fewer arms is due to the fact that its arms are longer and thus contribute more to the overall weight of the star.

Figure 2.5.C and **Figure 2.5.D** show the number of arms per star as a function of molecular weight. **S50-1** has slightly more arms per star compared to **S100-1** across the whole molecular weight range, which is in accordance with the Mark-Houwink plot. **S25-1** has an average of 61 arms per star, but it can be seen that at the highest molecular weights some stars reach over 200 arms. Furthermore, **S25-1** has a higher number of arms at any given molecular weight compared to **S50-1** and **S100-1**, showing that it has a higher number of arms per star due to the reduced steric hindrance of the arms, assuming the amount of cross-linker is proportional to the core size. The number of arms correlates well with the DLS star sizing, which shows that **S50-1** and **S100-1** have the same size (5.8 nm) whilst **S25-1** has a size of 9.5 nm due to it having the most arms (**Table 2.1.**).

The largest stars with 5 equivalents of cross-linker are found when DP25 arms are used. This is due to the combination of small cores being formed when only 5 equivalents of cross-linker are used and the reduced steric hindrance of DP25 arms. However, when longer arms are combined with more cross-linker, they are much more effective at forming large stars with high arm conversions. It seems there is a correlation between the arm length and the amount of cross-linker that can be incorporated. For example, stars formed with DP50 arms have the largest size when combined with 10 equivalents of cross-linker as can be seen from **S50-1** (5 eq cross-linker, 5.8 nm), **S50-4** (10 eq cross-linker, 9.3 nm), and **S50-7** (20 eq cross-linker, 8.7 nm). Stars formed with DP100 arms form larger stars with 20 equivalents of cross-linker as can be seen by **S100-1** (5 eq cross-linker, 5.8 nm), **S100-3** (10 eq cross-linker, 15.1 nm), and **S100-5** (20 eq cross-linker, 28.5 nm). In general, this trend is also observed with the number of arms per star; however, **S50-7** is the one anomaly to this trend and is discussed in the next section on the effect of the number of equivalents of cross-linker.

S25-1 shows a trimodal peak in the RI trace (**Figure 2.5.A**), which is a common feature of many of the stars formed in this study. (See **Figure 2.21.** and **Figure 2.22**, additional info) The lowest mass peak is attributed to residual arms, and the largest peak is the major star structure. The middle peak can be assigned as a smaller star-like structure as opposed to a dimer (see below). When the molecular weight distribution is overlaid with the Mark-Houwink plot (**Figure 2.6.**), features in the molecular weight distribution can be correlated to their changes in viscosity and thus their degrees of branching.

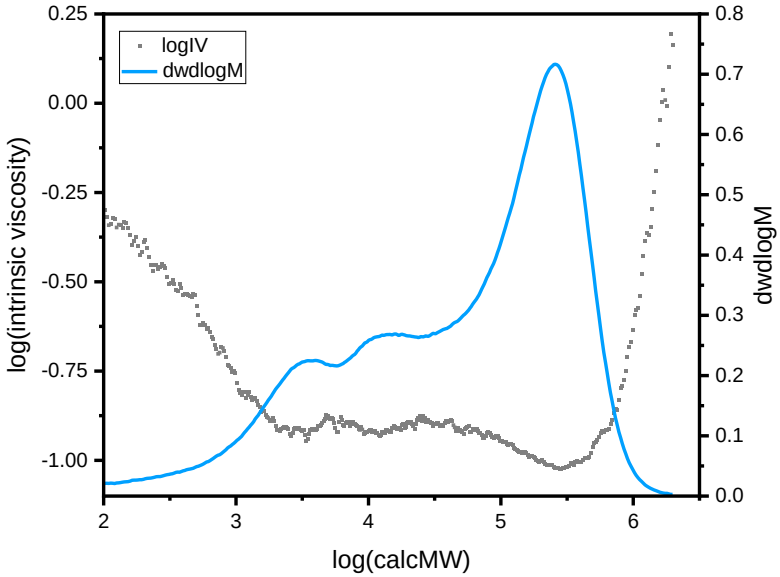

Figure 2.6. Plot overlaying the molecular weight distribution of **S25-1** with its Mark-Houwink plot. Sample was measured on a DMF GPC instrument.

Since a DP25 arm dimer has an analogous structure to a DP50 linear arm, there is no branching and thus no associated decrease in viscosity. However, the middle peak can be seen to have an associated reduction in viscosity which is indicative of a branched structure and not a dimer. It is not clear at this stage whether the reaction forms small and large stars in parallel or stars begin forming and then run out of cross-linker later on in the cross-linking process.

2.2.1.4. The Effect of Cross-linker Quantity on Star Formation

CCS stars typically have large cores that are highly suited to encapsulating small molecules and therefore the amount of cross-linker able to be incorporated was an important variable to investigate. The number of equivalents of cross-linker appears to have a significant effect on arm conversion. In the case where arm length is fixed at DP100 and the concentration is fixed at 0.5 M, as the number of equivalents of cross-linker is increased from 5 equivalents **(S100-1)** to 20 equivalents **(S100-5)** the leftover

arms decrease from 68% to 14%. Moreover, this trend can generally be seen across all stars formed. **Figure 2.7.** shows the GPC analysis of **S100-1**, **S100-3** and **S100-5** and highlights the effect of the amount of cross-linker on star formation.

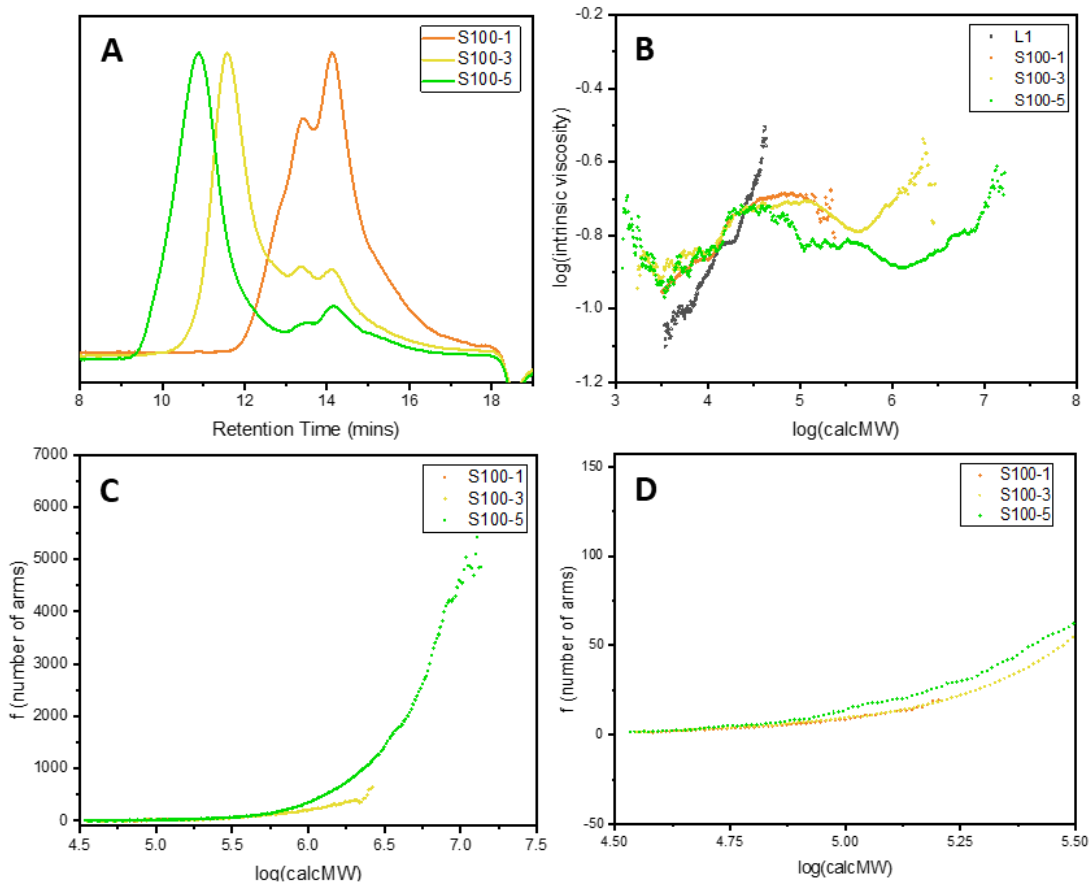

Figure 2.7. Plots showing the influence of cross-linker (5, 10, and 20 eqs) on star formation. **(A)** Hydrodynamic volume of stars as measured by GPC refractive index (RI). **(B)** Mark-Houwink plots of stars. **(C)** Number of arms, f, as a function of log(calcMW) (Assuming a polydisperse model with ε=0.75). **(D)** Zoomed into region of (C) at lower log(calcMW) for better comparison. All samples were measured on a DMF GPC.

Figure 2.7.A shows the RI traces of the three stars and shows a clear trend with increasing the amount of cross-linker and an increase in star hydrodynamic volume and arm conversion. As previously mentioned, **S100-5** and **S100-3** both have trimodal peaks which is attributed to a smaller star structure. **S100-1** does not form a larger star structure and only appears to form these smaller star species. These features can be seen in **Figure 2.7.B**

which shows the Mark-Houwink plot of the three stars. **S100-1** does form a small, branched structure as can be seen from its deviation from the linear reference plot. As mentioned earlier, the reason for this is due to the large amount of steric hindrance associated with DP100 arms and the small core size attributed to using only 5 equivalents of cross-linker. **S100-3** follows **S100-1** before it extends to a molecular weight of ~log6.5 with a more significant drop in viscosity highlighting an increase in the number of arms. **S100-5** reaches a much higher molecular weight than both than of these stars, ~log7.5. These high molecular weight stars have molecular masses in the tens of millions of Da, and are still soluble in solution highlighting the fascinating solution behaviour of this type of highly branched star structure.

As the number of equivalents of BisOx is increased from 5 to 10 and then to 20 the average number of arms the stars have are 7, 108 and 1002, respectively. When the reaction concentration and arm DP are fixed, increasing the amount of cross-linker always increases the number of arms across all polymers tested, *via* steric relief. There is a clear influence of the amount of cross-linker, and this can be used to carefully modify the number of arms per star. This trend is also seen in the DLS sizing, which shows that the size of **S100-1**, **S100-3**, and **S100-5** increases from 5.8 nm to 15.1 nm and to 28.5 nm. One interesting finding is that of **S50-5** and **S50-7**. **S50-7**, despite using 20 equivalents of cross-linker, appears to have a smaller core than **S50-5** as evidenced by having more arms but a smaller hydrodynamic size (**S50-7** – average of 213 arms, size of 8.7 nm, **S50-5** – average of 107 arms, size of 12.0 nm). This is also true for **S50-4** and **S50-7** where **S50-4** (average of 60 arms, size of 9.3 nm) also has a larger core.

Figure 2.7.C shows the functionality plots of **S100-1**, **S100-3**, and **S100-5.** For any given molecular weight, **S100-5** has a higher number of arms than both **S100-1** and **S100-3**. Moreover, it can be seen in **Figure 2.7.C** that some stars in **S100-5** have over 4000 arms. This shows that the observed increase in molecular weight of the stars when the amount of cross-linker is increased is due at least partly to an increase in the number of arms per star. If increasing the equivalents of cross-linker resulted in more stars forming, the average number of arms per star would decrease. This would result in less overall branching within the system, leading to an increase in intrinsic viscosity, which is not observed. Therefore, the most likely explanation is that increasing the number of equivalents of cross-linker increase the core size, which reduces steric hindrance and allows for more arms to be incorporated into each star.

2.2.1.5. The Effect of Reaction Concentration

The concentration at which a reaction is carried out is critical and CCS polymers are no different. In this chapter, it was found that stars synthesised at lower reaction concentrations were more able to incorporate cross-linker before gelation occurred. For example, **S50-8** and **S50-7** were formed with 20 equivalents of cross-linker. **S50-8** was performed at a concentration of 1 M and formed an insoluble gel whilst **S50-7** was performed at 0.5 M and formed a soluble star. Very low concentrations of 0.1 M were investigated, but the arm formation took several hours, and little star formation was seen, so the lowest concentration deemed acceptable was 0.5 M. 4 M was investigated as a higher reaction concentration, but this concentration limited the amount of cross-linker that could be incorporated to 5 equivalents and stars that formed had very low arm to star conversion.

The reaction concentration appears to have an effect on the size of the core as can be seen from **S100-2** (2 M) and **S100-1** (0.5 M). These stars used the same number of equivalents of cross-linker and the same arm DP, and had similar numbers of arms, averaging 8 arms and 7 arms respectively. However, their sizes as measured by DLS were 7.4 nm and 5.8 nm respectively, indicating that at higher concentrations the core size likely increases. It must be noted that this trend was not observed across all the series, notably stars with 5 equivalents of cross-linker tended to not follow this trend and were approximately the same size when the arm DP was fixed. The reason for this could be due to the small amount of cross-linker preventing significant core growth.

There appeared to be a trend when DP50 arms were incorporated with 10 equivalents of cross-linker. Although there was little effect on the arm conversion, increasing the reaction concentration resulted in larger star polymers as can be seen in **Figure 2.8.A**, which compares **S50-4** (0.5 M), **S50-5** (1 M), and **S50-6** (2 M).

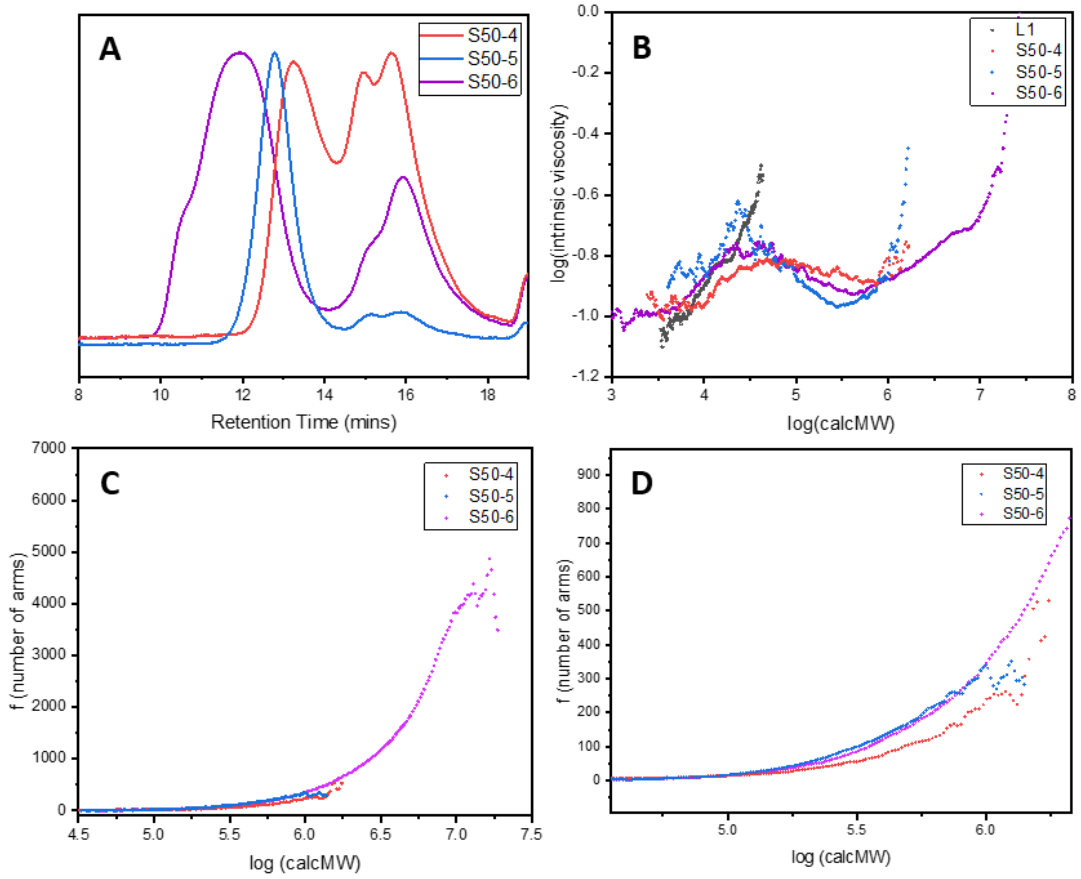

Figure 2.8. Plots showing the influence of reaction concentration (0.5 M, 1.0 M, and 2.0 M) on star formation. **(A)** Hydrodynamic volume of stars as measured by GPC RI. **(B)** Mark-Houwink plots of stars. **(C)** Number of arms, f, as a function of log(MW) (Assuming a polydisperse model with ε=0.75). **(D)** Zoomed into region of (C) at lower log(calcMW) for better comparison. All samples were measured on a DMF GPC.

As the concentration is increased, the size of the star also increases. Interestingly, **S50-4** and **S50-6** are much more disperse than **S50-5,** which incidentally had a much higher arm conversion. The Mark-Houwink plot shows that **S50-5** reaches the lowest viscosity of any of the three polymers, which indicates that it has the highest amount of branching on these stars. **S50-6** forms very large stars which have an average number of arms of 877, however the Mark-Houwink plot suggests that at log5.5 **S50-6** has fewer arms per star than **S50-5** as it does not reach as low a viscosity**. S50-4** forms the smallest stars that also have the lowest number of arms. The reason for these observations is not clear but could be due to a dilution effect. At high

concentrations, arms are in closer proximity to each other and so are more likely to agglomerate to form large stars.

Coupling between stars is a feature of star polymers, and it is normally seen as a high molecular weight shoulder in the RI trace as can be seen in **Figure 2.8.A**. However, another feature of star-star coupling is a sharp increase in the intrinsic viscosity due to the increase in size without an associated increase in branching. In this case, the high molecular weight shoulder corresponds to the small dip in the Mark-Houwink plot at log7. These features can be seen in **Figure 2.9,** where the molecular weight distribution of **S50-6** has been overlaid with the Mark-Houwink plot. This suggests that the high molecular weight shoulder is not due to star-star coupling but is the formation of larger stars.

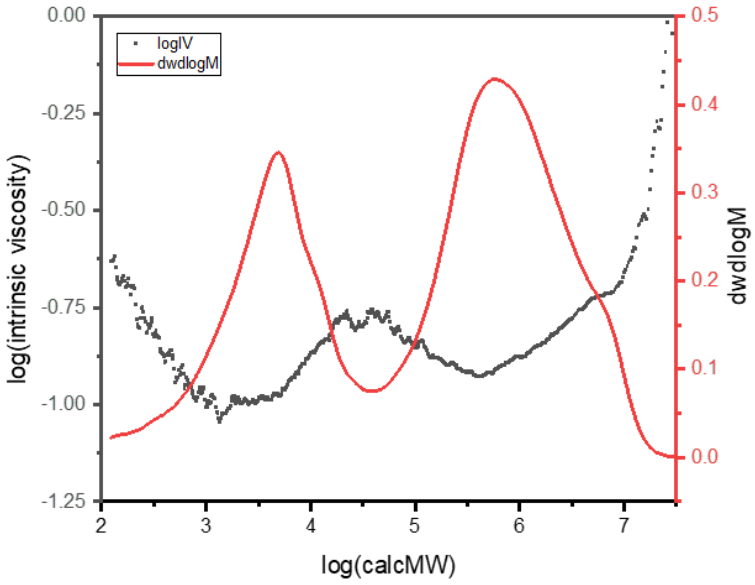

Figure 2.9. Plot overlaying the molecular weight distribution of **S50-6** with its Mark-Houwink plot. Sample was measured on a DMF GPC.

2.2.1.6. Drug Encapsulation Studies

Star polymers are often tested for their ability to encapsulate and transport drugs. The cores are dense networks of hydrophobic linkers and are able to capture hydrophobic molecules. To investigate the CCS polymers' ability to encapsulate, DHA was used as a model drug. DHA is a small hydrophobic dye that is frequently used for modelling as it absorbs ultraviolet (UV) light and so can easily be detected by utilising UV-Vis spectroscopy.[54] The star polymers were dissolved at a concentration of 3 mg/mL in water, and DHA was suspended in the polymer solution at a concentration of 5 mg/mL. The mixture was left for 24 hours to allow for DHA to be encapsulated in the hydrophobic core of the star polymer. DHA is not soluble in water and so a calibration line could not be made to determine quantities of DHA encapsulated into each star. Therefore, a relative approach was taken from the literature.[20] **S50-4** showed the highest degree of encapsulation by UV absorption so was set to 100% and the other polymer encapsulation values were derived from this.

All stars encapsulated DHA to some degree, whilst the linear reference **L1** did not encapsulate any. This is a promising sign that these stars can encapsulate molecules within their cores. Furthermore, correlations between the stars' ability to encapsulate drugs and the amount of cross-linker, arm DP, and reaction concentration were observed.

In general, drug encapsulation was seen to improve when the number of equivalents of cross-linker was increased, when the reaction concentration and arm DP were fixed. For example, **S100-1** (5 eq cross-linker), **S100-3** (10 eq cross-linker), and **S100-5** (20 eq cross-linker) had relative absorbances of

38%, 38%, and 75%, respectively. However, **S50-4** (10 eq cross-linker, 100% relative encapsulation) is the one notable exception to this as it encapsulates more than **S50-7** (20 eq cross-linker, 55% relative encapsulation) despite using less cross-linker. Furthermore, there appears to be an optimum ratio between the number of equivalents of cross-linker and the arm DP. The best encapsulation is seen for small arms when they are combined with small amounts of cross-linker (**S25-1**) and for larger arms when they are combined with large amounts of cross-linker (**S100-5**). This trend can be observed in **Figure 2.10**. For 5 equivalents of cross-linker, the whole range of arm lengths was tested. In this set, the shorter armed stars appeared to be more effective at encapsulating DHA and this is due to the lower steric hindrance associated with shorter arms allowing easier access to the core.

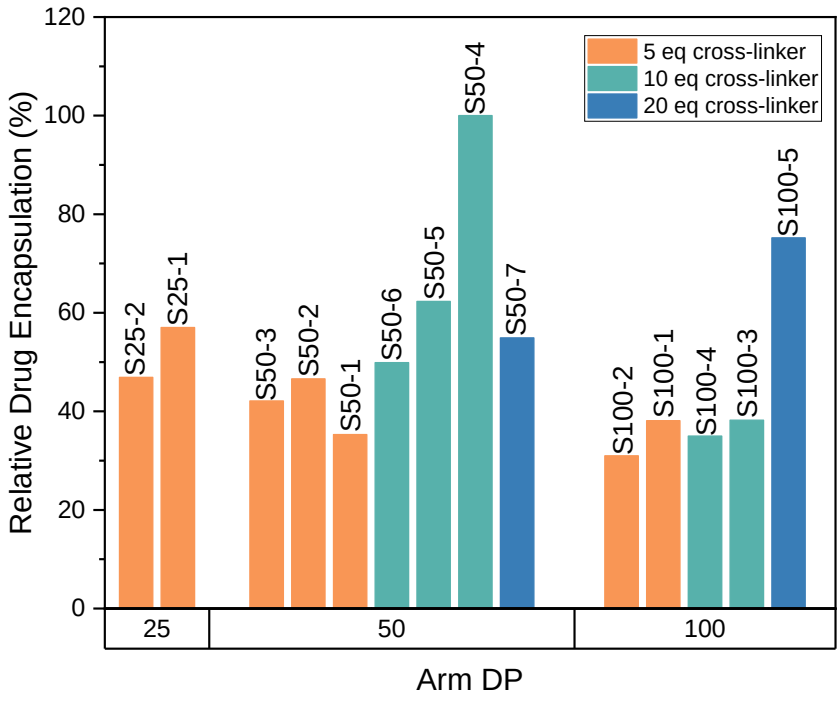

Figure 2.10. Bar chart showing arm DP against relative drug encapsulation. Percentage calculated based on the UV absorbance, and bars are colour coded based on the amount of cross-linker used.

Interestingly, decreasing the reaction concentration also improved drug encapsulation. This observation explains why **S50-4** shows the best encapsulation; it has short enough arms to minimise steric hindrance whilst also being able to incorporate 10 equivalents of cross-linker, and was synthesised at low concentration. From the previous discussion it was observed in the Mark-Houwink plot (**Figure 2.8.B)** that **S50-4** has a lower number of arms per star compared to **S50-5** and **S50-6**, and thus has lower steric hindrance allowing easier access to the core of the star by the DHA. Furthermore, **S25-1** has half the number of arms as **S25-2** and shows a higher degree of encapsulation.

2.2.2. Hyperbranched Poly(2-oxazoline)s

In this part of the chapter, the bisfunctional 2-oxazoline cross-linker used for the star polymer synthesis was employed to generate hyperbranched poly(2-oxazoline) structures in a one-pot system with EtOx and an end capping agent (**Scheme 2.2.**). As discussed in the introduction to this chapter, branched polymers are a more pragmatic alternative to dendrimers, which can be laborious to synthesise. The Strathclyde method is a very popular route for the synthesis of branched polymers from vinyl monomers and a chain transfer agent. [32, 55, 56] This method involves the combination of a linear monomer, a bifunctional monomer, and a chain transfer agent, which is typically a thiol.[57] The chain transfer agent is used to control the degree of branching and hence the molecular weight of the branched polymer. For poly(2-oxazoline)s, chemicals designed specifically for chain transfer do not exist and so the molecular weight of the branched polymers can be controlled by the addition of a small amount of a sterically hindered nucleophile at the start of the

polymerisation. The sterically hindered nucleophile terminates living chain ends, whilst competing with the ongoing polymerisation reaction in order to limit the molecular weight and prevent gelation.

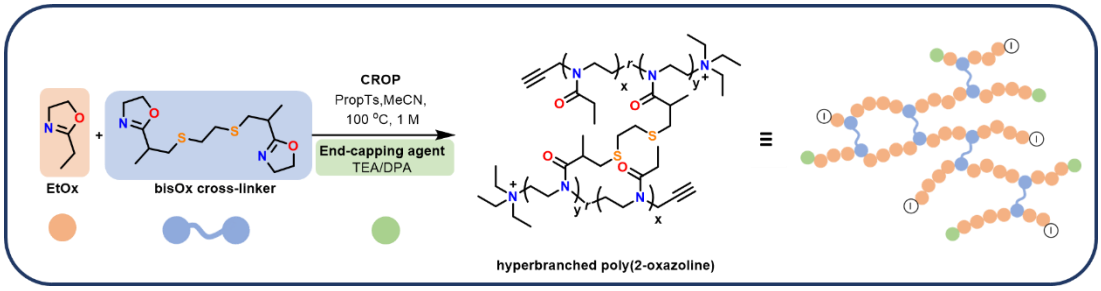

Scheme 2.2. Overall reaction mechanism for the synthesis of hyperbranched poly(2-oxazoline)s using BisOx.

Several sterically hindered bases have been explored in order to find the most suitable end-capping agent. An end-capping agent that is too nucleophilic or unhindered prevents polymerisation from occurring, whilst an end-capping agent that is not nucleophilic enough or too bulky does not terminate chains effectively and results in gelation.

In **Table 2.2**, the synthesised branched poly(2-oxazoline)s along with their end-capping agents, their BisOx/EtOx molar ratio as determined by ^{1}H NMR spectroscopy, the average degree of branching ($g'_{(n)}$), and the cloud point of each polymer can be seen. The BisOx/EtOx ratio was used as an indication of the amount of branching derived from ^{1}H NMR spectroscopy, whilst the degree of branching ($g'_{(n)}$) was calculated from viscosity GPC. Lastly, the cloud point of each polymer was measured to observe how branching affected the physical properties of the polymers.

Table 2.2. List of hyperbranched polymers prepared *via* CROP along with the BisOx/EtOx ratios, average g'$_{(n)}$, and cloud point.

Entry	*Base (eq)*	*Gelation*	*EtOx (eq)*[a]	*BisOx (eq)*[a]	$M_{n(GPC)}$ *(kDa)*[b]	*Đ*[b]	*BisOx/ EtOx ratio*	*g'$_{(n)}$*[c]	*Cloud point (°C)*[d]
P1	0	No	100	4	22.0	170	0.04	0.87	66
P2	0	No	100	6	19.8	106	0.06	0.75	62
P3	0	Yes	100	12	N.D.	N.D.	0.12	N.D.	N.D.
P4	0	No	200	6	11.0	17	0.03	0.94	70
P5	TEA (1)	No	66	3	4.9	12	0.05	0.90	66
P6	TEA (1)	No	53	3	3.2	3	0.06	0.83	60
P7	TEA (1)	No	60	5	3.7	8	0.08	0.80	51
P8	TEA (1)	No	57	6	4.7	52	0.11	0.82	44
P9	TEA (1)	No*	39	5	3.2	29	0.13	1.18	47
P10	TEA (0.5)	Yes	60	6	N.D.	N.D.	0.10	N.D.	N.D.
P11	TEA (5)	No polymer	43	5	N.D.	N.D.	0.12	N.D.	N.D.
P12	DPA (1)	No	100	7	7.5	62	0.07	0.85	55
P13	DPA (1)	No	72	6	5.3	75	0.08	0.78	60
P14	DPA (1)	No	38	4	9.1	27	0.11	0.73	47
P15	IPA (1)	Yes	90	9.6	N.D.	N.D.	0.11	N.D.	N.D.
P16	DIPEA (1)	Yes	56	6	N.D.	N.D.	0.11	N.D.	N.D.

[a]As calculated by ^{1}H NMR spectroscopy. Note that for gelled samples, values are calculated from T_0 samples. For the others, these are the amounts incorporated into the polymer.
[b]As calculated from RI from conventional GPC.
[c]As measured by advanced viscometry GPC.
[d]As measured by UV-Vis turbidimetry (See experimental).
*__P9__ was at the limit of solubility and was likely bordering on a hydrogel structure.
Triethylamine (TEA), diisopropylamine (DPA), isopropanol (IPA), diisopropylethylamine (DIPEA)

2.2.2.1. Calculation of the Branching Factor, g'

As for the star polymers discussed, earlier, the branching factor g' can again be used for hyperbranched polymers to analyse the degree of branching present in each polymer. Calculation of g' is exactly the same as for the star

polymers, i.e. the intrinsic viscosity of the branched polymer is compared to the intrinsic viscosity of a linear reference. Here, as g' tends towards 1, the degree of branching in the branched polymer reduces to that of a linear sample at the same molecular weight, i.e. there is no branching present. As g' tends towards 0, the branching increases *ad infinitum.* The branching factor, g, was calculated across the whole molecular weight range of the branched polymer by comparison to the linear reference, and a mean value was obtained to give an average of the amount of branching present per polymer – $g'_{(n)}$. It must be noted that small deviations in the line of best fit can drastically change the calculated amount of branching, which is a disadvantage to this approach. Nonetheless, this method is a suitable approach for relative comparison of branched polymers as long as all the polymers are analysed in the same manner. The line of best fit extrapolated from the linear reference can be seen in **Figure 2.11.A**, along with a branched polymer to highlight the lower overall viscosity of the branched polymer compared to the linear sample. From **Figure 2.11.A**, it is evident that **P1** has lower viscosity than the linear reference and thus contains more branching points across the whole polymer. In **Figure 2.11.B** the plot of g' as a function of logM can be seen for **P1**, showing a decrease in g' as logM increases. i.e. as the branched polymer gets larger, the amount of branching it contains increases. The red dashed lines indicate sections of the plots that were cut off for the $g'_{(n)}$ calculation. The reason for this cut-off was because the low polymer concentration at the extremities caused noise in the plots resulting in data that was erroneous.

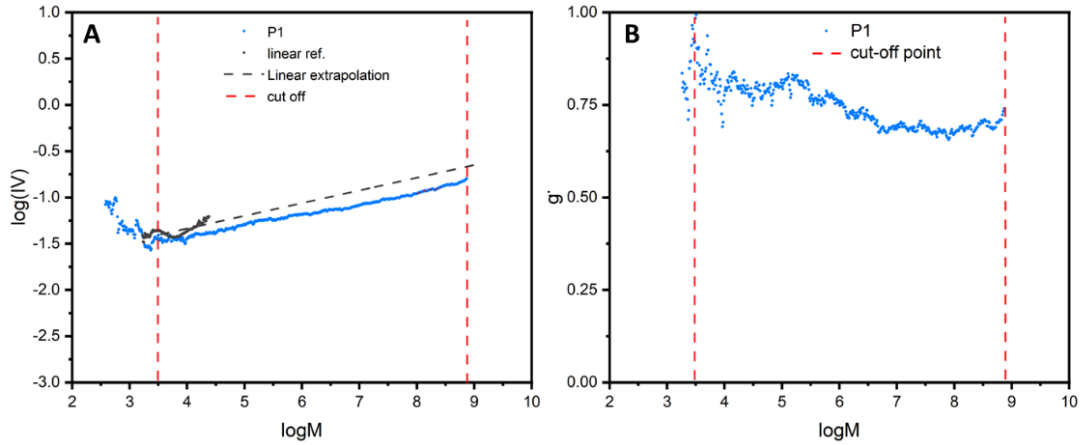

Figure 2.11. (A) Mark-Houwink plot of **P1** overlaid with the linear reference. **(B)** Plot of g' as a function of logM. Red dashed lines indicate cut-offs for low concentration extremities. Samples were measured on a THF GPC.

2.2.2.2. Branched Polymers with No End Capping Agent

To begin the discussion on branched polymers, a series of three polymers were synthesised with an increasing ratio of BisOx to EtOx (**P1-P3**). The EtOx DP was set to 100, and the equivalents of the BisOx cross-linker were increased from 4 to 12 equivalents. **P1** had the lowest amount of cross-linker and had a $g'_{(n)}$ value of 0.87. Once the amount of cross-linker had been increased from 4 eq (**P1**) to 6 eq (**P2**) the $g'_{(n)}$ value decreased from 0.87 to 0.75, corresponding to an associated drop in intrinsic viscosity, and thus higher degree of branching for **P2**. Next, the cross-linker amount was again increased from 6 eq to 12 eq (**P3**), increasing the BisOx/EtOx ratio from 0.06 to 0.12. This increase in cross-linker resulted in a gel forming that could not be analysed further by ^{1}H NMR spectroscopy and GPC. It should be noted that for the gelled polymers, the BisOx/EtOx ratio was determined from the ^{1}H NMR T_0 spectrum. Two example gels can be seen in **Figure 2.12**. **Figure 2.12.A** shows a desolvated version of **P3** that was brittle and had poor viscoelastic

properties, whilst **Figure 2.12.B** shows a solvated version of **P3** that had poor structural integrity and was easily broken up.

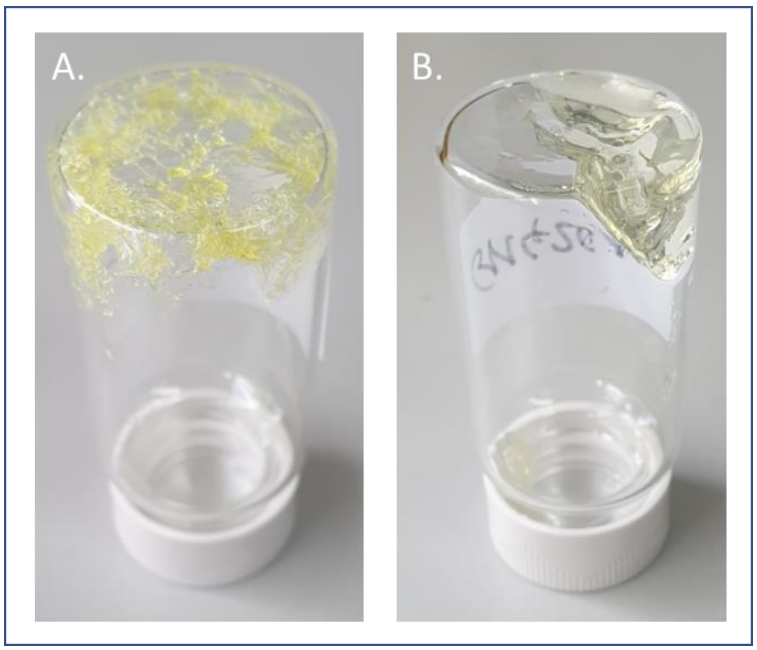

Figure 2.12. (A) Hydrogel (**P3**) with solvent removed. **(B)** Solvated hydrogel (**P3**).

Finally, to examine how increasing the amount of EtOx to change the BisOx/EtOx ratio affected the amount of branching, the equivalents of EtOx were doubled from 100 (**P2**) to 200 (**P4**). This halved the BisOx/EtOx ratio from 0.06 to 0.03 and had the result of driving the $g'_{(n)}$ upwards to 0.94 and reducing $M_{n(GPC)}$ by approximately half (19.8 kDa to 11.0 kDa). This high value of $g'_{(n)}$ is indicative of a minimal amount of branching and the lower observed $M_{n(GPC)}$ and $Đ$ are likely due to the reduced amount of branching. Nonetheless, of all the polymers investigated, **P1** and **P2** had the largest $M_{n(GPC)}$ values, and the highest values for $Đ$ indicating a lack of control when no terminating agent was used.

2.2.2.3. Triethylamine as a Terminating Agent

In order to maximise the amount of branching whilst retaining solubility, a terminating agent was added at the beginning of the reaction in an attempt to prevent uncontrolled cross-linking and gel formation. Here, inspiration was provided by the Strathclyde method of branched polymer formation where a chain transfer agent is added to suppress cross-linking. In order to prevent complete and instantaneous termination of all polymer chains by the end-capping agent, two factors needed to be considered. Firstly, the amount of terminating agent needed to be tuned so as not to immediately terminate all living chain ends, but also sufficient amounts needed to be added to suppress gelation. Secondly, a terminating agent needed to be chosen that would react slowly enough to ensure polymer formation, but not so slowly that gelation occurred. For this reason, triethylamine (TEA) was selected as it is sterically hindered non-nucleophilic base.

To investigate the effect of adding TEA as a terminating agent at the start of the polymerisation, a series of polymers with increasing BisOx/EtOx were synthesised (**P5**-**P9**). For this series, the BisOx/EtOx ratio was increased from 0.05 to 0.13 whilst keeping the amount of end-capper at 1 equivalent. From **P5** to **P8**, the $g'_{(n)}$ value decreased from 0.9 to 0.82, indicative of an increase in branching. The $M_{n(GPC)}$ values are also noticeably reduced compared to **P1**-**P4** and the $Đ$ of the polymers is much lower. Although branched polymers clearly form, the monomer conversion is low (**Table 2.5.**) showing that TEA does end-cap quite effectively. Nevertheless, the branched polymers do form, with decreasing $g'_{(n)}$ values correlating with increased end-capping. The BisOx/EtOx ratio was then increased to 0.13 (**P9**), which was higher than **P3**

(which formed a gel). However, the solubility of **P9** in tetrahydrofuran (THF) was extremely poor, which is reflected in the calculated $g'_{(n)}$ value of 1.18. This value is not possible, as it would mean the polymer has less branching than linear pEtOx. However, the poor solubility in THF is indicative of a highly branched polymer which has become accessible through the addition of TEA as a terminating agent. Interestingly, the branched polymers tended to be more easily soluble in water than THF. Regarding the poor solubility of **P9**, it is likely that the highest molecular weight, most branched polymers in the sample were the least soluble and so were filtered out of the GPC sample resulting in the higher than expect $g'_{(n)}$ value. The poor solubility of the sample could result in column interactions within the GPC causing the Mark-Houwink plot to be misrepresented.

As TEA was shown to be an effective terminating agent for the branched polymers described here, further reaction optimisation was continued with TEA. As previously mentioned, the amount of end-capping agent is an important factor to consider, and was the next parameter explored. Here, two polymers were synthesised with a targeted BisOx/EtOx ratio of 0.10. For **P10**, 0.5 equivalents of TEA were used, and 5 equivalents were used for **P11**. For **P10**, a gel was formed despite the BisOx/EtOx ratio of 0.10, which was lower than for **P9** (0.13) which formed a soluble sample. The BisOx/EtOx ratio provided is an estimate given that the amount of each monomer incorporated in the gel are unknown. Clearly, 0.5 equivalents of end-capper were not enough to control branching in this system. Meanwhile, for **P11**, there was no monomer conversion at all as measured by ^{1}H NMR spectroscopy. The high quantity of TEA added terminates the living polymer very effectively halting

any monomer conversion. Thus, there is a middle ground to be found for the amount of end-capper. Too much prevents polymerisation whereas too little results in gelation. It must be noted that the amount of terminating agent required for a specific system will likely depend on many factors, including the monomer, reaction concentration, end-capping agent used, and amount of cross-linker.

2.2.2.4. Diisopropylamine as a Terminating Agent

Once the limits of branching had been reached with TEA as the end-capper, the conditions were repeated with diisopropylamine (DPA) as the terminating agent. A branched polymer with a BisOx/EtOx ratio of 0.07 was synthesised (**P12**). This was similar to the BisOx/EtOx ratio of **P6** (0.06). These results were reflected in the similar $g'_{(n)}$ values of 0.85 (**P12**) and 0.83 (**P6**). **P12** had a much higher $M_{n(GPC)}$ of 7.5 kDa compared to 3.2 kDa for **P6** however. Observing the Mark-Houwink plot in **Figure 2.13**, it can be seen that both polymers have similar intrinsic viscosities and thus similar amounts of branching up to around log6, which was the maximum size of **P6**. **P12** reached much larger molecular weights than **P6** however, with some species with molecular weights above log8. The reason for this is likely due to the higher monomer conversion for **P12** compared to **P6**. **P12** used a higher DP of EtOx at the start of the reaction and this could be one possible reason for the larger size polymers. Moreover, the monomer conversion is generally higher for polymers using DPA as the terminating agent compared to TEA. This suggests that DPA is not as effective at end-capping as TEA although the reasons for this is not clear.

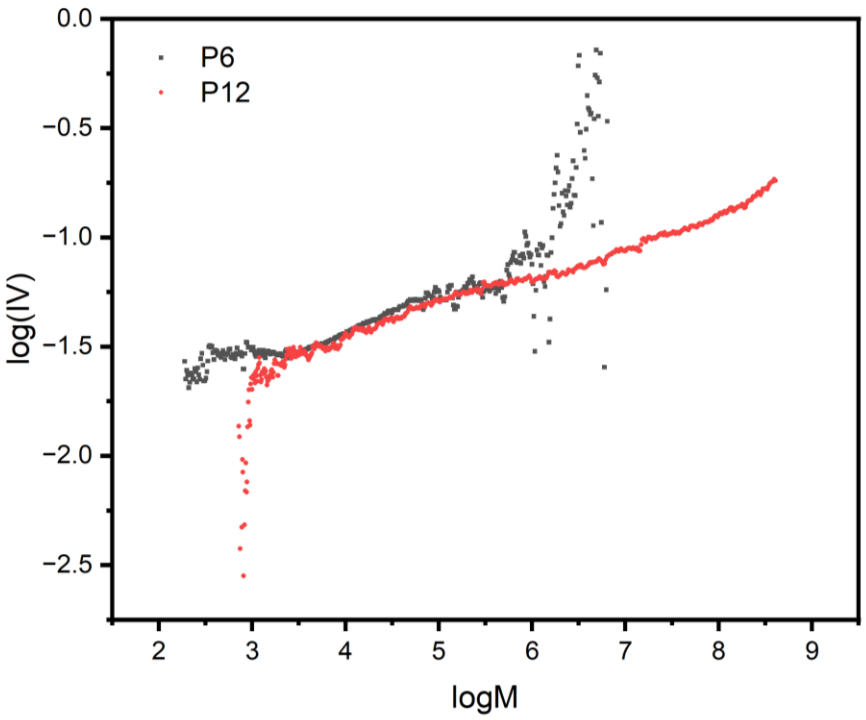

Figure 2.13. Mark-Houwink plot comparing **P6** and **P12**. Samples were measured on a THF GPC.

Next, the BisOx/EtOx ratio was then increased from 0.07 for **P12** to 0.08 for **P13**. This resulted in a reduction in $g'_{(n)}$ from 0.85 to 0.73 for **P12** to **P13** respectively. Then, the BisOx/EtOx ratio was increased to 0.11 for **P14** which resulted in a further decrease in $g'_{(n)}$ to 0.73, the lowest value of the entire set. All of the polymers end-capped with DPA had higher $M_{n(GPC)}$ values and dispersity when compared to TEA. Also, the monomer conversion for these polymers was much higher. These results suggest that DPA terminates less effectively than TEA, allowing for higher monomer conversion and larger polymers.

2.2.2.5. Testing Other Terminating Agents

As well as TEA and DPA, the non-nucleophilic base diisopropylethylamine (DIPEA) was selected, and 2-propanol (IPA) was chosen as a poor

nucleophile. Initially, 1 equivalent of each end-capper was tested (**P15** and **P16**). The BisOx/EtOx ratio was increased to 0.11, which was chosen to ensure gelation under normal circumstances without the presence of an end-capping agent. Nonetheless, gelation was seen for both **P15** (IPA) and **P16** (DIPEA). When TEA and DPA were used as terminating agents and the BisOx/EtOx ratio was 0.11 or higher (**P9**, TEA and **P14**, DPA) soluble branched polymers formed. This suggests that DIPEA is too sterically hindered to terminate chains. These important results suggest that TEA does end-cap polymer chains slowly whilst DIPEA does not end-cap to any significant degree. Furthermore, this result demonstrates that when preparing carboxylates for end-capping poly(2-oxazoline)s, DIPEA is a better choice of base than TEA. Using TEA will likely result in a mixture of chain ends that are partially terminated with the carboxylate, whilst others are terminated with TEA. This could be the reason for low end capping efficiencies where TEA and 2-bromo-2-methylpropionic acid are used as an end-capping mixture.[58]

2.2.2.6. Correlations Between $g'_{(n)}$, Cloud point, and BisOx/EtOx Ratio

To study the relationships between the BisOx/EtOx ratio, $g'_{(n)}$ value, and cloud point, three scatter plots were constructed (**Figure 2.14.**) using the data from **Table 2.2**. It must be noted that due to the poor solubility of **P9**, the measured values of $g'_{(n)}$ and the cloud point were affected. Nonetheless, it has been kept for observation in each graph, and can be seen highlighted by the red circle. Furthermore, each point has been coloured depending on the type of terminating agent used.

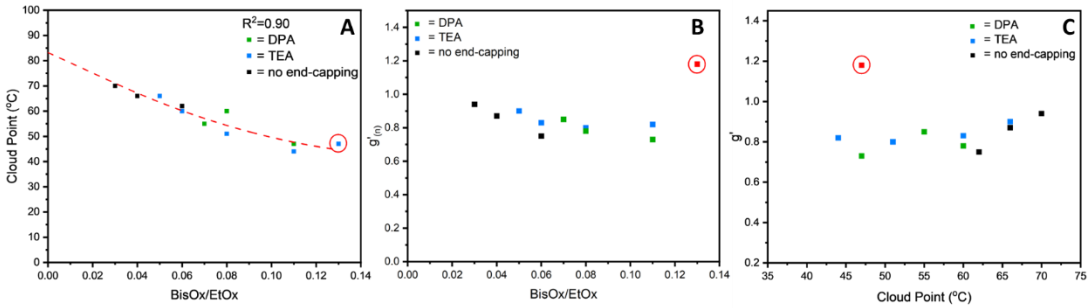

Figure 2.14. Scatter plots of **(A)** Cloud point vs. BisOx/EtOx ratio **(B)** BisOx/EtOx ratio vs g'$_{(n)}$. **(C)** g' value vs cloud point.

In **Figure 2.14.A**, the scatter plot of BisOx/EtOx ratio vs. cloud point has been plotted. A polynomial line of best fit has been derived that shows reasonable correlation between the two variables, with an R^2 value of 0.90. Interestingly, the cloud point appears to begin to plateau at around 50 °C once the BisOx/EtOx ratio reaches above 0.1, suggesting that further addition of cross-linker will not reduce the cloud point further. Extrapolating the fit to the y axis allows for prediction of the cloud point for linear pEtOx , suggesting that it is around 85-90 °C, which is an excellent fit for DP 100-150 pEtOx according to literature data.[59] It should be noted that it is not clear as to whether the decrease in cloud point is due to branching, the addition of the more hydrophobic BisOx monomer, an increase in molecular weight, or a combination thereof.

In addition, the BisOx/EtOx ratio has been plotted against g'$_{(n)}$. As can be seen in **Figure 2.14.B** the branched polymers with no end-capping have the highest g'$_{(n)}$ values and lowest BisOx/EtOx values, indicating that they have the least amount of branching of the set, despite having the highest $M_{n(GPC)}$ values. There is no apparent difference between the amount of branching between polymers end-capped with DPA and those with TEA, however. There is a clear

trend with decreasing $g'_{(n)}$ and increasing the BisOx/EtOx ratio for the polymers with no added terminating agent, however when a terminating agent is added the trend is not as clear.

Figure 2.14.C shows the relationship between $g'_{(n)}$ and polymer cloud point. As $g'_{(n)}$ increases, the cloud point increases alongside it. These results suggest that it may be possible to synthesise a hyperbranched poly(2-oxazoline) that has a cloud point of around body temperature. Hyperbranched polymers can be used for drug delivery,[60, 61] and so a hyperbranched polymer with thermoresponsivity at around body temperature is an exciting proposition because it could be used for targeted drug delivery.

2.3. Conclusions

In conclusion, the one-pot synthesis of core cross-linked star polymers *via* the CROP of 2-oxazolines using a bis 2-oxazoline cross-linker has been demonstrated. Moreover, all steps of the synthetic process were simple and efficient, with all three reaction parameters being influential on the structure of the poly(2-oxazoline) stars. It was shown that the amount of cross-linker incorporated influenced the number of arms per star, which varied from less than 10 to over 1000. The reaction concentration was found to be critical for the amount of cross-linker that could be incorporated, as well as the number of arms per star. Furthermore, it was shown that steric hindrance of the arms was an important factor that should be taken into account when considering the effective formation of a star polymer *via* this method, with shorter arms being more beneficial. Correlations were demonstrated between the chosen variables and the stars' ability to encapsulate DHA, highlighting a versatile

method to explore other factors such as the monomer R group. The best star to encapsulate was found to have DP50 arms and 10 equivalents of cross-linker, whilst being synthesised at a concentration of 0.5 M. This combination created stars with suitably sized cores for encapsulation and minimal steric hindrance from the arms. To build on this synthesis, chain extension of the arms with a more hydrophobic monomer could lead to self-assembly behaviour in a suitable solvent. Once self-assembled, a cross-linker could be added to generate star polymers. This method could make for more well-controlled core cross-linked star polymers that could allow for higher arm conversions.

As well as star polymers, hyperbranched poly(2-oxazoline)s have been synthesised for the first time using a bis-oxazoline cross-linker. Furthermore, a novel approach was taken as demonstrated by the addition of end-capping agents at the beginning of the polymerisation in order to control the degree of cross-linking. Various parameters were explored including the type of end-capping agent, amount of end-capping agent, and variation in the mono-functional monomer and bis-functional cross-linker ratio. Furthermore, correlations were drawn between the BisOx/EtOx ratio, average branching factor $g'_{(n)}$, and the cloud point. To explore branched poly(2-oxazoline)s further, the Strathclyde method could be implemented where the ratio of difunctional monomer to initiator is carefully controlled to maximise branching without gelation. Furthermore, drug encapsulation potential would be a useful application for these polymers and so analysing this would be beneficial.

2.4. Experimental

2.4.1. Materials Used

Anhydrous acetonitrile (99.9%, Acros Organics, extra dry), triethylamine (>99% Sigma-Aldrich), diisopropylethylamine (99%, Thermofisher), diisopropylamine (99%, Sigma-Aldrich), 2-propanol (99.9%, Sigma-Aldrich), diethyl ether (99.9%, Sigma-Aldrich), 1,2-ethanedithiol (98%, Sigma-Aldrich) were used as received.

2-ethyl-2-oxazoline (99%, Sigma-Aldrich) and 2-isopropenyl-2-oxazoline (98%, Sigma-Aldrich) were distilled over calcium hydride prior to use.

Propargyl *p*-toluenesulphonate (Sigma Aldrich, >97%) and methyl *p*-toluenesulphonate (>97%, Fisher Scientific) were distilled prior to use.

2.4.2. Instrument Methods Used

2.4.2.1. Nuclear Magnetic Resonance Spectroscopy

^{1}H NMR spectroscopy was measured on a Bruker DPX-300 or DPX-400 instrument and all samples were measured at either 300 MHz or 400 MHz in $CDCl_3$ at 298 K. The resonance signal of residual $CHCl_3$ at 7.26 ppm served as the reference peak for chemical shifts. Conversion of the polymers was determined from monitoring the disappearance of the 2-oxazoline ring peaks at 3.7 and 4.2 ppm.

2.4.2.2. Gel Permeation Chromatography

GPC measurements of star polymers were carried out with known concentration on an Agilent 1260 Infinity II MDS instrument equipped with differential refractive index, viscometry, dual angle light scattering and variable wavelength UV detectors. The system was equipped with 2 × PLgel Mixed-D columns (300 × 7.5 mm) and a PLgel 5 µm guard column. The eluent was dimethylformamide (DMF) with 5 mmol NH_4BF_4 additive. Samples were run at 1 mL min^{-1} at 50 °C. Poly(methyl methacrylate) standards (Agilent EasiVials) were used for calibration. Analyte samples were filtered through a nylon membrane with 0.22 μm pore size before injection. Experimental molar mass ($M_{n,GPC}$) and dispersity ($Đ$) values of synthesised polymers were determined by conventional calibration and universal calibration using Agilent GPC software.

GPC measurements of hyperbranched polymers were carried out on an Agilent Infinity II MDS instrument equipped with differential refractive index, viscometry, dual angle light scatter and multiple wavelength UV detectors. The system was equipped with 2 x PLgel Mixed C columns (300 x 7.5 mm) and a PLgel 5 µm guard column. The eluent is THF with 2% triethylamine and 0.01% butylated hydroxytoluene additives. Samples were run at 1 ml min^{-1} at 30 °C. Poly(methyl methacrylate) and polystyrene standards (Agilent EasiVials) were used for calibration. Analyte samples were filtered through a GVHP membrane with 0.22 μm pore size before injection. Respectively, experimental molar mass ($M_{n(GPC)}$) and dispersity ($Đ$) values of synthesised polymers were determined by conventional calibration using Agilent GPC software.

2.4.2.3. UV-Vis Measurements

For the drug encapsulation, UV−Vis measurements were performed on an Agilent Cary Series UV−Vis spectrophotometer. The polymers (3 mg/mL) were dissolved in distilled water and were added to vials containing dihydroxyanthroquinone (DHA) (5 mg/mL) which was suspended. The solutions were stirred for 24-76 h and were filtered using 0.45 µm nylon filters before performing the measurements at ambient temperature. Each polymer was run in triplicate and an average value taken.

For the cloud point measurements of the hyperbranched polymers, UV measurements were measured on a Cary 3500 UV-Vis Spectrophotometer. Samples were prepared at a concentration of 5 mg/mL in distilled water and experiments were run in Suprasil® quartz cuvettes (Hellman, 100-QS, light path = 10.00 mm). Samples were subjected to a heat/cool cycle from 25 °C to 85 °C and back to 25 °C at a ramp rate of 5 °C/min at a λ = 600 nm. The cloud point was determined as the temperature at which 50% transmittance was observed.

2.4.2.4. Dynamic Light Scattering

Dynamic light scattering measurements were carried out on a Malvern Nano-series dynamic light scattering instrument. The measurements were carried out in water at 25 °C in triplicate. Samples were prepared at a concentration of 5 mg/mL and filtered through a nylon membrane with 0.22 *µ*m pore size before measurement. Measurements were run in triplicate and average on the intensity setting.

2.4.2.5. Mass Spectrometry Measurements

Mass spectrometry measurements were carried out at a sample concentration of 10 ng/mL in acetonitrile before filtering through a 0.45 µm nylon filter. Samples were run on an Agilent 6130B single quad electrospray ionisation mass spectrometer with a mass range of 50-3000 m/z. The 6130B was coupled to an isocratic Agilent 110 HPLC (without column) as an automatic sample delivery system.

2.4.3. Synthesis of Bis-oxazoline Cross-linker

To an oven dried 30 mL round bottom flask 2-isopropenyl-2-oxazoline (iPOx) (5.0 g, 2 eq, 45.0 mmol) was added and the flask sealed under a nitrogen atmosphere. Next, 1,2-ethanedithiol (2.12 g, 1 eq, 22.5 mmol) was added dropwise and the reaction was left to stir overnight at room temperature. The reaction mixture was then analysed by ^{1}H NMR spectroscopy and dried under vacuum to yield the bis-oxazoline (yield – 99%).

^{1}H NMR (400 MHz, $CDCl_3$) δ 4.25 (t, *J* = 9.17 Hz, 4H) δ 3.85 (t, *J* = 9.17 Hz, 4H) δ 2.89 (m, 2H) δ 2.66 (m, 8H) δ 1.29 (d, *J* = 6.97 Hz, 6H)

^{13}C NMR (400 MHz, $CDCl_3$, DEPT) δ CH_2 67.36 CH_2 δ 54.30 δ CH_2 36.19 δ CH 34.24 δ CH_2 32.60 δ CH_3 17.25

2.4.4. Synthesis of Linear Poly(2-ethyl-2-oxazoline)s *via* CROP

The synthesis of linear poly(2-ethyl-2-oxazoline) (pEtOx) reference polymers was achieved *via* CROP in acetonitrile *via* the following typical procedure. To an oven dried and nitrogen purged microwave vial, EtOx (1.5 g, 100 eq, 15.1 mmol) and methyl *p*-toluenesulphonate (MeOTs) (22.8 µL, 1 eq, 0.15 mmol) were dissolved in acetonitrile (7.5 mL). The resulting mixture was heated at

140 °C for 10 minutes using microwave heating (Biotage Initiator+ microwave reactor). Upon cooling, a sample was taken for monomer conversion (>99%) and the reaction mixture was precipitated in diethyl ether before drying under vacuum at 40 ˚C.

2.4.1. Synthesis of Star Shaped Poly(2-ethyl-2-oxazoline)s *via* CROP

The synthesis of star shaped core cross-linked polymers was achieved by following an arm-first approach *via* CROP in acetonitrile in the following typical procedure. To an oven dried and nitrogen purged microwave vial, EtOx (0.5 mL, 50 eq, 4.95 mmol) and propargyl *p*-toluenesulphonate (PropTs) (17.1 µL, 1 eq, 0.099 mmol) were dissolved in 9.5 mL, 4.5 mL, and 2 mL acetonitrile, to obtain 0.5 M, 1 M, and 2 M reaction concentration, respectively (the density of 2-ethyl-2-oxazoline was set at 0.982 g/mL). The resulting mixture was heated at 120 °C for 60-466 minutes. Detailed reactions conditions including reaction time, temperature and concentration, for each polymer are listed in **Table 2.3**. After this time a pressure relief needle was inserted and a sample taken to determine the monomer conversion in the arm formation. Neat nitrogen purged bis 2-oxazoline cross-linker (0.173 g, 5 eq, 1 mmol) was then injected and the relief needle was removed. The reaction mixture was then left for 18 hours at 120 °C. Upon cooling, a sample was taken for monomer conversion (determined by the disappearance of the 2-oxazoline ring peaks at 3.7 and 4.2 ppm) and the mixture was precipitated in diethyl ether three times before drying under vacuum at 40 °C to yield the product, **S50-1.**

Table 2.3. Reaction conditions of the arm formation for each star polymer prepared in this study.

Entry	*Arm DP*	*BisOx (eq)*	*[Monomer] (M)*	*EtOx (g)*	*MeCN (mL)*	*Arm reaction time (mins)*	*Arm reaction temperature (°C)*
L1	100	ND	ND	0.5	0.75	60	120
S25-1	25	5	0.5	0.5	9.5	120	120
S25-3	25	5	2.0	0.5	2.0	85	100
S25-4	25	10	0.5	0.5	9.5	120	120
S50-1	50	5	0.5	0.5	9.5	240	120
S50-2	50	5	1.0	0.5	4.5	120	120
S50-3	50	5	2.0	0.5	2.0	166	100
S50-4	50	10	0.5	0.5	9.5	240	120
S50-5	50	10	1.0	0.5	4.5	120	120
S50-6	50	10	2.0	0.5	2.0	166	100
S50-7	50	20	0.5	0.5	9.5	240	120
S50-8	50	20	1.0	0.5	4.5	120	120
S100-1	100	5	0.5	0.5	9.5	466	120
S100-2	100	5	2.0	0.5	2.0	116	120
S100-3	100	10	0.5	0.5	9.5	466	120
S100-4	100	10	2.0	0.5	2.0	116	120
S100-5	100	20	0.5	0.5	9.5	466	120
S100-6	100	20	2.0	0.5	2.0	116	120

2.4.2. Synthesis of Hyperbranched Polymers *via* CROP

The synthesis of the branched polymers was achieved by following an arm-first approach *via* CROP in acetonitrile in the following typical procedure. To an oven dried and nitrogen purged microwave vial BisOx (0.10 g, 0.31 mmol, 4.2 eq) was added with a stirrer bar. The microwave vial was then sealed and

placed under a nitrogen atmosphere. To this, EtOx (0.76 g, 7.52 mmol, 100 eq) was added using a syringe. Acetonitrile (6.7 mL) was added to ensure a reaction concentration of 1 M (assuming density of BisOx and 2-ethyl-2-oxazoline is ~ 1 g/mL). Next, PropTs (16 mg, 0.075 mmol, 1 eq) was added and a sample taken for T_0. The nitrogen line was removed, and the reaction flask was stirred at 100 °C in an oil bath for 16 hours. A sample was taken for T_{final} before precipitating the polymer twice in diethyl ether and drying in a vacuum oven at 40 °C. (**P1**)

For other polymers using an end-capping agent e.g., **P5** the following procedure was used. Note: quantities of reagents used for **P5**-**P16** can be found in **Table 2.4.** BisOx (100 mg, 0.32 mmol, 6 eq) was added to a clean and dry microwave vial with a stirrer bar. The microwave vial was then sealed and placed under a nitrogen atmosphere. To this, EtOx (506 mg, 5.11 mmol, 97 eq) and TEA (5 mg, 0.05 mmol, 1 eq) were added. Acetonitrile (4.5 mL) was added to ensure a reaction concentration of 1 M (assuming density of BisOx and EtOx is ~ 1 g/mL). Next, PropTs (11 mg, 0.053 mmol, 1 eq) was added and a sample taken for T_0. The nitrogen line was removed, and the reaction flask was stirred at 100 °C in an oil bath for 16 hours. A sample was taken for T_{final} before precipitating the polymer twice in diethyl ether and drying in a vacuum oven at 40 °C.

Table 2.4. Quantities of reagents used for each hyperbranched polymer reaction.

Polymer	EtOx			BisOx			PropTs			Terminating agent				MeCN
	mg	eq	mmol	mg	eq	mmol	mg	eq	mmol	type	mg	eq	mmol	vol (mL)
P1	746	100	7.52	100	4.2	0.32	16	1	0.075	N.D.	N.D.	N.D.	N.D.	6.7
P2	522	100	5.27	100	6	0.32	11	1	0.053	N.D.	N.D.	N.D.	N.D.	4.6
P3	261	100	2.63	100	12	0.32	6	1	0.026	N.D.	N.D.	N.D.	N.D.	2.3
P4	1044	200	10.53	100	6	0.32	11	1	0.053	N.D.	N.D.	N.D.	N.D.	9.4
P5	506	97	5.11	100	6	0.32	11	1	0.053	TEA	5	1	0.05	4.5
P6	359	126	3.62	100	11	0.32	6	1	0.029	TEA	3	1	0.03	3.2
P7	285	100	2.87	100	11	0.32	6	1	0.029	TEA	3	1	0.03	2.5
P8	244	78	2.46	100	10	0.32	7	1	0.032	TEA	3	1	0.03	2.1
P9	269	43	2.72	100	5	0.32	13	1	0.063	TEA	6	1	0.06	2.3
P10	376	60	3.79	100	5	0.32	13	1	0.063	TEA	3	0.5	0.03	3.3
P11	269	43	2.72	100	5	0.32	13	1	0.063	TEA	32	5	0.32	2.3
P12	352	110	3.55	100	9.8	0.32	7	1	0.032	DPA	3	1	0.03	3.1
P13	298	95	3.00	100	10	0.32	7	1	0.032	DPA	3	1	0.03	2.6
P14	326	47.9	3.29	100	4.6	0.32	14	1	0.069	DPA	7	1	0.07	2.9
P15	294	90	2.96	100	9.6	0.32	7	1	0.033	IPA	2	1	0.03	2.6
P16	292	56	2.95	100	6	0.32	11	1	0.053	DIPEA	7	1	0.05	2.6

Table 2.5. Equivalents of EtOx and BisOx at T_0 and T_{final}, and their overall conversions for each polymer, as calculated by ^{1}H NMR Spectroscopy.

Polymer	*Terminating agent*	*Terminating agent (eq)*	*T_0 (eq)*		*T_{final} (eq)*		*EtOx conversion (%)*	*BisOx conversion (%)*
			EtOx	**BisOx**	**EtOx**	**BisOx**		
P1	N.D.	N.D.	100	4.2	100	4.2	100	100
P2	N.D.	N.D.	100	6	100	6	100	100
P3	N.D.	N.D.	100	12	100	12	100	100
P4	N.D.	N.D.	200	6	200	6	100	100
P5	TEA	1	97	6	66	3	68	50
P6	TEA	1	126	11	53	3	42	27
P7	TEA	1	100	11	60	5	60	45
P8	TEA	1	78	10	57	6	73	60
P9	TEA	1	43	5	39	5	91	100
P10	TEA	0.5	60	5	N.D.	N.D.	N.D.	N.D.
P11	TEA	5	43	5	N.D.	N.D.	N.D.	N.D.
P12	DPA	1	110	9.8	100	7	91	71
P13	DPA	1	95	10	72	6	76	60
P14	DPA	1	47.9	4.6	38	4	79	87
P15	IPA	1	90	9.6	N.D.	N.D.	N.D.	N.D.
P16	DIPEA	1	56	6	N.D.	N.D.	N.D.	N.D.

2.5. Additional Data

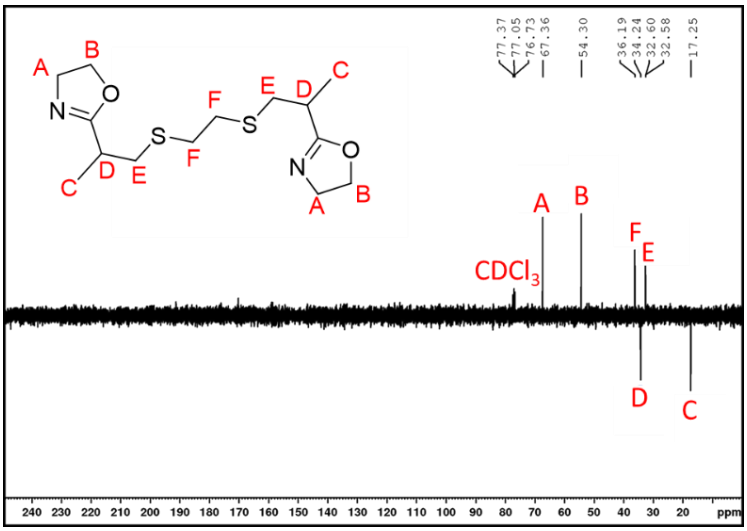

Figure 2.15. ^{13}C NMR Spectrum of BisOx. Spectra was measured using $CDCl_3$ as the solvent.

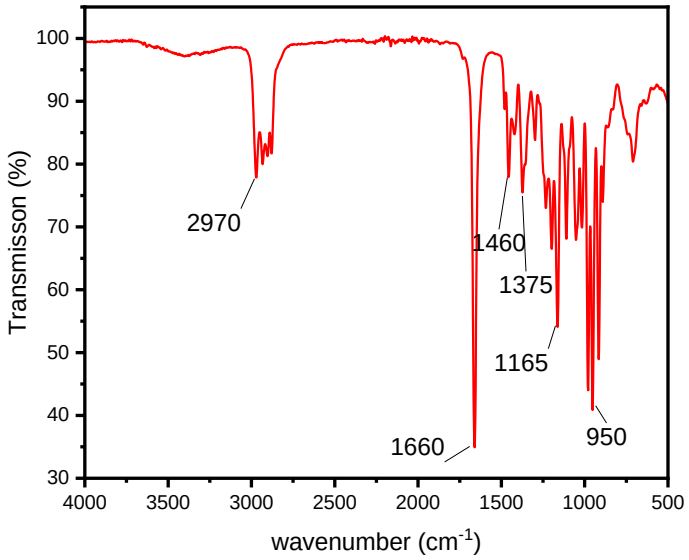

Figure 2.16. FTIR spectrum of BisOx. v_{max}/cm^{-1} 2970 (CH) 1660 (CN) 1460 (CH) 1375

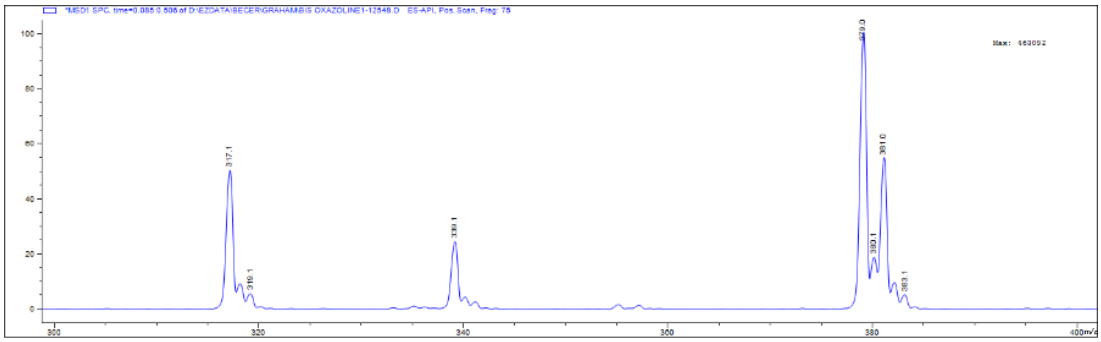

Figure 2.17. Mass spectrum of BisOx. *m/z* 316.48, 317.1 ($M + H^+$), 339.1 ($M + Na^+$), 379.0 ($M + Na^+ + K^+$)

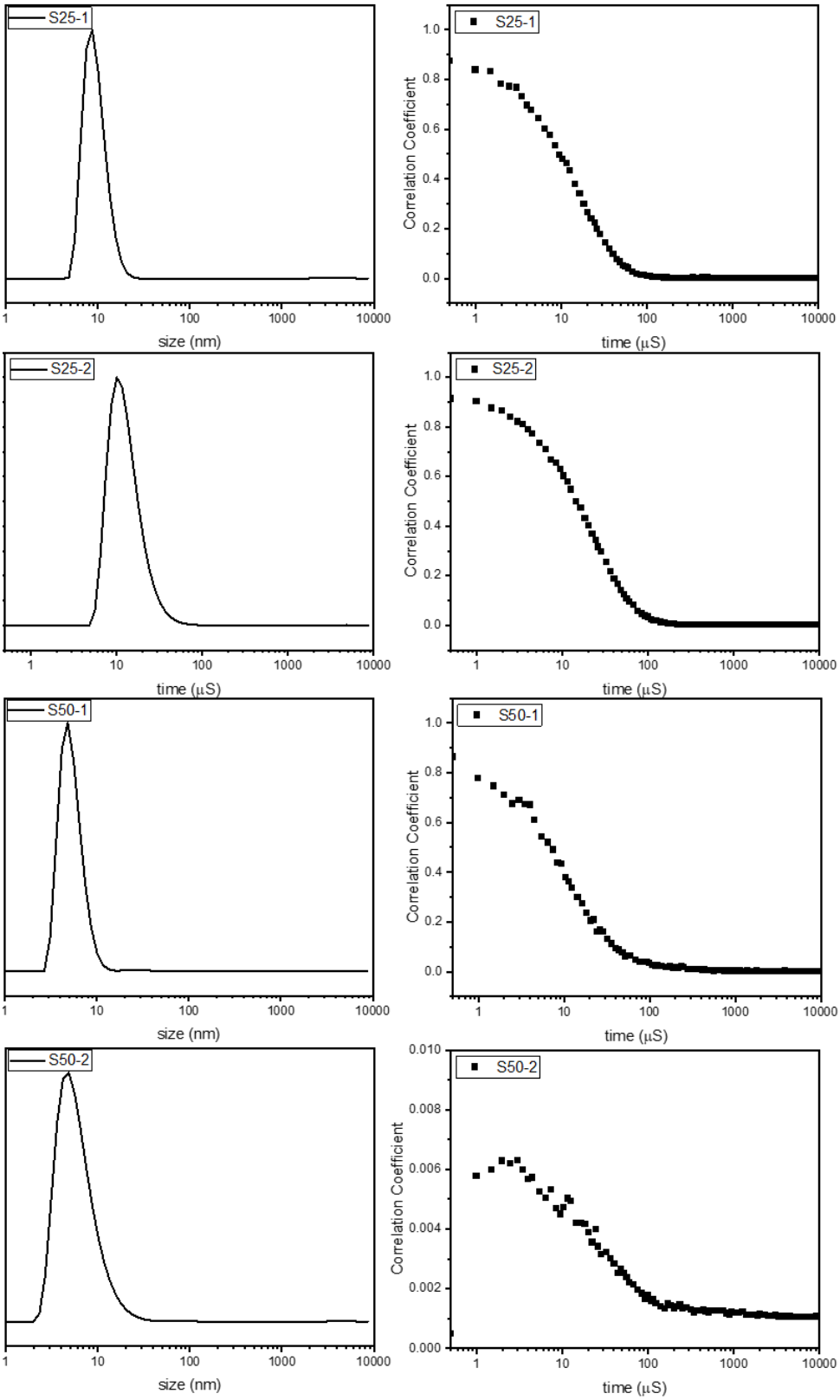

Figure 2.18. DLS plots of stars **S25-1**, **S25-2**, **S50-1**, **S50-2**. Number average plots (left), correlation function (right).

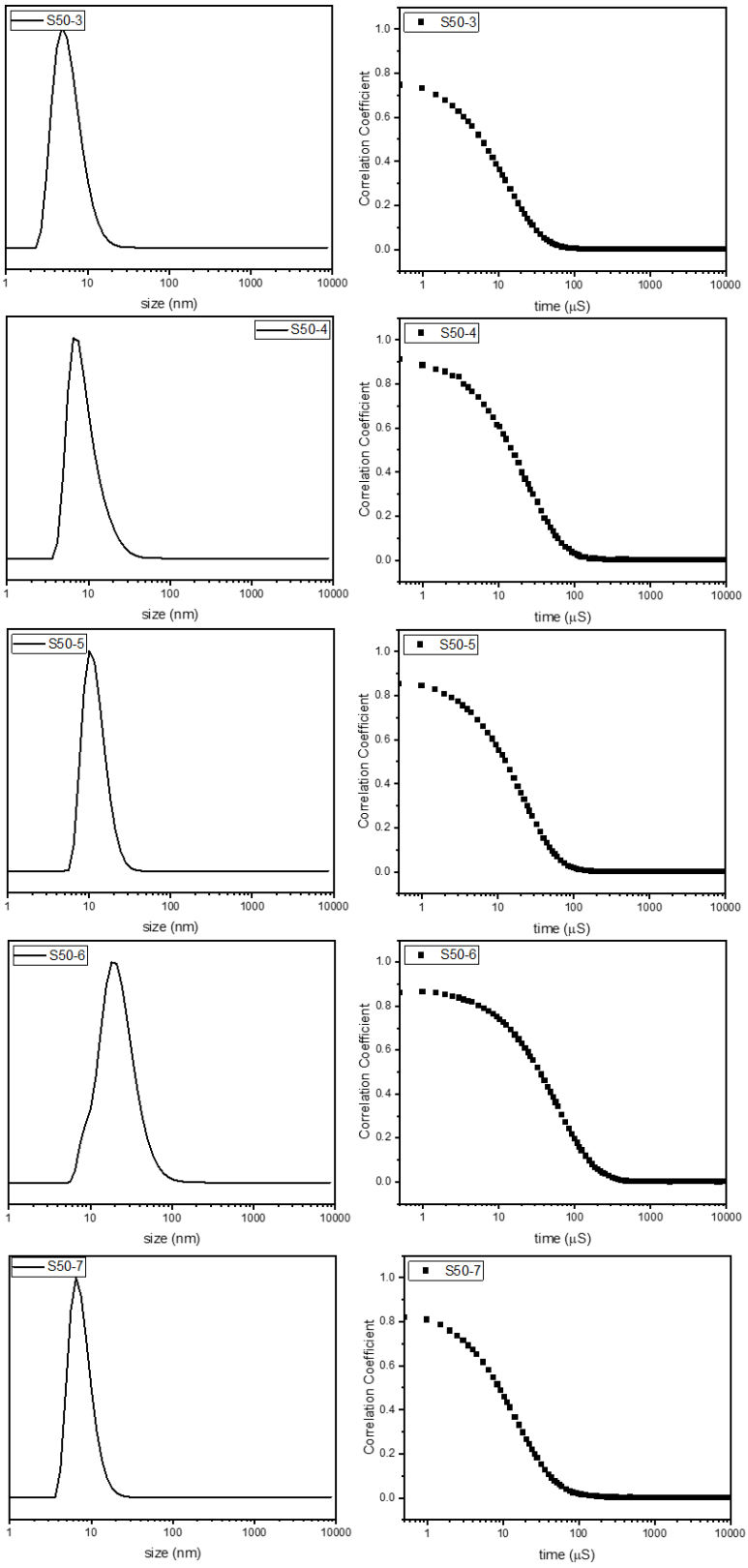

Figure 2.19. DLS plots of stars **S50-3**, **S50-4**, **S50-5**, **S50-6**, **S50-7**. Number average plots (left), correlation function (right).

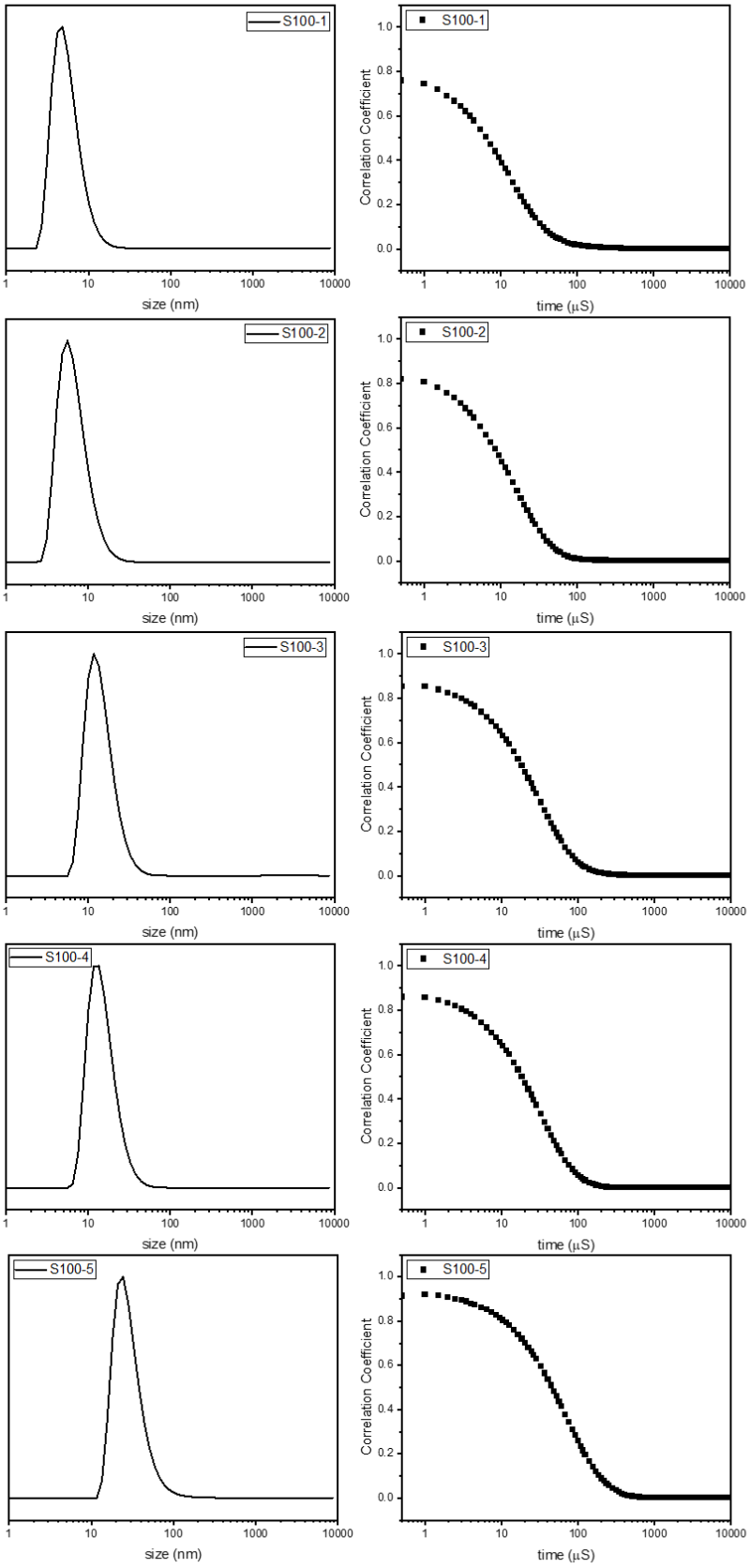

Figure 2.20. DLS plots of **S100-1**, **S100-2**, **S100-3**, **S100-4**, **S100-5**. Number average plots (left), correlation function (right).

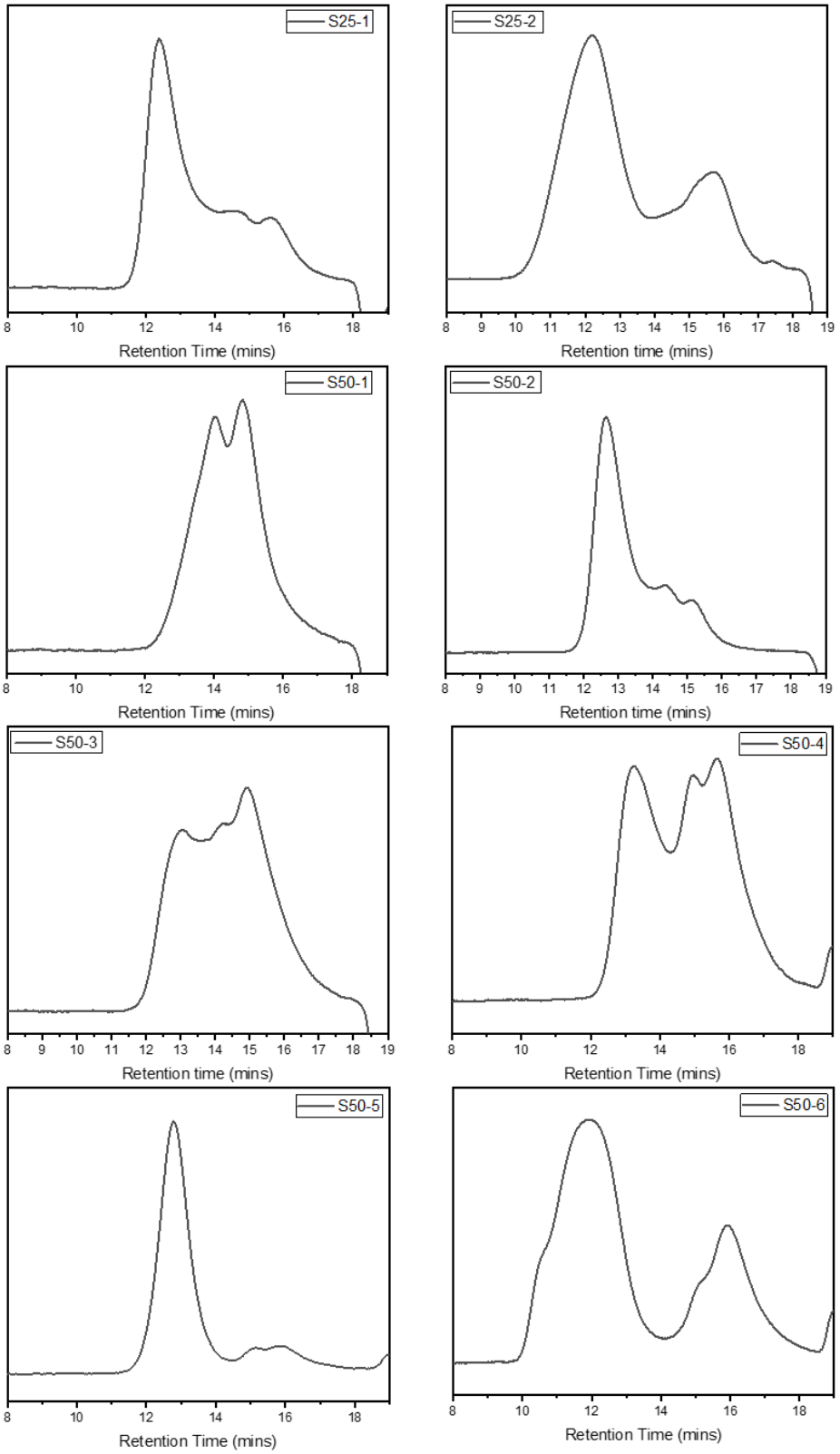

Figure 2.21. GPC RI Traces of **S25-1**, **S25-2**, **S50-1**, **S50-2**, **S50-3**, **S50-4**, **S50-5**, **S50-6** as measured on a DMF GPC.

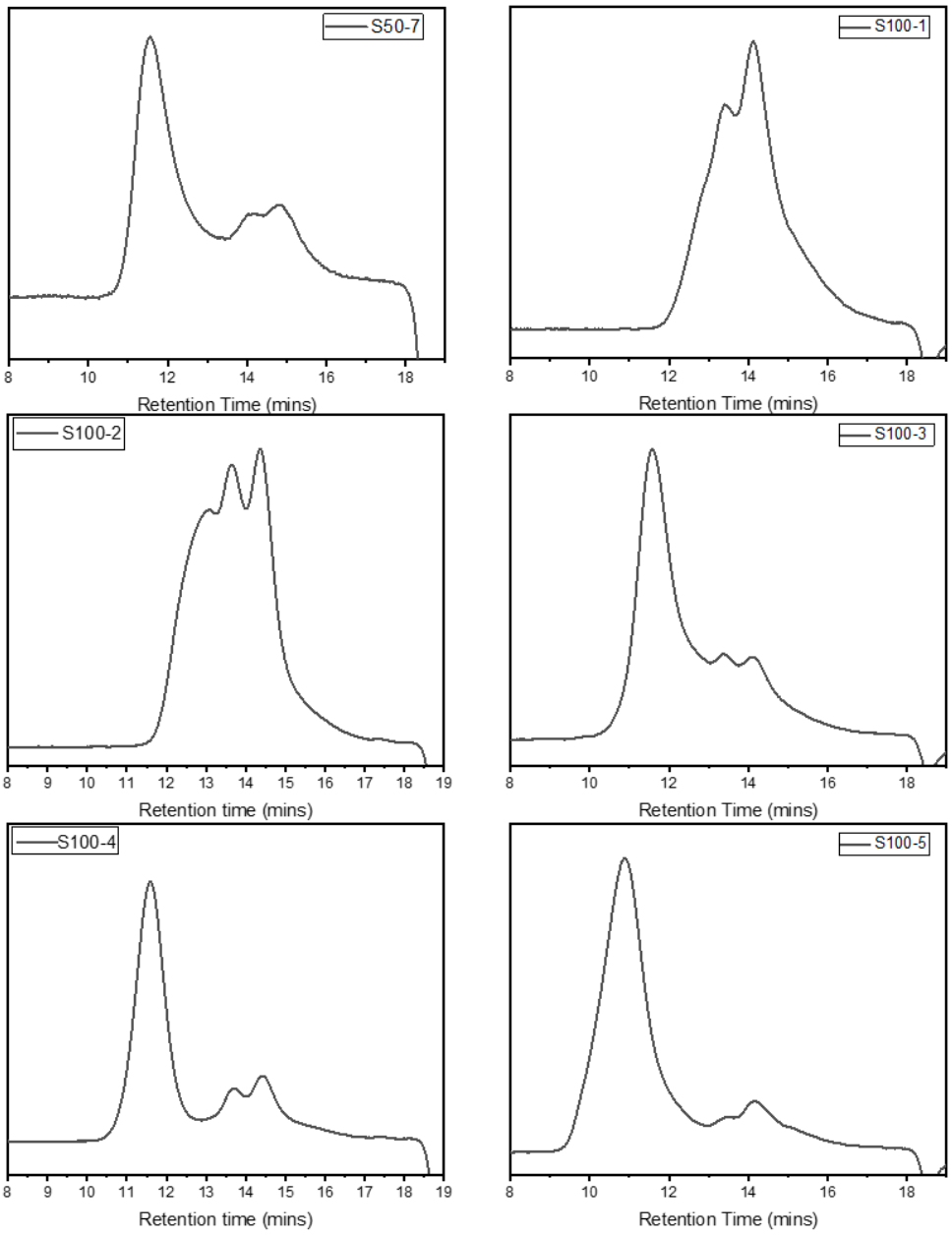

Figure 2.22. GPC RI Traces of **S50-7**, **S100-1**, **S100-2**, **S100-3**, **S100-4**, **S100-5** as measured on a DMF GPC.

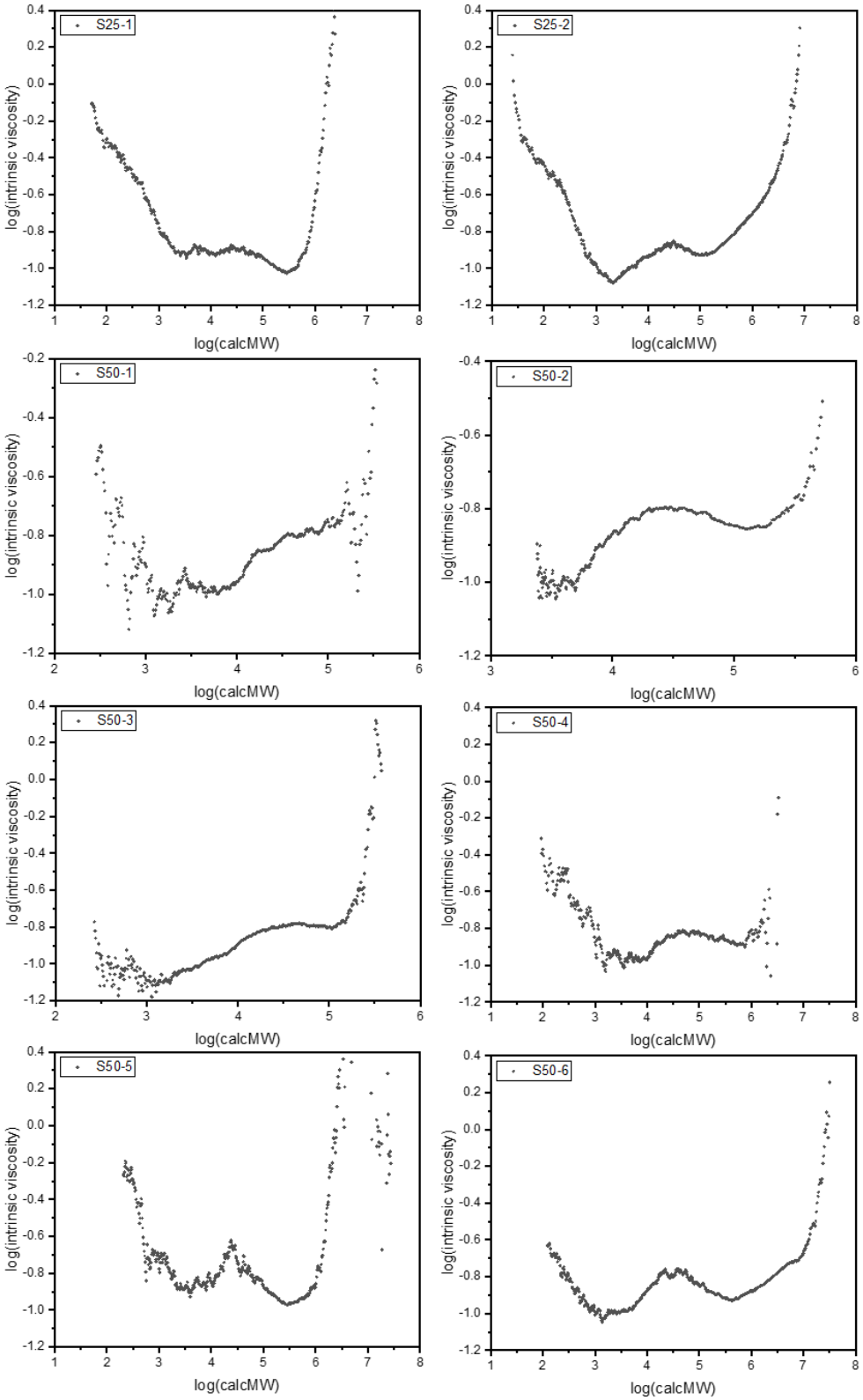

Figure 2.23. Mark-Houwink plots of **S25-1**, **S25-2**, **S50-1**, **S50-2**, **S50-3**, **S50-4**, **S50-5**, **S50-6** as measured on a DMF GPC.

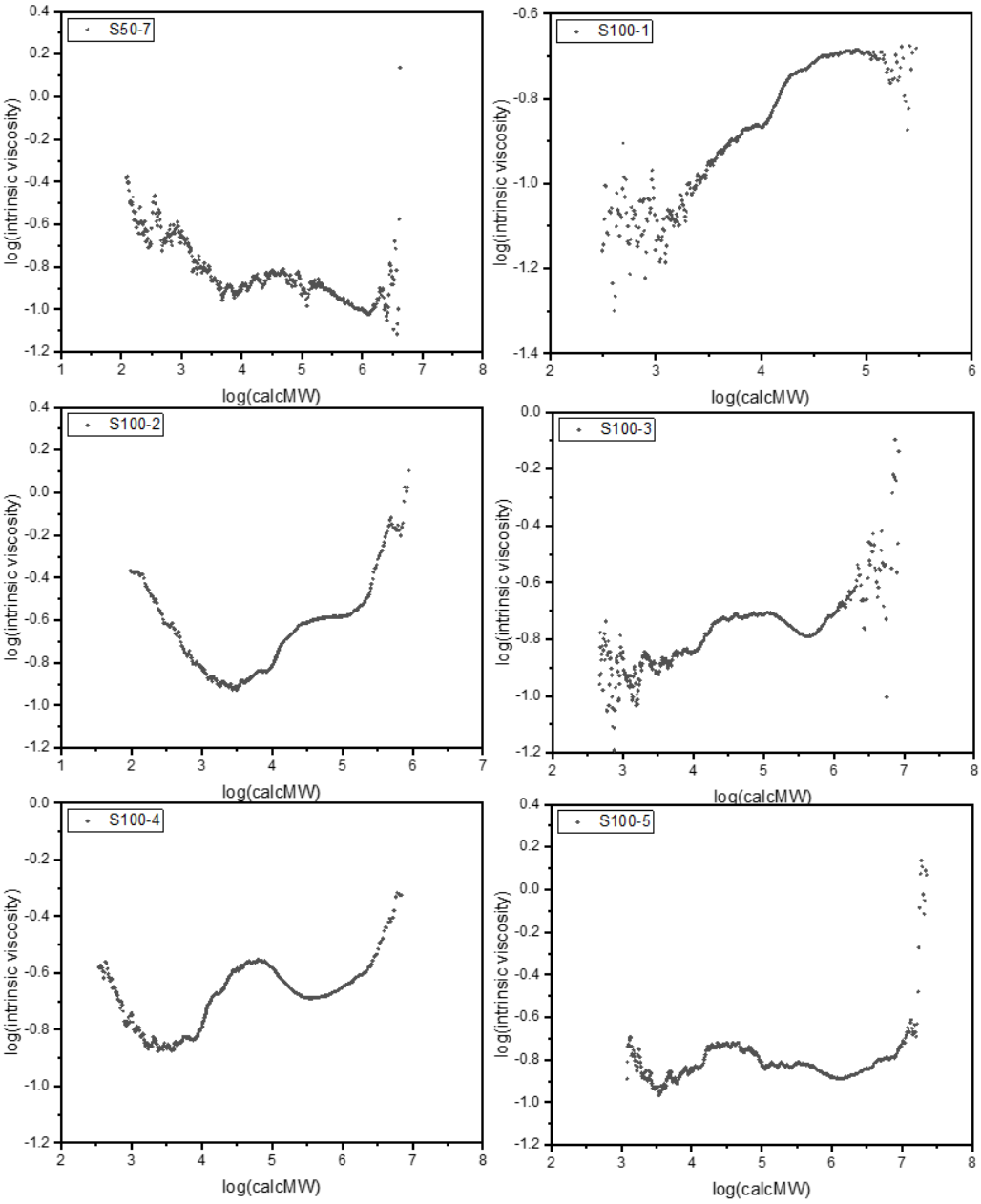

Figure 2.24. Mark-Houwink plots of **S50-7**, **S100-1**, **S100-2**, **S100-3**, **S100-4**, **S100-5** as measured on a DMF GPC.

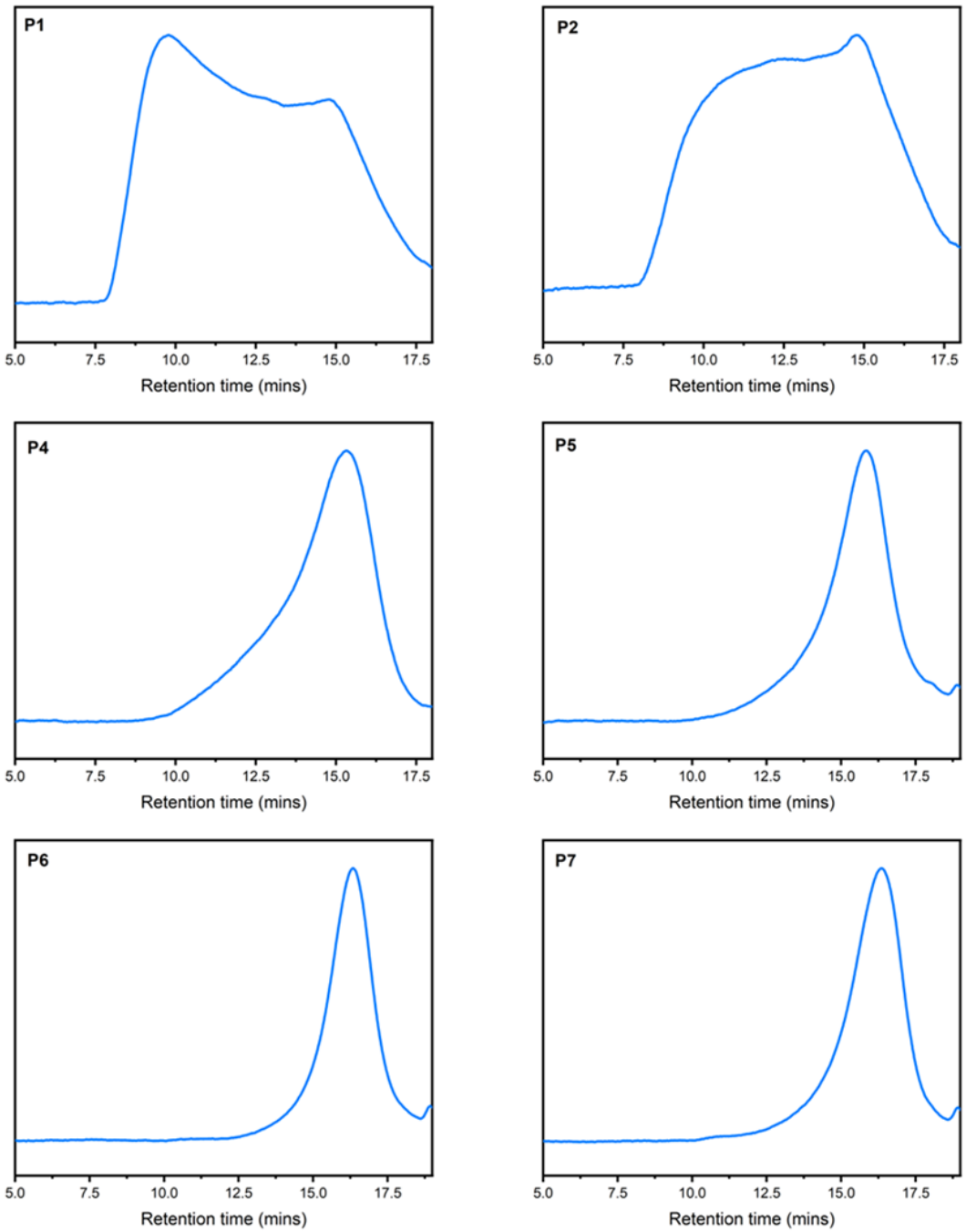

Figure 2.25. RI GPC traces of hyperbranched polymers **P1**-**P7** as measured on a THF GPC.

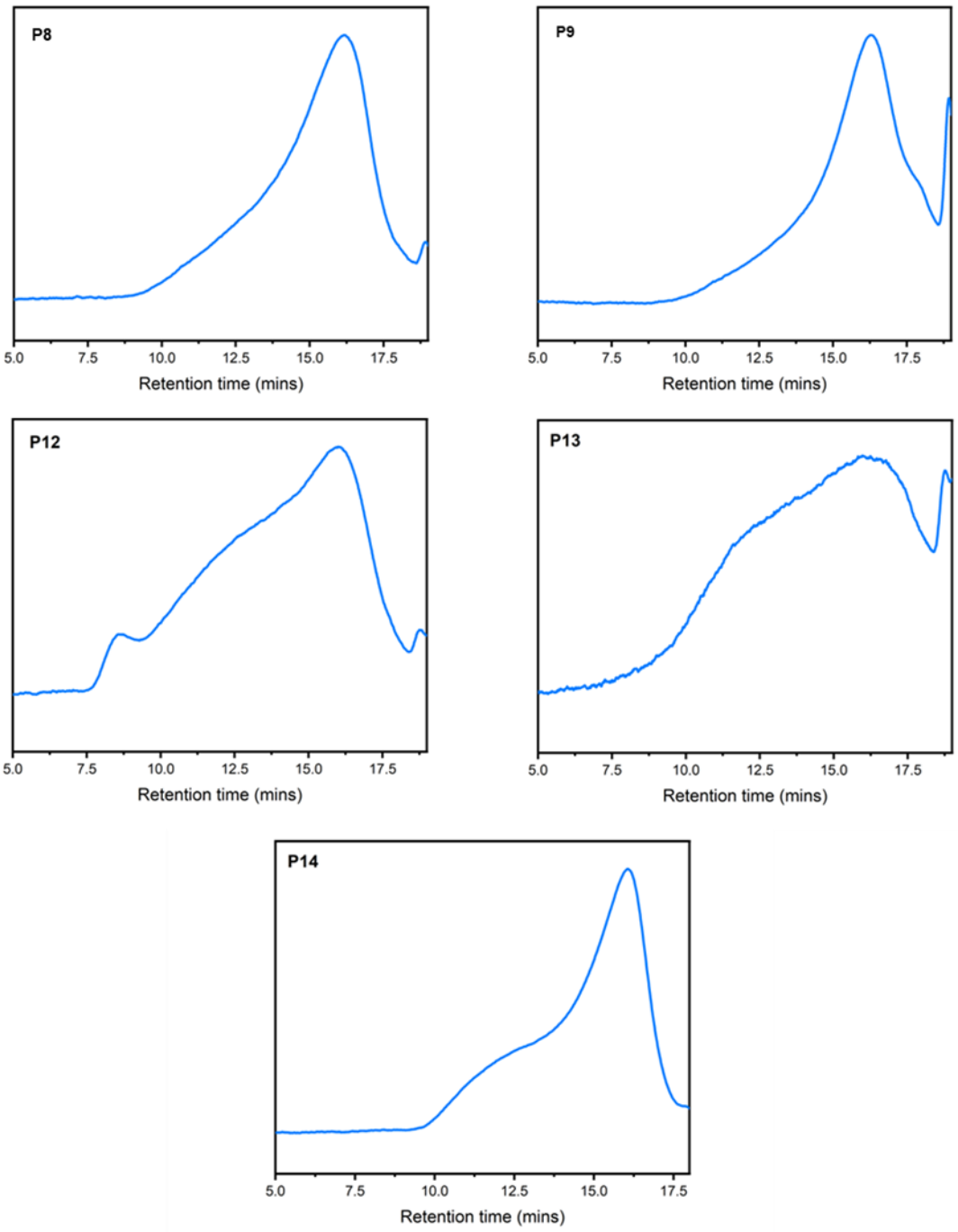

Figure 2.26. RI GPC traces of hyperbranched polymers **P8**-**P14** as measured on a THF GPC.

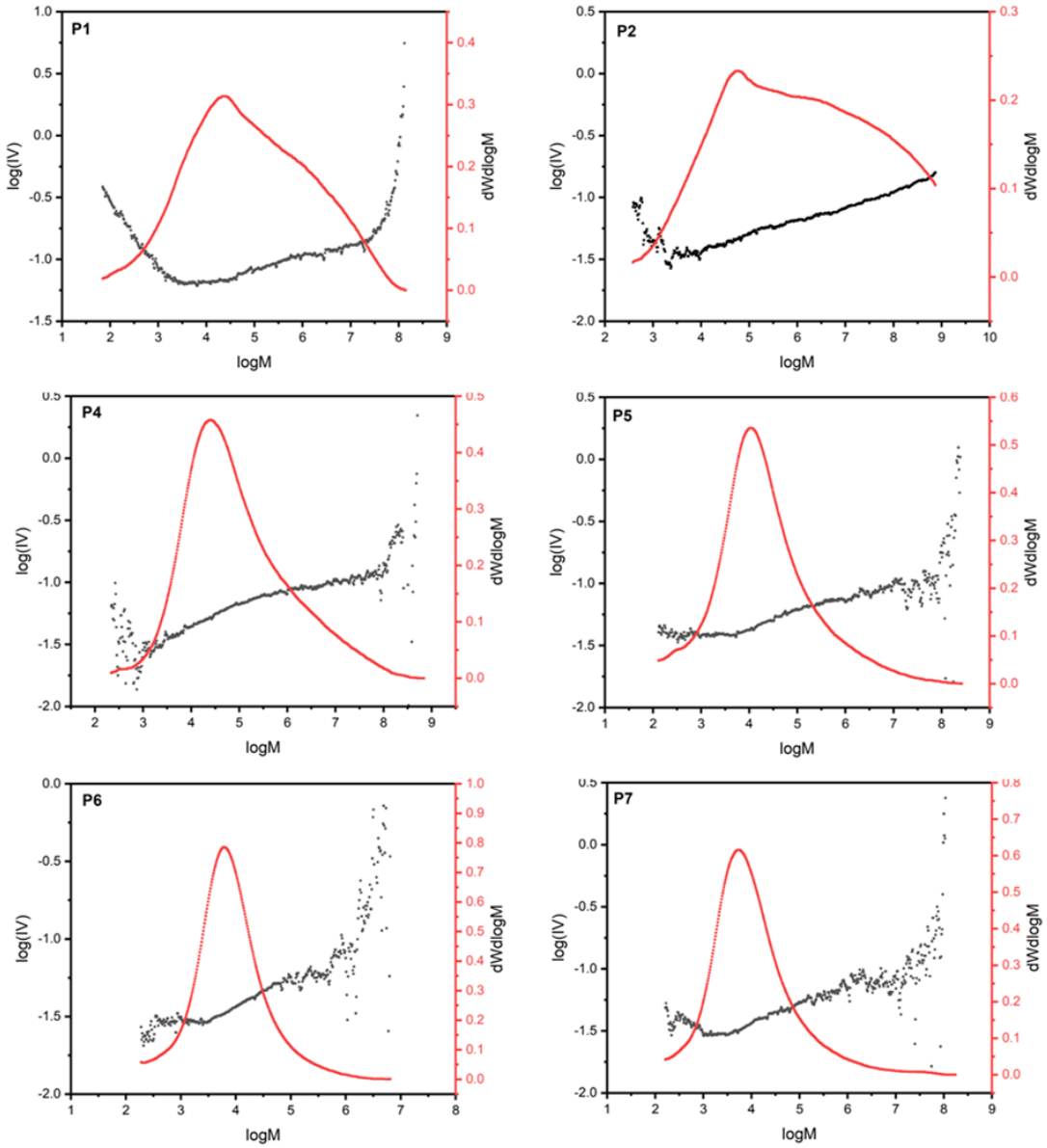

Figure 2.27. Mark-Houwink plots of hyperbranched polymers **P1**-**P7** overlaid with their dWdLogM traces, as measured on a THF GPC.

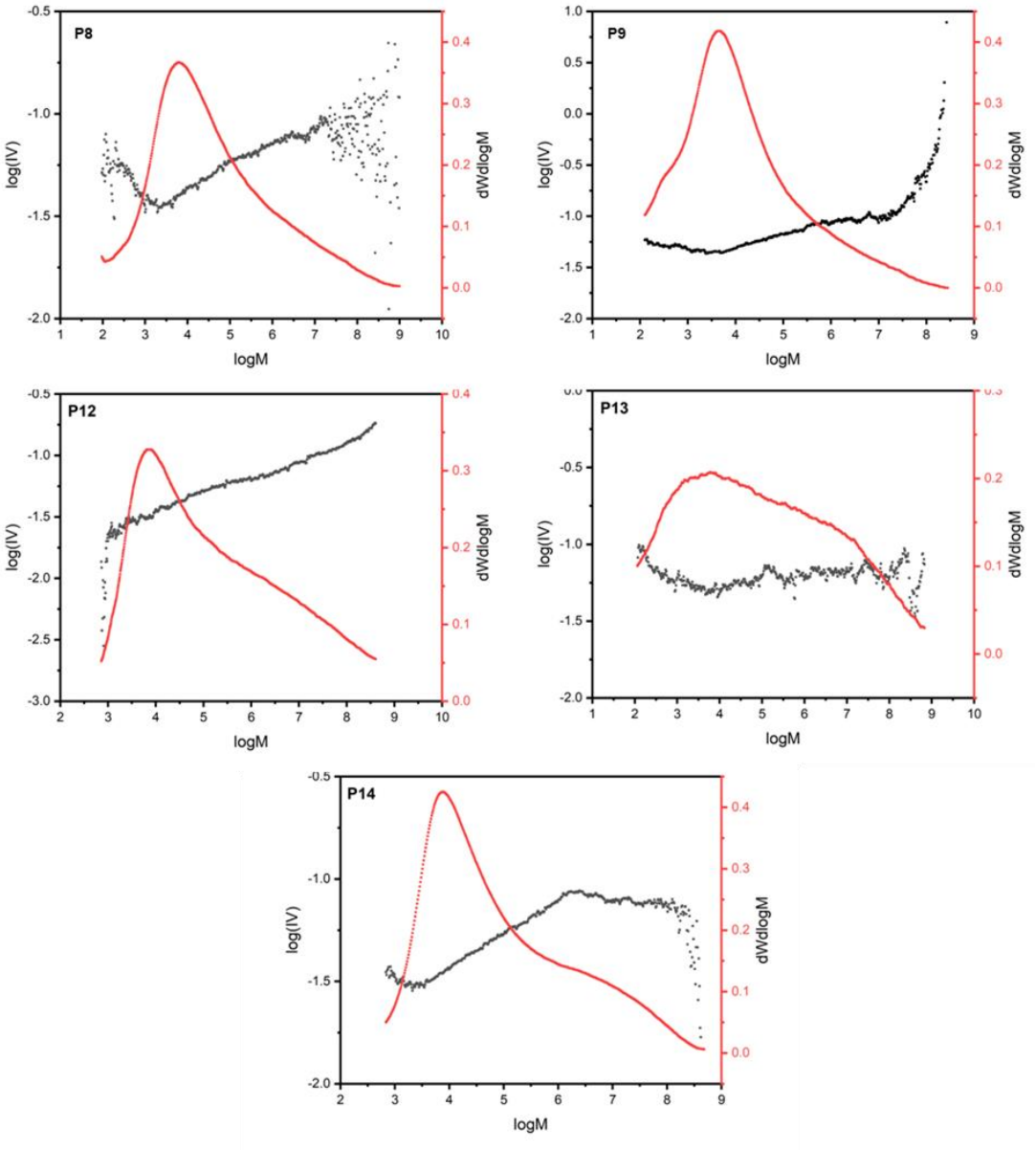

Figure 2.28. Mark-Houwink plots of hyperbranched polymers **P8**-**P14** overlaid with their dWdLogM traces, as measured on a THF GPC.

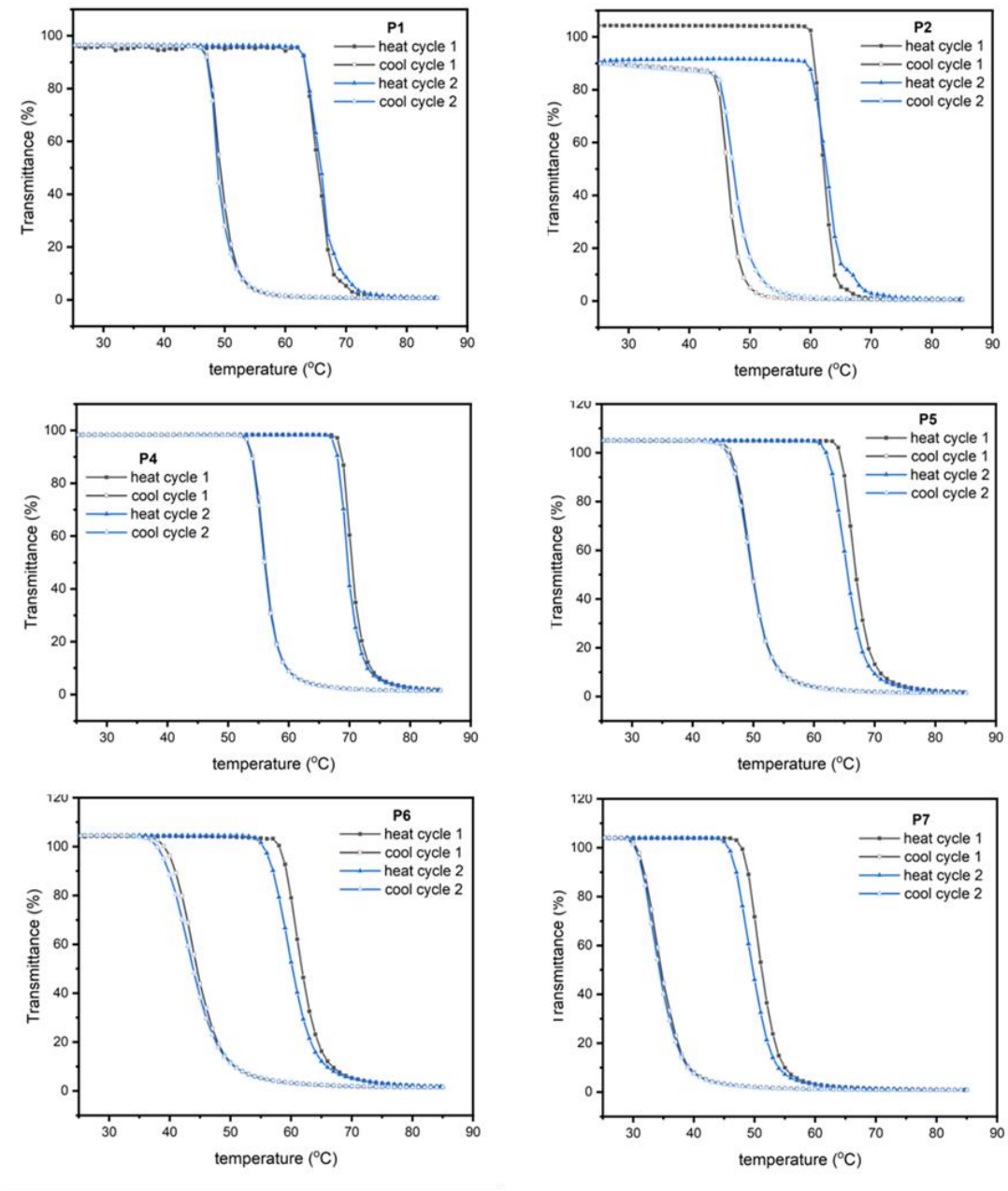

Figure 2.29. Cloud point curves for hyperbranched polymers **P1**-**P7** as determined by UV-Vis turbidimetry.

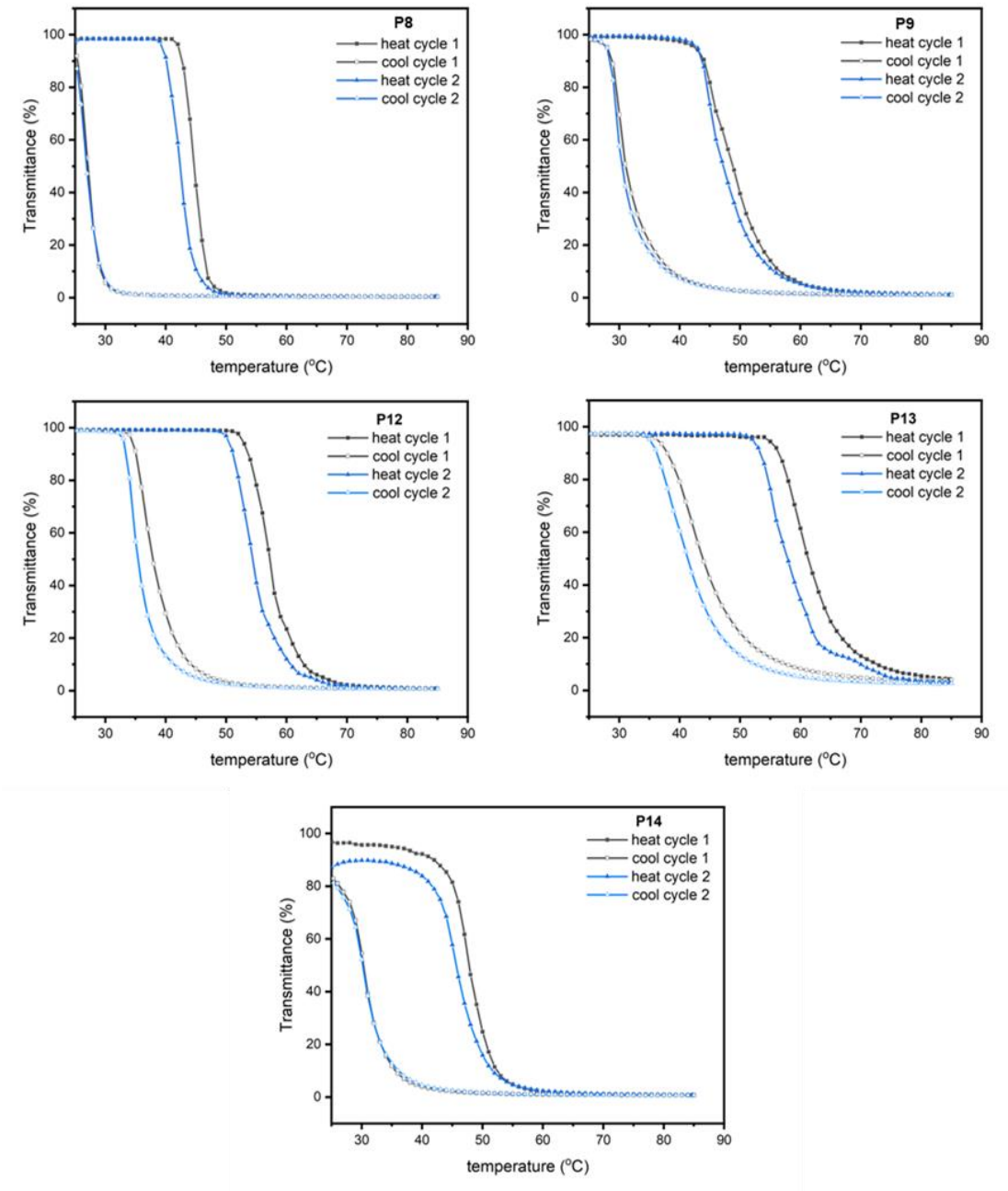

Figure 2.30. Cloud point curves for hyperbranched polymers **P8**-**P14** as determined by UV-Vis turbidimetry.

2.6. References

1. Ren, J. M.; McKenzie, T. G.; Fu, Q.; Wong, E. H. H.; Xu, J.; An, Z.; Shanmugam, S.; Davis, T. P.; Boyer, C.; Qiao, G. G., *Chemical Reviews* **2016,** *116* (12), 6743-6836.

2. Georgiou, T. K., *Polymer International* **2014,** *63* (7), 1130-1133.

3. Mitchell, D. A.; Zhang, Q.; Voorhaar, L.; Haddleton, David M.; Herath, S.; Gleinich, A. S.; Randeva, H. S.; Crispin, M.; Lehnert, H.; Wallis, R.; Patterson, S.; Becer, C. R., *Chemical Science* **2017,** *8* (10), 6974-6980.

4. Wu, W.; Wang, W.; Li, J., *Progress in Polymer Science* **2015,** *46*, 55-85.

5. Bates, M. W.; Barbon, S. M.; Levi, A. E.; Lewis, R. M.; Beech, H. K.; Vonk, K. M.; Zhang, C.; Fredrickson, G. H.; Hawker, C. J.; Bates, C. M., *ACS Macro Letters* **2020,** *9* (3), 396-403.

6. Skey, J.; Willcock, H.; Lammens, M.; Du Prez, F.; O'Reilly, R. K., *Macromolecules* **2010,** *43* (14), 5949-5955.

7. Fetters, L. J.; Kiss, A. D.; Pearson, D. S.; Quack, G. F.; Vitus, F. J., *Macromolecules* **1993,** *26* (4), 647-654.

8. Shi, Z.; Guo, F.; Tan, R.; Niu, H.; Li, T.; Li, Y., *Polymer Chemistry* **2017,** *8* (9), 1449-1453.

9. Tezel, A. K.; Leal, L. G., *Macromolecules* **2006,** *39* (13), 4605-4614.

10. van Ravensteijn, B. G. P.; Bou Zerdan, R.; Seo, D.; Cadirov, N.; Watanabe, T.; Gerbec, J. A.; Hawker, C. J.; Israelachvili, J. N.; Helgeson, M. E., *ACS Applied Materials & Interfaces* **2019,** *11* (1), 1363-1375.

11. Derry, M. J.; Smith, T.; O'Hora, P. S.; Armes, S. P., *ACS Applied Materials & Interfaces* **2019,** *11* (36), 33364-33369.

12. Monaco, A.; Beyer, V. P.; Napier, R.; Becer, C. R., *Biomacromolecules* **2020,** *21* (9), 3736-3744.

13. Zhang, Q.; Su, L.; Collins, J.; Chen, G.; Wallis, R.; Mitchell, D. A.; Haddleton, D. M.; Becer, C. R., *Journal of the American Chemical Society* **2014,** *136* (11), 4325-4332.

14. Gibson, T. J.; Smyth, P.; Semsarilar, M.; McCann, A. P.; McDaid, W. J.; Johnston, M. C.; Scott, C. J.; Themistou, E., *Polymer Chemistry* **2020,** *11* (2), 344-357.

15. Meier, M. A. R.; Gohy, J.-F.; Fustin, C.-A.; Schubert, U. S., *Journal of the American Chemical Society* **2004,** *126* (37), 11517-11521.

16. Plet, L.; Delecourt, G.; Hanafi, M.; Pantoustier, N.; Pembouong, G.; Midoux, P.; Bennevault, V.; Guégan, P., *European Polymer Journal* **2020,** *122*, 109323.

17. Vysochinskaya, Y. S.; Anisimov, A. A.; Peregudov, A. S.; Dubovik, A. S.; Orlov, V. N.; Malakhova, Y. N.; Stupnikov, A. A.; Buzin, M. I.; Nikiforova, G. G.; Vasil'ev, V. G.; Shchegolikhina, O. I.; Muzafarov, A. M., *Journal of Polymer Science Part A: Polymer Chemistry* **2019,** *57* (11), 1233-1246.

18. Huang, J.; Xiao, Z.; Liang, Hui; Lu, J., *Polymer International* **2014,** *63* (6), 1122-1128.

19. Learsch, R.; Miyake, G. M., *Journal of Polymer Science Part A: Polymer Chemistry* **2018,** *56* (7), 732-740.

20. Monaco, A.; Drain, B.; Becer, C. R., *Polymer Chemistry* **2021,** *12* (36), 5229-5238.

21. Vrijsen, J. H.; Osiro Medeiros, C.; Gruber, J.; Junkers, T., *Polymer Chemistry* **2019,** *10* (13), 1591-1598.

22. Uchiyama, M.; Satoh, K.; McKenzie, T. G.; Fu, Q.; Qiao, G. G.; Kamigaito, M., *Polymer Chemistry* **2017,** *8* (38), 5972-5981.

23. Wiltshire, J. T.; Qiao, G. G., *Macromolecules* **2008,** *41* (3), 623-631.

24. Luxenhofer, R.; Bezen, M.; Jordan, R., *Macromolecular Rapid Communications* **2008,** *29* (18), 1509-1513.

25. Zhang, C.; Liu, S.; Tan, L.; Zhu, H.; Wang, Y., *Journal of Materials Chemistry B* **2015,** *3* (27), 5615-5628.

26. Zhao, T.; Drain, B.; Yilmaz, G.; Becer, C. R., *Polymer Chemistry* **2021,** *12* (44), 6392-6403.

27. Kesharwani, P.; Jain, K.; Jain, N. K., *Progress in Polymer Science* **2014,** *39* (2), 268-307.

28. Svenson, S.; Tomalia, D. A., *Advanced Drug Delivery Reviews* **2012,** *64*, 102-115.

29. Abbasi, E.; Aval, S. F.; Akbarzadeh, A.; Milani, M.; Nasrabadi, H. T.; Joo, S. W.; Hanifehpour, Y.; Nejati-Koshki, K.; Pashaei-Asl, R., *Nanoscale Research Letters* **2014,** *9* (1), 247.

30. Liu, B.; Kazlauciunas, A.; Guthrie, J. T.; Perrier, S., *Macromolecules* **2005,** *38* (6), 2131-2136.

31. Zheng, Y.; Li, S.; Weng, Z.; Gao, C., *Chemical Society Reviews* **2015,** *44* (12), 4091-4130.

32. Isaure, F.; Cormack, P. A. G.; Graham, S.; Sherrington, D. C.; Armes, S. P.; Bütün, V., *Chemical Communications* **2004,** (9), 1138-1139.

33. Bouhier, M.-H.; Cormack, P. A. G.; Graham, S.; Sherrington, D. C., *Journal of Polymer Science Part A: Polymer Chemistry* **2007,** *45* (12), 2375-2386.

34. Rosselgong, J.; Armes, S. P.; Barton, W. R. S.; Price, D., *Macromolecules* **2010,** *43* (5), 2145-2156.

35. Xiang, L.; Song, Y.; Qiu, M.; Su, Y., *Industrial & Engineering Chemistry Research* **2019,** *58* (47), 21312-21322.

36. Yong, H.; Miao, Y.; A, S.; Quan, D.; Ivankovic, A.; Singh, K.; Zhang, J.; Zhou, D.; Wang, W., *Polymer Chemistry* **2019,** *10* (7), 885-890.

37. Mann, J. L.; Grosskopf, A. K.; Smith, A. A. A.; Appel, E. A., *Biomacromolecules* **2021,** *22* (1), 86-94.

38. Li, W.; Yoon, J. A.; Zhong, M.; Matyjaszewski, K., *Macromolecules* **2011,** *44* (9), 3270-3275.

39. Hawker, C. J.; Frechet, J. M.; Grubbs, R. B.; Dao, J., *Journal of the American Chemical Society* **1995,** *117* (43), 10763-10764.

40. Zahoranová, A.; Kroneková, Z.; Zahoran, M.; Chorvát Jr, D.; Janigová, I.; Kronek, J., *Journal of Polymer Science Part A: Polymer Chemistry* **2016,** *54* (11), 1548-1559.

41. Schenk, V.; Rossegger, E.; Ebner, C.; Bangerl, F.; Reichmann, K.; Hoffmann, B.; Höpfner, M.; Wiesbrock, F., *Polymers* **2014,** *6* (2), 264-279.

42. Hartlieb, M.; Schubert, S.; Kempe, K.; Windhab, N.; Schubert, U. S., *Journal of Polymer Science Part A: Polymer Chemistry* **2015,** *53* (1), 10-14.

43. Hartlieb, M.; Pretzel, D.; Englert, C.; Hentschel, M.; Kempe, K.; Gottschaldt, M.; Schubert, U. S., *Biomacromolecules* **2014,** *15* (6), 1970-1978.

44. Kurniasih, I. N.; Keilitz, J.; Haag, R., *Chemical Society Reviews* **2015,** *44* (12), 4145-4164.

45. Choi, J.; Kwak, S.-Y., *Environmental Science & Technology* **2007,** *41* (10), 3763-3768.

46. Wiltshire, J. T.; Qiao, G. G., *Australian Journal of Chemistry* **2007,** *60* (10), 699-705.

47. Beyer, V. P.; Monaco, A.; Napier, R.; Yilmaz, G.; Becer, C. R., *Biomacromolecules* **2020,** *21* (6), 2298-2308.

48. Wei, X.; Moad, G.; Muir, B. W.; Rizzardo, E.; Rosselgong, J.; Yang, W.; Thang, S. H., *Macromolecular Rapid Communications* **2014,** *35* (8), 840-845.

49. Bohdanecky, M., *Macromolecules* **1977,** *10* (5), 971-975.

50. Adam, M.; Delsanti, M., *Macromolecules* **1977,** *10* (6), 1229-1237.

51. Litt, M.; Levy, A.; Herz, J., *Journal of Macromolecular Science: Part A - Chemistry* **1975,** *9* (5), 703-727.

52. Gao, H.; Matyjaszewski, K., *Macromolecules* **2006,** *39* (9), 3154-3160.

53. Connal, L. A.; Gurr, P. A.; Qiao, G. G.; Solomon, D. H., *Journal of Materials Chemistry* **2005,** *15* (12), 1286-1292.

54. Thiele, C.; Auerbach, D.; Jung, G.; Qiong, L.; Schneider, M.; Wenz, G., *Polymer Chemistry* **2011,** *2* (1), 209-215.

55. Konkolewicz, D.; Gray-Weale, A.; Perrier, S., *Polymer Chemistry* **2010,** *1* (7), 1067-1077.

56. Durie, S.; Jerabek, K.; Mason, C.; Sherrington, D. C., *Macromolecules* **2002,** *35* (26), 9665-9672.

57. O'Brien, N.; McKee, A.; Sherrington, D. C.; Slark, A. T.; Titterton, A., *Polymer* **2000,** *41* (15), 6027-6031.

58. Menezes, R. N. L. d.; Felisberti, M. I., *Polymer Chemistry* **2021,** *12* (32), 4680-4695.

59. Hoogenboom, R.; Thijs, H. M. L.; Jochems, M. J. H. C.; van Lankvelt, B. M.; Fijten, M. W. M.; Schubert, U. S., *Chemical Communications* **2008,** (44), 5758-5760.

60. Kavand, A.; Anton, N.; Vandamme, T.; Serra, C. A.; Chan-Seng, D., *Journal of Controlled Release* **2020,** *321*, 285-311.

61. Wan, W.; Ouyang, H.; Long, W.; Yan, W.; He, M.; Huang, H.; Yang, S.; Zhang, X.; Feng, Y.; Wei, Y., *ACS Sustainable Chemistry & Engineering* **2019,** *7* (23), 19202-19212.

Chapter 3. Hybrid Multiblock Copolymers of 2-Oxazolines and Acrylates *via* a Cu Catalysed Azide-Alkyne Cycloaddition Step-Growth Mechanism

Part of this chapter has been accepted for publication:

Hayes, G.; Drain, B.; Lefley, J. Becer, C.R.; Macromolecules, 2022

3.1. Introduction

Block polymers are a very interesting type of polymeric architecture as they can be used to covalently link polymers of different polarities that are normally non-miscible. This can have interesting results, including self-assembly into micelles and other structures. Furthermore, block polymers have a range of potential applications, including being employed to span the phase boundary between non-miscible materials such as polyethylene/isotactic polypropylene.[1, 2] The non-miscibility of polyethylene/isotactic polypropylene is of scientific interest because it makes recycling these polymers challenging. Also, block polymers can be used to create highly ordered soft materials[3] which allow for applications in drug delivery,[4] microelectronics,[5] and advanced plastics.[6] Poly(2-oxazoline)s have previously been used in the synthesis of multiblock polymers, including hybrid polymers combining different polymerisation techniques.[7] Previous examples of this include a heterofunctional initiator that was used to combine poly(2-oxazoline) with styrene,[8] and poly(2-oxazoline)s end-capped with an appropriate initiator for another polymerisation technique such as reversible addition-fragmentation chain transfer polymerisation (RAFT)[9] and copper (0)-mediated reversible deactivation radical polymerisation (Cu(0)-RDRP).[10, 11] Furthermore, the different chemistry of each polymer block can lead to interesting physical behaviour such as amphiphilicity.[12]

Frequently, post polymerisation click reactions such as the thiol-ene reaction[13] and copper(I) catalysed azide-alkyne cycloaddition (CuAAC) [14, 15] are used as simple techniques to access higher orders of polymeric architecture such as stars,[16] brushes,[17] cyclic polymers,[18] and multiblock polymers.[19] Click

chemistry can be used in conjunction with suitably designed heterotelechelic polymers to generate high molecular weight multiblock step-growth polymers *via* intermolecular reaction.[20] Moreover, click reactions have the advantage of proceeding rapidly and effectively in various solvents.[21] The competing intramolecular click reaction forming the cyclic product can be undesired and careful reaction optimisation is often required.[18, 22] Despite this, cyclic polymers also have unique physical properties [23, 24] and similarly minimising the intermolecular step-growth reaction can be desirable in some cases. For instance, cyclic polymers have lower hydrodynamic volumes,[25] lower intrinsic viscosities,[26] are less susceptible to degradation,[23, 27] and demonstrate different cloud point temperatures to their linear counterparts.[28] Furthermore, they are a promising biointerface as they typically produce a denser and thicker surface film compared to linear equivalents.[29] However, the synthesis of cyclic polymers can be challenging, often requiring very dilute conditions to minimise the amount of linear polymers *via* step-growth mechanism. [23, 30]

In this chapter, a simple reaction mechanism involving the end-capping of a propargyl initiated poly(2-oxazoline) chain with an initiator for Cu(0)-RDRP is demonstrated, followed by subsequent polymerisation and conversion of the polymer chain end from a bromide into an azide. CuAAC of the polymers was then carried out to study the effects of 2-oxazoline block length, acrylate block length, solvent polarity, and copper concentration on the ratio of step-growth to cyclisation (see **Scheme 3.1.**). Furthermore, the structures of the formed hybrid multiblock products were evaluated *via* advanced gel permeation chromatography (GPC) and their self- assembly behaviour into stomatocyte-like nanoparticles was investigated.

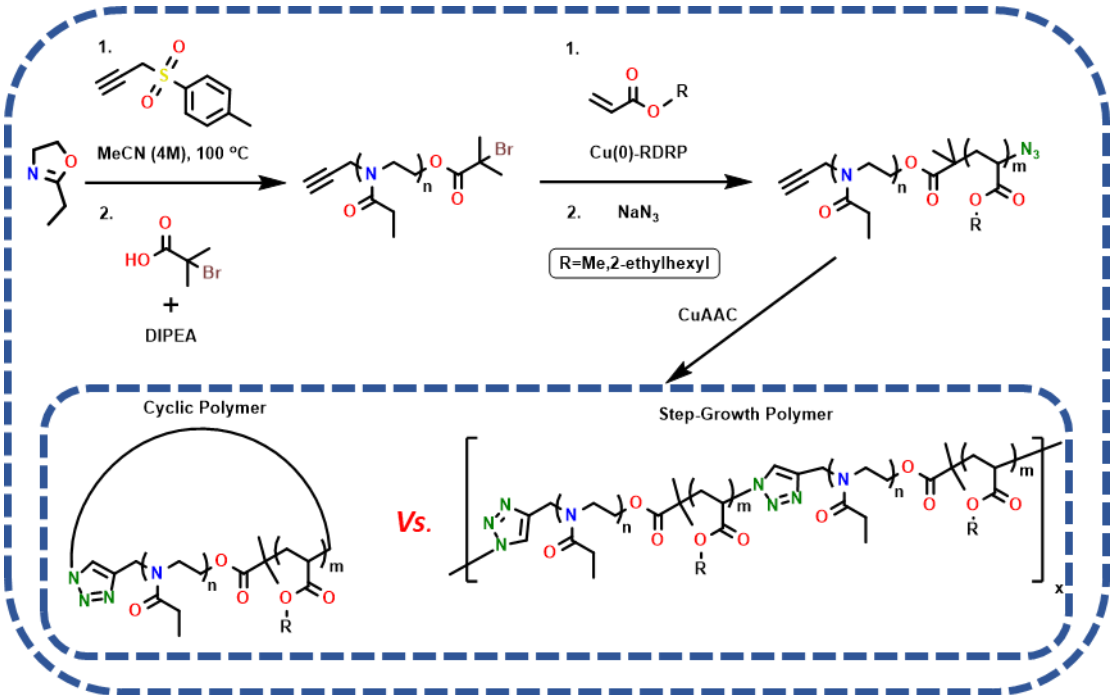

Scheme 3.1. Synthetic pathway for the 2-oxazoline macroinitiator synthesis *via* cationic ring opening polymerisation (CROP), subsequent chain extension of acrylates *via* Cu(0) RDRP, and final CuAAC reaction generating hybrid multiblock/cyclic polymers *via* step growth mechanism.

3.2. Results and Discussion

3.2.1. Synthesis of Poly(2-ethyl-2-oxazoline)-Acrylate Macromonomers

Firstly, the poly(2-ethyl-2-oxazoline) (pEtOx) macroinitiator was synthesised *via* end-capping of the living polymer chains with 2-bromo-2-methylpropionic acid (BMPA). Three macroinitiators were synthesised, with monomer to initiator ratios ([M]:[I]) of 19, 25, and 40. In this section discussing the synthesis of the macroinitiators, the macroinitiator with an [M]:[I] of 19 ($pEtOx_{19}$-I) is focussed on as the other macroinitiators were synthesised in the same way. Firstly, to calculate the end-capping efficiency of the polymer chains, ^{1}H nuclear magnetic resonance (NMR) spectroscopy was used demonstrating that at least 90% of the chains had been successfully end-capped, by

comparing the integral of peak **F** to the other polymer peak integrals.(**Figure 3.1.**).

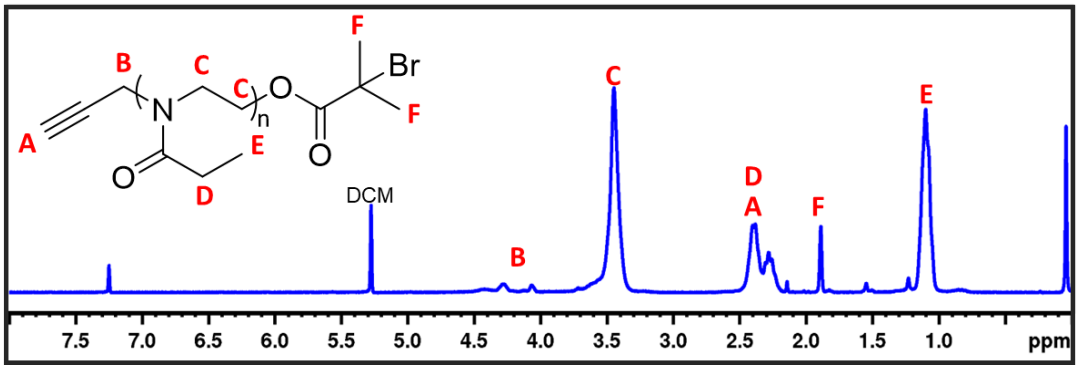

Figure 3.1. ^{1}H NMR spectrum of PEtOx-I. Spectra was measured using $CDCl_3$ as a solvent.

To confirm the end-capping, the matrix assisted laser desorption ionisation time of flight mass spectrum (MALDI-TOF-MS) of the polymer was also obtained and is shown in **Figure 3.2**. The spectrum shows a major distribution which corresponds to the sodium adduct of the polymer with both a propargyl group on the α chain end and BMPA on the Ω chain end. There are also two minor distributions (see magnified region, **Figure 3.2.**) however these distributions could not be assigned.

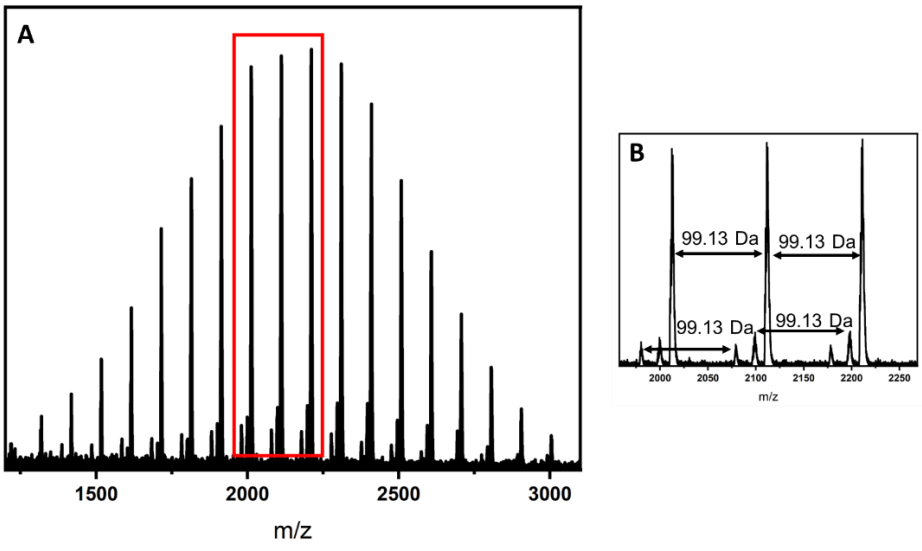

Figure 3.2. MALDI-TOF-MS for BMPA end-capped pEtOx macroinitiator (pEtOx-I). **(A)** Full spectrum, **(B)** magnified insert. [M+Na$^+$] calc = 2110.44 Da, [M+Na$^+$] found = 2111.36 Da.

In addition to the MALDI-TOF-MS data, the chain extension was attempted for $pEtOx_{19}$-I using 2-ethylhexyl acrylate (EHA) *via* Cu(0)-RDRP (**Scheme 3.1.**). To enable the measurement of the Ω chain end functionality of $pEtOx_{19}$-I, a large degree of polymerisation was employed such that any leftover $pEtOx_{19}$-I would be apparent in the GPC and the functionality could be calculated. Due to the hydrophobic nature of EHA, trifluoroethanol (TFE) was used because literature reports indicate that TFE is a good solvent for the Cu(0)-RDRP of hydrophobic acrylates.[31] The [EHA]:[$PEtOx_{19}$-I] was set at 93:1. As can be seen from **Figure 3.3.A**, a complete shift was observed in the GPC chromatogram and no residual $pEtOx_{19}$-I is detected. Therefore, this further indicated that the majority of the chains had the end-group desired. It should be noted that this end-capping reaction with BMPA and subsequent chain-extension has been previously reported with styrene monomers.[10, 11] The chain extension of the other synthesised macroinitiators $pEtOx_{25}$ and $pEtOx_{40}$ were tested with methyl acrylate (MA), and can be seen in **Figure 3.3.B** and **Figure 3.3.C**. In each case, a complete shift in the entire polymer peak demonstrated that the end-group fidelity of each synthesised macroinitiator was excellent. Furthermore, the dispersity of each polymer *post*-chain extension was low, indicating that the polymerisation was living.

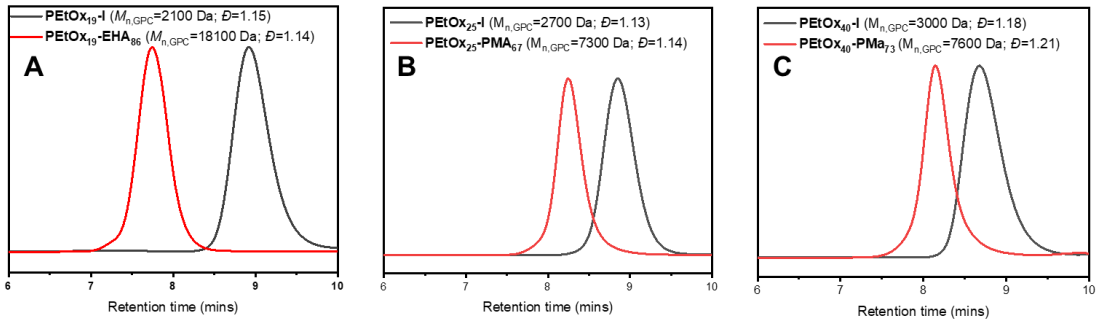

Figure 3.3. GPC traces of **(A)** Successful chain extension of pEtOx$_{19}$-I with EHA to form a pEtOx$_{19}$-EHA$_{86}$ macromonomer**. (B)** Chain extension of pEtOx$_{25}$-I with methyl acrylate to form a pEtOx$_{25}$-MA$_{67}$ macromonomer. **(C)** Chain extension of pEtOx$_{40}$-I with MA to form a pEtOx$_{40}$-EHA$_{73}$ macromonomer. All chromatograms were measured on a THF GPC.

Next, the kinetics of the Cu(0)-RDRP of both EHA and MA were measured to examine the livingness of the chain extension and to ensure that there were no issues with the macroinitiators such as slow initiation. For the chain extension with EHA, TFE was used because as mentioned, it is reported as a good solvent for hydrophobic acrylates. Nonetheless, there was a long induction period presumably due to an imbalance in the copper species. For this reason, a small amount of Cu(II)Br was added (0.05 eq) to help the system equilibrate. Cu(II)Br- Tris(2-(dimethylamino)ethyl)amine (Me$_6$TREN) is not soluble in TFE however, and so this was formed in a minimal amount of dimethylformamide (DMF) first. As can be seen from **Figure 3.4.A**, the first order kinetic plot follows a linear trend indicating a constant concentration of propagating species, and shows that the initiation is fast. Furthermore, the addition of Cu(II)Br has removed any induction period, with the polymerisation starting immediately. The final GPC trace demonstrates a very well-controlled polymerisation with a *Đ* of less than 1.10. For the chain extension with MA, DMF could be used as the solvent and there was no induction period. The first order kinetic plot initially demonstrated a linear trend indicating no termination

events were occurring (**Figure 3.4.B**) until around log2.5. At high monomer conversion however, there was some loss of control as demonstrated by the increasing *Đ* at 90% conversion and above, and the deviation from the linear first order kinetic plot above log2.5. This is also reflected in the GPC traces (**Figure 3.4.B**) that start to show a high molecular weight shoulder at high conversions, suggesting that polymer-polymer coupling could be occurring. For this reason, polymerisations were typically stopped at around 90% conversion to prevent coupling from arising.

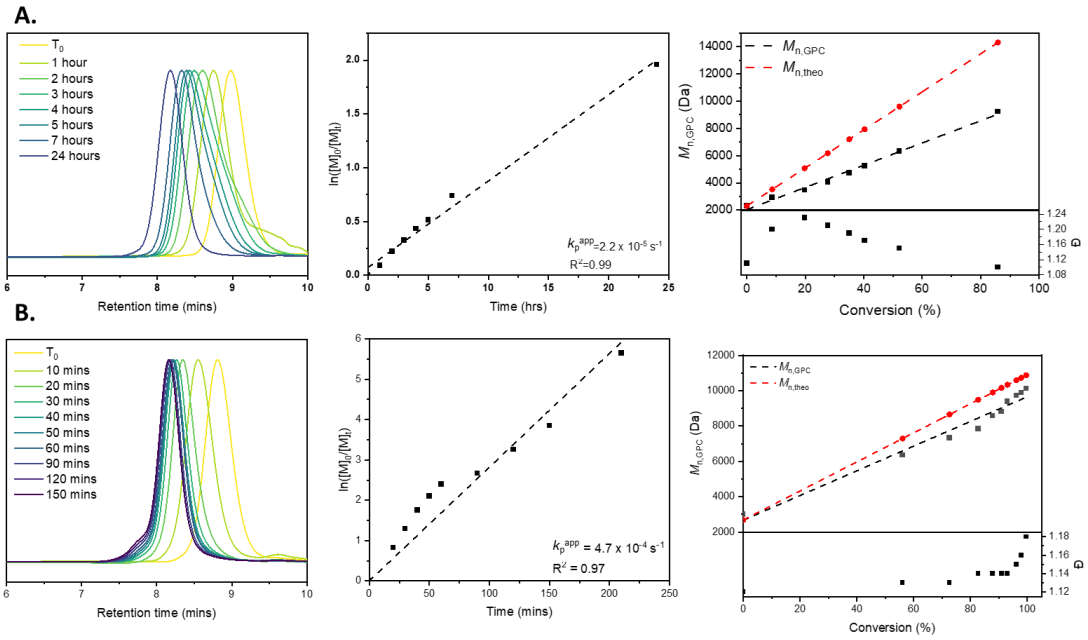

Figure 3.4. (A) Kinetic of chain extension with EHA using Cu(0)-RDRP. Conditions: EHA in TFE with 8.7% DMF, Me_6TREN (0.16 eq) and copper(II) bromide (0.05 eq) with a solvent to monomer ratio of 1:1 v/v and [M]:[I]=94:1. The Cu(II)Br was added and degassed before addition of Cu(0) wire. **(B)** Kinetic of chain extension with MA using Cu(0)-RDRP. Conditions: MA in DMF, Me_6TREN (0.16 eq) and copper(II) bromide (0.05 eq) with a solvent to monomer ratio of 1:1 v/v and [M]:[I]=100:1. The Cu(II)Br was added and degassed before addition of Cu(0) wire.

The poly(2-ethyl-2-oxazoline)-poly(acrylate) (pEtOx-pA) A-B block copolymers were then converted into macromonomers *via* the nucleophilic substitution of the terminal bromine with sodium azide (**Scheme 3.1.**). This formed a diblock 2-oxazoline/acrylate polymer with an alkyne functionality on the α chain end and an azide group on the Ω chain end.

3.2.2. AB Step-Growth Polymerisation

Having established that the chain extension of all three macroinitiators yielded well-controlled pEtOx-pA A-B block copolymers for both EHA and MA, click reactions were carried out using CuAAC, and the effect of various parameters on the degree of cyclisation versus step-growth were investigated. These parameters included effect of 2-oxazoline block length, acrylate block length, acrylate type, copper concentration, and reaction concentration (**Table 3.1.**).

Table 3.1. Conditions, molecular weight averages and %cyclic for all reactions in this work.

Entry	*pOx DP*	*Acrylate (DP)*	*Solvent*	*[Polymer] (mg/mL)*	*$M_{n,GPC}$[a] (kDa)*	*$M_{w,GPC}$[a] (kDa)*	*Đ*	*CuBr (eq)*	*PMDETA (eq)*	*%Cyclic[b] (wt%)*
SG1	19	EHA (86)	THF	100	60.3	150.8	2.50	0.3	0.3	16
SG2	19	EHA (86)	THF	400	79.3	197.3	2.49	0.3	0.3	9
SG3	19	EHA (86)	THF	600	94.5	215.2	2.28	0.3	0.3	7
SG4	19	EHA (86)	THF	733	84.1	194.4	2.31	0.3	0.3	6
SG5	25	MA (7)	THF/MeOH 4:1	26	4.9	16.4	3.37	0.3	0.3	41
SG6	25	MA (7)	THF	26	5.1	17.3	3.36	0.3	0.3	43
SG7	25	MA (7)	THF/hexane 4:1	26	3.9	7.7	1.97	0.3	0.3	58
SG8	25	MA (118)	THF/MeOH 4:1	102	45.3	54.2	2.61	0.3	0.3	13
SG9	25	MA (118)	THF	102	57.0	281.1	4.93	0.3	0.3	13
SG10	25	MA (118)	THF/hexane 4:1	102	47.8	398.6	8.34	0.3	0.3	18
SG11	25	EHA (7)	THF/MeOH 4:1	32	6.5	17.6	2.72	0.3	0.3	42
SG12	25	EHA (7)	THF	32	6.2	15.7	2.52	0.3	0.3	46
SG13	25	EHA (7)	THF/hexane 4:1	32	5.8	12.9	2.23	0.3	0.3	53
SG14	25	EHA (90)	THF/MeOH 4:1	154	54.2	140.2	2.59	0.3	0.3	15
SG15	25	EHA (90)	THF	154	59.4	158.1	2.66	0.3	0.3	13
SG16	25	EHA (90)	THF/hexane 4:1	154	57.3	145.4	2.54	0.3	0.3	12
SG17	25	MA (7)	THF/MeOH 1:1	26	5.2	17.0	3.28	0.3	0.3	43
SG18	25	MA (67)	THF	68	17.4	100.6	5.77	0.3	0.3	22
SG19	25	MA (67)	THF/hexane 4:1	68	15.2	88.5	5.82	0.3	0.3	26
SG20	25	EHA (60)	THF	110	39.1	95.1	2.43	0.3	0.3	23
SG21	25	EHA (60)	THF/hexane 4:1	110	38.8	93.5	2.42	0.3	0.3	22
SG22	40	MA (73)	THF	84	18.1	38.8	2.15	0.3	0.3	24
SG23	40	MA (73)	THF/hexane 4:1	84	13.9	29.3	2.11	0.3	0.3	35
SG24	25	MA (7)	THF	26	4.7	29.2	6.21	0.6	0.6	42
SG25	25	MA (67)	THF	68	21.4	123.4	5.79	0.15	0.15	14
SG26	25	MA (67)	THF	68	20.2	128.9	6.39	0.6	0.6	19
SG27	25	MA (67)	THF	68	18.8	128.6	6.82	1.2	1.2	21
SG28	40	MA (73)	THF	84	18.0	36.5	2.02	0.6	0.6	19
SG29	25	EHA (60)	THF	110	38.9	105.6	2.72	0.15	0.15	24
SG30	25	EHA (60)	THF	110	42.3	94.5	2.23	0.6	0.6	21
SG31	25	EHA (60)	THF	110	40.6	123.8	3.05	1.2	1.2	20
SG32	40	MA (7)	THF	38	5.3	10.5	2.00	0.3	0.3	51
SG33	40	MA (7)	THF	19	4.9	9.9	2.03	0.15	0.15	58
SG34	25	MA (118)	THF/MeOH 1:1	408	70.6	287.1	4.06	0.3	0.3	8

[a] Calculated using poly(methyl methacrylate) PMMA standards
[b] Percentage cyclisation calculated using a GPC RI integration method
Tetrahydrofuran (THF), MeOH (methanol).

To calculate the degree of cyclisation, a previously reported integration method was used in order to calculate the *wt*% of step-growth product.[30] In this method, the area of the cyclic peak is divided by the total area (**Figure 3.5.**) to give the *wt*% of the cyclic product from which the amount of step-growth can then be calculated.

$$degree\ of\ cyclisation\ \% = \frac{2(red\ area)}{blue\ area} \times 100 \qquad \textbf{Equation 3.1}$$

It must be noted that this method does not provide an absolute value for the degree of cyclisation. However, if all the polymers within the set are treated in the same manner, this method does provide a relative approach to comparing the polymers. There are three assumptions that are required for this approach. Firstly, there is no leftover starting material skewing the amount of cyclisation. Secondly, the dn/dc of both the step-growth material and the cyclic material is similar/the same. This is a reasonable assumption because both the step-growth and the cyclic material are made from the same starting material. Thirdly, that the cyclic peak is Gaussian in nature.

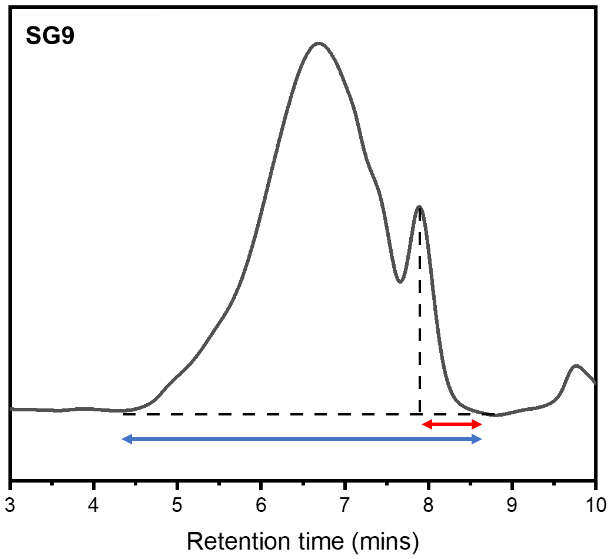

Figure 3.5. GPC trace of **SG9** demonstrating areas used to calculate degree of cyclisation. Sample was measured on a THF GPC.

3.2.2.1. Effect of Reaction Concentration on CuAAC

Firstly, the effect of reaction concentration on the CuAAC was investigated, using the $pEtOx_{19}$-EHA_{86} macromonomer. The CuAAC was initially carried out at a polymer concentration of 100 mg/mL. As can be seen in **Figure 3.6**, this polymerisation (**SG1**) (see **Table 3.1.** for full details) has a low molecular weight peak that shifts to longer retention time compared to the starting macromonomer. Such shifts to lower molecular weights are typical of cyclisation side reactions on account of the smaller hydrodynamic volume of the cyclic polymer.[18, 32-38] Therefore, to improve the step-growth polymerisation the polymer concentration was increased from 100 mg/mL to 400 mg/mL (**SG2**) and then again to 600 mg/mL (**SG3**) to suppress cyclisation by increasing the concentration of reactive end-groups. It should be noted that to enable a fair comparison, the concentration of Cu(I)Br and 1,1,4,7,7-pentamethyldiethylenetriamine (PMDETA) used for CuAAC were scaled proportionally with the concentration (**Table 3.1.**). At a macromonomer concentration of 100 mg/mL the *wt*% of step-growth was found to be 84%. As the concentration was increased to 400 and then 600 mg/mL the *wt*% increased to 91 and 93%, respectively. The data also suggests that most of the benefit from increasing the polymer concentration happens at lower concentrations. At the highest polymer concentration of 733 mg/mL (**SG4**) the step-growth increased further to 94%. 733 mg/mL was chosen as the highest concentration because beyond this point, $pEtOx_{19}$-EHA_{86} was not sufficiently soluble. It is worth noting that at 733 mg/mL the reaction solution was extremely viscous and became even more viscous as the polymerisation

proceeded. However, even under these conditions, cyclisation appeared to persist albeit to a significantly reduced extent.

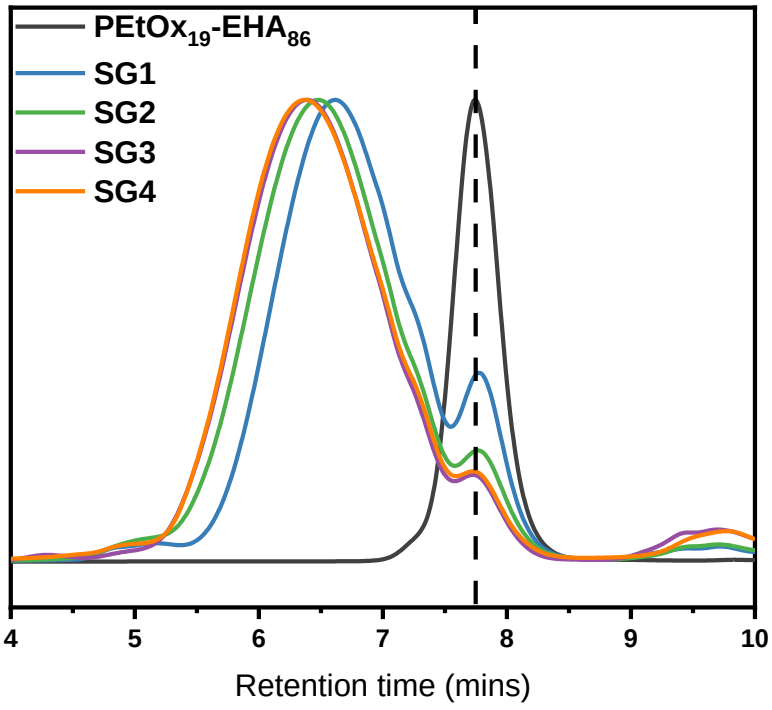

Figure 3.6. Step-growth polymerisation at four different polymer concentrations: 100 mg/mL (**SG1**, blue), 400 mg/mL (**SG2**, green), 600 mg/mL (**SG3**, purple) and 733 mg/mL (**SG4**, orange). All samples were measured on a THF GPC.

Although all reactions were left for extended reaction times (16 h), the polymerisation appears to be rapid. For **SG4**, the GPC chromatogram was obtained after a significant increase in viscosity was observed (~ 15 min). The GPC was then measured again at 18 h. Remarkably, the GPC chromatograms (**Figure 3.7.**) indicate that there was no further growth after just 15 minutes. These results imply that the reaction is fast. Although a full kinetic investigation was not carried out, it is expected that all step-growth polymerisations reported here are rapid.

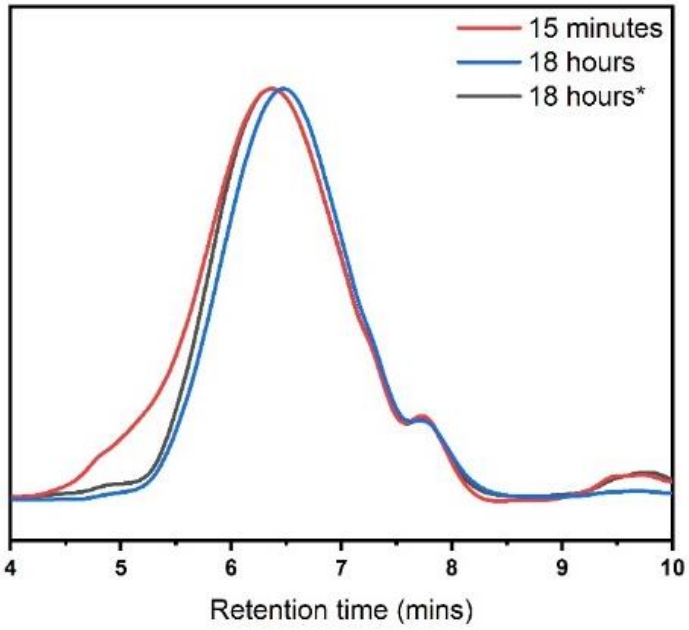

Figure 3.7. GPC Chromatograms for **SG4** after 15 min (red), 18 h (blue) and 18 h measured at a low concentration (black). Samples were measured on a THF GPC.

3.2.2.2. Effect of Solvent Composition on CuAAC

In previous work on the cyclisation of heterotelechelic poly(2-oxazoline)s a solvent dependency was observed.[18] By changing the solvent composition, it was possible to change the proportion of cyclisation to step-growth. To study the effect of solvent polarity on the step-growth of the A-B macromonomers in this case, four polymer compositions were synthesised utilising a $pEtOx_{25}$-I macroinitiator. The four compositions were $pEtOx_{25}$-MA_7, $pEtOx_{25}$-MA_{118}, $pEtOx_{25}$-EHA_7, and $pEtOx_{25}$-EHA_{90}. These compositions were selected in order to study short and long lengths of polar and non-polar chain extensions. Step-growth polymerisation of the polymers was then carried out in several different solvent systems to examine the effect of polarity on cyclisation vs. step-growth (**Figure 3.8.**). Tetrahydrofuran (THF) was selected as a base solvent, with THF/hexane 4:1 being used to decrease polarity, and THF/methanol 4:1 being used to increase polarity.

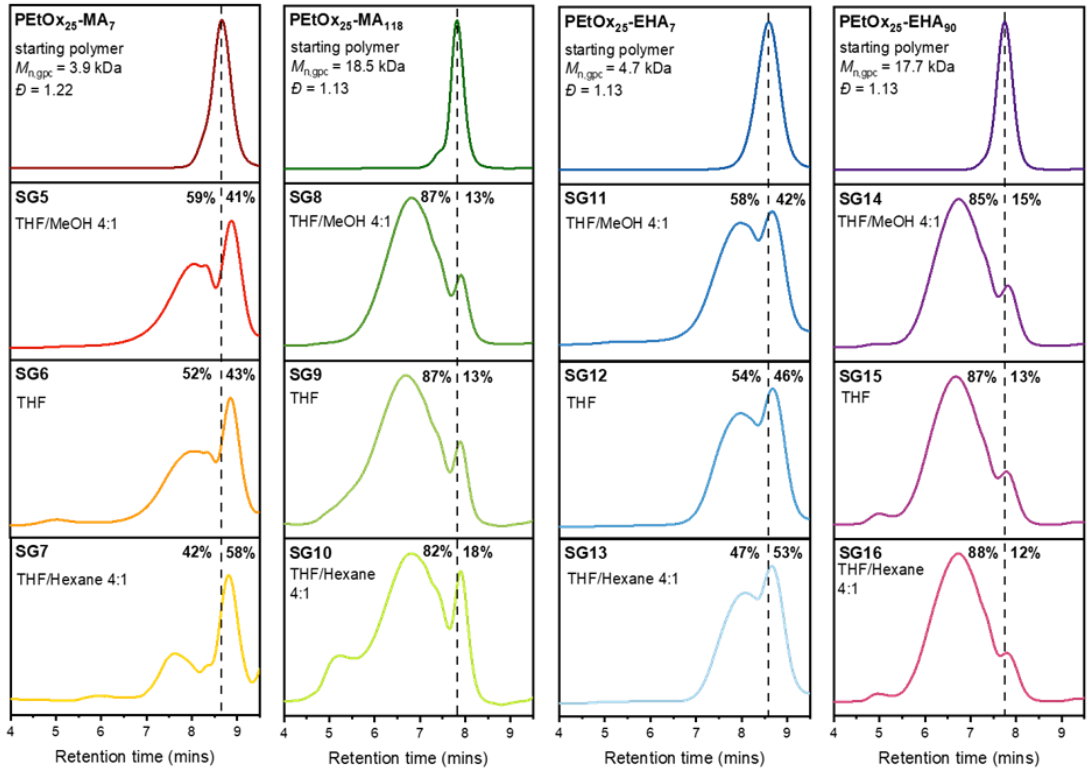

Figure 3.8. GPC chromatograms showing the effect of solvent on the step-growth polymerisation of $pEtOx_{25}$-MA_7, $pEtOx_{25}$-MA_{118}, $pEtOx_{25}$-EHA_7 and $pEtOx_{25}$-EHA_{90}. All reactions were carried out at 50 °C with a polymer concentration of 8 mM and 0.3 equivalents of CuBr and PMDETA. All samples were measured on a THF GPC.

Interestingly, the block composition appears to affect how much of a shift to longer retention time occurs when cyclisation is observed. For example, the small MA and EHA blocks shows a more significant shift than the longer blocks, and MA shows a more significant shift than EHA. Due to the relative change in hydrodynamic volume between the cyclic polymer and its linear counterpart, the shorter polymers result in a more compact cyclic structure with a more pronounced shift to longer retention time. The cyclic structures associated with the longer polymers are not so compact and thus have a smaller relative shift.

The GPC chromatograms for **SG5-SG16** are also shown in **Figure 3.8**. In keeping with the results presented earlier (**Figure 3.6.**), in all cases there is cyclisation present as observed from the shift to lower apparent molecular

weight (indicated by the dashed line). To begin the discussion on the effect of solvent, $pEtOx_{25}$-MA_7 will be considered first. As the solvent polarity decreases from THF/methanol 4:1 (**SG5**) to THF/hexane 4:1 (**SG7**)**,** the amount of cyclisation increases from 41% to 58%. Both the pEtOx and pMA blocks are better solvated in more polar solvents. In less polar solvents, the solvent-polymer interaction is less favourable, and the polymer chains collapse in solution. This results in the α and Ω chain ends of an individual polymer being in close proximity to each other, increasing the probability of cyclisation compared to step-growth. Indeed, this trend is consistent with other literature examples suggesting poor solvation leads to increased cyclisation.[18, 39] The effect of increasing the solvent polarity beyond 20% methanol was also tested on $pEtOx_{25}$-MA_7 (**Table 3.1.**). The polarity of the solvent was further increased from THF/methanol 4:1 to THF/methanol 1:1 (**SG5** and **SG17**, respectively) to test the effect on the degree of cyclisation. Nonetheless, **SG17** and **SG5** showed very similar amounts of cyclisation indicating that making the solvent system more polar than THF/methanol 4:1 does not reduce the cyclisation further.

A macromonomer with a longer methyl acrylate block was also investigated, $pEtOx_{25}$-MA_{118}. The effect of solvent was much less pronounced in this case, with both THF/methanol 4:1 (**SG8**) and 100% THF (**SG9**) showing 13% cyclisation. Once the solvent polarity was decreased to THF/hexane 4:1, the amount of cyclisation increased marginally to 18%. The chain length of $pEtOx_{25}$-MA_{118} is much longer (see discussion below) and the polarity of the polymer chain is different. The longer MA block reduces the polarity of the chain which causes there to be less solvent dependency. In a similar way to

$pEtOx_{25}$-MA_7, $pEtOx_{25}$-EHA_7 was also investigated. However, the effect of solvent polarity was the same for $pEtOx_{25}$-EHA_7 as for $pEtOx_{25}$-MA_7 (**Figure 3.8.**). **SG11,** which was carried out in THF/methanol 4:1 had 42% cyclisation, which increased to 46% cyclisation in 100% THF (**SG12**) and then 53% for THF/hexane 4:1 (**SG13**). $pEtOx_{25}$-EHA_{90}, showed a different trend where decreasing the polarity of the solvent appeared to have a minimal effect. In THF/methanol 4:1, there was 15% cyclisation (**SG14**) which subsequently reduced to 12% in the non-polar solvent mixture of THF/hexane 4:1 (**SG16**). $pEtOx_{25}$-EHA_{90} contains a long EHA block, which is much more hydrophobic than the methyl acrylate blocks and so is better solvated by non-polar solvents. This trend is not observed for $pEtOx_{25}$-EHA_7 however, because the EHA block is much shorter and has less influence over the polymer behaviour in solution compared to the longer, more hydrophilic pEtOx block.

3.2.3. Effect of Block Length on CuAAC

The effect of 2-oxazoline block lengths was also explored. Generally, it was observed that increasing the acrylate block length reduced the amount of cyclisation, whilst increasing the 2-oxazoline block length increased the amount of cyclisation. One possible reason for these opposing trends is the different chemistries of the polymer blocks – the acrylate block has a hydrophobic saturated hydrocarbon backbone whilst the 2-oxazoline block is a more hydrophilic pseudo-peptide. As the acrylate block length was increased, it always resulted in a reduction in the amount of cyclisation when the other reaction conditions were fixed (**Figure 3.9.**).

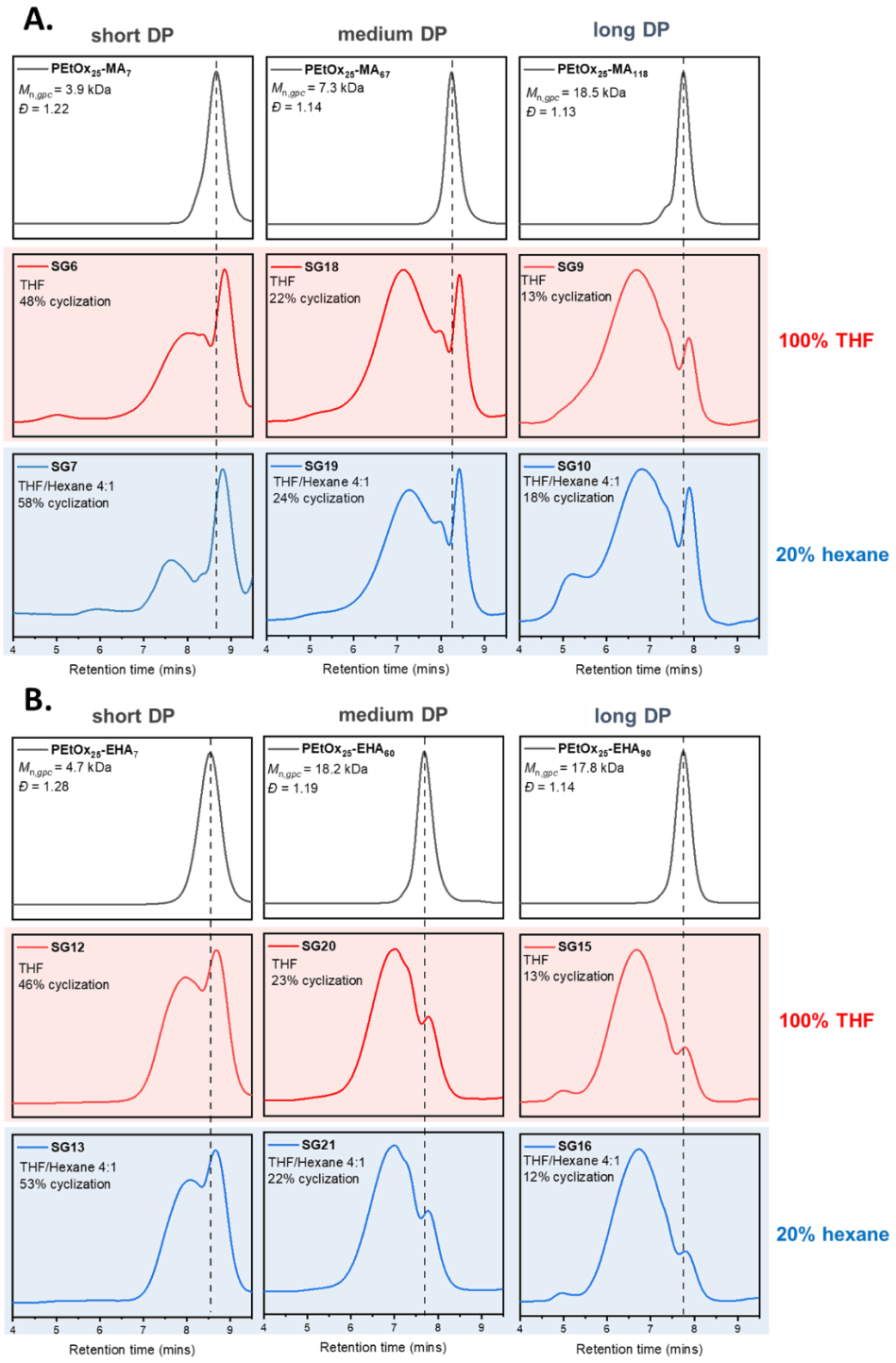

Figure 3.9. (A) GPC chromatograms demonstrating the effect of methyl acrylate block length on the degree of cyclisation. **(B)** GPC Chromatograms demonstrating the effect of 2-ethylhexyl acrylate block length on the degree of cyclisation. Red traces are run in the 100% THF solvent system, blue traces are run in the 4:1 THF:hexane solvent system. The dashed lines are to help the reader observe the shift to longer retention time indicating cyclisation. All samples were measured on a THF GPC.

For example, when the pEtOx$_{25}$-MA$_x$ (x = 7, 67, 118) polymers underwent step-growth in 100% THF, the degree of cyclisation decreased from 48% to

22%, and then 13% as the methyl acrylate block was increased from DP7 to DP67 and then DP118 (**SG6, SG18, SG9**) (**Figure 3.9.A**). This trend was also seen when the same polymers underwent step-growth in the non-polar solvent system, THF:hexane 4:1. The degree of cyclisation reduced from 58% for DP7, to 26% for DP67, and then to 18% for DP118 (**SG7**, **SG19**, **SG10**).

In the case of the EHA blocks, the trend observed was identical to the MA case. When the $pEtOx_{25}$-(EHA)y (y= 7, 59, 90) macromonomer underwent step-growth in 100% THF, the degree of cyclisation reduced from 46% for DP7 (**SG12**), to 23% for DP59 (**SG20**), and finally to 13% for DP90 (**SG15**). Again, this trend was seen when the non-polar solvent mixture was used: DP7 had 53% cyclisation (**SG13**), DP60 had 22% cyclisation (**SG21**), and DP90 had 12% cyclisation (**SG16**) (**Figure 3.9.B**). Given the results obtained, it is likely that there is an acrylate block length dependency on the step-growth of these macromonomers. Moreover, the same trends were observed regardless of solvent ruling out a polarity effect. It should be noted that in previous work utilising purely heterotelechelic $pEtOx_{25}$, step-growth polymerisation *via* CuAAC in THF led to no cyclisation at all.[18] In these results, by adding a short poly(acrylate) block, cyclisation occurs with a *wt%* of 46-48%. Although the previous work utilised a higher polymer concentration, this does not account for the high weight percentages observed here. Therefore, it suggests that this system has an overall increased tendency to cyclise due to the addition of the acrylate block.

As well as studying the effect of acrylate length, the effect of 2-oxazoline block length was investigated. For this, two separate block lengths were synthesised, $pEtOx_{25}$-I and $pEtOx_{40}$-I. To study the effect of macroinitiator

length, both macroinitiators were chain extended with MA by a DP of ~70. When the CuAAC was carried out in 100% THF, the degree of cyclisation marginally increased from 22% (**SG18**) to 24% (**SG22**) when the macroinitiator length was increased from DP25 to DP40 respectively. This trend was also observed when the CuAAC was carried out in THF/hexane 4:1 (**SG19** and **SG23**) which showed an increase from 26% cyclisation for **SG19** to 35% cyclisation for **SG23**. The results here suggest that a macromonomer with a higher proportion of pEtOx in the backbone cyclises more favourably, particularly in more non-polar solvent. This is likely due to the difference in polarity of the backbones of the two polymer types. The quasi-peptoid nature of the poly(2-oxazoline) backbone is likely to favour solvation in more polar solvents and so will collapse in on itself in non-polar solvents. This reduces the distance between the chain ends promoting cyclisation over step-growth.

3.2.4. Effect of CuBr Concentration on CuAAC

Previous work synthesised telechelic poly(2-oxazoline)s that could undergo CuAAC and form cyclic and step-growth polymers.[18, 22] Furthermore, various factors affecting the ratio of step-growth to cyclisation were investigated, including the equivalents of copper used. For simple homopolymers of 2-oxazolines, it was demonstrated that a 6-fold increase in copper concentration resulted in an increase in the amount of cyclisation from 34% to 53%.[18] To investigate the effect of copper on the step-growth polymers synthesised in this study, the polymerisation was carried out with the amount of copper ranging from 0.15 to 1.2 equivalents. Note that the equivalents of ligand were also increased proportionally. The GPC plots can be seen in **Figure 3.10**. In general, the copper concentration had minimal effect on the degree of

cyclisation vs. step-growth. However, one notable outlier is **SG25** which showed a significant decrease in the amount of cyclisation (14%) compared to **SG18**, **SG26**, and **SG27** which corresponds to the trend seen in previous study on telechelic poly(2-oxazoline)s,[18] however the reason why **SG25** showed a reduction in cyclisation is not clear.

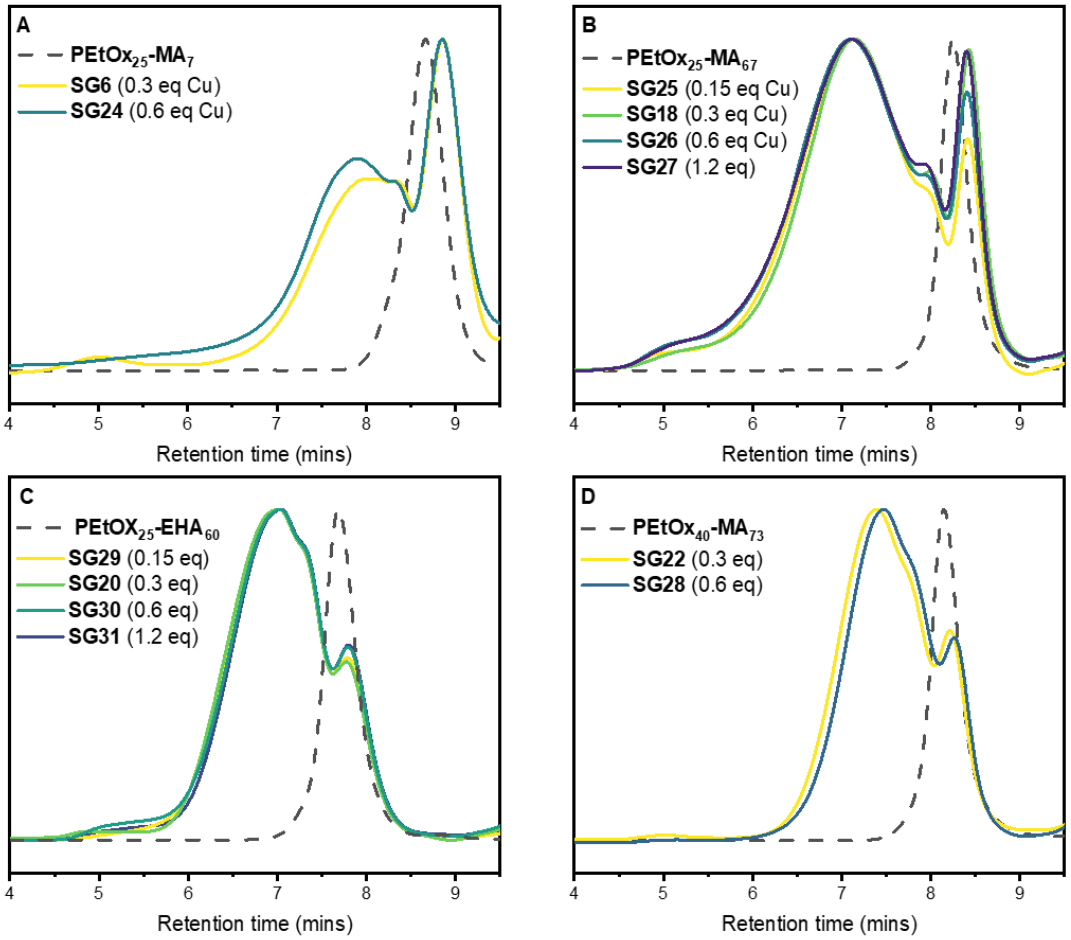

Figure 3.10. Effect of different number of equivalents of copper on the step-growth polymerisation of **(A)** pEtOx$_{25}$-MA$_7$ **(B)** pEtOx$_{25}$-MA$_{67}$ **(C)** pEtOx$_{25}$-EHA$_{60}$ **(D)** pEtOx$_{40}$-EHA$_{67}$. All the reactions were carried out in 100% THF with a polymer concentration of 8 mM**.** Samples were measured on a THF GPC.

Previously it was postulated that an excess of copper beyond the catalytic amount required for the CuAAC can coordinate to the 2-oxazoline backbone and thus increases cyclisation. For this reason, it could be expected that changing the 2-oxazoline block length might have an effect on the amount of

cyclisation. However, no obvious effect was observed in this study (**Figure 3.10.B,D**) Nonetheless, the step-growth was shown to be consistent at a range of copper concentrations, and effective even at copper amounts as low as 0.15 equivalents, highlighting this robust method to obtain multiblock polymers *via* CuAAC.

3.2.5. Maximising Step-Growth and Cyclisation

To maximise cyclisation, the longer DP40 oxazoline block was used with a short MA block as these were shown to promote cyclisation. Ideally, the solvent polarity should be decreased with the addition of hexane as this was shown to increase cyclisation, however the polymer (**SG33**) was not soluble due to the polarity of the polymer blocks. Nonetheless, at a polymer concentration of 38 mg/mL in 100% THF, there was 51 wt% cyclisation. Decreasing the polymer concentration further to 19 mg/mL resulted in 58% cyclisation, the joint highest of the entire set analysed here, and the highest wt% of cyclic material of any CuAAC reaction performed here in purely THF. To maximise the amount of step-growth, factors that were found to be conducive for step-growth were combined. These were: high polymer concentration, the shorter oxazoline block, the longest MA block, and also the most polar solvent. These conditions were combined for **SG34**, which had an overall step-growth of 92 wt%. Unfortunately, the concentration could not be increased further for comparison to **SG3** and **SG4** because the polymer was not sufficiently soluble.

3.2.6. Advanced GPC Analysis

So far, the analysis that has been carried out only provides an indication of the amount of cyclisation present. It does not account for the associated stunted step-growth observed (e.g. **SG5**). When the polymer chains undergo cyclisation the stoichiometric balance of end-groups is preserved, however, the concentration of reactive end groups decreases. Therefore, one possible explanation of the stunted step-growth is a system that grows and then cyclises such that a macrocyclic structure results. This seems logical given that steps taken to promote cyclisation are likely to affect the whole system. Such an outcome of macrocyclisation is not necessarily negative given that large macrocyclic polymers would be expected to have different physical and solutional properties compared to a linear equivalent. Nevertheless, it is important to understand what structures are being formed in the reaction for any future application.

To investigate the structures of the polymers, advanced GPC was utilised (**Figure 3.11.**). Specifically, viscosity measurements can give information on the structure of a polymer given that a cyclic polymer always has a lower intrinsic viscosity (IV) than its linear equivalent.[26] Even in the best step-growth case, a monocyclic peak is present which can act as reference. This peak is known to be cyclic as evidenced by the shift to lower apparent molecular weight. In the cases where step-growth and larger cyclic structures are present, the viscosity will be a weighted average of the species.

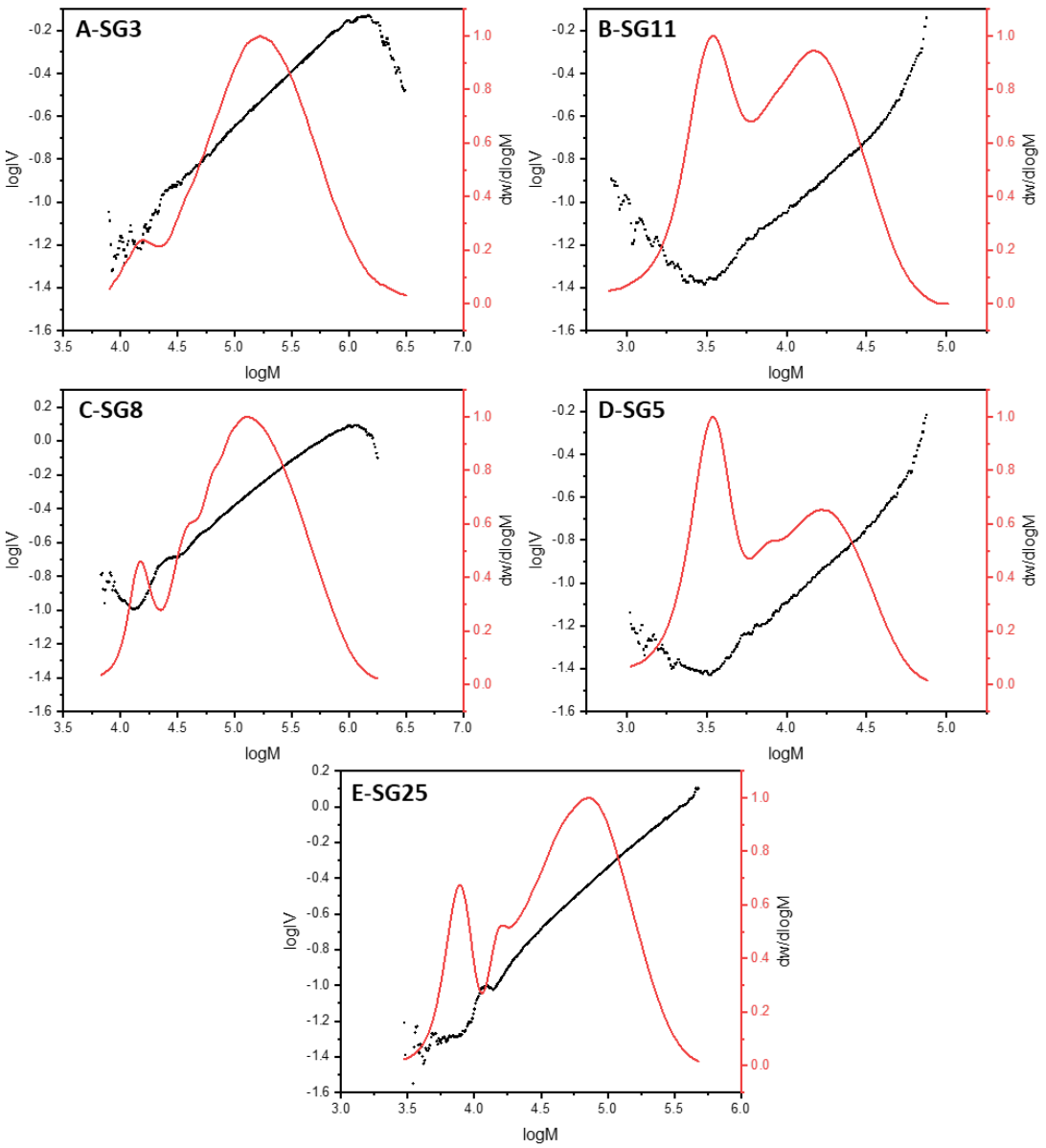

Figure 3.11. Mark-Houwink plots overlaid with the distribution for (**A) SG3, (B) SG11, (C) SG8, (D) SG5 and (E) SG25**. Samples were measured on a chloroform GPC.

Figure 3.11. shows the Mark-Houwink plots for **SG3**, **SG11**, **SG8**, **SG5** and **SG25** which have been overlaid with the distribution data. By overlaying intrinsic viscosity with the GPC chromatogram, analysis is simpler as changes in viscosity can easily be attributed to different sections of the GPC chromatogram. Consider **SG3** and **SG11** which were synthesised from macromonomers with similar pEtOx blocks but with different length EHA blocks (86 for **SG3**, 7 for **SG11**). As discussed previously, these polymers

have a different proportion of cyclisation to step-growth. In the case of **SG3** a drop in intrinsic viscosity is observed which corresponds to the cyclic peak. The intrinsic viscosity then rises and increases proportionally with the molecular weight up to log6 Da. Given the shift to lower apparent molecular weight the cyclisation is confirmed with the rest of the material appearing to be predominately step-growth. The drop in IV after log6 Da could be evidence of further cyclisation at high molecular weight, however the concentration of polymeric species at the extremities of the Mark-Houwink plots is low and so signal noise is a significant factor. Conversely, **SG11** had a much higher proportion of cyclic material. Given that the lower molecular weight peak is cyclic material a significant change in gradient would be expected to occur (as seen for **SG3**) upon step-growth. However, as can be seen from **Figure 3.11.B** the gradient through the entirety of the Mark-Houwink plot is very similar. This data highly suggests that the material is not exclusively step-growth but also macromonomers that have undergone step-growth and then cyclisation. This possibility has been described in the literature previously to account for stunted step-growth observed in other similar systems.[18, 40-42]

In a similar way, looking at **SG8** and **SG5** the same behaviour is observed (**Figure 3.11.C, D**). Here the EHA blocks were replaced with similar length MA blocks. **SG8** had less cyclisation and shows a change in gradient in the Mark-Houwink plot consistent with the formation of primarily step-growth products whereas **SG5** does not show this change of gradient. As discussed above, this indicates the formation of larger cyclic structures. **SG25** had a similar starting macromonomer to that of **SG5** and **SG8**, but with a MA block length in between. Despite the relatively low level of cyclisation observed, the Mark-

Houwink plot suggests that cyclic product is almost exclusively obtained. Overall, the data obtained suggests that when cyclisation is promoted, larger cyclic structures are also promoted. Given the results of **SG25**, it appears likely that there is a pEtOx-acrylate composition at which step-growth is the predominant species, although more work would be needed to confirm this. These findings would probably apply to other similar polymer systems of this type that aim to synthesise cyclic polymers *via* intramolecular cyclisation of telechelic polymers using click chemistry, however, a detailed study would be required to investigate this further.

3.2.7. Aqueous Self-Assembly

Finally, the aqueous self-assembly of selected polymers, **SG9, SG6**, **SG12** and **SG15** was analysed by dynamic light scattering (DLS) and transmission electron microscopy (TEM). It should be noted that the TEM images were carried out by James Lefley of the Becer group. **SG9** is similar to **SG8** in that it has a DP25 EtOx block and a long DP118 MA block and is expected to be comprised of predominately step-growth species. As observed from the TEM, self-assembly is observed (**Figure 3.12.A**) with the formation of stomatocyte-like nanoparticles. The average size of the particles was found to be 80.6 ± 21.0 nm which is in good agreement with the dynamic light scattering obtained size of 85 ± 17 nm (**Figure 3.12.E**). The large range of sizes is to be expected given the disperse nature of the polymer giving rise to a range of chain lengths and compositions. Given the long hydrophobic acrylate block and the short 2-oxazoline block this behaviour is expected. Conversely **SG6,** which is analogous to **SG5** in that it has a DP25 EtOx block and a short DP7 MA block, and the polymer is likely to be exclusively cyclic with chains that have grown

and then cyclised. In the TEM images obtained (**Figure 3.12.B**), there is extensive aggregation which is supported by DLS (**Figure 3.12.E**). The absence of self-assembly was expected given the very short acrylate block and hydrophilicity of pEtOx.

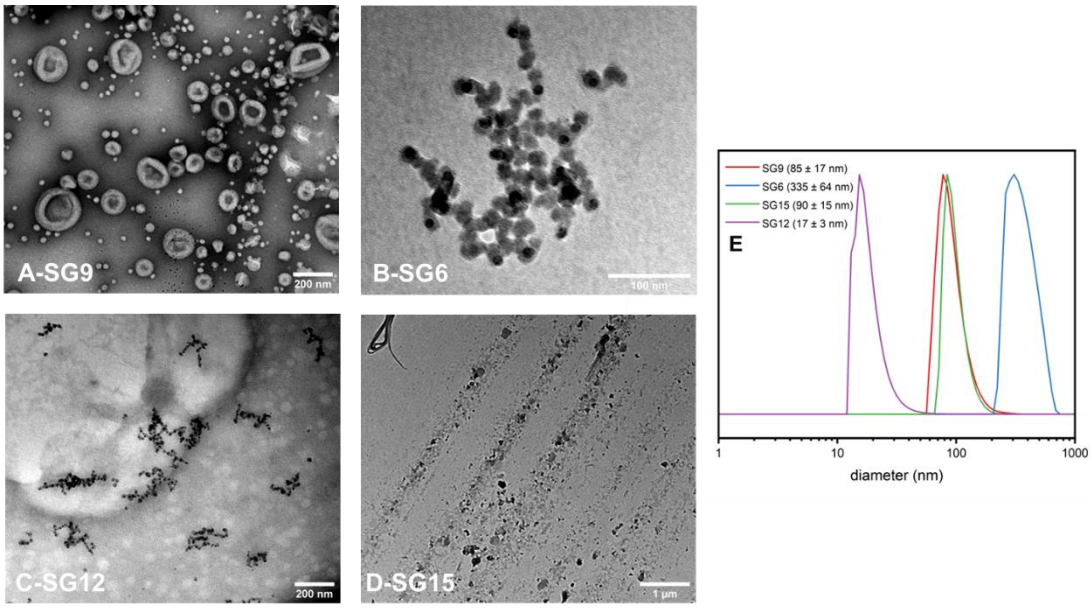

Figure 3.12. TEM images for **(A) SG9, (B) SG6, (C) SG12, (D) SG15, (E)** DLS plot for **SG9, SG6, SG12** and **SG15**.

In addition, the aqueous self-assembly behaviour of the EHA equivalents to **SG9** and **SG6** (**SG12**, **SG15**) was explored. The TEM image for **SG12**, with the short EHA segment, is shown in **Figure 3.12.C**. In the same way as with **SG6**, there appears to be aggregation. Noting that **SG12** is similar to **SG11**, even at higher molecular weights, the polymer would be expected to be predominately cyclic. The reasons for aggregation have already been described for **SG6**. Similarly, **SG15** with a long EHA block was investigated. Despite having an acrylate block length similar to that of **SG9**, the self-assembly behaviour was entirely different. In the DLS measurements (**Figure 3.12.E**) the polymer was found to have a size of 90 ± 15 nm which was similar to **SG9**, however, in the TEM, no particles were observed. Moreover, the

appearance in TEM was characteristic of a film rather than self-assembled particles (**Figure 3.12.D**). The drying process in conventional TEM, as opposed to Cryo-TEM, can have an effect on the final structure seen under the microscope.[43] The self-assembled structures can potentially disassemble and/or produce drying artifacts hence why a dried film may have been observed. The reason for this behaviour in the DLS, is likely self-assembly due to the very hydrophobic nature of the acrylate block. Therefore, there is a fine balance to be made with these polymers to generate self-assembled structures.

3.3. Conclusions

In conclusion, a novel way of making poly(2-oxazoline)-poly*(*acrylate) multi-block polymers *via* CuAAC has been presented. As has been found with previous studies, the conditions of the reaction such as solvent composition had an influence on the product mix. Herein, a full analysis has been carried out attempting to optimise conditions for cyclisation and step-growth, achieving 58 wt% and 92 wt% respectively. Interestingly, copper concentration was found to have a negligible effect on cyclisation in contrast to exclusively poly(2-oxazoline) systems where the effect is dramatic. Moreover, the nature of the acrylate used and the length of the acrylate block had a strong effect on the resulting cyclic to step-growth mixture with shorter acrylate blocks favouring cyclisation. Advanced GPC measurements showed that where cyclisation is favoured the resulting high molecular weight species is unlikely to be oligomers from step-growth but macrocyclic polymers that have grown and then cyclised as has been suggested in the literature previously. Finally, polymers with long acrylate blocks show self-assembly behaviour in aqueous

media. Future work would involve an in-depth study into the exact nature of the species formed in the reaction and the associated self-assembly. Lastly, these polymers appear to have useful mechanical properties such as high elasticity and so future work would be to investigate these features.

3.4. Experimental

3.4.1. Materials Used

Anhydrous acetonitrile (99.9%, Acros Organics, extra dry), sodium azide (Sigma Aldrich, >99%), *N,N*-diisopropylethylamine (Sigma Aldrich, >99%), 2-bromo-2-methylpropionic acid (Sigma Aldrich, 99%), 1,1,4,7,7-pentamethyldiethylenetriamine (Acros Organics, 98+%), trifluoroethanol (Sigma Aldrich, 99%) and 2-ethylhexyl acrylate (Sigma Aldrich, 98%) were all used as received.

2-ethyl-2-oxazoline (Sigma Aldrich, >99%) was distilled over calcium hydride prior to use. Propargyl p-toluene sulfonate (Sigma Aldrich, >97%) was distilled prior to use. Copper (I) bromide (Sigma Aldrich, 99.99%) was purified by stirring overnight in acetic acid followed by filtration and washing with ethanol and drying in a vacuum oven.

Cu(0) wire (Fisher Scientific, 99.99%, 0.25 mm diameter) was activated by being placed in 35% hydrochloric acid(aq) for 2 min followed by washing with water and acetone. Tris[2-(dimethylamino)ethyl]amine (Me_6TREN) was synthesised using a published procedure.[44]

3.4.2. Instrument Methods Used

3.4.2.1. GPC Measurements

All GPC chromatograms were measured on an Agilent Technologies 1260 Infinity instrument fitted with a refractive index detector, a PLgel 5 µm guard column and a PLgel 5 µm mixed D column (300 x 7.5 mm). tetrahydrofuran (THF) with 2% triethylamine was used as the eluent. Samples were run at 40 °C with a flow rate of 1 mL min^{-1} and measured against narrow poly(methyl methacrylate) standards. The viscosity GPC measurement of the step-growth polymers was carried out at known concentration on an Agilent 1260 Infinity II-MDS instrument with two PLgel Mixed-C columns operating in THF with 0.01% butylated hydroxytoluene. Samples were run at 30 °C with a flow rate of 1 mL min^{-1}. The following detectors were used for the analysis of the step-growth polymer: a refractive index detector and viscometer. Narrow linear poly(methyl methacrylate) standards were used to calibrate the instrument (1-1020 kDa). All samples were left overnight, with stirring, before being filtered over 0.2 µm PTFE syringe filters before analysis.

3.4.2.2. NMR Measurements

^{1}H NMR spectroscopy was measured on a Bruker DPX-300 or DPX-400 and all samples were measured at either 300 MHz or 400 MHz in $CDCl_3$ at 298 K. The resonance signal of residual $CHCl_3$ at 7.26 ppm served as the reference peak for chemical shifts. Conversion of the polymers was determined from the disappearance of the 2-oxazoline ring peaks at 3.7 and 4.2 ppm.

3.4.2.3. MALDI Measurements

All MALDI-TOF was performed on a Bruker Autoflex Speed mass spectrometer using a nitrogen laser delivering 2 ns pulses at 337 nm with positive ion ToF detection performed using an accelerating voltage of 25 kV. The matrix used was trans-2-[3-(4-tertbutylphenyl)-2-methyl-2-propylidene]malonitrile dissolved in tetrahydrofuran and sodium trifluoroacetate used as a cationic agent (solution in ethanol). Samples were measured in reflective mode and calibrated against poly(methyl methacrylate) standards.

3.4.2.4. Preparation of Nanoparticles *via* Direct Injection

Modified literature procedure.[45] 6 mg (± 0.1 mg) of polymer was dissolved in 1 mL extra dry THF (Acros Organics) in a 20 mL scintillation vial charged with a stirrer bar and stoppered with a Suba-seal® septum. The polymer/THF solution was allowed to stir for 30 minutes before 3 mL of Mili-Q® deionised water was added to the vial dropwise using a New Era NE-1000 Syringe Pump set to deliver the solution at a rate of 1 mL min^{-1} from a 5 mL syringe and needle. The solution was allowed to stir for 10 minutes before being placed in an oil bath set at 30 °C. The Suba-seal was removed and the THF was allowed to evaporate. After 4 hours the THF had been removed from the solution. The nanoparticle solution was then filtered using a 0.45 µm Nylon syringe filter ready for dynamic light scattering and transmission electron microscopy analysis.

3.4.2.5. DLS Measurements

Measurements were carried out on an Anton Paar Litesizer 500 particle size analyser. A sample (1 mL) of each nanoparticle solution as described above was measured in a Hellma Analytics high precision quartz cell. A backscattering measuring angle of 175˚ was used and each sample was measured in triplicate. Poly(2-ethyl-2-oxazoline) refractive index used was 1.52.

3.4.2.6. TEM Measurements

All nanoparticle solutions were imaged after a negative staining treatment. A 10 µL aliquot of a nanoparticle solution was drop-casted on a 300-mesh carbon-coated copper transmission electron microscopy grid (Agar Scientific, Stansted, U.K.). After 3 minutes, excess solution was removed by blotting with filter paper before 10 µL of a 0.75% phosphotungstic acid solution was drop-casted onto the same grid and incubated for 1 minute. Excess stain was removed by blotting with filter paper and dried under vacuum before imaging. Bright-field transmission electron microscopy imaging was performed on a JEOL 2100 Plus Transmission Electron Microscope operated at an acceleration voltage of 200 kV. All the images were recorded on a Gatan Orius 11 megapixel digital camera and at least six areas were analysed.

3.4.3. Synthesis of pEtOx$_{19}$-I

To an oven dried and nitrogen purged microwave vial, 2-ethyl-2-oxazoline (EtOx) (4 g, 40.3 mmol, 19 eq) and propargyl p-toluenesulphonate (PropTs) (37 µL, 2.12 mmol, 1 eq) were dissolved in acetonitrile (6.1 mL). The resulting solution was heated at 100 °C, with stirring, for 45 minutes. After this time, a

solution of 2-bromo-2-methylpropionic acid (BMPA) (1.4 g, 8.5 mmol, 4 eq) and diisopropylethylamine (DIPEA) (1.4 mL, 8.5 mmol, 4 eq) in acetonitrile (2 mL) was added to the reaction with the aid of a relief needle. The heating was turned off and the mixture left to cool, with stirring, overnight. A sample was taken for conversion before the polymer was precipitated into cold diethyl ether. The resulting solids were then dissolved in dichloromethane (50 mL), washed with water (50 mL), saturated sodium hydrogen carbonate (2 x 50 mL) and brine (50 mL). The organic phase was dried over magnesium sulphate, filtered and the solvent removed *in vacuo* to yield the polymer, **pEtOx$_{19}$-I**, as a yellow solid (Conversion: 99%).

A similar approach was taken for the DP25 and DP40 macroinitiators except the quantities of reagents were as follows:

(**DP25**) EtOx (8.0 g, 25.0 eq, 80. 7 mmol), PropTs (0.67 g, 0.55 mL, 1.0 eq, 3.2 mmol) were dissolved in acetonitrile (12.3 mL). The end-capping solution was as follows: DIPEA (5.4 mL, 31 mmol, 10 eq) BMPA (5.2 g, 31 mmol, 10 eq) in acetonitrile (5 mL).

(**DP40**) EtOx (8.0 g, 50 eq, 80. 7 mmol), PropTs (0.34 g, 0.28 mL, 1.6 mmol, 1.0 eq) were dissolved in acetonitrile (16 mL). The end-capping solution was as follows: DIPEA (2.1 g, 2.83 mL, 16.1 mmol, 10 eq) BMPA (2.69 g, 16 mmol, 10 eq) in acetonitrile (2.5 mL).

3.4.4. Chain Extension with EHA

A typical procedure was as follows:

pEtOx-I (0.29 g, 0.12 mmol, 1 eq) was dissolved in trifluoroethanol (2.3 mL) and 2-ethylhexyl acrylate (EHA) (2.04 g, 11.1 mmol, 93 eq) and Me_6TREN (33 mg, 0.12 mmol, 1 eq) added. The mixture was purged with nitrogen for 30 minutes before a sample was taken for T_0. After purging, 5 cm of hydrochloric acid activated Cu(0) wire (0.22 mm) wrapped around a magnetic stirrer bar was added and the polymerisation left to proceed, with stirring, for 20 h. A sample was taken for conversion before being precipitated three times in acetonitrile (dissolving in the minimum amount of THF for precipitations 2 and 3) to yield **pEtOx-PEHA** as a colourless semi-solid and used in the subsequent step as obtained (Conversion: 92%).

For the quantities used for the other polymers, see **Table 3.2.**

3.4.5. Chain Extension with MA

A typical procedure was as follows:

pEtOx-I (0.5 g, 0.19 mmol, 1 eq) and methyl acrylate (MA) (2.40 g, 27.9 mmol, 150 eq) were dissolved in dimethylformamide (DMF) (2.4 mL). A stock solution of 20.8 mg Cu(II)Br dissolved in DMF (1 mL) was prepared, of which 0.1 mL (Cu(II)Br 2.08 mg, 0.009 mmol, 0.05 eq) was added to the **pEtOx-I** reaction mixture. The reaction mixture was then purged with nitrogen for 30 minutes before Me_6TREN (6.9 mg, 8 µL, 0.16 eq) was added. 5 cm of hydrochloric acid activated Cu(0) wire was wrapped around a magnetic stirrer bar which was then added to the reaction solution and a sample taken for T_0. The

polymerisation was left for 4.5 hours before a sample taken for conversion. The polymer was then precipitated into ice cold diethyl ether 3 times to yield the polymer as a colourless solid, which was then used as obtained.

For the quantities used for the other polymers, see **Table 3.2**.

Table 3.2. Quantities of reagents used for chain extensions with MA and EHA.

Polymer	*Macroinitiator*				*Acrylate*				*Me_6TREN*			*Cu(II)Br*			*Solvent*		*Reaction time (hrs)*
	type	*(g)*	*(mmol)*	*(eq)*	*type*	*(g)*	*(mmol)*	*(eq)*	*(mg)*	*(mmol)*	*(eq)*	*(mg)*	*(mmol)*	*(eq)*	*type*	*(mL)*	
P1	DP19	1	0.48	1	EHA	8.32	45.2	100	106	0.46	1	-	-	-	TFE	9.4	26
P2	DP25	1	0.37	1	MA	0.64	7.5	20	13.8	0.06	0.16	4.2	0.02	0.05	DMF	0.5	0.5
P3	DP25	0.5	0.19	1	MA	2.41	28.0	150	6.9	0.03	0.16	2.1	0.01	0.05	DMF	1	4.5
P4	DP25	1	0.37	1	EHA	0.69	3.7	10	13.8	0.06	0.16	4.2	0.02	0.05	IPA	0.7	9
P5	DP25	0.5	0.19	1	EHA	3.85	20.9	112	43.0	0.19	1	-	-	-	TFE	3.5	18
P6	DP25	1	0.37	1	MA	2.73	31.7	85	13.8	0.06	0.16	4.2	0.02	0.05	DMF	2.7	3
P7	DP25	0.5	0.19	1	EHA	2.41	13.1	70	43.0	0.19	1	-	-	-	TFE	2	9
P8	DP40	0.5	0.12	1	MA	0.88	10.2	85	4.4	0.02	0.16	1.3	0.01	0.05	DMF	0.9	2.5
P9	DP40	1	0.24	1	EHA	2.96	16.1	67	55.2	0.24	1	-	-	-	TFE	3	18
P10	DP40	1	0.24	1	MA	0.21	2.4	10	8.8	0.04	0.16	2.3	0.01	0.05	DMF	0.6	2

Table 3.3. Acrylate monomer conversions for polymers **P1**-**P10**.

Polymer	*Monomer Eq T_0[a]*	*Conversion (%)[b]*
P1	100	86
P2	18	40
P3	134	88
P4	11	67
P5	103	87
P6	79	86
P7	67	90
P8	78	93
P9	68	88
P10	10	70

3.4.6. Bromo-Azide Exchange

The precipitated polymer (2.5 g, 0.20 mmol, 1 eq) after the chain extension step was dissolved in acetone (7 mL) and DMF (15 mL). Sodium azide (130 mg, 2.0 mmol, 10 eq) was then added and the reaction mixture was stirred at 50 °C overnight. During this reaction step, a colour change from colourless to pale yellow/green was observed. After this time, the polymer solution was diluted in THF and the now insoluble excess sodium azide was removed by centrifugation. The solvent was then removed *in vacuo* and the polymer dried prior to CuAAC.

3.4.7. Step-Growth *via* CuAAC

A typical procedure was as follows:

pEtOx-PEHA macromonomer (100 mg) was dissolved in THF (0.8 mL) and purged with nitrogen for 15 minutes. Separately in a nitrogen purged vial, CuBr (2.6 mg) and 1,1,4,7,7-pentamethyldiethylenetriamine (PMDETA) (8 µL) were dissolved in THF (5.2 mL). 0.2 mL of this stock solution such that the CuBr and PMDETA were both 0.3 equivalents with respect to the **pEtOx-PEHA** macromonomer was then added to the reaction and the reaction was heated, with stirring, at 50 °C for 16 h. For the quantities for the other polymers, see **Table 3.1.**

3.5. References

1. Kay, C. J.; Goring, P. D.; Burnett, C. A.; Hornby, B.; Lewtas, K.; Morris, S.; Morton, C.; McNally, T.; Theaker, G. W.; Waterson, C.; Wright, P. M.; Scott, P., *Journal of the American Chemical Society* **2018,** *140* (42), 13921-13934.

2. Eagan James, M.; Xu, J.; Di Girolamo, R.; Thurber Christopher, M.; Macosko Christopher, W.; LaPointe Anne, M.; Bates Frank, S.; Coates Geoffrey, W., *Science* **2017,** *355* (6327), 814-816.

3. Bates, F. S.; Fredrickson, G. H., *Physics Today* **1999,** *52* (2), 32-38.

4. Meng, F.; Zhong, Z.; Feijen, J., *Biomacromolecules* **2009,** *10* (2), 197-209.

5. Ruiz, R.; Kang, H.; Detcheverry François, A.; Dobisz, E.; Kercher Dan, S.; Albrecht Thomas, R.; de Pablo Juan, J.; Nealey Paul, F., *Science* **2008,** *321* (5891), 936-939.

6. Bates, F. S.; Fredrickson, G. H.; Hucul, D.; Hahn, S. F., *American Institute of Chemical Engineers. AIChE Journal* **2001,** *47* (4), 762.

7. Drain, B. A.; Becer, C. R., *European Polymer Journal* **2019,** *119*, 344-351.

8. Becer, C. R.; Paulus, R. M.; Höppener, S.; Hoogenboom, R.; Fustin, C.-A.; Gohy, J.-F.; Schubert, U. S., *Macromolecules* **2008,** *41* (14), 5210-5215.

9. Krieg, A.; Weber, C.; Hoogenboom, R.; Becer, C. R.; Schubert, U. S., *ACS Macro Letters* **2012,** *1* (6), 776-779.

10. Menezes, R. N. L. d.; Felisberti, M. I., *Polymer Chemistry* **2021,** *12* (32), 4680-4695.

11. Tran, H.; Bergman, H. M.; de la Rosa, V. R.; Maji, S.; Parenti, K. R.; Hoogenboom, R.; Campos, L. M., *Journal of Polymer Science Part A: Polymer Chemistry* **2019,** *57* (12), 1349-1357.

12. Cui, S.; Yu, L.; Ding, J., *Macromolecules* **2019,** *52* (10), 3697-3715.

13. Durham, O. Z.; Chapman, D. V.; Krishnan, S.; Shipp, D. A., *Macromolecules* **2017,** *50* (3), 775-783.

14. Lava, K.; Verbraeken, B.; Hoogenboom, R., *European Polymer Journal* **2015,** *65*, 98-111.

15. Laurent, B. A.; Grayson, S. M., *Journal of the American Chemical Society* **2006,** *128* (13), 4238-4239.

16. Hayes, G.; Drain, B.; Becer, C. R., *Macromolecules* **2022,** *55* (1), 146-155.

17. Kim, J.; Waldron, C.; Cattoz, B.; Becer, C. R., *Polymer Chemistry* **2020,** *11* (42), 6847-6852.

18. Drain, B. A.; Beyer, V. P.; Cattoz, B.; Becer, C. R., *Macromolecules* **2021,** *54* (12), 5549-5556.

19. Beyer, V. P.; Cattoz, B.; Strong, A.; Phillips, D. J.; Schwarz, A.; Remzi Becer, C., *Polymer Chemistry* **2019,** *10* (31), 4259-4270.

20. Zhao, T.; Drain, B.; Yilmaz, G.; Becer, C. R., *Polymer Chemistry* **2021,** *12* (44), 6392-6403.

21. Kolb, H. C.; Finn, M. G.; Sharpless, K. B., *Angewandte Chemie International Edition* **2001,** *40* (11), 2004-2021.

22. Huettner, N.; Goldmann, A. S.; Hoogenboom, R.; Dargaville, T. R., *Polymer Chemistry* **2022,** *13* (27), 3975-3980.

23. Haque, F. M.; Grayson, S. M., *Nature Chemistry* **2020,** *12* (5), 433-444.

24. Cortez, M. A.; Godbey, W. T.; Fang, Y.; Payne, M. E.; Cafferty, B. J.; Kosakowska, K. A.; Grayson, S. M., *Journal of the American Chemical Society* **2015,** *137* (20), 6541-6549.

25. Wang, T.-W.; Golder, M. R., *Polymer Chemistry* **2021,** *12* (7), 958-969.

26. Jeong, Y.; Jin, Y.; Chang, T.; Uhlik, F.; Roovers, J., *Macromolecules* **2017,** *50* (19), 7770-7776.

27. Nasongkla, N.; Chen, B.; Macaraeg, N.; Fox, M. E.; Fréchet, J. M. J.; Szoka, F. C., *Journal of the American Chemical Society* **2009,** *131* (11), 3842-3843.

28. Wu, Z.; Zhang, H.; Liu, C.; Hong, C., *Macromolecular Rapid Communications* **2021,** *42* (12), 2100136.

29. Morgese, G.; Trachsel, L.; Romio, M.; Divandari, M.; Ramakrishna, S. N.; Benetti, E. M., *Angewandte Chemie International Edition* **2016,** *55* (50), 15583-15588.

30. Muramatsu, Y.; Takasu, A., *Polymer Journal* **2022,** *54* (2), 121-132.

31. Samanta, S. R.; Levere, M. E.; Percec, V., *Polymer Chemistry* **2013,** *4* (11), 3212-3224.

32. Divandari, M.; Morgese, G.; Ramakrishna, S. N.; Benetti, E. M., *European Polymer Journal* **2019,** *110*, 301-306.

33. Ramakrishna, S. N.; Morgese, G.; Zenobi-Wong, M.; Benetti, E. M., *Macromolecules* **2019,** *52* (4), 1632-1641.

34. Yan, W.; Divandari, M.; Rosenboom, J.-G.; Ramakrishna, S. N.; Trachsel, L.; Spencer, N. D.; Morgese, G.; Benetti, E. M., *Polymer Chemistry* **2018,** *9* (19), 2580-2589.

35. Morgese, G.; Cavalli, E.; Rosenboom, J.-G.; Zenobi-Wong, M.; Benetti, E. M., *Angewandte Chemie International Edition* **2018,** *57* (6), 1621-1626.

36. Jung, Y.; Kim, J.-H.; Jang, W.-D., *European Polymer Journal* **2017,** *88*, 605-612.

37. Ali, M. W.; Muhammad, Z.; Jia, Q.; Li, L.; Saleem, M.; Siddiq, M.; Chen, Y., *Polymer Chemistry* **2020,** *11* (25), 4164-4171.

38. Kricheldorf, H. R., *Journal of Polymer Science Part A: Polymer Chemistry* **2010,** *48* (2), 251-284.

39. Tsarevsky, N. V.; Sumerlin, B. S.; Matyjaszewski, K., *Macromolecules* **2005,** *38* (9), 3558-3561.

40. Kricheldorf, H. R., *Macromolecular Rapid Communications* **2008,** *29* (21), 1695-1704.

41. Tsarevsky, N. V.; Sumerlin, B. S.; Matyjaszewski, K., *Macromolecules* **2005,** *38* (9), 3558-3561.

42. Kricheldorf, H. R.; Schwarz, G., *Macromolecular Rapid Communications* **2003,** *24* (5-6), 359-381.

43. Michen, B.; Geers, C.; Vanhecke, D.; Endes, C.; Rothen-Rutishauser, B.; Balog, S.; Petri-Fink, A., *Scientific Reports* **2015,** *5* (1), 9793.

44. Ciampolini, M.; Nardi, N., *Inorganic Chemistry* **1966,** *5* (1), 41-44.

45. Meeuwissen, S. A.; Bruekers, S. M. C.; Chen, Y.; Pochan, D. J.; van Hest, J. C. M., *Polymer Chemistry* **2014,** *5* (2), 489-501.

Chapter 4. Synthesis of Charged Poly(2-oxazoline) Glycopolymers for Non-viral Gene Delivery

Manuscript in preparation for publication. Authors:

Hayes,G.; Dias Barbieri, B.; Yilmaz, Shattock, R.J.; G. Becer, CR.

4.1. Introduction

Gene delivery is one of the most novel and exciting techniques for the conveyance of therapeutics and vaccinations at present.[1] For example, ribonucleic acid (RNA) vaccines were used extensively against the SARS-CoV-19 pandemic with great effect.[2] Theoretically, RNA vaccines could be used to provide protection against a wide range of infectious diseases including Influenza,[3] Rabies,[4] Human immunodeficiency virus,[5] and Ebola.[6]

RNA vaccines have several advantages over traditional vaccines that use direct injection of antigens or deactivated viruses. Traditional vaccines require large scale bioreactors that grow batches of cells which then produce the virus or antigen protein, in a costly and time-consuming process. For RNA vaccines, the RNA is produced synthetically and then combined with a delivery vehicle. Lipid nanoparticles (LNPs) are typically used to deliver RNA vaccines, although the stability and storage of LNPs can be problematic.[7] Another issue is that the general population experience side effects to the RNA vaccines due to an innate ability to detect RNA, and so minimising the amount of RNA injected is currently of interest.[8] One method of reducing the payload of RNA required is to use self-amplifying RNA (saRNA). As well as encoding the antigen, saRNA also encodes a replicase protein that can replicate the original strand of injected RNA, and thus amplify protein expression.[9] Nonetheless, one of the problems with saRNA is that it is much larger than mRNA and is more difficult to deliver.[10] Several different nanocarriers have been used to deliver RNA effectively, including LNPs,[11] cationic polymers,[12] dendrimers,[13] and nanofibre-type materials.[14]

Regarding polyplexes, various polymers have been extensively studied including poly(ethylene imine) (PEI),[15] poly(2-oxazoline)s,[16] poly(ethylene glycol),[17] and peptides.[18] Amongst the different polymers tested, PEI is generally viewed as the optimal transfection agent.[19] PEI is synthesised *via* either the ring opening polymerisation of aziridine,[20] or the hydrolysis of linear poly(2-ethyl-2-oxazoline).[21] Nonetheless, both of these methods have the disadvantages of an associated lack of control which results in uncertainty about the exact polymeric structure, and PEI has been shown to have toxicity issues.[22] Partially hydrolysed poly(2-oxazoline)s have also been used for RNA delivery,[23] but again, this method is imprecise and does not allow for the formation of complex structures such as defined, functionalised, cationic block polymers. These well-controlled cationic poly(2-oxazoline) structures may show a selective targeting ability for certain cell types, which is of interest as it can be used to reduce the amount of RNA required to produce a response. Indeed, it has been demonstrated that complex poly(2-oxazoline) architectures such as graft copolymers are able to selectively target different types of liver cell.[24]

Lectins are proteins that regulate biological processes such as cell recognition and intracellular communication.[25, 26] They achieve this by binding to glycans such as oligosaccharides on the surface of cells and viruses, and play an important role in human disease.[27] Since lectins bind sugars, glycopolymers can be used to target specific cells for applications such as drug delivery.[28] Indeed, the type of sugar used and its spatial configuration in relationship to the polymer backbone have been shown to be able to influence the lectin selectivity.[29] Furthermore, poly(2-oxazoline)s decorated with sugar moieties

have been demonstrated to be effective at targeting specific cells.[30] Nonetheless, the synthetic route used in this case limits the polymer architecture to random copolymers which reduces the polymer definition and can impact lectin selectivity. Interactions with lectins are greatly enhanced by the so-called 'glycocluster effect' where large numbers of carbohydrates in close proximity have a multivalency effect.[31] Therefore, a method combining charged poly(2-oxazoline)s with sugars in a manner that enables access to more complex architectures such as blocks is highly desirable.

In this chapter, a library of poly(2-oxazoline)s was synthesised by combining three discrete monomer types. 2-ethyl-2-oxazoline (EtOx), 2-butenyl-2-oxazoline (butenylOx), and a protected amine oxazoline (BocAmineOx) were combined in various ratios. The butenylOx was then used to attach acetylated glucose units *via* a thiol-ene reaction. The glucose units were then deacetylated to yield the unprotected glucose (GluOx), followed by the deprotection of the BocAmineOx resulting in a cationic amine (AmineOx). (**Scheme 4.1.**). Using these monomers, various statistical copolymers and block copolymers were synthesised in order to study the effect of polymer structure on saRNA transfection efficiency in different cell types. The aims here were firstly to demonstrate good transfection ability, and secondly to investigate potential for targeted delivery to specific cell types. Firstly, the polyplexes were characterised by dynamic light scattering (DLS), then each polymer was tested at different N/P ratios to investigate the best ratio for transfection. The N/P ratio is the ratio of positively charged nitrogen atoms on the polymer chain to negatively charged phosphate groups on the genetic material. Next, the polymer encapsulation efficiencies were examined using a

RiboGreen assay, and their transfection efficiency and toxicity were tested in various cell lines including HEK293T/17 (human embryonic kidney cells), HeLa (immortalised epithelial cells), hSkMC (human skeletal muscle cells), and THP-1 (human monocytic cells).

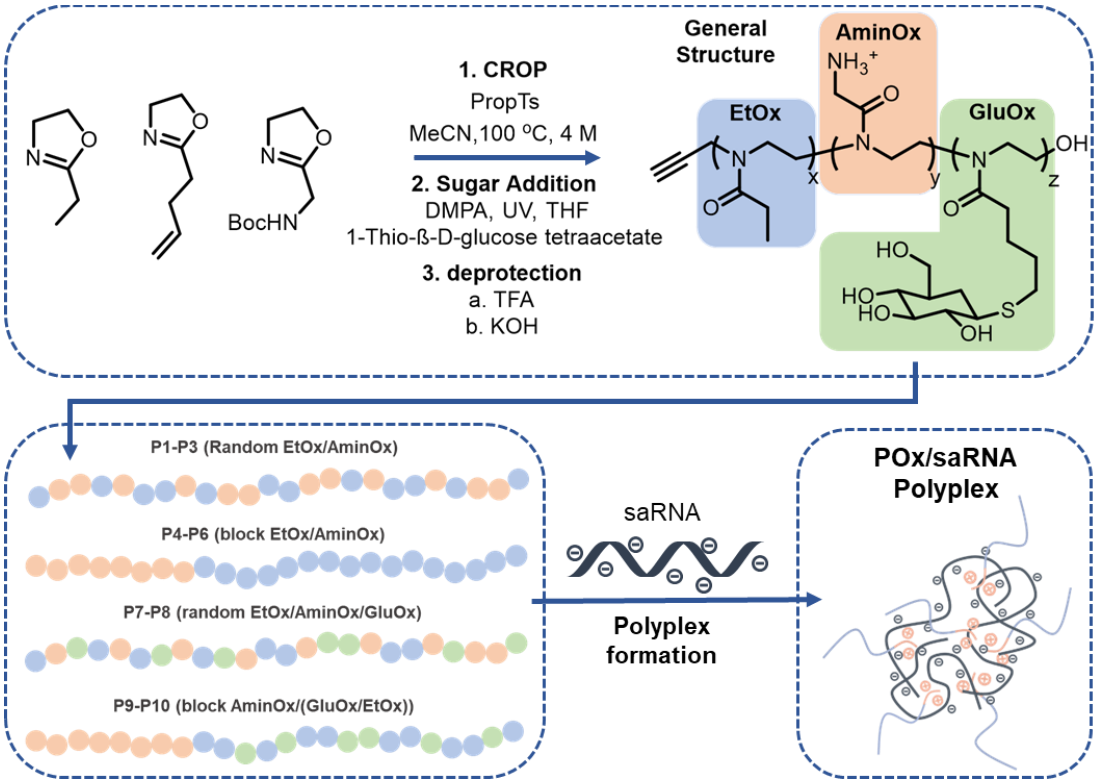

Scheme 4.1. Overall scheme for glycosylated cationic poly(2-oxazoline) synthesis, and the four general polymer structures synthesised herein.

4.2. Results and Discussion

As mentioned in **Chapter 1**, many poly(2-oxazoline)s are regarded as being non-toxic and this is one of the main reasons for the intensive research into them currently.[32-34] They can be water soluble and exhibit stealth-like behaviour in the body, meaning they can circulate in the body whilst remaining undetected by the immune system.[24, 35] Furthermore, the versatility of poly(2-oxazoline)s allows for a wide range of R groups that can be used for various applications. In this study, the two main R groups used were a positively

charged quaternary amine for polyplex formation with negatively charged RNA, and a glucose moiety intended for targeted delivery of the polyplexes. These were combined with EtOx in order to aid water solubility. A small library of polymers containing these 2-oxazolines in various configurations was synthesised, and they were compared for transfection efficiency.

In **Table 4.1**, the synthesised polymers used in this study can be seen. **P1**-**P3** are statistical copolymers of various compositions of EtOx and AmineOx. **P4**-**P6** are block polymers of various length of EtOx and AmineOx. **P7** and **P8** are statistical polymers of EtOx, GluOx, and AmineOx. Finally, **P9** and **P10** are block polymers, with the first block being a random combination of EtOx and GluOx, with the second block being purely AmineOx.

Table 4.1. Summary of polymers used for transfection studies, along with their monomer conversions, number average molar masses ($M_{n(GPC)}$), dispersity ($Đ$), and encapsulation efficiency (EE).

Entry	*Polymer Structure*	*EtOx Conv. (%) (DP)*[a]	*BocAmineOx conv. (%) (DP)*[a]	*ButenylOx conv. (DP)*[a]	$M_{n(GPC)}$ *(kDa)*[b]	$M_{n(theor.)}$ *(kDa)*[b]	*Đ*	*EE (%)*[c]
P1	p(EtOx$_{70}$/AmineOx$_{11}$)	>99 (70)	90 (11)	-	6.6	9.1	1.31	14
P2	p(EtOx$_{95}$/AmineOx$_{10}$)	>99 (95)	90 (10)	-	7.3	11.4	1.23	19
P3	p(EtOx$_{90}$/AmineOx$_{10}$)	>99 (90)	>99 (10)	-	10.1	11.0	1.11	14
P4	p(EtOx)$_{40}$-*b*-P(AmineOx)$_{10}$	>99 (40)	>99 (10)	-	4.9	5.2	1.31	93
P5	p(EtOx)$_{60}$-*b*-P(AmineOx)$_{10}$	>99 (60)	>99 (10)	-	6.2	8.2	1.34	85
P6	p(EtOx)$_{80}$-*b*-P(AmineOx)$_{18}$	>99 (80)	87 (18)	-	10.5	11.7	1.13	95
P7	p(EtOx$_{52}$/AmineOx$_{10}$/GluOx$_{9}$)	>99 (52)	>99 (10)	90% (9)	13.4	12.0	1.39	31
P8	p(EtOx$_{27}$/AmineOx$_{9}$/GluOx$_{27}$)	>90 (27)	90 (9)	90% (27)	13.7	17.7	1.73	30
P9	p(EtOx$_{56}$/GluOx$_{9}$)-*b*-AmineOx$_{5}$	>99 (56)	60 (5)	>99% (9)	12.6	11.1	1.23	64
P10	p(EtOx$_{53}$/GluOx$_{10}$)-*b*-AmineOx$_{10}$	>99 (53)	83 (10)	>99% (10)	15.0	12.2	1.35	93

[a]As measured by ^{1}H NMR Spectroscopy
[b]As measured by GPC compared to poly(methyl methacrylate) standards
[c]Encapsulation efficiency, calculated using a RiboGreen Assay.

4.2.1. Polymer Analysis

GPC traces were measured for each stage of the polymerisation, and these can be seen in **Figure 4.1**. The statistical polymers **P1**-**P3** show a single trace that is representative of the polymer at T_{final}. Overall, the statistical polymers were well-controlled, although there is some tailing to low molecular weight which could be due to a column interaction effect from the BocAmineOx. For the block polymers **P4**-**P6,** two GPC traces can be seen, representing the first polymer block (black), followed by the sequential addition of the second BocAmineOx block (red). The second block addition appears to have been successful in each case as a clear shift in the GPC is evident. Both sides of the GPC peak shift equally providing evidence that termination events are minimal. It should be noted that once the BocAmineOx was deprotected, the polymer was no longer soluble in THF and so this GPC trace could not be overlaid. The sugar addition can be seen by the blue traces in **P7-P10**. In each case, a high molecular weight shoulder can be observed which is thought to be due to polymer-polymer coupling *via* the double bonds. The reason for this is not clear, however the sugar addition required UV radiation and a photoinitiator which could result in some undesired radical reactions resulting in polymer-polymer coupling, despite a large excess of the thio-glucose being used (5 eq).

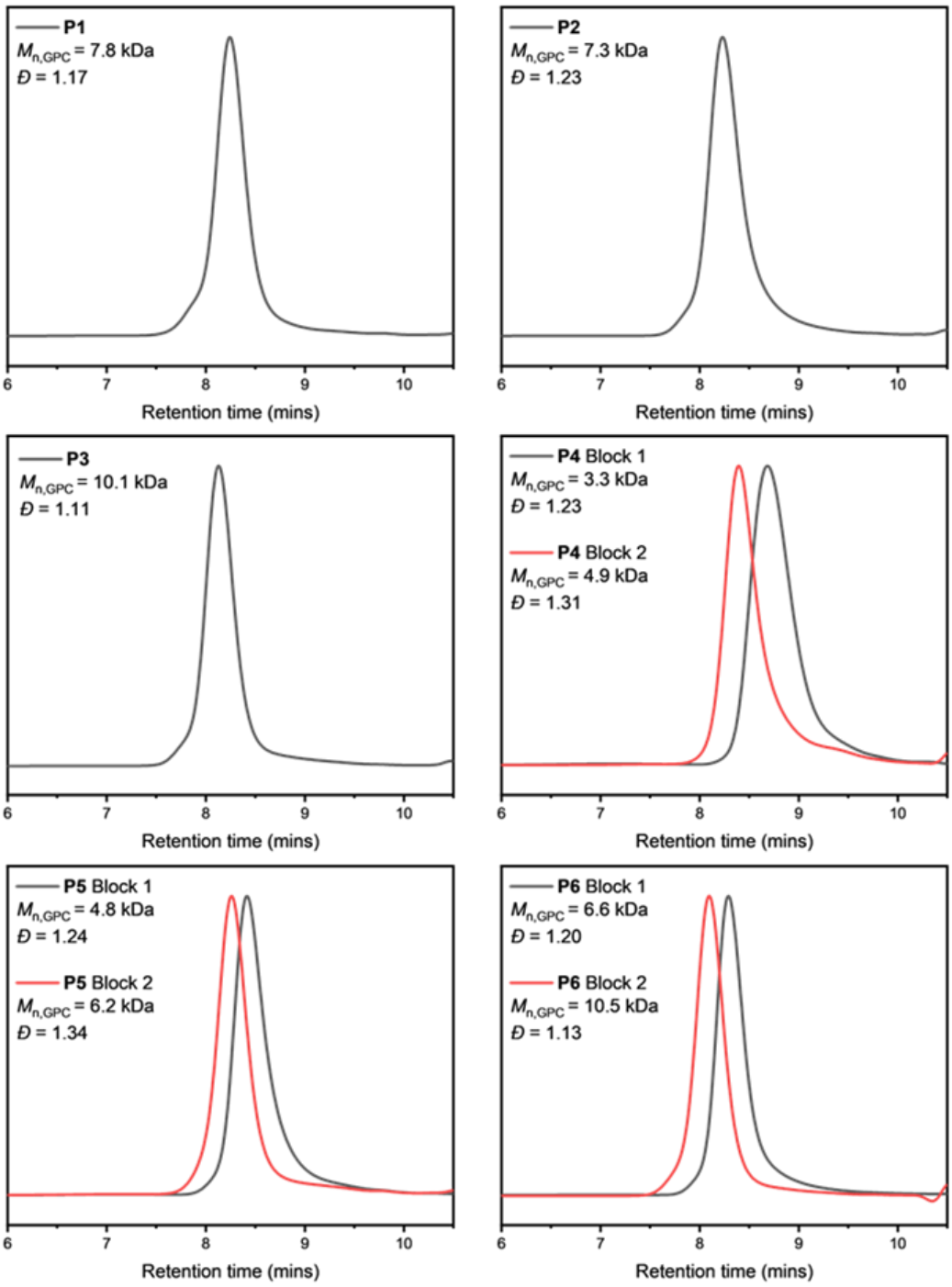

Figure 4.1. GPC traces of all non-glycosylated polymers. Red traces indicate addition of the second block. All samples were measured on a THF GPC.

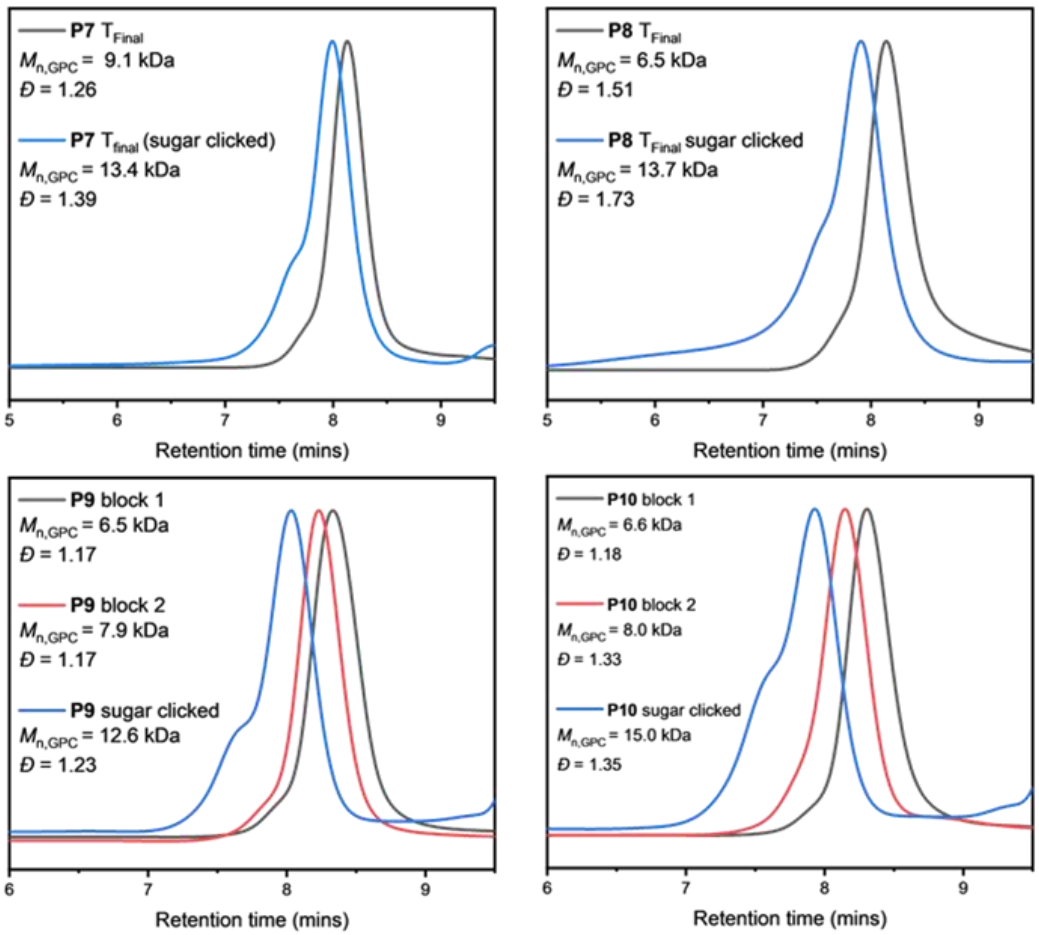

Figure 4.2. GPC traces of all glycosylated polymers. Red traces indicate addition of the second block, blue traces indicate addition of the acetylated glucose. All samples were measured on a THF GPC.

As well as GPC, ^{1}H nuclear magnetic resonance (NMR) spectroscopy was used to monitor each stage of the polymer formation, and the ^{1}H NMR spectra of each transformation for **P7** can be seen in **Figure 4.3.** For the other polymers, the ^{1}H NMR spectra can be seen in **Figure 4.12.** and **Figure 4.13.** (**4.4. Additional Data**). The monomer conversion was monitored by the disappearance of the 2-oxazoline ring protons between 3.5 and 4.5 ppm (red dashed box). Sugar addition was monitored by disappearance of the butenylOx double bond peak at 5.7 ppm (green dashed box). Removal of the boc protecting group was monitored by disappearance of the singlet peak at

1.4 ppm (blue dashed box), and removal of the acetyl protecting groups was monitored by disappearance of the multiplet at 2.0 ppm (gold dashed box).

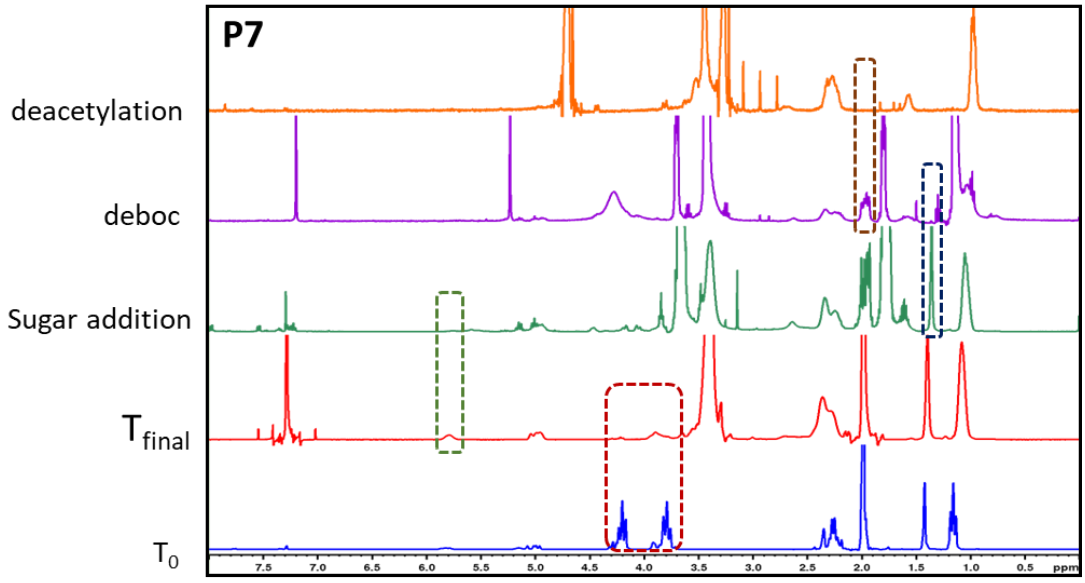

Figure 4.3. ^{1}H NMR spectra of each transformation for the glycosylated polymer **P7.** Key peak disappearances are highlighted by the coloured dashed boxes. Spectra were measured using $CDCl_3$ as the solvent.

To investigate the composition of the copolymers **P1**, **P2**, and **P3**, kinetic studies were performed. The kinetic plots can be seen in **Figure 4.4.A**. The first order plots show no deviation from the linear lines of best fit indicating that there are negligible termination events and that initiation is fast. Furthermore, the plot of molecular mass ($M_{n(GPC)}$) vs. conversion is linear, showing the absence of any chain-chain coupling reactions or chain transfer. The reactivity ratios for both monomers were calculated from the apparent propagating rate ($k_{p,app}$) derived from the first order kinetic plot for each monomer. The different reactivity ratios of the two monomers (0.65 for BocAmineOx/EtOx and 1.53 for EtOx/BocAmineOx) show that a statistical polymer has likely been formed. For the terpolymers **P7** and **P8**, the same trend is seen. The reactivities of the butenylOx and EtOx are similar, whilst the BocAmineOx again polymerises slower and so a statistical polymer is likely formed. The polymerisation is

reasonably well-controlled with *Đ* of the final polymer being ~1.4, and no evidence of termination, chain transfer, or polymer coupling reactions can be observed.

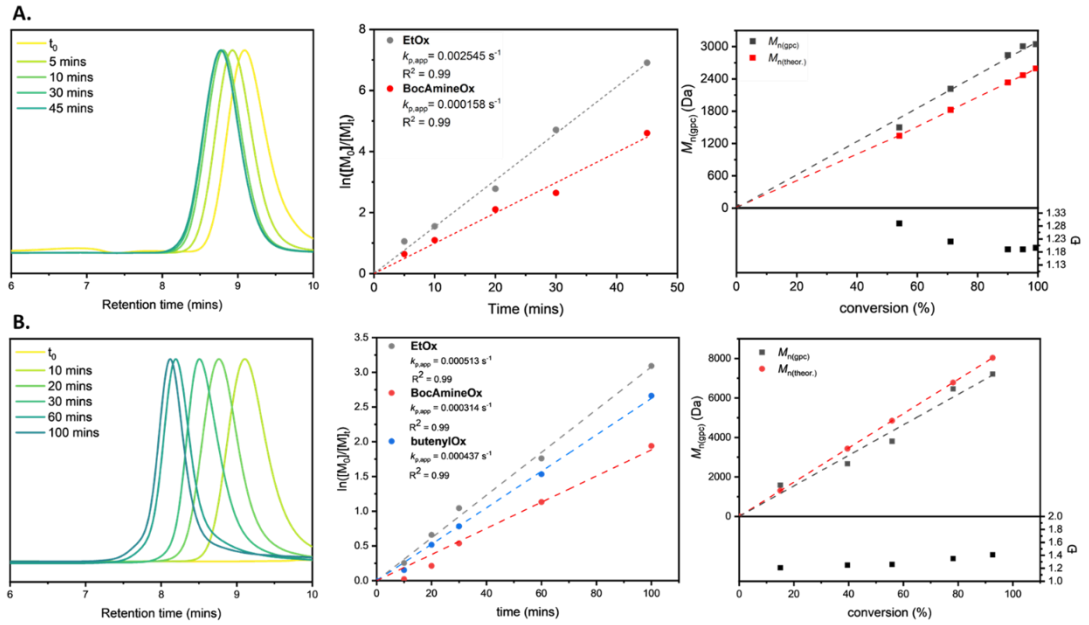

Figure 4.4. (A) Kinetic of EtOx and BocAmineOx. Conditions: Initiated with propargyl tosylate. Carried out at a concentration of 4 M. Conditions: Solvent was acetonitrile:dimethylacetamide 1:1 vol/vol, run at 120 °C **(B)** kinetic of EtOx, BocAmineOx, and butenylOx. Conditions: the initiator was propargyl tosylate. Carried out at a concentration of 4 M. Solvent was MeCN, run at 100 °C.

4.2.2. Optimising the N/P Ratio

It must be noted that the encapsulation efficiency, cell transfection, and cell viability experiments were carried out by Beatriz Dias Barbieri from the Shattock group at Imperial College London. In **Figure 4.5.** various N/P ratios were tested from 0.5 to 50. These values were derived from the ratio of polymer concentration to RNA concentration in solution, and do not indicate the optimal N/P ratio to prevent an excess of polymer being used. Initially, the size, polydispersity index and zeta potentials of each polyplex were measured by DLS (**Figure 4.5.**). In general, the polyplexes were smaller at higher N/P ratios, and the zeta potentials were much closer to neutral. Ideally, the polyplex

size should be around 100-300 nm as particles smaller than this are quickly eliminated by renal excretion and larger particles are taken up by monomolecular phagocytic cells.[36] The zeta potential is important as it affects polyplex stability can prevent aggregation. For an N/P ratio of 20, the polyplex sizes were amongst the smallest with the lowest dispersity, and their zeta potentials were positive compared to the other ratios. Interestingly, the glycosylated polymers were smaller and had lower dispersity than the non-glycosylated polymers. One obvious outlier to this trend was **P8**, which although glycosylated, formed abnormally large particles.

For the non-glycosylated polymers (**P1-P6**), the statistical copolymers **P1**-**P3** generally formed larger, more disperse particles than the block polymers (**P4**-**P6**), and at higher N/P ratios (20,50) the block polymers had higher zeta potentials. For the glycosylated polymers, the block polymers (**P9** and **P10**) were smaller than the statistical polymers (**P7** and **P8**), especially at high N/P ratios. **P8** had the highest zeta potential of all the polymers and formed the largest particles of all the polymers tested, however the reason for these features is not clear. Lastly, for the glycosylated block polymers, **P10** had higher zeta potential values when compared to **P9.** This can be attributed to having twice the amount of positively charged units in the polymer (5 per polymer for **P9**, 10 per polymer for **P10**).

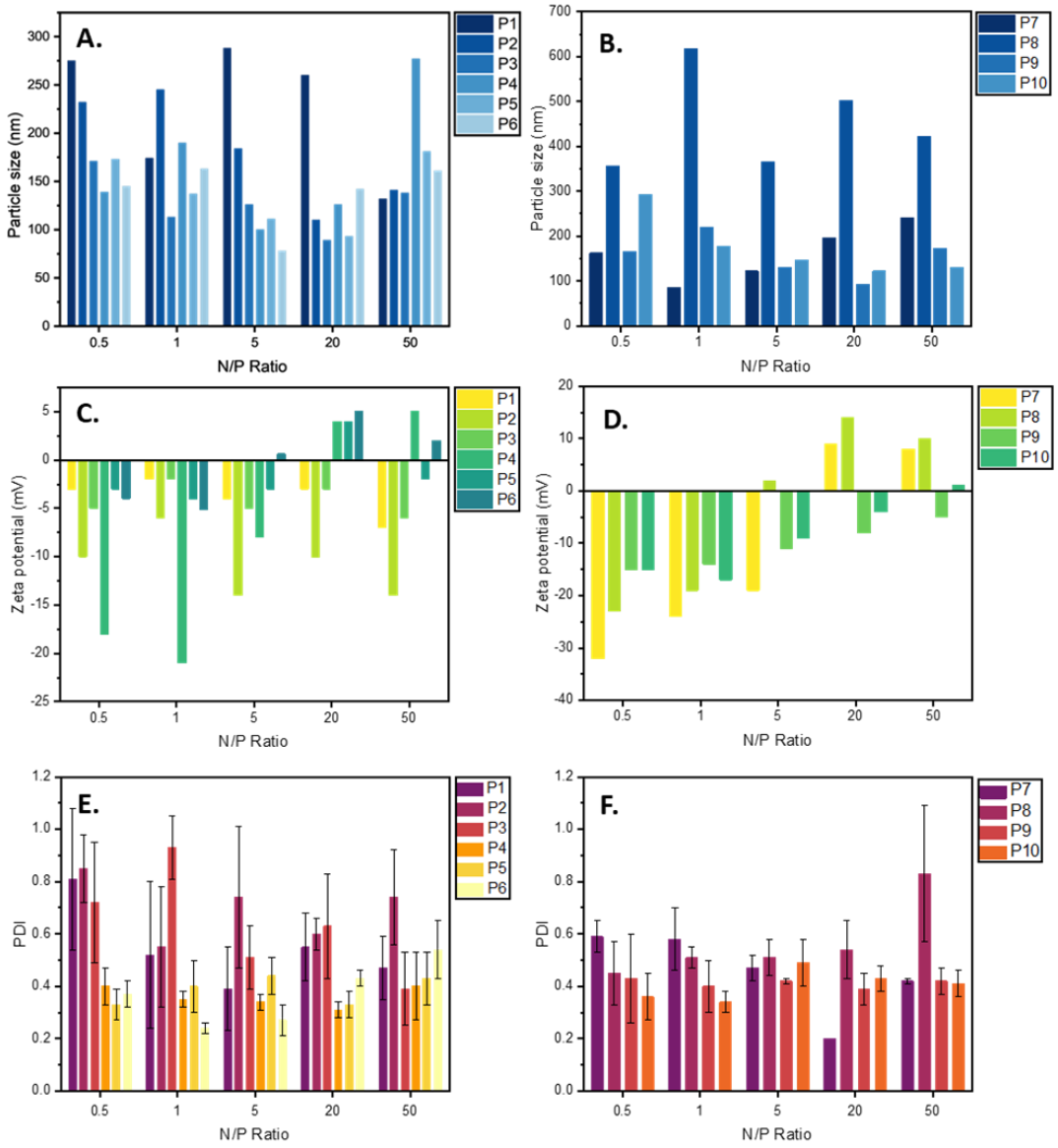

Figure 4.5 (A) particle sizes of non-glycosylated polymers **P1**-**P6 (B)** particle sizes of glycosylated polymers **P7**-**P10 (C)** zeta potentials of non-glycosylated polymers **P1**-**P6 (D)** zeta potentials of glycosylated polymers **P7**-**P10 (E)** PDI of non-glycosylated polymers **P1**-**P6 (F)** PDI of glycosylated polymers **P7**-**P10**.

Next, the transfection efficiency was measured at each N/P ratio for all the polymers (**Figure 4.6.**). Here, polyplexes were formed with saRNA that encoded the firefly luciferase enzyme. Firefly luciferase bioluminesces and can be used as a proxy for transfection efficiency as the amount of luminescence can be used to quantify transfection. Improved transfection was observed with higher N/P ratios, however the non-glycosylated statistical polymers (**P1**-**P3**) performed poorly across the whole N/P ratio, with minimal

transfection observed. The block polymers **P4**-**P6** had much higher transfection efficiencies, showing the effect of polymer architecture on transfection efficiency. These polymers have a higher concentration of charged species at one terminus of the polymer, as opposed to the statistical polymers which have the charged species distributed throughout the polymer which could explain the improved transfection seen. Indeed, a correlation between increased charge density on the polymer and improved transfection has already previously been established.[23] Within the subset of non-glycosylated block polymers, transfection improved with increasing polymer size, with **P6** performing better at low N/P ratios compared to **P5**, and **P5** performing better than **P4** at low N/P ratios.

For the statistical glycosylated polymers, **P8** had improved transfection compared to **P7** at higher N/P ratios, whilst also having a higher glucose content. Comparing the effect of block polymer vs. statistical glycosylated polymer, **P10** performed slightly better than **P7** at lower N/P ratios, but they were similar at higher N/P ratios. Comparison of **P7** and **P10** is important because they have the same quantities of EtOx, AmineOx, and GluOx, but **P10** has the charged AmineOx groups in a block structure whilst they are statistically distributed for **P7**. Doubling the charged block length from 5 to 10 (**P9** to **P10**) improved transfection at the lower N/P ratios, but at higher N/P ratios (20,50) there was minimal difference. Due to these preliminary transfection results along with the DLS results, an N/P ratio of 20 was selected for future experiments as these polyplexes had suitable sizes and had comparable transfection results to an N/P ratio of 50.

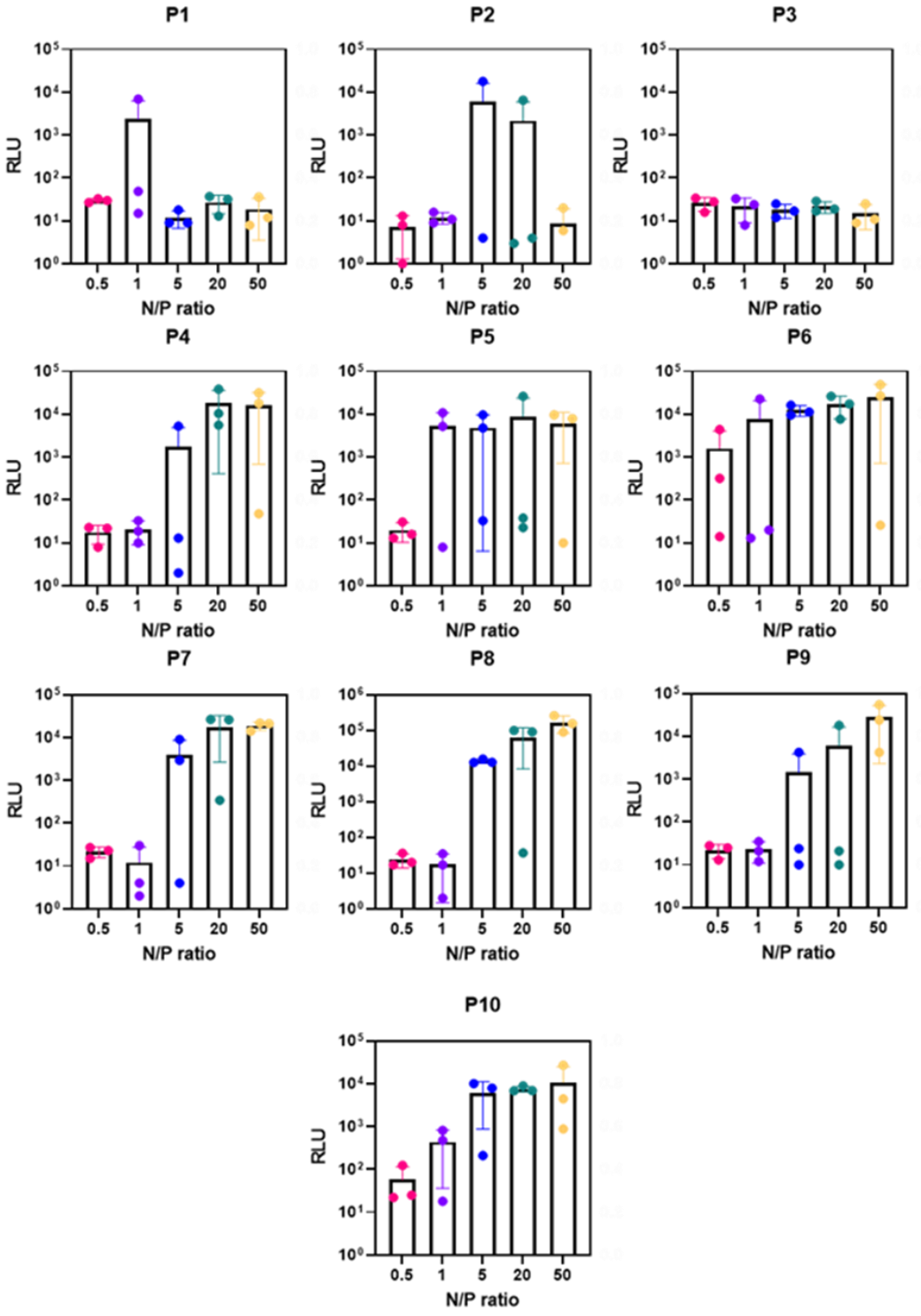

Figure 4.6. Transfection efficiencies for all polymers at N/P ratios of 0.5, 1, 5, 20, 50.

4.2.3. Encapsulation Efficiency of the Polymers

To measure the encapsulation efficiency of the polymers, a RiboGreen RNA assay was performed, the results of which can be seen in **Figure 4.7**. For the assay, a dye that can bind with nucleic acids is mixed with the polyplexes. The dye cannot access nucleic acids that are bound within the polyplex and so only binds to unbound material. When the dye binds to a nucleic acid, it fluoresces strongly and this can be used to quantify the amount of unbound genetic material by subtraction from 100%. It should be noted that polymers do not 'encapsulate' *per se* but form a mesh-like complex with the genetic material. For the non-glycosylated statistical polymers (**P1**-**P3**), the encapsulation efficiency was very low with all three polymers having encapsulation efficiencies of under 20% (see **Table 4.1**). The polymer length has only a marginal effect on the encapsulation efficiency, with the longer chain (**P2**) having slightly improved encapsulation efficiency compared to **P1** and **P3**. The non-glycosylated block polymers (**P4**-**P6**) showed considerably better encapsulation efficiency than their statistical counterparts, with the encapsulation efficiency increasing to over 80% for all three polymers. The block structure increases the positive charge density at the chain end, and this is likely the reason for the improved encapsulation efficiency. For the glycosylated polymers, the same trend was seen between the statistical polymers and the block polymers, i.e. the block polymers **P9** and **P10** demonstrated better encapsulation than the statistical polymers **P7** and **P8**. Interestingly, glycosylation appeared to increase the encapsulation efficiency for the statistical polymers slightly as both **P7** and **P8** showed better encapsulation than **P1**, **P2**, and **P3**. **P10** had slightly improved encapsulation

efficiency compared to **P5**, which is of similar degree of polymerisation (DP) with a similar amount of charged units, but without glycosylation. Lastly, **P9** had much worse encapsulation efficiency than **P10**, which is due to the much shorter charged block length. In order to maximise encapsulation efficiency, glycosylated block polymers are ideal, with longer charged blocks showing improved encapsulation.

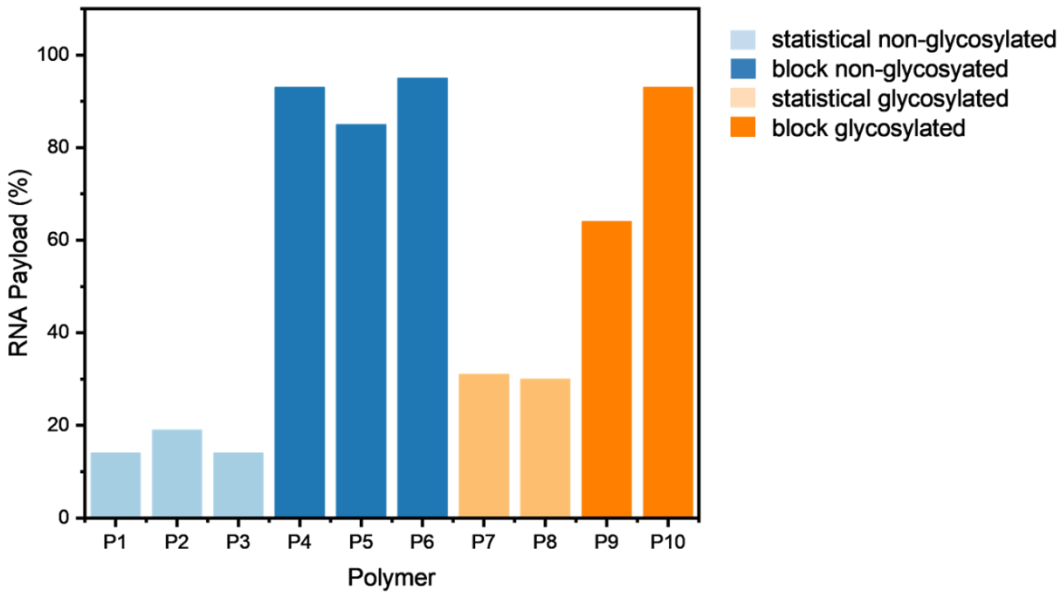

Figure 4.7. Encapsulation efficiency results for all polymers from the RiboGreen Assay. Colours are provided to aid in distinguishing between the polymer types.

4.2.4. Polymer Toxicity Study

A CellTiter-Glo 2.0 assay test was run to examine cell viability after they had been exposed to the different polyplexes (**Figure 4.8.**). For this assay, cells were incubated for 24 hours with the polyplexes, before luciferin was added to the cell cultures. Luciferin reacts in the presence of adenosine triphosphate (ATP) to form oxyluciferin, which is fluorescent and can be used to quantify the amount of ATP. It is important to quantify the amount of ATP as this is a direct indicator of active metabolic cells (i.e. living cells). Four separate cell

lines were investigated - HEK293T/17, HeLa, hSkMC, and THP-1 lines. HEK293T/17 cells are a type of human embryonic kidney (HEK) cells that are useful for transfections studies because they are easy to grow and transfect with genes, as they have little regulation on RNA expression.[37] HeLa cells are an immortalised epithelial cell line, whilst hSkMC are human skeletal muscle cells, and THP-1 is a monocyte immune cell type. These three cell lines were chosen for transfection as they are some of the most common cell types found in the human body. Moreover, the cell viability was above 80% for all polymers used in all the cell lines. Furthermore, all polymers demonstrated comparable cell viability levels to PEI, with improved viability showed particularly for the HeLa cells. It should be noted that the polymer concentration for the cell viability and cell transfection was low (1 μg/1 mL) and this explains the high cell viability of PEI and the polymers tested in this study. For many of the polymers in the HeLa and THP-1 cells, the polymers actually showed increased cell viability compared to the control, further demonstrating their outstanding cell viability. For the HEK293 t/17 cell line, the polymers showed excellent cell viability with over 90% of cells surviving in most cases. **P6** showed some reduction in cell viability for this cell line, which may be due to the greater number of amine units on the polymer compared to the other samples tested. For the HeLa cell line, the polymers showed minimal toxicity, with some cell viability results increasing to over 100% demonstrating cell growth. There was again a reduction in cell viability for **P6**, although the cell viability was still high for this sample. For the hSkMC cell line, all polymers again showed excellent cell viability, however the glycosylated polymers **P7**-**P9** showed a slight decrease in cell viability compared to the other polymers

tested. Finally, the THP-1 macrophage cell line was tested, with all polymers showing excellent cell viability, with results demonstrating that around 100% of the cells survived exposure to the polymers.

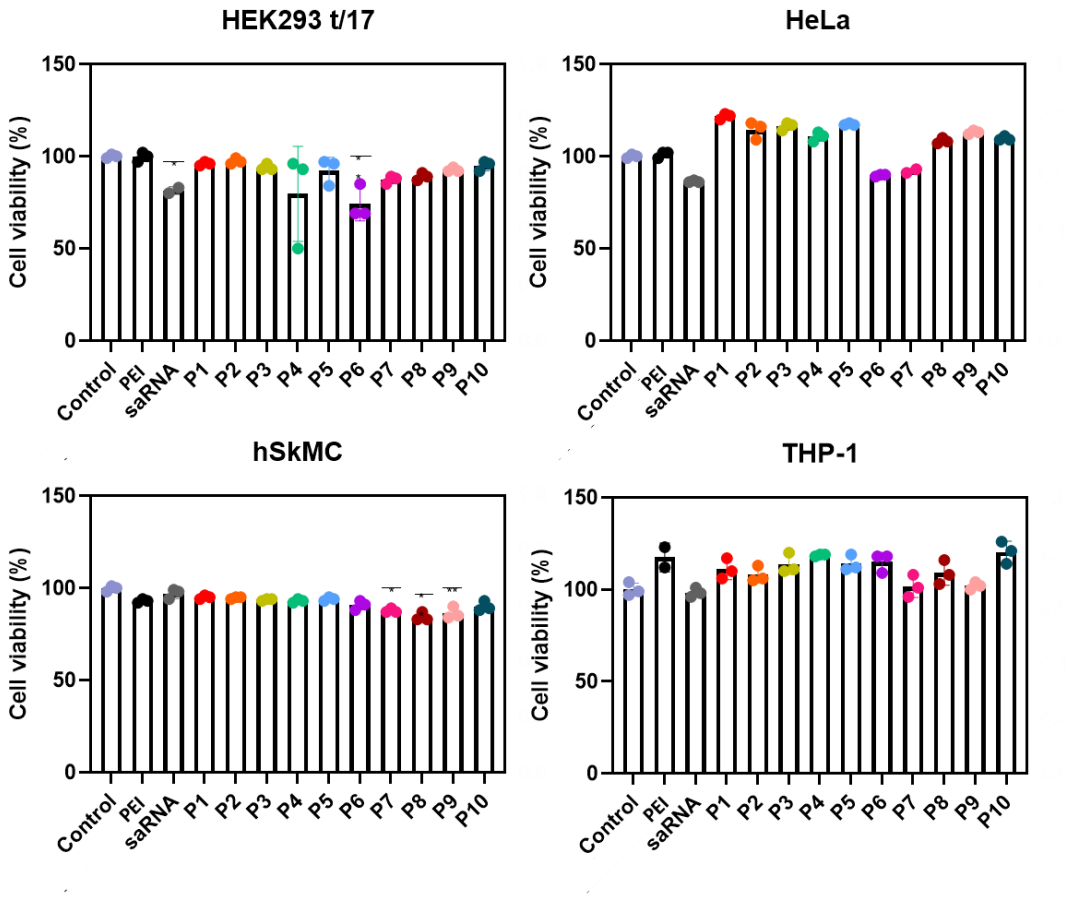

Figure 4.8. Cell viability of different cell lines upon incubation with the polymers for 24 hours, as calculated using the CellTiter-Glo 2.0 assay test. Polymer concentration was 1 ng/µL, see experimental for cell seeding density.

4.2.5. Polyplex Transfection in Various Cell Lines

To explore the effect of structure and glycosylation of the polymers on saRNA transfection, transfection efficiency was measured in the various cell lines – HEK293T/17, HeLa, hSkMC, and THP-1 (**Figure 4.9.**). It should be noted that the amount of polyplex used was adjusted depending on the encapsulation efficiency of the polymer. i.e. **P3** required a much higher mass of the polyplex

to attain the same level of encapsulated saRNA as, for example, **P4**. This is because the encapsulation efficiency of **P3** was much less than for **P4**.

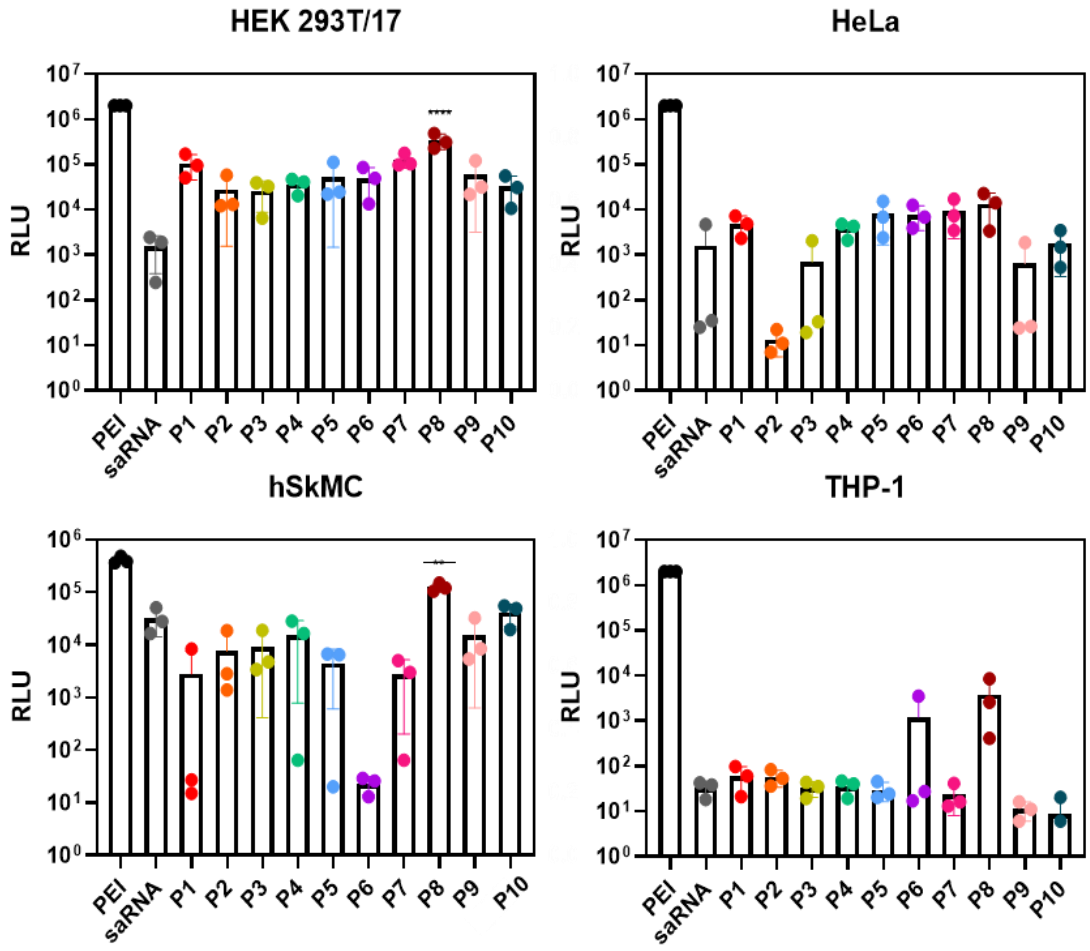

Figure 4.9. Polyplex efficiency for polymers P1-P10 using the cell lines HEK 293T/17, HeLa, hSkMC, and THP-1. Polymer concentration was 1 ng/µL, see experimental for cell seeding density.

Firstly, the transfection efficiency with the HEK 293T/17 was investigated. As expected, all polyplexes for this cell line demonstrated higher transfection efficiency compared to saRNA, although none performed to the same standard as PEI due to the high molecular weight of the PEI used (40 kDa) in relation to the synthesised polymers.[23] There was not a significant difference between the non-glycosylated statistical (**P1**-**P3**) and block copolymers (**P4**-**P6**), although much less polyplex was required for **P4**, **P5**, and **P6** due to their

increased encapsulation efficiency. The glycosylated polymers **P7**, **P9**, and **P10** were also comparable to the non-glycosylated polymers, however **P8** showed improved levels of transfection compared to all the other polymers.

P8 has a higher density of glucose moieties along its backbone compared to the other glycosylated polymers, and this is likely the reason why it shows improved transfection. It is not clear as to whether this improved transfection is due to a lectin binding effect or for some other reason whereby glycosylation aids transfection. Further testing is required to elucidate the reason behind this improved transfection. For the HEK 293T/17 cell line, heavily glycosylated block polymers are likely to lead to the most potent transfection agent as they demonstrate the best saRNA expression, whilst the block polymer structure allows for more polymer to be encapsulated per polyplex.

Next, the HeLa cell line was considered. Here, all the polymers performed worse than PEI, with some appearing to inhibit the transfection of saRNA. The reduction in cell transfection efficiency could be explained by the fact that HeLa cells are interferon competent, while HEK cells are not. Interferons are proteins that cells express to trigger an immune response when exposed to a pathogen. An excess of a type I IFN response may lead to the activation of the eukaryotic translation initiation factor 2A, which impairs the activity of eIF2. eIF2 is a protein that is involved in the initiation phase of translating RNA into the corresponding protein. Consequently, if this protein function is impaired, mRNA translation and protein synthesis are inhibited (i.e. less fluorescence is shown).[38, 39] Interestingly, for the non-glycosylated statistical copolymers, an increase in polymer length (**P1** compared to **P2**/**P3**) caused a drastic reduction in transfection efficiency of the polymers. The cause of this reduction in

transfection may be due to the low charge density on the polymers **P2** and **P3** as a consequence of the large amount of EtOx compared to AmineOx. Furthermore, the large difference in transfection between **P1** and **P2** is surprising and warrants further investigation. The non-glycosylated block copolymers **P4**, **P5**, and **P6** were comparable to **P1**, as were the glycosylated statistical polymers. Interestingly, the glycosylated block polymers **P9** and **P10** did not appear to perform as well as the glycosylated statistical polymers **P7** and **P8**. The block polymer **P9** possesses a very short cationic block and this may be the cause of the poor transfection for this sample as it has only a few charged units to bind the RNA, however the reason for the reduction in transfection for **P10** is not clear.

Continuing from the HeLa cell line, the hSkMC cell line was investigated. Overall, the polyplexes performed similarly to saRNA on its own, except for **P8** which showed improved transfection efficiency when compared to saRNA and was almost as effective as PEI. This is a promising result considering the difference in molecular weight between PEI (40 kDa) and **P8** (17.7 kDa). For the statistical non-glycosylated polymers, increasing the polymer length appeared to improve transfection, although all three polymers (**P1**-**P3**) performed worse than saRNA. Interestingly, **P6** showed much lower transfection efficiency than all other polymers for the hSkMC cell line. **P6** contains more charged amine units than all the other polymers, which is a potential cause of this observation. Conflictingly, PEI also contains a large amount of charged amines along the backbone of the polymer, whilst retaining high transfection efficiency. Moreover, the polymers in this series contain exclusively primary amines and so increasing the number of primary amines

appears to reduce transfection to hSkMC cells. This suggests that charged primary amines may prevent transfection to specific types of cell such as hSkMC, which warrants further research into how the substituent profile of the amine affects transfection. As mentioned, comparing **P7** and **P10** shows the effect of block vs statistical for the glycosylated polymers. There is a clear difference between these polymers for the hSkMC line, with **P10** demonstrating much higher transfection than **P7**. As well as this, reducing the charged block length from 10 (**P10**) to 5 (**P9**) caused a small reduction in transfection. Overall, glycosylation appears to have the biggest impact on transfection in skeletal muscle cells for these polymers, as can be seen by **P8**, and there is some evidence to suggest that block polymers improve transfection over statistical polymers, particularly for the glycosylated polymers.

The last cell line explored was the THP-1 cells, which typically show a significant immune response. Therefore, it was especially important to demonstrate promising transfection without drastically reducing the cell viability and interfering with their behaviour. Moreover, THP-1 macrophages possess a wide range of carbohydrate-binding lectins, and so should be sensitive to glycosylated polymers.[40] In this cell line, polymers **P1**-**P7** performed similarly to saRNA i.e. they showed minimal transfection potential. **P6** showed some better transfection efficiency compared to saRNA however there was significant error associated with the sample. Once again, **P8** showed optimum transfection efficiency within the polymers tested, presumably due to the large amount of glycosylation being able to target the THP-1 cells. Nonetheless, the other glycosylated polymers **P7**,**P9**, and **P10** did not perform

as well, although these polymers do not have as many glucose units attached per polymer chain. It must be noted that it is not clear whether the improved transfection of **P8** is purely due to glycosylation, or a synergy between the glycosylation and charged primary amines. Although the significantly higher amount of glycosylation of **P8** shows improved transfection, it is not clear at this stage as to whether this is due to a lectin binding interaction or for some other reason. Nonetheless, it would be of interest to synthesize more heavily glycosylated polymers as there is a clear improvement demonstrated here by adding more glucose units.

Next, the polymers were compared across cell types to examine any potential targeting ability. All polymers showed good transfection in the HEK cell line, which was expected as the HEK cell line was chosen as it is easy to transfect. Therefore, for ease of comparison the HEK cell line was ignored and the polymer transfection ability in the other cell types was compared. The statistical non-glycosylated polymers **P2** and **P3** demonstrated better transfection in the skeletal muscle cells compared to the THP-1 immune cells and the HeLa epithelial cells, whilst the statistical block polymer **P6** showed improved transfection in the HeLa epithelial cells compared to the skeletal muscle cells and THP-1 immune cells. Although the glycosylated polymer **P8** performed well compared to the other polymers in the study across all cell lines, it demonstrated the best transfection for the skeletal muscle cells. This was also observed for the glycosylated block polymers **P9** and **P10** which showed the best transfection in the skeletal muscle cell line. The individual polymers clearly have different transfection efficiencies in the different cell

lines, however further work is required to observe whether the targeting observed in this study is real.

4.2.6. Conclusions

In this chapter, the successful synthesis of charged and glycosylated poly(2-oxazoline)s was demonstrated. The synthesised polymers were combined with saRNA to form polyplexes, which were systematically tested for encapsulation efficiency, transfection in various cell lines, and cell viability. The polymer structure was shown to be influential over encapsulation efficiency of the saRNA, with block polymers showing encapsulation efficiencies of up to 95%. Furthermore, longer polymers also improved the encapsulation efficiency, and glycosylated polymers showed improved encapsulation compared to their non-glycosylated counterparts. Interestingly, **P8** which has the highest number of sugar units on the polymer chain generally had the best transfection efficiency in different cell lines, despite having an encapsulation efficiency of only 30%. The statistical glycosylated polymers **P7** and **P8** performed better in HEK 293 T/17 and HeLa cells, whilst **P8** outperformed all polymers in the hSkMC and THP-1 cell lines. Clearly the degree of glycosylation is a key factor in transfection efficiency. Whilst the difference between block and statistical polymers also influenced transfection, it was of secondary importance compared to glycosylation. There is some evidence to suggest that the polymers can be used to target cells for gene transfection, however further work is required to investigate this. Lastly, the polymers showed excellent cell viability across all cell lines and were comparative to the control. Future work in this area would be to increase the glycosylation of the polymers further and to maximize block lengths to increase transfection.

Furthermore, evaluating the polymers in mixed cell cultures could be used to demonstrate targeted transfection at specific cell types.

4.3. Experimental

4.3.1. Polymer Synthesis and Analysis

4.3.1.1. Materials Used

Boc-glycine (98%), *N*-(3-dimethylaminopropyl)-*N'*-ethylcarbodiimide (97%), 4-dimethylaminopyridine (99%), 2,2-dimethyl-2-phenyl-acetophenone (99%), 1-Thio-β-D-glucose tetraacetate (97%) Sodium chloride (>99%), Tetrahydrofuran (anhydrous), and triethylamine (>99%) were purchased from Sigma-Aldrich and used as received. Chloroethylamine.HCl (98%), acetonitrile (anhydrous), and hydrochloric acid (37%) were purchased from Fisher Scientific and used as received. Trifluoroacetic acid (99%), and 4-pentenoic acid (98%) were purchased from Alfa-Aesar and used as received.

Methyl *p*-toluenesulphonate (98%) (Fisher Scientific) was distilled prior to use. 2-ethyl-2-oxazoline (99%) (Fisher Scientific) was stirred over calcium hydride for 16 hours before purification by distillation.

4.3.1.2. Instrument Methods Used

4.3.1.2.1. GPC Measurements

The eluent used was tetrahydrofuran (THF) with 2% triethylamine and 0.01% Butylated hydroxytoluene. The Agilent Technologies 1260 Infinity instrument was equipped with a refractive index and 308 nm UV detectors, a PLgel 5 μm guard column, and a PLgel 5 μm mixed D column (300 × 7.5 mm). Samples were run at 1 mL min^{-1} at 40 °C. Poly(methyl methacrylate) standards (Agilent

PMMA calibration kits, M-M-10 and M-L-10) were used for the calibration. Before injection (100 µL), the samples were filtered through a PTFE membrane with 0.2 µm pore size.

4.3.1.2.2. NMR Spectroscopy Measurements

Proton and carbon nuclear magnetic resonance spectra (^{1}H and ^{13}C NMR) were measured on a Bruker DPX-300 or DPX-400 and all samples were measured at either 300 MHz or 400 MHz in $CDCl_3$ at 298 K. The resonance signal of residual $CHCl_3$ at 7.26 ppm served as the reference peak for chemical shifts.

4.3.1.3. Synthesis of BocAmineOx

Taken from a literature procedure.[41] To a 500 mL round bottomed flask, *N*-(*tert*-Butoxycarbonyl)glycine (10.00 g, 57.1 mmol, 1 eq), chloroethylamine.HCl (7.28 g, 62.8 mmol, 1.1 eq), and 4-dimethylaminopyridine (DMAP) (0.697 g, 5.7 mmol, 0.1 eq) were added along with a magnetic stirrer bar. Dichloromethane (DCM) (200 mL) was added, and the reaction was stirred under a nitrogen blanket and cooled to 0 °C using an ice bath. Once the reaction mixture had cooled to 0 °C, triethylamine (TEA) (11.55 g, 110 mmol, 2 eq) was added dropwise. Next, *N*-(3-dimethylaminopropyl)-*N'*-ethylcarbodiimide (EDAC) (9.74 g, 62.8 mmol, 1.1 eq) was added dropwise and the reaction mixture was allowed to stir overnight. Next, the reaction mixture was washed with 0.5 M $HCl_{(aq)}$ (3 x 100 mL), saturated $NaHCO_3$ solution (3 x 100 mL), distilled water (3 x 100 mL) and brine (2 x 100 mL) before being dried over magnesium sulphate. The solvent was removed *in vacuo* to yield the amide intermediate.

For the ring closure step to form the 2-oxazoline, potassium hydroxide (4.8 g, 85 mmol, 1.5 eq) was dissolved in methanol (50 mL). The amide intermediate was added to a 100 mL round bottomed flask with a stirrer bar and placed under a nitrogen blanket. To this, the methanolic potassium hydroxide solution was added slowly, and the reaction mixture was then heated to 50 °C and left for 16 hours. The reaction mixture was then filtered, and the residual methanol was removed *in vacuo*. The reaction mixture was then redissolved in DCM (100 mL) before being washed with distilled water (3 x 100 mL) and then brine (2 x 100 mL) before being dried over magnesium sulphate. The organic solvent was the removed *in vacuo*, before the 2-oxazoline was purified by vacuum distillation to yield a white crystalline solid. (overall yield = 70%). NMR spectra can be seen in **Figure 4.10**.

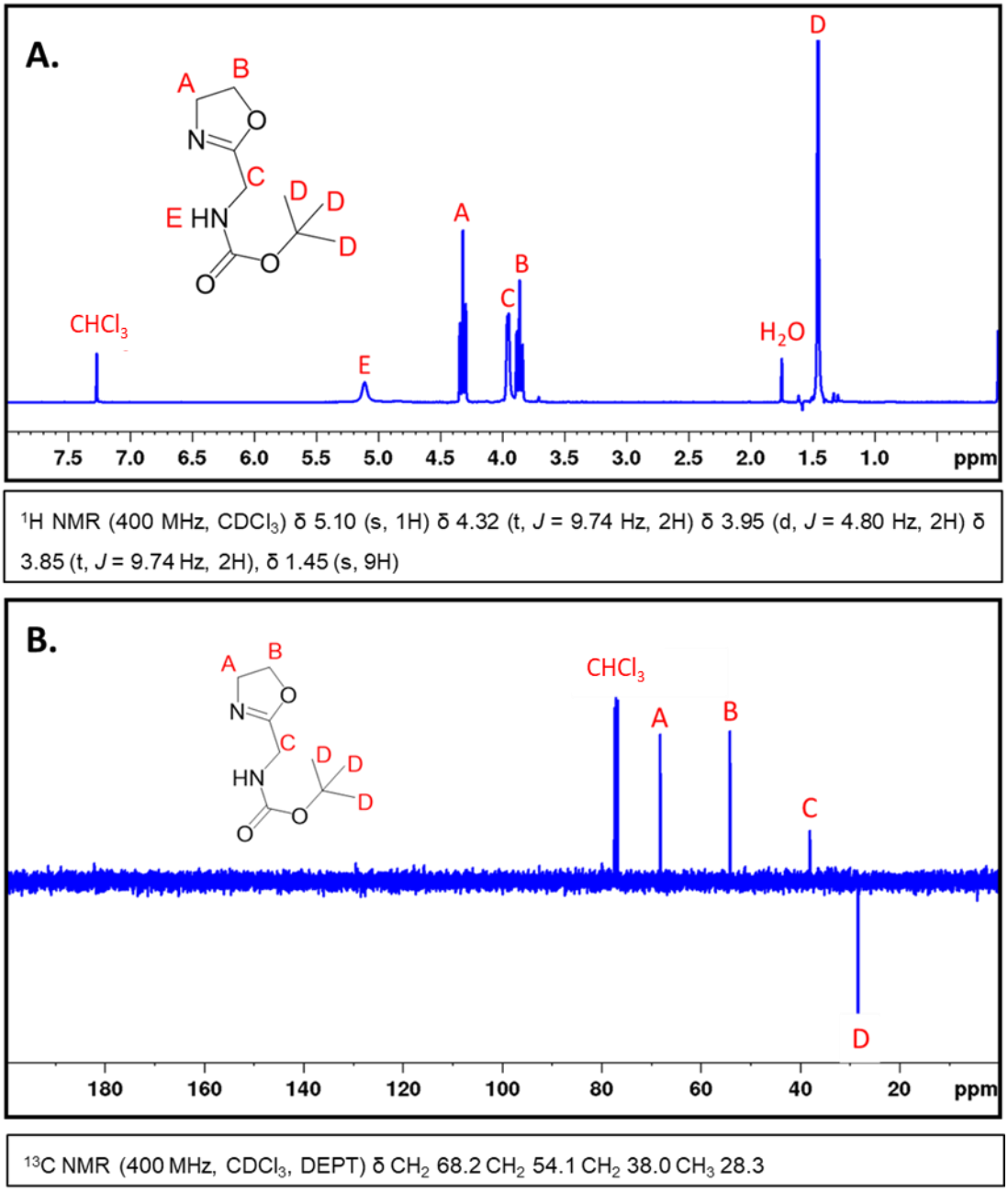

Figure 4.10. (A) ^{1}H NMR Spectrum of BocAmineOx **(B)** ^{13}C NMR spectrum of BocAmineOx. Both spectra were measured using $CDCl_3$ as the solvent.

4.3.1.4. Synthesis of ButenylOx

Based on a literature procedure.[42] To a 500 mL round bottomed flask, 4-pentenoic acid (10.00 g, 99.8 mmol, 1 eq), chloroethylamine.HCl (12.74 g, 109.9 mmol, 1.1 eq), and DMAP (1.22 g, 10.0 mmol, 0.1 eq) were added along with a magnetic stirrer bar. DCM (200 mL) was added, and the reaction was

stirred under a nitrogen blanket and cooled to 0 °C using an ice bath. Once the reaction mixture had cooled to 0 °C, triethylamine (20.2 g, 199.9 mmol, 2 eq) was added dropwise. Next, EDAC (17.06 g, 109.9 mmol, 1.1 eq) was added dropwise and the reaction mixture was allowed to stir overnight. Next, the reaction mixture was washed with 0.5 M $HCl_{(aq)}$ (3 x 100 mL), saturated $NaHCO_3$ solution (3 x 100 mL), distilled water (3 x 100 mL) and brine (2 x 100 mL) before being dried over magnesium sulphate. The solvent was removed *in vacuo* to yield the intermediated amide.

For the ring closure step to form the 2-oxazoline, potassium hydroxide (8.4 g, 149.8 mmol, 1.5 eq) was dissolved in methanol (50 mL). The amide intermediate was added to a 100 mL round bottomed flask with a stirrer bar and placed under a nitrogen blanket. To this, the methanolic potassium hydroxide solution was added slowly, and the reaction mixture was then heated to 50 °C and left for 16 hours. The reaction mixture was then filtered and the residual methanol was removed *in vacuo*. The reaction mixture was then redissolved in DCM (100 mL) before being washed with distilled water (3 x 100 mL) and then brine (2 x 100 mL) before being dried over magnesium sulphate. The organic solvent was the removed *in vacuo*, before the 2-oxazoline was purified by vacuum distillation to yield a white crystalline solid. (overall yield = 40%). The NMR spectra can be seen in **Figure 4.11**.

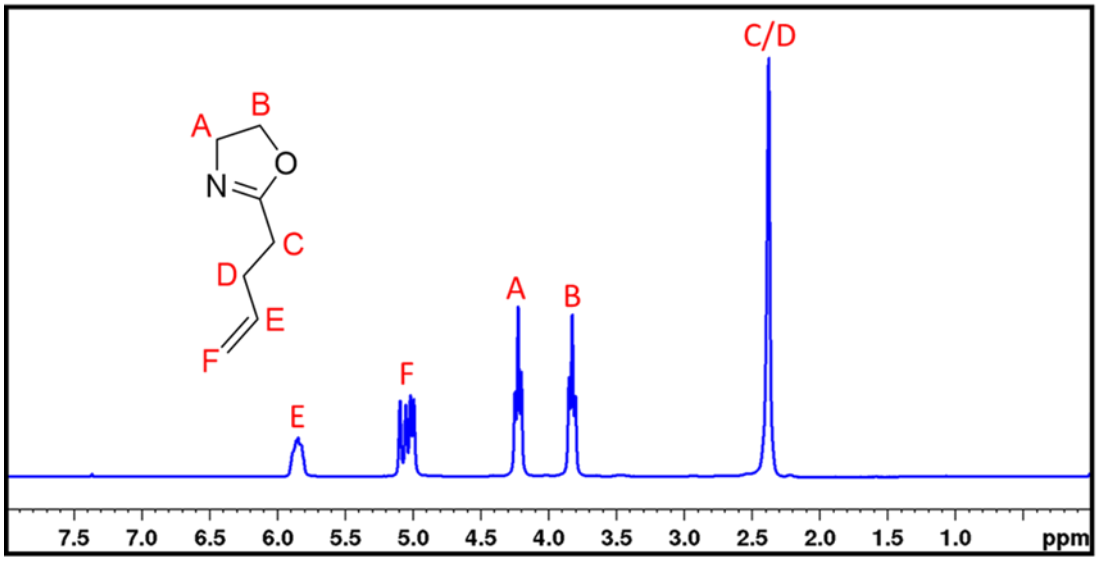

^{1}H NMR (400 MHz, $CDCl_3$) δ 5.84 (m, 1H) δ 5.04 (m, 2H) δ 4.22 (t, *J* = 9.23 Hz, 2H) δ 3.82 (t, *J* = 9.23 Hz, 2H), δ 2.38 (s, 4H)

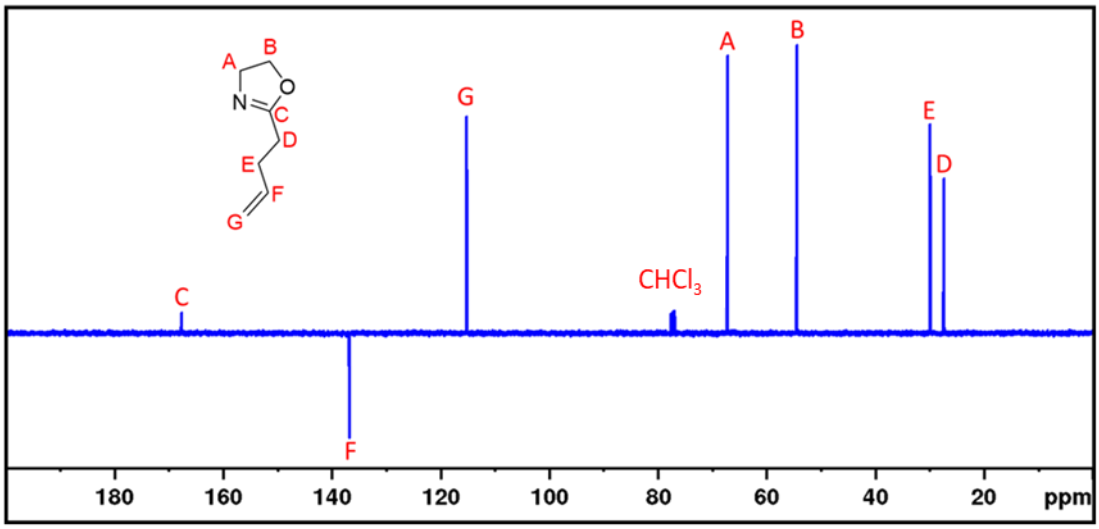

^{13}C NMR (400 MHz, $CDCl_3$, DEPT) δ C 167.7 CH 136.8 CH_2 115.3 CH_2 67.1 CH_2 54.3 CH_2 29.8 CH_2 27.3

Figure 4.11. (A) ^{1}H NMR Spectrum of ButenylOx **(B)** ^{13}C NMR spectrum of ButenylOx. Both spectra were measured using $CDCl_3$ as the solvent.

4.3.1.5. Synthesis of Statistical Poly(2-oxazoline) Copolymer (P7)

To a clean and dry microwave vial, bocAmineOx (0.16 g, 0.8 mmol, 10 eq) was added with a stirrer bar, before the flask was sealed and placed under a nitrogen atmosphere. To this, butenylOx (0.10 g, 0.8 mmol, 10 eq), 2-ethyl-2-oxazoline (EtOx) (0.39 g, 0.40 mL, 4.0 mmol, 50 eq), and acetonitrile (0.75 mL) were added. The reaction mixture was then degassed with nitrogen for 10

minutes, before methyl *p*-toluenesulphonate (PropTs) (14.8 mg, 12.0 µL, 0.0799 mmol, 1 eq) was added. A sample was taken for T_0 before the reaction was placed in an oil bath at 100 °C for 100 minutes. Next, a sample was taken for T_{final} before the polymer was precipitated twice in diethyl ether.

The same procedure was followed for polymers **P1**, **P2**, **P3**, and **P8.** Quantities of reagents, reaction times, and monomer conversions can be seen in **Table 4.2.**

4.3.1.6. Synthesis of p(EtOx)-p(AmineOx) Block Poly(2-oxazoline)s (P4)

To a clean and dry microwave vial, EtOx (0.495 g, 4.99 mmol, 40 eq), and acetonitrile (0.75 mL) were added. The reaction mixture was then degassed with nitrogen for 10 minutes, before PropTs (26.0 mg, 0.12 mmol, 1 eq) was added. A sample was taken for T_0 before the reaction was placed in an oil bath at 100 °C for 75 minutes. After this time, bocAmineOx (0.250 mg, 1.24 mmol, 10 eq) was added to the reaction flask. The reaction flask was then left for a further 25 minutes at 100 °C. Next, a sample was taken for T_{final} before the polymer was precipitated twice in diethyl ether.

The same procedure was followed for polymers **P5** and **P6**. Quantities of reagents, reaction times, and monomer conversions can be seen in **Table 4.2.**

4.3.1.7. Synthesis of p(EtOx)-*r*-p(GluOx))-*b*-p(AmineOx) Block Poly(2-oxazoline)s (P9)

To a clean and dry microwave vial, EtOx (0.495 g, 4.99 mmol, 40 eq), butenylOx (0.100 g, 0.08 mmol, 10 eq) and acetonitrile (0.75 mL) were added. The reaction mixture was then degassed with nitrogen for 10 minutes, before

methyl *p*-toluenesulphonate (MeOTs) (15.0 mg, 0.08 mmol, 1 eq) was added. A sample was taken for T_0 before the reaction was placed in an oil bath at 100 °C for 100 minutes. After this time, bocAmineOx (0.160 mg, 0.8 mmol, 10 eq) was added to the reaction flask. The reaction flask was then left for a further 20 minutes at 100 °C. Next, a sample was taken for T_{final} before the polymer was precipitated twice in diethyl ether. The polymer then underwent post-polymerisation to add the glucose (see glycosylation step), before deprotection of the bocAmineOx and then deprotection of the glucose.

The same procedure was followed for polymers **P10**. Quantities of reagents, reaction times, and monomer conversions can be seen in **Table 4.2.**

Table 4.2. Quantities of all reagents used for all polymers synthesised in this chapter.

Polymer	*initiator*	*initiator*			*EtOx*			*BocAmineOx*			*ButenylOx*			*concentration (M)*	*Reaction time (mins) (block 1)*	*Reaction time* (mins) (block 2)	*Reaction Temperature*
		mass (g)	*eq*	*moles (mmol)*	*mass (g)*	*eq*	*moles (mmol)*	*mass (g)*	*eq*	*moles (mmol)*	*mass (g)*	*eq*	*moles (mmol)*				
P1	PropTs	0.030	1	0.14	1.000	70	10.09	0.289	10	1.44	-	-	-	4	135	-	100
P2	PropTs	0.023	1	0.11	1.000	95	10.09	0.213	10	1.06	-	-	-	4	175	-	100
P3	PropTs	0.024	1	0.11	1.000	90	10.09	0.224	10	1.12	-	-	-	4	170	-	100
P4	PropTs	0.026	1	0.12	0.495	40	4.99	0.250	10	1.24	-	-	-	4	75	25	100
P5	PropTs	0.035	1	0.16	1.000	60	10.09	0.337	10	1.68	-	-	-	4	100	20	100
P6	PropTs	0.053	1	0.25	2.000	80	20.18	1.010	20	5.04	-	-	-	4	135	35	100
P7	MeOTs	0.015	1	0.08	0.395	50	3.99	0.160	10	0.80	0.100	10	0.80	4	100	-	100
P8	MeOTs	0.005	1	0.03	0.079	30	0.80	0.053	10	0.27	0.100	30	0.80	4	115	-	100
P9	MeOTs	0.015	1	0.08	0.395	50	3.99	0.16	10	0.80	0.100	10	0.80	4	100	20	100
P10	MeOTs	0.015	1	0.08	0.395	50	3.99	0.16	10	0.80	0.100	10	0.80	4	100	20	100

4.3.1.8. Deprotection of BocAmineOx

The protected polymer was dissolved in DCM (2 mL) and trifluoroacetic acid (1 mL) was added to the reaction mixture. The mixture was left to stir overnight at room temperature, before the polymer was precipitated in diethyl ether, and subsequently dried *in vacuo,* before being dialysed against a 0.5 M sodium chloride solution using 1 kDa cut-off dialysis tubing.

4.3.1.9. Addition and Deprotection of Thioglucose to Polymer Chains

Polymer **P9** (100 mg), 2,2-dimethoxy-2-phenylacetophenone (DMPA) (10 mg, 0.5 eq per butenylOx), and 1-thio-β-D-glucose tetraacetate (59 mg, 2 eq per butenylOx) were dissolved in dry THF (0.75 mL). The reaction mixture was stirred under UV radiation for 16 hours before precipitation of the polymer in diethyl ether.

For the glucose deprotection, polymer **P9** (50 mg) was dissolved in methanol (2.5 mL). To this, 2 M sodium methoxide in methanol (0.5 mL) was added, and the reaction mixture was stirred at room temperature for 3 hours before addition of 1 M HCl to obtain a reaction mixture pH of ~3. The polymer was then precipitated in diethyl ether and subsequently dialysed against 0.5 M NaCl solution using 1 kDa cut-off dialysis tubing. Quantities of DMPA and 1-Thio-β-D-glucose tetraacetate used can be found in **Table 4.3.**

Table 4.3. Quantities of 1-thio-β-D-glucose tetraacetate and DMPA used for **P7**-**P10**.

Polymer	*Polymer amount (mg)*			*double*	*mmoles of*	*DMPA*			*sugar*		
	Mass (mg)	*RMM (g/mol)*	*moles (mol)*	*bonds per chain*	*double bond*	*Eq*	*mmoles*	*mass (mg)*	*Eq*	*mmoles*	*mass*
P7	100	12,000	8.3E-06	9	0.0001	0.5	0.04	10	5	0.375	138
P8	100	17700	5.6E-06	27	0.0002	0.5	0.08	20	5	0.763	278
P9	100	11100	9.0E-06	9	0.0001	0.5	0.04	10	5	0.405	147.5
P10	100	12200	8.2E-06	10	0.0001	0.5	0.04	11	5	0.410	150

4.3.2. Polyplex Formation and RNA Transfection

This work was carried out by Beatriz Dias Barbieri from the Shattock Group at Imperial College London. Furthermore, these experimental procedures were provided by the Shattock group.

4.3.2.1. *In Vitro* Transcription of Self-amplifying mRNA

Self-amplifying mRNA (saRNA) derived from VEEV alphavirus genome and encoding firefly luciferase (fLuc) was prepared by *in vitro* transcription. pDNA was linearised using MluI (New England BioLabs, UK) for 2 h at 37 °C, MluI was added again and incubated for another 1 h at 37 °C. Linearisation was confirmed by agarose gel electrophoresis. For transcription into saRNA, 6 µl of linearised DNA template was synthesised into RNA transcripts *via* the mMessage mMachine kit (Invitrogen, Thermo Fisher Scientific, UK) according to manufacturer's instructions. Transcripts were then purified by lithium chloride precipitation. Briefly, transcripts were frozen overnight at -20 °C and precipitated the next morning by centrifugation at 14000 rpm for 20 min at 4 °C. Pellets were resuspended in 70% ethanol and centrifuged at 14000 rpm for 5 min at 4 °C. The ethanol was removed, pellets were allowed to dry for 5

min, and transcripts were resuspended in ultrapure water. RNA quantification was done using a NanoDrop One (Thermo Fisher Scientific, UK) and RNA integrity was evaluated by RNA gel electrophoresis using a FlashGel™ System (Lonza, UK).

4.3.2.2. Formation of Polyplexes

Stock solutions of the polymers (**P1**-P**10**) at 1 mg/mL were prepared in ultrapure H_2O. Polyplexes were prepared at different N/P ratios (0.5, 1, 5, 20 and 50). The required amount of polymer at different N/P ratios was added to a fixed amount of RNA (20 µg). Polymers were added in a drop-wise manner to the RNA solution in HEPES buffer with 5% glucose (pH = 5). Samples were mixed for 30 min at 500 rpm and at 20 °C, using a Thermomixer comfort (Eppendorf, Germany). The raw polyplex DLS data can be seen in **Table 4.4** and **Table 4.5.**

.

Table 4.4. Size, PDI, and zeta potential (as measured by DLS) for polymers **P1**-**P5** at N/P ratios of 0.5, 1, 5, 20, 50.

P1	Size (nm)	PDI	Zeta Potential (mV)
N/P 0.5	660 ± 906	0.81 ± 0.27	-3 ± 1
N/P 1	174 ± 43	0.52 ± 0.28	-2 ± 0
N/P 5	195 ± 28	0.39 ± 0.16	-4 ± 2
N/P 20	143 ± 33	0.55 ± 0.13	-3 ± 1
N/P 50	132 ± 16	0.47 ± 0.12	-7 ± 5

P2	Size (nm)	PDI	Zeta Potential (mV)
N/P 0.5	141 ± 57	0.85 ± 0.13	-10 ± 12
N/P 1	151 ± 23	0.55 ± 0.23	-6 ± 4
N/P 5	163 ± 31	0.74 ± 0.27	-14 ± 5
N/P 20	287 ± 77	0.60 ± 0.06	-10 ± 1
N/P 50	237 ± 49	0.74 ± 0.18	-14 ± 0

P3	Size (nm)	PDI	Zeta Potential (mV)
N/P 0.5	177 ± 14	0.72 ± 0.23	-5 ± 6
N/P 1	113 ± 25	0.93 ± 0.12	-2 ± 0
N/P 5	126 ± 16	0.51 ± 0.12	-5 ± 4
N/P 20	89 ± 10	0.63 ± 0.20	-8 ± 9
N/P 50	138 ± 18	0.39 ± 0.14	-6 ± 1

P4	Size (nm)	PDI	Zeta Potential (mV)
N/P 0.5	350 ± 62	0.40 ± 0.07	-18 ± 6
N/P 1	190 ± 14	0.35 ± 0.03	-21 ± 7
N/P 5	252 ± 24	0.34 ± 0.03	-10 ± 4
N/P 20	200 ± 41	0.31 ± 0.03	+4 ± 1
N/P 50	215 ± 47	0.40 ± 0.13	+5 ± 1

P5	Size (nm)	PDI	Zeta Potential (mV)
N/P 0.5	173 ± 14	0.33 ± 0.06	-3 ± 2
N/P 1	137 ± 10	0.40 ± 0.10	-4 ± 2
N/P 5	111 ± 7	0.44 ± 0.07	-3 ± 1
N/P 20	93 ± 4	0.33 ± 0.05	+4 ± 1
N/P 50	181 ± 40	0.43 ± 0.10	-2 ± 1

Table 4.5. Size, PDI, and zeta potential (as measured by DLS) for polymers **P6**-**P10** at N/P ratios of 0.5, 1, 5, 20, 50.

P6	Size (nm)	PDI	Zeta Potential (mV)
N/P 0.5	145 ± 22	0.37 ± 0.05	-10 ± 3
N/P 1	163 ± 5	0.24 ± 0.02	-51 ± 13
N/P 5	78 ± 4	0.27 ± 0.06	+1 ± 0
N/P 20	92 ± 13	0.43 ± 0.03	+5 ± 3
N/P 50	105 ± 8	0.54 ± 0.11	+2 ± 1

P7	Size (nm)	PDI	Zeta Potential (mV)
N/P 0.5	797 ± 233	0.59 ± 0.06	-32 ± 1
N/P 1	507 ± 69	0.58 ± 0.12	-24 ± 7
N/P 5	412 ± 40	0.47 ± 0.05	-19 ± 3
N/P 20	196 ± 6	0.20 ± 0.00	+9 ± 1
N/P 50	241 ± 7	0.42 ± 0.01	+8 ± 0

P8	Size (nm)	PDI	Zeta Potential (mV)
N/P 0.5	334 ± 38	0.45 ± 0.12	-23 ± 7
N/P 1	617 ± 75	0.51 ± 0.04	-19 ± 3
N/P 5	249 ± 24	0.51 ± 0.07	+2 ± 0
N/P 20	309 ± 43	0.54 ± 0.11	+14 ± 1
N/P 50	190 ± 38	0.83 ± 0.26	+10 ± 0

P9	Size (nm)	PDI	Zeta Potential (mV)
N/P 0.5	170 ± 95	0.43 ± 0.17	-15 ± 12
N/P 1	220 ± 29	0.40 ± 0.10	-14 ± 7
N/P 5	130 ± 6	0.42 ± 0.01	-15 ± 7
N/P 20	110 ± 28	0.39 ± 0.06	-8 ± 2
N/P 50	189 ± 43	0.42 ± 0.05	-5 ± 1

P10	Size (nm)	PDI	Zeta Potential (mV)
N/P 0.5	206 ± 42	0.36 ± 0.09	-11 ± 6
N/P 1	177 ± 34	0.34 ± 0.04	-17 ± 5
N/P 5	147 ± 14	0.49 ± 0.09	-15 ± 7
N/P 20	122 ± 2	0.43 ± 0.05	-4 ± 0
N/P 50	130 ± 6	0.41 ± 0.05	+1 ± 0

4.3.2.3. Cell Line and Culture Conditions

HEK293T.17 and HeLa cells (ATCC, US) were routinely grown in Dulbecco's Modified Eagle's Medium (DMEM) (Gibco, Thermo Fisher, UK) supplemented with 10% (v/v) foetal bovine serum (FBS), 1% (v/v) L-glutamine, and 1% (v/v) penicillin/streptomycin (Thermo Fisher, UK), at 37 °C under 5% CO2. When confluent, cells were washed with DPBS 1X (Gibco, UK) and treated with trypsin (TrypLE Express 1X) (Gibco, UK) for seeding in new culture flasks (Corning, US).

THP-1 cells (ATCC, US) were routinely grown in RPMI-1640 Medium (Sigma, UK) supplemented with 10% (v/v) foetal bovine serum (FBS), 1% (v/v) L-glutamine, and 1% (v/v) penicillin/streptomycin (Thermo Fisher, UK), at 37 °C under 5% CO_2. When confluent, the whole cell suspension in culture media was centrifuged at 1750 rpm for 5 min, and the pellet was re-suspended in fresh RPMI-1640 medium for seeding in new culture flasks (Corning, US).

Finally, an immortalised cell line of human skeletal muscle cells (hSkMC) (PromoCell, UK) was routinely grown in Skeletal Muscle Cell Growth Medium (PromoCell, Germany), supplemented with SupplementMix (PromoCell, Germany). When confluent, cells were washed with DPBS 1X (Gibco, UK) and treated with trypsin. Neutralisation was done with DPBS 1X containing 10% FBS, and cells were centrifuged and re-suspended in the skeletal muscle cell growth medium for seeding in new culture flasks (Corning, US).

4.3.2.4. Cell Transfection and Luciferase Assay

The cell experiments were carried out *via* the following procedure: Transfection assay was performed similar to as previously described by Blakney *et al*.[3] For both HEK293T.17 and HeLa cell lines, a concentration of $5x10^4$ cells per well were seeded in a 96-well plate 24 h prior to the experiment. For THP-1 cells, the concentration was $8x10^4$ cells per well, and for the immortalised hSkMC, the concentration was $10x10^4$ cells per well.

On the day of the experiment, 100 ng of polyplexes in 100 µL of ultrapure H_2O was added to each well. Samples were allowed to transfect for 24 h. After, the transfection efficiency was analysed by removing 50 µL of medium and adding 50 µL of Bright-Glo™ luciferin substrate (Promega, UK) to each well. The total volume was transferred to a white plate (Falcon®, US) and luminescence intensity was analysed on a FLUOstar Omega plate reader (BMG LABTECH, UK).

4.3.2.5. Quantification of Encapsulation Efficiency

The saRNA loading in polyplexes was quantified using a Quant-iT RiboGreen assay (Thermo Fisher, UK) similar to as previously described.[43] Samples were diluted to 3 µg/mL in 1× TE buffer in PBS (Sigma Aldrich, UK). Standard solutions were also prepared in 1× TE buffer to account for any variation in fluorescence. The assay was performed according to the manufacturer's protocol. RiboGreen reagent was diluted 200-fold in 1× TE buffer. Samples were loaded on a black, 96-well plate, and analysed for fluorescence on a microplate reader (BMG LABTECH, UK) at an excitation of 485 nm and emission at 528 nm. Fluorescence values correspond to the RNA that was not

loaded into polyplexes and percentage of saRNA loading was calculated subtracting it from 100%.

4.3.2.6. Cell Viability Assay

Cells were seeded at the appropriate concentrations as mentioned previously and transfected the next day with 100 ng of RNA complexed with polymers. Cells were incubated with polyplexes for 24 h. Plates were equilibrated at room temperature for 30 min and an equal volume of the CellTiter-Glo® 2.0 (Promega, UK) reagent was added to the wells (100 µL). Contents were mixed for 2 min using an orbital shaker and plates were incubated for 10 min at room temperature. The total volume was transferred to a white plate (Falcon®, US) and luminescence intensity was analysed on a FLUOstar Omega plate reader (BMG LABTECH, UK).

4.4. Additional Data

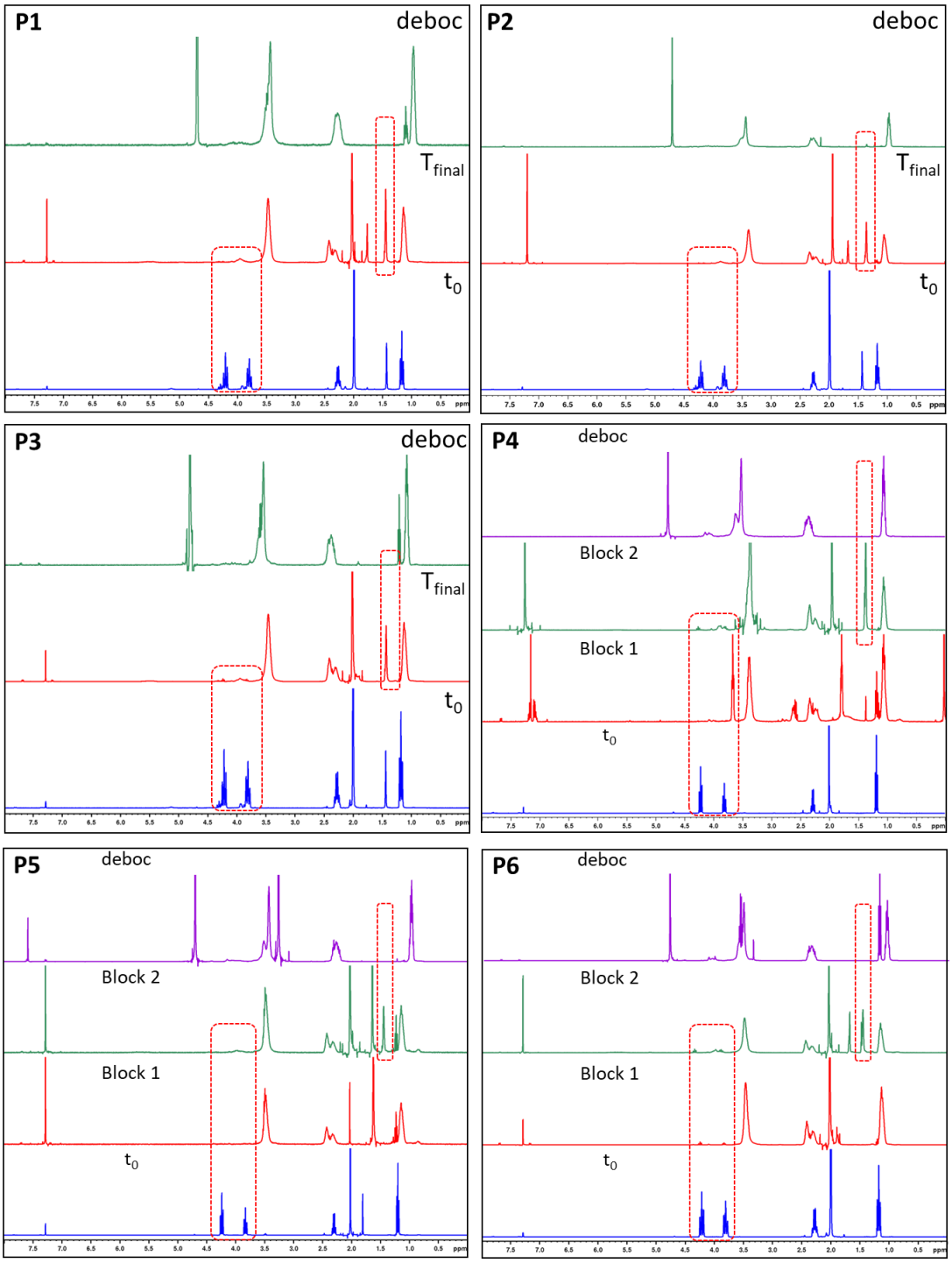

Figure 4.12. ^{1}H NMR Spectra for each step of the polymerisation for polymers **P1**-**P6**, including deprotection of the boc-amine functionalities. All spectra were measured using $CDCl_3$ as the solvent.

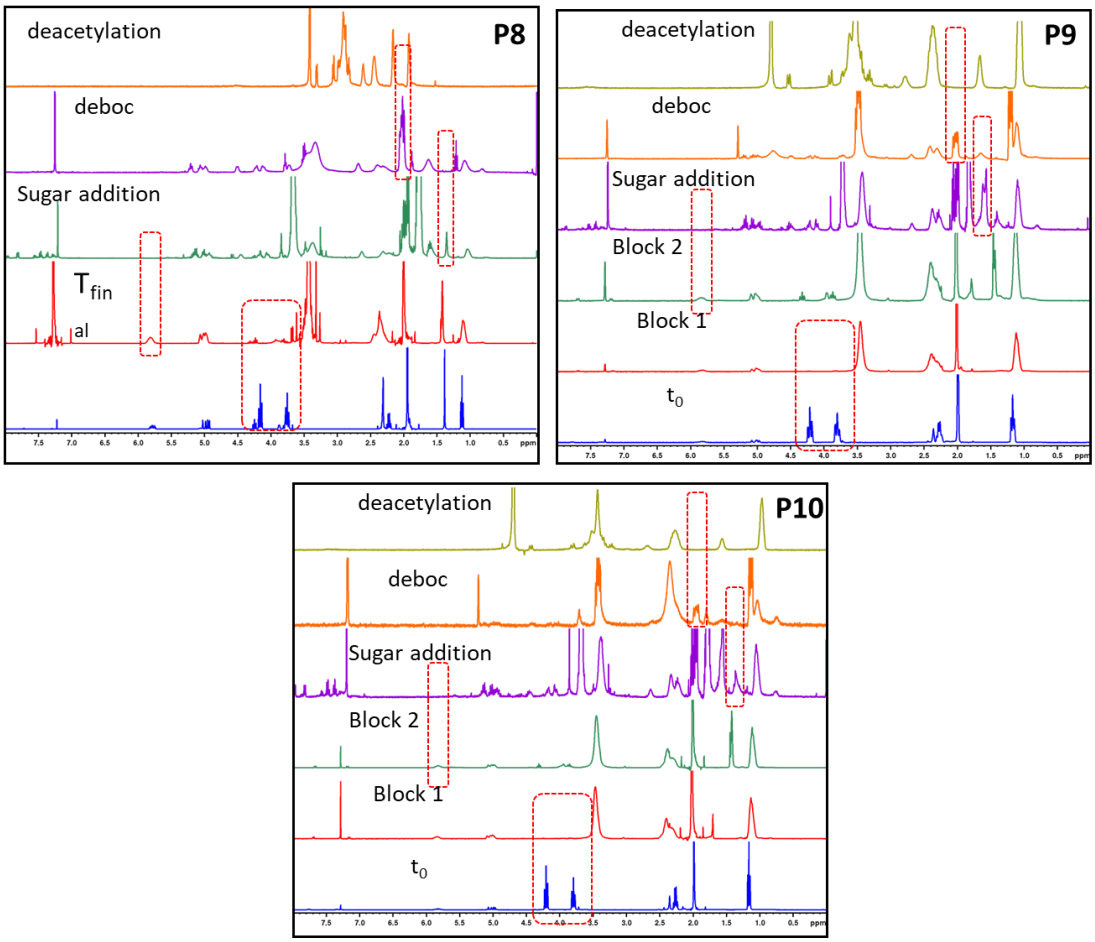

Figure 4.13. ^{1}H NMR Spectra for each step of the polymerisation for polymers **P8**-**P10**, including deacetylation of the polymers and deprotection of the boc-amine functionalities. All spectra were measured using $CDCl_3$ as the solvent.

4.5. References

1. Gupta, A.; Andresen, J. L.; Manan, R. S.; Langer, R., *Advanced Drug Delivery Reviews* **2021,** *178*, 113834.
2. Verbeke, R.; Lentacker, I.; De Smedt, S. C.; Dewitte, H., *Journal of Controlled Release* **2021,** *333*, 511-520.
3. Blakney, A. K.; Zhu, Y.; McKay, P. F.; Bouton, C. R.; Yeow, J.; Tang, J.; Hu, K.; Samnuan, K.; Grigsby, C. L.; Shattock, R. J.; Stevens, M. M., *ACS Nano* **2020,** *14* (5), 5711-5727.
4. Stokes, A.; Pion, J.; Binazon, O.; Laffont, B.; Bigras, M.; Dubois, G.; Blouin, K.; Young, J. K.; Ringenberg, M. A.; Ben Abdeljelil, N.; Haruna, J.; Rodriguez, L.-A., *Regulatory Toxicology and Pharmacology* **2020,** *113*, 104648.
5. Moyo, N.; Vogel, A. B.; Buus, S.; Erbar, S.; Wee, E. G.; Sahin, U.; Hanke, T., *Molecular Therapy - Methods & Clinical Development* **2019,** *12*, 32-46.
6. Bloom, K.; van den Berg, F.; Arbuthnot, P., *Gene Therapy* **2021,** *28* (3), 117-129.
7. Uddin, M. N.; Roni, M. A., *Vaccines* **2021,** *9* (9), 1033.
8. Machado, B. A.; Hodel, K. V.; Fonseca, L. M.; Mascarenhas, L. A.; Andrade, L. P.; Rocha, V. P.; Soares, M. B.; Berglund, P.; Duthie, M. S.; Reed, S. G.; Badaró, R., *Vaccines* **2021,** *9* (11), 1345.
9. Rodriguez-Gascon, A.; del Pozo-Rodriguez, A.; Solinis, M. A., *International Journal Of Nanomedicine* **2014,** *9*, 1833-1843.
10. Chang, Y.-H.; Lin, M.-W.; Chien, M.-C.; Ke, G.-M.; Wu, I. E.; Lin, R.-L.; Lin, C.-Y.; Hu, Y.-C., *Journal of Controlled Release* **2021,** *338*, 694-704.
11. Goswami, R.; Chatzikleanthous, D.; Lou, G.; Giusti, F.; Bonci, A.; Taccone, M.; Brazzoli, M.; Gallorini, S.; Ferlenghi, I.; Berti, F.; O'Hagan, D. T.; Pergola, C.; Baudner, B. C.; Adamo, R., *ACS Infectious Diseases* **2019,** *5* (9), 1546-1558.
12. Seok, H.; Noh, J. Y.; Lee, D. Y.; Kim, S. J.; Song, C. S.; Kim, Y. C., *J Control Release* **2017,** *265*, 66-74.
13. Chahal, J. S.; Khan, O. F.; Cooper, C. L.; McPartlan, J. S.; Tsosie, J. K.; Tilley, L. D.; Sidik, S. M.; Lourido, S.; Langer, R.; Bavari, S.; Ploegh, H. L.; Anderson, D. G., *Proc. Natl. Acad. Sci. U.S.A* **2016,** *113* (29), E4133-42.
14. Tian, Y.; Wang, H.; Liu, Y.; Mao, L.; Chen, W.; Zhu, Z.; Liu, W.; Zheng, W.; Zhao, Y.; Kong, D.; Yang, Z.; Zhang, W.; Shao, Y.; Jiang, X., *Nano Letters* **2014,** *14* (3), 1439-1445.

15. Tierney, E. G.; Duffy, G. P.; Hibbitts, A. J.; Cryan, S.-A.; O'Brien, F. J., *Journal of Controlled Release* **2012,** *158* (2), 304-311.

16. Lorson, T.; Lubtow, M. M.; Wegener, E.; Haider, M. S.; Borova, S.; Nahm, D.; Jordan, R.; Sokolski-Papkov, M.; Kabanov, A. V.; Luxenhofer, R., *Biomaterials* **2018,** *178*, 204-280.

17. Nelson, C. E.; Kintzing, J. R.; Hanna, A.; Shannon, J. M.; Gupta, M. K.; Duvall, C. L., *ACS Nano* **2013,** *7* (10), 8870-8880.

18. Coolen, A.-L.; Lacroix, C.; Mercier-Gouy, P.; Delaune, E.; Monge, C.; Exposito, J.-Y.; Verrier, B., *Biomaterials* **2019,** *195*, 23-37.

19. Hall, A.; Lächelt, U.; Bartek, J.; Wagner, E.; Moghimi, S. M., *Molecular Therapy* **2017,** *25* (7), 1476-1490.

20. Gleede, T.; Reisman, L.; Rieger, E.; Mbarushimana, P. C.; Rupar, P. A.; Wurm, F. R., *Polymer Chemistry* **2019,** *10* (24), 3257-3283.

21. Mees, M. A.; Hoogenboom, R., *Polymer Chemistry* **2018,** *9* (40), 4968-4978.

22. Taranejoo, S.; Liu, J.; Verma, P.; Hourigan, K., *Journal of Applied Polymer Science* **2015,** *132* (25).

23. Blakney, A. K.; Yilmaz, G.; McKay, P. F.; Becer, C. R.; Shattock, R. J., *Biomacromolecules* **2018,** *19* (7), 2870-2879.

24. Muljajew, I.; Huschke, S.; Ramoji, A.; Cseresnyés, Z.; Hoeppener, S.; Nischang, I.; Foo, W.; Popp, J.; Figge, M. T.; Weber, C.; Bauer, M.; Schubert, U. S.; Press, A. T., *ACS Nano* **2021,** *15* (7), 12298-12313.

25. Figdor, C. G.; van Kooyk, Y.; Adema, G. J., *Nat. Rev. Immunol* **2002,** *2* (2), 77-84.

26. Varki, A., *Glycobiology* **2017,** *27* (1), 3-49.

27. Sharon, N.; Lis, H., *Science* **1989,** *246* (4927), 227-234.

28. Stenzel, M. H., *Macromolecules* **2022,** *55* (12), 4867-4890.

29. Hartweg, M.; Jiang, Y.; Yilmaz, G.; Jarvis, C. M.; Nguyen, H. V. T.; Primo, G. A.; Monaco, A.; Beyer, V. P.; Chen, K. K.; Mohapatra, S.; Axelrod, S.; Gómez-Bombarelli, R.; Kiessling, L. L.; Becer, C. R.; Johnson, J. A., *JACS Au* **2021,** *1* (10), 1621-1630.

30. Blakney, A. K.; Abdouni, Y.; Yilmaz, G.; Liu, R.; McKay, P. F.; Bouton, C. R.; Shattock, R. J.; Becer, C. R., *Biomacromolecules* **2020,** *21* (6), 2482-2492.

31. Ting, S. R. S.; Chen, G.; Stenzel, M. H., *Polymer Chemistry* **2010,** *1* (9), 1392-1412.

32. Luxenhofer, R.; Sahay, G.; Schulz, A.; Alakhova, D.; Bronich, T. K.; Jordan, R.; Kabanov, A. V., *Journal of Controlled Release* **2011,** *153* (1), 73-82.

33. Tong, J.; Zimmerman, M. C.; Li, S.; Yi, X.; Luxenhofer, R.; Jordan, R.; Kabanov, A. V., *Biomaterials* **2011,** *32* (14), 3654-3665.

34. Luxenhofer, R.; Han, Y.; Schulz, A.; Tong, J.; He, Z.; Kabanov, A. V.; Jordan, R., *Macromolecular Rapid Communications* **2012,** *33* (19), 1613-1631.

35. Tavano, R.; Gabrielli, L.; Lubian, E.; Fedeli, C.; Visentin, S.; Polverino De Laureto, P.; Arrigoni, G.; Geffner-Smith, A.; Chen, F.; Simberg, D.; Morgese, G.; Benetti, E. M.; Wu, L.; Moghimi, S. M.; Mancin, F.; Papini, E., *ACS Nano* **2018,** *12* (6), 5834-5847.

36. Troiber, C.; Kasper, J. C.; Milani, S.; Scheible, M.; Martin, I.; Schaubhut, F.; Küchler, S.; Rädler, J.; Simmel, F. C.; Friess, W.; Wagner, E., *European Journal of Pharmaceutics and Biopharmaceutics* **2013,** *84* (2), 255-264.

37. Thomas, P.; Smart, T. G., *Journal of Pharmacological and Toxicological Methods* **2005,** *51* (3), 187-200.

38. Buschmann, M. D.; Carrasco, M. J.; Alishetty, S.; Paige, M.; Alameh, M. G.; Weissman, D., *Vaccines* **2021,** *9* (1), 65.

39. Ivashkiv, L. B.; Donlin, L. T., *Nature Reviews Immunology* **2014,** *14* (1), 36-49.

40. Forrester, M. A.; Wassall, H. J.; Hall, L. S.; Cao, H.; Wilson, H. M.; Barker, R. N.; Vickers, M. A., *Cellular Immunology* **2018,** *332*, 58-76.

41. Zhou, M.; Qian, Y.; Xie, J.; Zhang, W.; Jiang, W.; Xiao, X.; Chen, S.; Dai, C.; Cong, Z.; Ji, Z.; Shao, N.; Liu, L.; Wu, Y.; Liu, R., *Angewandte Chemie International Edition* **2020,** *59* (16), 6412-6419.

42. Gress, A.; Völkel, A.; Schlaad, H., *Macromolecules* **2007,** *40* (22), 7928-7933.

43. Geall Andrew, J.; Verma, A.; Otten Gillis, R.; Shaw Christine, A.; Hekele, A.; Banerjee, K.; Cu, Y.; Beard Clayton, W.; Brito Luis, A.; Krucker, T.; O'Hagan Derek, T.; Singh, M.; Mason Peter, W.; Valiante Nicholas, M.; Dormitzer Philip, R.; Barnett Susan, W.; Rappuoli, R.; Ulmer Jeffrey, B.; Mandl Christian, W., *Proceedings of the National Academy of Sciences* **2012,** *109* (36), 14604-14609.

Chapter 5. Summary and Outlook

The aim of this thesis was to further develop the field of poly(2-oxazoline) architectures. From **Chapter 1**, it was seen that a wide variety of poly(2-oxazoline) architectures are available, including random and block copolymers, cyclic polymers, star polymers, and branched polymers. These polymeric architectures have a wide range of applications including drug delivery, gene delivery, lubricating coatings, and contrast agents. Nonetheless, there are clear areas within the literature that have not been fully explored and these areas warrant further investigation.

In **Chapter 2**, the use of a bisfunctional 2-oxazoline monomer was used to synthesise core cross-linked poly(2-oxazoline) star polymers for the first time. Bisfunctional 2-oxazolines are not novel themselves and have been used to synthesise highly cross-linked hydrogels previously. However, core cross-linked star polymers are an intriguing type of polymer, with the high degree of branching allowing for access to large macromolecules with molecular weights in the millions of Daltons. Importantly, and opposingly to hydrogels, these structures are still highly soluble in a range of solvents allowing for more advanced analysis to be performed. One of the disadvantages to the core cross-linked approach to star polymers is the difficulty in analysing the structure of the core, and this was again the case for the polymers synthesised in **Chapter 2**. Nonetheless, the synthesised stars were shown to be able to encapsulate a small hydrophobic model drug, whilst linear references could not encapsulate any. Further work for these star polymers would be to improve their potential for biomedical applications. This could be achieved by glycosylating the polymers to allow for targeted delivery, using a pH responsive monomer for the arms, or using a biodegradable cross-linker.

These further additions could allow for a more targeted delivery and release of any drug encapsulated.

In **Chapter 3**, hybrid multiblock and cyclic copolymers of poly(2-oxazoline)s and poly(acrylate)s were synthesised using a copper azide-alkyne cycloaddition step-growth mechanism for the first time. This was the first known example of multiblock and cyclic copolymers combining these two types of polymer. One of the issues with the synthesis of cyclic polymers is that extremely dilute conditions are generally required in order to suppress the competing step-growth reaction. In this chapter, an extensive investigation was carried out in order to discover factors favouring either step-growth or cyclisation. These factors were combined in order to maximise the yield of step-growth polymers and cyclic polymers, eventually achieving a yield of 92% and 58% respectively. Advanced GPC analysis was used to analyse the structure of the polymers, providing evidence that the polymers underwent step-growth and then cyclisation. As shown in **Chapter 1**, cyclic poly(2-oxazoline)s are frequently used for biolubricating purposes and show better performance than linear counterparts, and so future work for these cyclic polymers would be to investigate their friction modifying potential.

In **Chapter 4**, 2-oxazoline monomers were synthesised with tuneable R groups. These monomers were then polymerised together to access more complex poly(2-oxazoline)s such as positively charged and glycosylated block copolymers. These polymers were used for transfection of self-amplifying RNA into various cell lines. It was shown that the block copolymers had a much higher encapsulation efficiency compared to the statistical copolymers, whilst glycosylation improved transfection of the RNA into the different cell lines.

Furthermore, all polymers were shown to have excellent cell viability in all cell types. Future work for these polymers is to further increase the block lengths and the degree of glycosylation on the polymers since these were the major contributors to improved encapsulation and transfection of RNA.

The field of poly(2-oxazoline)s has already moved from exploring synthetic capabilities to looking at real applications. From **Chapter 1**, it is clear that many of these applications are centred on their use as therapeutic agents. The versatility of the poly(2-oxazoline) chain ends and R groups allow for drug conjugation, whilst block polymers can be self-assembled and used to encapsulate drugs. Similarly, star polymers can be used to encapsulate and protect drugs in their cores. Cyclic poly(2-oxazoline)s have been shown to improve the lubricity of surfaces compared to linear polymers and can even be attached to cartilage to act as a biolubricant. The hydrolysis of poly(2-oxazoline)s allows for access to positively charged polymers that can be used to form polyplexes with genes and used for transfection. The field of poly(2-oxazoline)s appears to be heading towards more complex structures for biomedical applications, for example by the attachment of sugar moieties for targeted delivery of material within the body, or self-assembled structures for drug encapsulation. Ultimately though, these complex polymers will need to be tested in clinical trials to really demonstrate their potential. Nonetheless, clinical trials using poly(2-oxazoline)s are beginning to emerge, for example, a poly(2-oxazoline)-Rotigotine conjugate has recently undergone stage 1 clinical trials.